Technische Universität Berlin

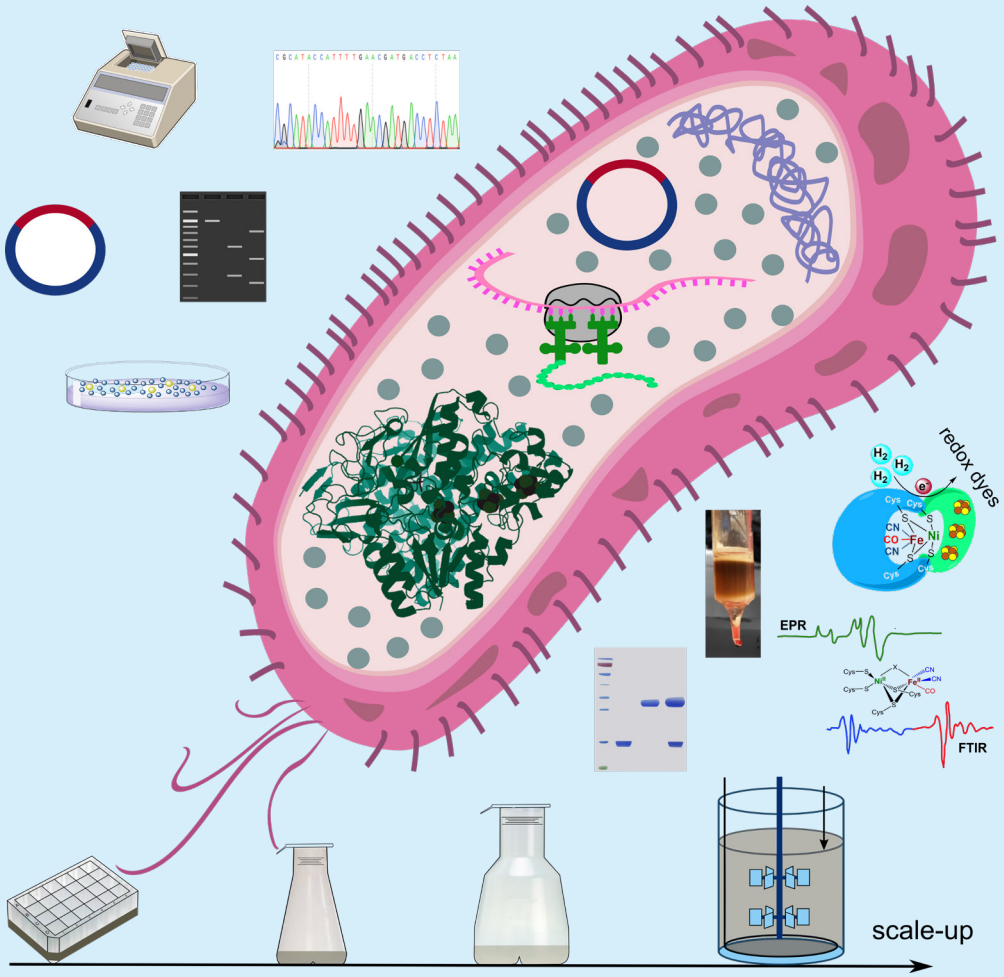

Development of a Bioprocess for Heterologous Hydrogenase Production in *Escherichia coli*

Qin Fan - Dissertation

Institute of Biotechnology
Technische Universität Berlin
Bioprocess Engineering

Development of a bioprocess for heterologous hydrogenase production in *Escherichia coli*

vorgelegt von

M. Sc.

Qin Fan

ORCID: 0000-0001-5801-8690

an der Fakultät III – Prozesswissenschaften

der Technischen Universität Berlin

zur Erlangung des akademischen Grades

Doktor der Ingenieurwissenschaften

- Dr.-Ing. -

genehmigte Dissertation

Promotionsausschuss:

Vorsitzender:	Prof. Dr. Jens Kurreck
Gutachter:	Prof. Dr. Peter Neubauer
Gutachter:	Prof. Dr. Gary R. Sawers, Institute of Biology/Microbiology, Martin-Luther University Halle-Wittenberg, Halle, Germany
Gutachter:	Dr. Oliver Lenz

Tag der wissenschaftlichen Aussprache: 13. Oktober 2022

Berlin 2022

Abstract

Concerns about exhaustion of natural resources and global warming have led to increasing attention to clean and renewable energy. Here, biohydrogen (H_2) is a very attractive alternative because of its various means of production, large energy content per mass and its environmental friendliness. In nature, the most efficient H_2 producers are hydrogenases. These metalloenzymes display fascinating redox-chemical properties with tremendous promise as a biocatalyst for H_2 production, bioanode in biofuel cells or H_2-driven cofactor generation systems. However, the catalytic center of most hydrogenases is irreversibly inactivated by even trace O_2 and CO which extremely restricts their biochemical investigations and potential applications. Thus, O_2-tolerant hydrogenases that sustain catalytic activity under oxic conditions, particularly from the "Knallgas" bacterium *Ralstonia eutropha* are promising candidates for biotechnological application. Since understanding of these highly complex enzymes has been severely hampered by low yields, heterologous production of hydrogenases in a robust and genetically tractable expression host is an attractive strategy to make these enzymes more accessible. In the study, the H_2-sensing regulatory [NiFe]-hydrogenase (RH) from *R. eutropha* H16, owing to its relatively simple architecture and extensive use in spectroscopic studies, was chosen as a model for development of a heterologous hydrogenase production system in *Escherichia coli*.

For this purpose, a plasmid-based expression system for the RH structural subunits under control of the IPTG inducible lac-promoter was designed followed by a production screening. Initial trials with fed-batch-like EnPresso B cultivations demonstrated the possibility of heterologous hydrogenase production. Based on the EnPresso growth system, IPTG and lactose autoinduction resulted in a remarkably higher productivity averaged over the whole process time in comparison with classic single-shot IPTG induction. Repeated boosting increased cell densities and soluble RH yield to about 360 mg L^{-1}, an increase of several 100-fold compared to the production in the native organism *R. eutropha*. Since spectroscopic studies showed the absence of the [NiFe]-cofactor, the production process was further improved by investigating different parameters e.g., strain, production temperature and duration, metal additions and co-expression of maturation genes. Hereby, it succeeded in producing a heterologous RH with similar activity to native RH, but with significantly higher yields and shorter process time. Finally, the process was transferred to a high cell density fed-batch cultivation in lab-scale bioreactors, confirming that active RH production of >130 mg per liter is possible in pure glucose-based mineral salt medium.

This study developed herein lays a good basis for the future production of difficult-to-produce functional hydrogenases for basic and applied science.

Zusammenfassung

Bedenken bezüglich des Verbrauchs natürlicher Ressourcen und der Klimaerwärmung haben zu einer gesteigerten Aufmerksamkeit auf saubere und erneuerbare Energien geführt. Hier ist Biowasserstoff (H_2) aufgrund seiner vielfältigen Herstellungsmöglichkeiten, seines hohen Energiegehalts pro Masse und seiner Umweltfreundlichkeit eine sehr attraktive Alternative. In der Nature sind die effizientesten H_2-Produzenten die Hydrogenases. Diese Metalloenzyme weisen faszinierende redox-chemische Eigenschaften auf und sind vielversprechend als Biokatalysatoren für die H_2-Produktion, als Bioanode in Brennstoffzellen oder als Teil H_2-betriebener Kofaktorregenerationsysteme. Das katalytische Zentrum der meisten Hydrogenases wird jedoch durch Spuren von O_2 and CO irreversibel inaktiviert, was ihre biochemischen Untersuchungen und potenziellen Anwendungen extrem einschrämkt. Daher sind O_2-tolerante Hydrogenases, insbesondere aus dem „Knallgas"-Bakterium *Ralstonia eutropha*, die ihre katalytische Aktivität unter oxischen Bedingungen aufrechterhalten, vielversprechende Kandidaten für die biotechnologische Anwendung. Die Erforschung dieser hochkomplexen Enzyme wird allerdings durch niedrige Ausbeuten stark behindert, weshalb die heterologe Produktion von Hydrogenasen in einem robusten und genetisch gut verstandenen Expressionswirt eine attraktive Strategie darstellt, um diese Enzyme besser herstellen zu können. Aufgrund ihrer relative einfachen Architektur und umfangreichen Verwendung in spektroskopischen Studien wurde in dieser Arbeit, die als H_2-Sensor fungierende, regulatorische [NiFe]-Hydrogenase (RH) aus *R. eutropha* H16 als Model für die Entwicklung eines heterologen Hydrogenase-Produktionssytems in *Escherichia coli* ausgewählt.

Zur diesem Zweck wurde ein plasmidbasiertes Expressionsystem für die Herstellung der RH-Strukturuntereinheiten unter der Kontrolle des IPTG-induzierbaren lac-Promotors entwickelt, und anschließend verschiedene Produktionsbedingungen evaluiert. Erste Versuche mit „Fed-batch-like" EnPresso B Kultiverungen zeigten die Möglichkeit einer heterologen Hydrogenase-Produktion. Die Nutzung von IPTG- und Laktose-Autoinduktion im EnPresso Wachstumsystems führte im Vergleich zur klassischen Induktion mit einmaliger IPTG-Zugabe zu einer bemerkenswert höheren Produktivität, gemittelt über die gesamte Prozessdauer. Wiederholte Nährstoffzugabe erhöhte die Zelldichte und die lösliche RH-Ausbeute auf ca. 360 mg L^{-1}, was einer 100-fach höheren Produktion im Vergleich zur Herstellung im nativen Organismus *R. eutropha* entspricht. Da spektroskopische Untersuchungen das Fehlen des [NiFe]-Cofaktors zeigten, wurde der Produktionsprozess durch die Untersuchungen verschiedener Parameter, z.B. Stamm, Produktionstemperature und -dauer, Zugabe von Metallionen und Koexpression von Reifungsgenen, weiter verbessert. Auf diese

Weise gelang es, eine heterologe RH mit ähnlicher Aktivität wie die native RH herzustellen, jedoch mit deutlich höherer Ausbeute und kürzerer Prozessdauer. Schließlich wurde der Prozess auf eine Hochzelldichte Fed-Batch-Kultiverung in Bioreaktoren im Labormaßstab übertragen. Dies bestätigte, dass eine aktive RH-Produktion von >130 mg pro Liter in reinem Glukose-basiertem Mineralsalzmedium möglich ist.

Diese Studie bildet eine gute Grundlage für die künftige Produktion von schwierig herzustellenden funktionellen Hydrogenasen für Grundlagen- und angewandten Forschung.

List of contents

Acknowledgements

I would like to thank all people who supported me during the making of this thesis, the numerous coworkers involved, and my colleagues at the Chair of Bioprocess Engineering and at the Max-Volmer Laboratory for Biophysical Chemistry, especially

- Prof. Dr. Peter Neubauer for placing his trust in me even before I started my bachelor thesis and for further giving me the opportunity to prepare this thesis in an independent yet well supported manner, helpful discussions and general encouragement in science and life,
- Dr. Matthias Gimpel for numerous opportunities to express myself and develop in most interesting scientific projects and collaborations, valuable advice, guidance and fruitful as well as inspiring discussions in every part of the work, good and always exciting interaction specially for manuscript writing prior to publication on both personal and professional level,
- Dr. Oliver Lenz for giving me the opportunity for the pleasant collaboration at the Max-Volmer Laboratory for Biophysical Chemistry, his professional discussions, constructive advice and valuable support,
- Dr. Giorgio Caserta and Dr. Christian Lorent for the measurements using UV-visible, IR and EPR spectroscopy, data evaluation and supportive discussions,
- Janna Schoknecht for introduction of *in vitro* H_2-dependent activity measurement and chilled French Pressure, her kind help with booking service and preparation of buffer required,
- Dr. Sebastian L. Riedel and Saskia Waldburger for supervising and performing the bioreactor experiments,
- Dr. Robert Giessmann, Dr. Janina Preissler, Michelle Gerlach for their help with the practical work in molecular biology and protein analytical experiments,
- Sarah von Westarp for her kind help with downstream processing experiments and always nice talk during the lab work,
- Brigitte Burckhardt, Irmgard Maue-Mohn and Thomas Högl for their excellent technical support,
- my friends for keeping me aware of life beyond the lab, especially Yuwen for her loving patience in times of science-related bad temper and unnerving restlessness,
- my beloved parents who made all this possible.

I acknowledge the Cluster of Excellence “Unifying Systems in Catalysis” (UniSysCat) for funding this project, the Berlin International Graduate School of Natural Sciences and Engineering (BIG-NSE), and the Chinese Scholarship Council as well as the German Academic Exchange Service (DAAD) for supplying the funding that carried me through this project.

List of publications contributing to this work

I. **Fan, Q.**, Neubauer, P., Lenz, O., and Gimpel, M. (2020). Heterologous hydrogenase overproduction systems for biotechnology—An overview. Int. J. Mol. Sci. 21, 5890, https://doi.org/10.3390/ijms21165890.

II. **Fan, Q.**, Caserta, G., Lorent, C., Lenz, O., Neubauer, P., and Gimpel, M. (2021a). Optimization of culture conditions for oxygen-tolerant regulatory [NiFe]-hydrogenase production from *Ralstonia eutropha* H16 in *Escherichia coli*. Microorganisms 9, 1195, https://doi.org/10.3390/microorganisms9061195.

See Chapter 7 Publications, Paper I, page 65-81

III. **Fan, Q.**, Neubauer, P., and Gimpel, M. (2021b). Production of soluble regulatory hydrogenase from *Ralstonia eutropha* in *Escherichia coli* using a fed-batch-based autoinduction system. Microb. Cell Fact. 20, 1–22, https://doi.org/10.1186/s12934-021-01690-4.

See Chapter 7 Publications, Paper II, page 82-94

IV. **Fan, Q.**, Caserta, G., Lorent, C., Zebger, I., Neubauer, P., Lenz, O., et al. (2022). High-yield production of catalytically active regulatory [NiFe]-hydrogenase from *Cupriavidus necator* in *Escherichia coli*. Front. Microbiol. 13, 894375, https://doi.org/10.3389/fmicb.2022.894375.

See Chapter 7 Publications, Paper III, page 95-108

V. **Fan, Q.**, Waldburger, S., Neubauer, P., Riedel, S. L., and Gimpel, M. (2022). Implementation of a high cell density fed-batch for heterologous production of active [NiFe]-hydrogenase in *Escherichia coli*. Microb. Cell Fact. 21, 193, https://doi.org/10.1186/S12934-022-01919-W.

See Chapter 7 Publications, Paper IV, page 109-120

Author contributions

I. Q.F. wrote the first draft of the manuscript. Q.F. M.G. O.L. and P.N. contributed in writing and editing the manuscript. All authors have read and agreed to the published version of the manuscript.

II. Q.F. and M.G. designed experiments together with P.N. and O.L. Q.F. carried out all molecular biological and biochemical experiments. G.C. and C.L. performed the spectroscopic IR and EPR measurements and the data evaluation. All authors analyzed the data with major contributions from Q.F. and M.G. Q.F. prepared the original draft. M.G. P.N. G.C. and O.L. revised the manuscript. All authors have read and agreed to the published version of the manuscript.

III. Q.F. M.G. and P.N. participated in experiment design and interpretation of the results. Q.F. carried out all laboratory experiments, Q.F. and M.G. analysed the data. Q.F. drafted the manuscript. M.G. and P.N. revised the manuscript. All authors read and approved the final manuscript.

IV. Q.F. M.G. and O.L. participated in experimental design and interpretation of the results. Q.F. carried out all molecular biological and biochemical experiments. G.C. C.L. and I.Z. performed the spectroscopic IR and EPR measurements and the data evaluation. All authors analyzed the data with major contributions from Q.F. and M.G. Q.F. prepared the original draft. M.G., P.N. and O.L. revised the manuscript. All authors read and approved the final manuscript.

V. Q.F. and M.G. participated in experimental design and interpretation of the results. Q.F. carried out all molecular biological and biochemical experiments. Q.F. and S.W. performed the bioreactor cultivation experiments. S.R. supervised the bioreactor cultivation. All authors analyzed the data with major contributions from Q.F. and M.G. Q.F. drafted the original manuscript. M.G. S.W. P.N. and S.R. revised the manuscript. All authors read and approved the final manuscript.

1. Introduction

At the beginning of the 21st century, we are facing significant energy challenges around the world. Concerns about global climate change and limited supply of fossil fuel energy have increased interest in biomass and other alternative energy sources, such as hydrogen (H_2), which is considered as a potential and promising future viable energy carrier. H_2 has the highest energy gravimetric energy density of all known substances, nearly three times greater than of the fossil fuel (oil 42-45 MJ/kg) (Vijayaraghavan and Mohd Soom 2006). While water (H_2O) is the only product of H_2 combustion, the use of H_2 is less polluting and CO_2-neutral (Crabtree and Dresselhaus 2008). In addition, H_2 also acts as a low potential reductant (H_2/H^+, $E_0' = -420$ mV) for cellular energy generation and anaerobic processes (Lauermann et al. 2000; Shima et al. 2008). Hence, H_2 is strategically important for development of cleaner and more sustainable energy system. However, at present, the current industrial H_2 production methods, including stream reforming of fossil fuels and electrolysis of H_2O are not ideal due to several obvious shortcomings, e.g., the requirement of a huge energy input and costly precious metal-based catalysts, extremely low energy conversion efficiency, economic effects and availability (Armstrong et al. 2009). Moreover, there are also "biophotolysis" or "dark fermentation" of low-cost substrates to produce bio-H_2 from renewable resources, but these technologies regrettably have not reached industrial applications due to high production cost and low economic efficiency (Vijayaraghavan et al. 2006; Liao et al. 2012). Thus, the search and biosynthesis for alternative biocatalysts capable of cheap, efficient and stable H_2 production, inspired by nature could solve those problems mentioned above (Goff et al. 2009).

In nature, the most efficient bio-H_2 producers are hydrogenases, biotechnologically relevant metalloenzymes, that catalyze the reversible conversion of molecular H_2 into protons and electrons (Fontecilla-Camps et al. 2007). Nevertheless, due to the complex structure and maturation process of hydrogenases, their heterologous production has been a challenging task and their sensitivity to O_2, CO, etc has seriously hampered their potential applications (Friedrich et al. 2011; Fan et al. 2020). The O_2-tolerant [NiFe]-hydrogenases from *Ralstonia eutropha* (also known as *Cupriavidus necator*) are of particular interest as they maintain catalysis even in the presence of molecular O_2. Therefore, to meet the demands of scientific and applied research, the goal of this thesis is development of a bioprocess for heterologous

hydrogenase production in *Escherichia coli* by selecting a regulatory hydrogenase from *R. eutropha* as a model enzyme, from strain engineering, cultivation conditions and medium optimization to process improvement.

2. Scientific background

2.1. General background about hydrogenases

2.1.1. Hydrogenases for microbial biohydrogen production

In biological processes, hydrogenases capable of catalyzing the interconversion of H_2 and protons, are redox metallo-proteins. They are abundant in archaea, proteobacteria, actinobacteria, cyanobacteria and some photosynthetic microalgae (Vignais and Billoud 2007; Peters et al. 2011). In 1931, the first hydrogenase capable of oxidizing H_2 was described in a gram-negative bacillus (Stephenson and Stickland 1931). While the reversible hydrogenases catalyze both H_2 oxidation and production, uptake hydrogenases exclusively catalyze H_2 oxidation $H_2 \rightarrow 2H^+ + 2e^-$ (Benemann 1996). Both reactions are useful in microbes and catalyzed, but the direction depends on the presence of electron acceptors or donors. In the presence of electron acceptors and H_2 acting as an anergy source, H_2 oxidation proceeds, electrons of which is used to produce cellular reducing equivalents such as NADH and reduced ferredoxin (Wang et al. 2013). By contrast, H_2 production is often a by-product of formate metabolism and also a potential solar fuel in some photosynthetic organisms (Takács et al. 2008; Allakhverdiev et al. 2010; McDowall et al. 2014, 2015). Based on metal composition of the catalytic active center, hydrogenases are commonly classified into three phylogenetically distinct classes: the iron-sulfur-free [Fe]-, the [FeFe]- and the [NiFe]-hydrogenases (Vignais and Billoud 2007). Generally, [FeFe]-hydrogenases are more frequently involved in the production of H_2, whereas [NiFe]-hydrogenases are known to participate in the oxidation of H_2 (Frey 2002; Karyakin et al. 2005).

[Fe]-hydrogenases can only be found in some methanogenic archaea. Unlike the other two classes, they do not contain iron-sulfur clusters. The most widely studied [Fe]-hydrogenase is Hmd (**H**$_2$-forming **m**ethylene-tetrahydromethanopterin **d**ehydrogenase) from *Methanothermobacter marburgensis*. Hmd catalyzes the reversible, H_2-driven reduction of methenyl-H_4MPT$^+$ with H_2 to methylene-H_4MPT and H^+, an intermediate step during the reduction of CO_2 to methane (Fig 1.1A) (Huang et al. 2020). Hmd is a homodimer harboring a unique iron-guanylyl pyridinol (FeGP) cofactor at the active site that is typical for [Fe]-hydrogenases (Zirngibl et al. 1992). The FeGP cofactor contains a cysteine thiol, two CO, one acyl-carbon and one hybridized pyridinol nitrogen (Buurman et al. 2000; Korbas et al. 2006; Shima et al.

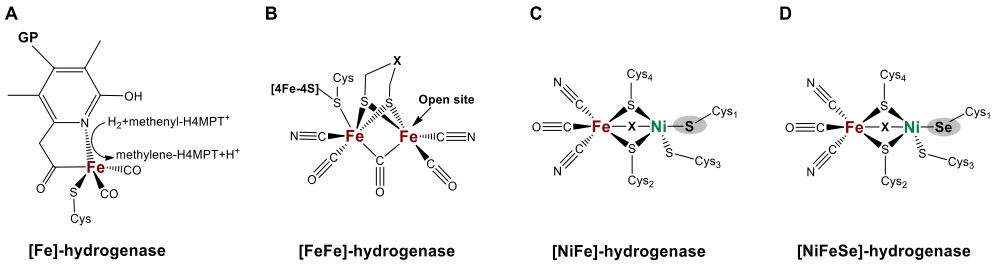

Figure 1.1 Structure of the catalytic centers of [Fe]-, [FeFe]- and [NiFe(Se)]-hydrogenase.
In the [FeFe]-hydrogenases, the distal Fe-atom, relative to the nearest [4Fe4S]-cluster, represents the H_2-binding site as well as the attack site for entry of the inhibitors like O_2 or CO ("open site"). The bridging ligand X might be NH/NH^{2+}, CH_2 or O for native or artificially matured [FeFe]-hydrogenases, while O, S, OH^--groups might be X in the oxidized form of [NiFeSe]-hydrogenases.

2008; Hiromoto et al. 2009; Schick et al. 2012). Hmd is extremely photosensitive and reversibly inhibited by CO and CN^-, but remains active in the presence of O_2 (Lyon et al. 2004a, 2004b; Shima et al. 2004; Shima and Thauer 2007).

[FeFe]-hydrogenases are widespread in strictly anaerobic bacteria (Peters et al. 2015), fungi, protists (Horner et al. 2002; van der Giezen et al. 2005), and in some unicellular green algae (Melis et al. 2004; Meyer 2007). Consequently, they are synthesized under strictly anoxic conditions (Vignais and Billoud 2007). Structurally, [FeFe]-hydrogenases occur as monomeric species, but hetero-dimeric, -trimeric and -tetrameric proteins are also known (Peters et al. 1998; Peters 1999; Vignais 2001; Nicolet et al. 2002). They possess a unique catalytic site, the so-called H-cluster (Ghirardi et al. 2007). Many of them also harbor additional iron-sulfur clusters (Peters et al. 1998). The H-cluster contains a di-iron [FeFe] sub-cluster, which is coordinated by carbonyl and cyanide ligands and connected to a [4Fe-4S] cluster via a bridging cysteine residue and a dithiolate bridging ligand between both Fe-atoms (Fig 1.1B) (Peters et al. 1998; Silakov et al. 2009; Mulder et al. 2011; Bortolus et al. 2018). The synthesis and insertion of the H-cluster into apo-[FeFe]-hydrogenase requires a number of maturation proteins (HydE, HydF and HydG) (Shepard et al. 2014; Caserta et al. 2017; Lampret et al. 2019). Sequence conservation in *Desulfovibrio desulfuricans* and *Clostridium pasteurianum* reveals a single hydrophobic channel for H_2 gas transport from the protein surface to the active center, but molecular dynamics show that H_2 can enter the enzyme interior through a variety of ways (Peters et al. 1998; Nicolet et al. 1999; Cohen et al. 2005; Fontecilla-Camps

et al. 2009). Under strictly anoxic conditions, [FeFe]-hydrogenases preferentially catalyze the production of H_2 at turnover rates two orders of magnitude higher than those of [NiFe]-hydrogenases ($2x10^4$ s^{-1}) (Frey 2002; Happe and Kaminski 2002; Friedrich et al. 2011). However, their catalytic center of the currently known [FeFe]-hydrogenases are generally extremely sensitive to irreversible inactivation by even trace O_2 or CO molecules, which extremely restricts their potential biotechnological applications.

[NiFe]-hydrogenases are the most diverse in structure, function and distribution of the three hydrogenase classes, and are mostly engaged in H_2 oxidation (Vignais and Colbeau 2004). They are found in bacteria and Archaea and characterized by lower specific activity in both H_2 uptake and production assays and more tolerant to O_2 and CO than [FeFe]-hydrogenases (Adams 1990; Vignais 2001; Frey 2002; Vignais and Colbeau 2004). Unlike [Fe]- and [FeFe]-hydrogenases, the minimal [NiFe]-hydrogenase is comprised of a core catalytic heterodimer having a large subunit (~60 kDa) harboring the [NiFe]-active center and a small electron-transferring subunit (~30 kDa) hosting one to three almost linearly arranged [FeS]-clusters with different compositions, which are termed the "proximal", "medial" and "distal cluster" according to their proximity to the active center (Lubitz et al. 2014). The unusual active center of [NiFe]-hydrogenases, the structure of which is remarkably conserved, consists of a Ni atom which is coordinated by the sulfurs of four cysteines, two of which are bridging to an Fe atom that is further coordinated by three non-protein diatomic ligands: one carbonyl (CO) and two cyanides (CN^-) (Fig 1.1C) (Bleijlevens et al. 2004; Fontecilla-Camps et al. 2007; Ohki et al. 2008). The bridging position between the Ni and Fe atoms is often occupied by oxygenic (OOH^- or OH^- in *Desulfovibrio vulgaris* Miyazaki F, *D. gigas* or *Allochromatium vinosum* [NiFe]-hydrogenase) or sulfenic species (S- or SH in *D. vulgaris*) in the oxidized inactive states, whereas in the some reduced active states it is replaced by a hydride (H^-) (Ohki et al. 2008; Lubitz et al. 2014; Volbeda et al. 2015). The [NiFeSe]-hydrogenases are a subgroup of the [NiFe]-hydrogenases with a selenocysteine residue coordinated to the active site Ni-center instead of a cysteine (Fig 1.1D). These [NiFeSe]-enzymes are found in sulfur-reducing bacteria like *Desulfomicrobium baculatum* and *D. vulgaris* (Valente et al. 2005; Baltazar et al. 2011). They are characterized by high H_2 productivity, lack of substantial inhibition of H_2 production by H_2 product, and higher O_2 tolerance due to a lower efficiency for O_2 permeation compared to standard [NiFe]-hydrogenases (Marques et al. 2010,

2017; Wombwell et al. 2015; Barbosa et al. 2020; Evans et al. 2021). As such, those advantageous properties make them more suited for H_2 production in biotechnological applications.

Since the core [NiFe]-active site is buried deeply in the center of the protein, the large subunit contains various hydrophobic gas channels connecting the buried [NiFe] center to the protein surface, which allow H_2 and other small molecules, such as O_2 or CO, to access the [NiFe] center (Fontecilla-Camps et al. 2007; Wang et al. 2011; Kalms et al. 2018). So far, the proposed proton transfer pathway from the [NiFe] center is still controversial (Sumner and Voth 2012; Abou-Hamdan et al. 2015; Evans et al. 2016; Ogata et al. 2016). Whilst [NiFe]-hydrogenases are reversibly inactivated by O_2, several enzymes can even catalyze H_2 conversion in the presence of O_2, thus they are referred to as "O_2-tolerant" hydrogenases (De Lacey et al. 2007; Lukey et al. 2011). This makes them of great interest for biotechnological applications, e.g., in biofuel cells (Vincent et al. 2005) or for H_2 production (Friedrich et al. 2011), as it is not necessary to make additional efforts to protect the production and operation process from the environmental O_2. Furthermore, the distance between [NiFe]-cofactor and proximal [FeS]-cluster is much larger than the respective distance in [FeFe]-hydrogenases, at 11 Å instead of 4 Å, respectively (Lubitz et al. 2014). The electrons produced by the heterolytic cleavage of H_2 in the active site are transferred via the [FeS]-clusters to the molecular surface and to the electron acceptors. This might contribute to almost 2 orders of magnitude lower activity observed in [NiFe]-hydrogenases than [FeFe]-hydrogenases, as more efficient electron delivery to the active site can be assured via the much shorter distance in [FeFe]-hydrogenases. After translation, it is necessary to insert Ni, Fe, CN, CO and other groups into the subunits for cofactor formation and their maturation systems are highly specific to structure of enzymes (Kalia et al. 2003; Vignais and Billoud 2007). Thus, all these factors make [NiFe]-hydrogenases extremely difficult to be efficiently processed into their mature form in heterologous hosts.

2.1.2. Potential biotechnological applications of hydrogenases

Over the last several decades, hydrogenases have been widely developed in a variety of potential biotechnological applications, including bio-H_2 production, biofuel cells, biosensors, wastewater treatment, prevention of microbial-induced corrosion, bioremediation, generation and regeneration of NADP cofactors (Mertens and Liese

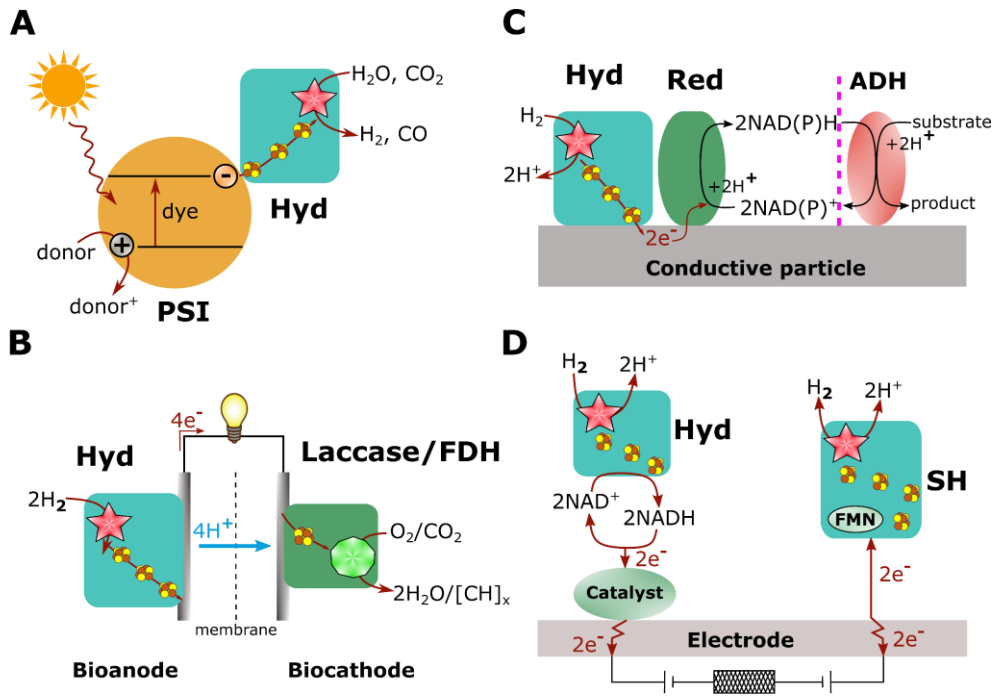

Figure 1.2 Potential biotechnological applications of hydrogenases.
(A) Light-driven biohydrogen production system consists of a PSI-hydrogenase hybrid complex. (B) Biofuel cell system based on a hydrogenase at the bioanode and a O_2/CO_2 reducing enzyme (e.g., laccase, bilirubin oxidase or formate dehydrogenase FDH for CO_2 reduction) at the biocathode. (C) H_2-driven NAD(P)H cofactor generation and regeneration recycling system. The carbon particles are modified with hydrogenase and the $NAD(P)^+$-reducing enzyme (e.g. FDH or glucose dehydrogenase GDH) moiety and extended to H_2-driven NAD(P)H supply for NAD(P)H-dependent enzymes, e.g. alcohol dehydrogenase (ADH) for highly selective H_2-driven ketone reduction. (D) Biosensors based on different electronic communication pathways between redox enzymes and conductive electrodes. Electrical communication using NAD^+/NADH cofactor re-oxidized and recycled electrocatalytically (exemplified with an enzyme oxidizing a substrate and reducing NAD^+ yielding NADH) (left), or via direct electron transfer from an enzyme active center to an electrode (exemplified with an enzyme oxidizing a substrate and generating anodic current at an electrode) (right). PSI: photosystem I; FDH: formate dehydrogenase; Red: $NAD(P)^+$ reductase; ADH: NAD(P)H-dependent alcohol dehydrogenase.

2004; Jugder et al. 2013). For bio-H_2 production (Fig 1.2A), one promising method has been demonstrated by integrating O_2-tolerant hydrogenases, e.g., *Ralstonia eutropha* membrane-bound [NiFe]-hydrogenase or *Clostridium acetobutylicum* [FeFe]-hydrogenase into the process of direct biophotolysis via *Synechocystis* sp. PCC6803 photosystem I (PSI) (Ihara et al. 2006;

Krassen et al. 2009; Lubner et al. 2010a, 2010b; Schwarze et al. 2010). Here, the redox potential of the terminal [FeS]-cluster of PSI-complex is used for direct proton reduction without the intermediate NAD(P)H. However, coupling of PSII, i.e., the H_2O splitting system, has yet to be established for photosynthetic H_2 production *in vitro* (Mersch et al. 2015; Teodor et al. 2020). Even though with high turnover numbers, *in vitro* systems render to cease their activity quickly and are generally short lived (1.5-4 h) as metabolic processes that support self-repair and maintenance are missing (Utschig et al. 2015). To overcome these obstaches, a recombinant *in vivo* system that generates H_2 using a hydrogenase enzyme directly coupled to a cyanobacterial photosystem, has been more recently developed (Appel et al. 2020; Kanygin et al. 2020; Lupacchini et al. 2021). Research on this recombinant system is now ongoing to improve the efficiency of sunlight-driven H_2 production from H_2O (Krishnan et al. 2018; Lenz 2020).

Apart from H_2 production, recent reports utilized the H_2 uptake activity of [NiFe]-hydrogenases from *R. eutropha* H16, *R. metallidurans* CH34, *Thiocapsa roseopersicina*, *Escherichia coli*, *D. gigas* and *D. vulgaris*, or [FeFe]-hydrogenases from *D. desulfuricans* to design enzymatic biofuel cells used for electricity generation (Fig 1.2B) (Karyakin et al. 2005; Vincent et al. 2005, 2006; Wait et al. 2010; Szczesny et al. 2020). Hydrogenases have several advantages over traditional platinum catalysts including bioavailability, biodegradability, very high turnover rates ($\sim 10^4$ s^{-1}), high selectivity toward H_2 and lower susceptibility to be poisoned by impurities, such as CO and H_2S, commonly present as contaminants of industrial H_2 gas (Vincent et al. 2007; Cracknell et al. 2008a, 2008b). Overall, approaches using [NiFe]-hydrogenases, e.g. MBH, as an anode catalyst and enzymatic oxidizing agents, e.g. laccase or biluribin/glucose oxidase on the cathode, allow operation of fuel cells at much more favorable moderate conditions, e.g., neutral pH, ambient temperatures (Ikeda and Kano 2001; Morozov et al. 2002; Vincent et al. 2005; Ruff et al. 2018). Additionally, electrochemical groups attempt to estabilish a H_2-driven CO_2 reduction hybrid system by coupling hydrogenases and CO_2 reductases, e.g., formate dehydrogenase (Ceccaldi et al. 2017; Ahmed et al. 2020; Goyal et al. 2020). This system is capable of converting CO_2 obtained from the air into more oxygen-poor and valuable hydrocarbon chemicals or fuels. Therefore, the hydrogenases as an alternative to platinum are one of the most promising bioelectrocatalysts in enzyme-driven biofuel cells.

Another possible application of interest is the use of redox enzymes such as dehydrogenases in the enzymatic generation and regeneration of cofactors (Tishkov and Popov 2006; Weckbecker et al. 2010). These cofactors are mostly NAD(H) and NADP(H), but their stoichiometric addition in industrial synthesis is not economical due to the low stability and high cost (Uppada et al. 2014). During synthesis, the reduced form NADH serves as a carrier of a hydride, producing oxidized NAD^+. In order to reduce the NAD^+ again, an effective and stable regeneration system is required. The use of a hydrogenase, for example, the soluble hydrogenases of *Pyrococcus furiosus* (SHI), *R. eutropha* (SH), *E. coli* (Hyd-2), in such a regeneration system offers efficient production. Regeneration of the reducing agents using inexpensive molecular H_2 generates no by-products other than protons (Ratzka et al. 2012; Reeve et al. 2015, 2017; Preissler et al. 2020). Recently, there is growing interest in harnessing the selectivity of NADH-dependent redox enzymes *in vitro* for fine chemical synthesis, in particular for hydrogenation and dehydrogenation reactions. One established H_2-driven particle system for regeneration of NADH-dependent biocatalysis has been developed (Fig 1.2C): Electrons from H_2 oxidation by a hydrogenase are transferred into an electronically conductive particle and subsequently used by an NAD^+ reductase for selective NAD^+ reduction to supply NADH to a co-immobilized NADH-dependent carbonyl reductase, e.g. alcohol dehydrogenase, for reduction of a ketone, e.g acetophenone (Reeve et al. 2017). Here, both atoms of H_2 are incorporated into the product, e.g., phenylethanol, to allow a 100% atom-efficient chemical synthesis without unwanted byproducts. Thus, this approach has a great positive impact on the economic and environmental viability of such enzyme cascade reactions.

Furthermore, another application using the H_2 oxidizing activity of hydrogenases is to develop biosensors (Lutz et al. 2005; Vincent et al. 2006). In biosensors based on direct electron transfer in redox proteins, efficient electron-transfer pathways between the immobilized redox protein and the electrode surface have to be established to allow a fast electron transfer and concomitantly avoiding free-diffusing redox species (Fig 1.2D) (Wu and Hu 2007; Bollella and Katz 2020). The enzyme can be potentially modified as film on various electrode surfaces using protein film voltammetry and rotating disc pyrolytic graphite “edge” electrode techniques (Jones et al. 2003; Léger et al. 2003; Mertens and Liese 2004). By increasing understanding of hydrogenases, they also have a potential biotechnological application in bioremediation of environments polluted by toxic heavy metals, as developed for the conversion of toxic

Cr(VI) to more reduced, less toxic Cr(III) by the [NiFe]-hydrogenase of the sulfur-reducing *D. vulgaris* (Goulhen et al. 2006).

However, at present those biotechnological applications of hydrogenases are still unfeasible for industrial purposes (Vincent et al. 2005; Schwarze et al. 2010; Atomi et al. 2011; Kim et al. 2011). There are large amounts of factors contributing to this point: (i) Most of these enzymes are sensitive to O_2, CO and (ii) unstable to wide range of pH and temperature in the fuel cell surrounding; (iii) Hydrogenases for potential use are not produced largely in their native hosts, and (iv) difficult to be recombinantly expressed in large quantities in heterologous hosts due to the complex enzyme structure and maturation process (Kalia et al. 2003; Vignais and Billoud 2007). Among those limitations, investigations and improvements of those biotechnological applications are still on-going. Furthermore, ever since the hydrogenase maturation pathways has been deciphered, numerous approaches for the recombinant production of hydrogenases using *in vivo* heterologous as well as *in vitro* maturation systems are realized (Fan et al. 2020). The availability of a number of different hydrogenases enables a deep understanding of their catalytic mechanisms, thereby laying the groundword for their biotechnological applications. Extremely low yields of active *in vivo*/ *in vitro* maturated hydrogenases greatly hindered the understanding of microbial hydrogenases and relevant potential applications, thus development of bioprocess for high-yield production of hydrogenases using an industrial robust cell factory, e.g., *E. coli* might be a solution at the moment.

2.1.3. Classification of [NiFe]-hydrogenases

[NiFe]-hydrogenases are the most divergently evolved enzymes among [Fe]-, [FeFe]-, and [NiFe]-hydrogenases in terms of higher specificity and unique or complex function. For a variety of reasons, the [NiFe]-hydrogenases are also of particular interest for a number of biotechnological applications. They have been characterized in a diverse range of physiological roles across species (Greening et al. 2015). According to their physiological function, composition and localization in the organism, [NiFe]-hydrogenases have so far been categorized into four groups: (1) Membrane-bound H_2-uptake hydrogenases; (2) Cyanobacterial uptake and H_2-sensing hydrogenases; (3) Bidirectional heteromultimeric cytoplasmic hydrogenases; (4) Membrane-associated energy-conserving and H_2-producing hydrogenases (Vignais and Billoud 2007; Constant et al. 2011; Greening et al. 2016). The function, features

of these groups and the commonly used genes based on the complete sequences of the small and subunits are summerized in the Table 1.1.

Table 1.1 Characterization of [NiFe]-hydrogenases and the genes commonly used based on the small and large subunits.

Group	Function	Features	Common genes
1	Membrane-bound H_2-uptake	- H_2-oxidation coupled with quinone reduction - Activity associated with cytochrome *b* or *c* complex	Bacteria: *hupSL, hydAB, hupAB, hyaAB, hoxKG, mbhSL, hybOC, hynSL, hysAB,* Archaea: *vhtGA, vhoGA*
2a	Cyanobacterial uptake	- Cytoplasmic - Aerobic respiration and recycling H_2	Bacteria: *hupSL, mbhSL*
2b	H_2-sensor	- H_2-sensing - Regulation of expression of uptake hydrogenases - O_2-tolerant - Low activity	Bacteria: *hupUV, hoxBC*
3a	F_{420}-reduction	- Bidirectional activity - Found in hyperthermophilic Archaea, methanogens	Archaea: *frhAG, fruAG, frcAG*
3b	Bifunctional NADP-linked		Bacteria: *hydDA, shyDA,* hyjSL Archaea: *hyhSL, hydDA, hyd$^{\delta a}$*
3c	Methyl-viologen-reduction		Archaea: *mvhGA, vhcGA, vhuGA, mvhSL*
3d	Bidirectional NAD(P)-linked		Bacteria: *hoxYH*
4	Membrane-bound energy conserving, H_2-production	- H_2-production coupled with CO, formate or acetate oxidation	Bacteria: *hyfIG, hycGE, cooLH, echFE* Archaea: *echFE, ehaNO, ehbMN*

2.1.4. [NiFe]-hydrogenases from *Escherichia coli*

E. coli is capable of producing four distinct [NiFe]-hydrogenases, Hyd-1 to Hyd-4, with different subunit compositions. All of them are known or predicted to be anchored to the inner membrane (Fig 1.3) exhibiting hydrogenase activity under physiological conditions (Sawers et al. 1985; Sargent 2016).

Hyd-1 is encoded by the *hyaABCDEF* operon (Fig 1.3A) (Menon et al. 1991). The *hyaABC* genes encode the structural components of Hyd-1, whereas the *hyaDEF* encoded proteins are required for the proper assembly of the enzyme. The large

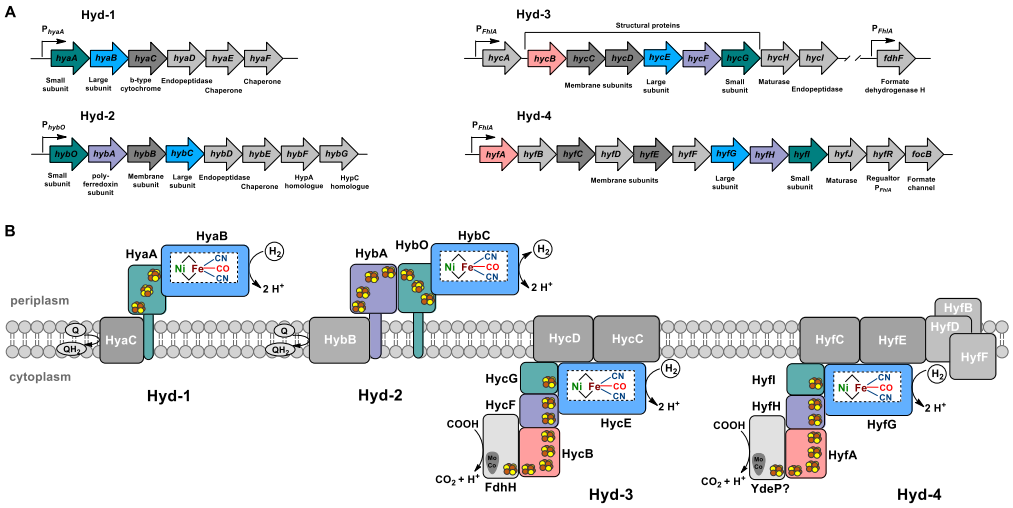

Figure 1.3 The genes (A) encoding four [NiFe]-hydrogenases of *E. coli* and structural composition (B).

The *hyaABC* genes encode the structural components of Hyd-1, whereas *hyaDEF* encode accessory proteins involved in enzyme assembly. The *hybOABC* genes encode the structural components of Hyd-2, whilst *hybDEFG* encode accessory proteins involved in enzyme assembly. The *hycBCDEFG* genes encode the structural components of Hyd-3, whilst *hycAHI* are accessory genes involved in both gene transcription and enzyme assembly. Together with formate dehydrogenase H encoded by *fdhF* located elsewhere in the genome, the formate hydrogenase lyase (FHL) complex is formed. The *hyfAGHI* genes encode the structural components of Hyd-4 soluble domains, whilst *hyfBCDEF* encode the Hyd-4 membrane domains, and *hyfJR* are accessory genes involved in gene regulation and enzyme assembly. The *focB* is a gene encoding a putative formate channel related to FocA. MoCo is molybdo-selenium cofactor. Q/QH_2: quinone/reduction of quinone.

subunit HyaB contains the [NiFe]-active site, while the small subunit HyaA hosts a C-terminal transmembrane helix anchor and three [FeS]-clusters, a proximal [4Fe-3S], a medial [3Fe-4S] and a distal [4Fe-4S] (Lukey et al. 2010; Volbeda et al. 2012). Hyd-1 is produced under anaerobic conditions. It belongs to the [NiFe]-hydrogense Group 1d, which is characterized by tolerance to O_2 attack (Lukey et al. 2010; Greening et al. 2016; Sargent 2016). Hyd-1 is co-expressed with a cytochrome oxidase HyaC, whose physiological role is mainly proposed as aerobic shock protection as soon as O_2 is encountered (Volbeda et al. 2013). More recent studies revealed native *E. coli* Hyd-1 is a dimer of a heterotrimer $(HyaABC)_2$, showing H_2-oxidizing activity (Lukey et al. 2010; Volbeda et al. 2012).

Hyd-2 is encoded by the *hybOABCDEFG* operon (Fig 1.3A) and belongs to the [NiFe]-hydrogenase group 1c. It is produced under anaerobic respiration with glycerol and fumarate, which allows H_2 to be used as an electron donor for fumarate reduction (Ballantine and Boxer 1985; Menon et al. 1994; Pinske et al. 2015a; Sargent 2016). As for Hyd-1, expression of Hyd-2 correlates with an increase in levels of FNR activation, the FNR-dependent expression of the *hyp* maturation proteins and *nik* nickel transporter operons (Sawers et al. 1985; Messenger and Green 2003). The expression of *hya* and *hyb* operons is inhibited under aerobic conditions by IscR, that is the negative transcriptional regulator of [FeS]-cluster biosynthesis (Sawers et al. 1985; Richard et al. 1999; Giel et al. 2006; Nesbit et al. 2009). Hyd-2 is characterized as a standard O_2-sensitive [NiFe]-hydrogenase that predicted carries a [4Fe4S]-cluster at the proximal position of the small subunit HybO (Richard et al. 1999; Lukey et al. 2010). Unlike Hyd-1, Hyd-2 has bidirectional catalytic activity and can oxidize or produce H_2 with high efficiency (Armstrong and Hirst 2011; Pinske et al. 2015a).

Hyd-3 is part of the H_2-evolving formate hydrogenlyase complex (FHL) that is produced under anerobic fermentative conditions and required for disproportionation of formate to CO_2 and H_2, consequently protecting the cell from acidic pH (Sawers et al. 1985; Sawers 2005; McDowall et al. 2014; Sargent 2016). Hyd-3 is encoded by the *hycABCDEFGHI* operon (Fig 1.3A) and a member of the group 4a of [NiFe]-hydrogenases dedicated to the majority of H_2 evolution in *E. coli* (Greening et al. 2016). More recently, FHL has been shown to be capable of unidirectional H_2-evolving activity under physiological conditions, even at high H_2 and CO_2 concentrations at an alkaline pH conditions (Pinske and Sawers 2016). Thus, these desirable features, coupled with the fact that FHL is by far the predominant H_2 production pathway in *E. coli*, make Hyd-3 a particularly important enzyme for bio-H_2 production in research and industrial scale.

The putative Hyd-4 is encoded by the *hyfABCDEFGHIJRfocB* operon which is similar to Hyd-3 in terms of complex architecture and sequence homology (82% similarity of HyfG and HycE, 73% similarity of HyfI and HycG) (Andrews et al. 1997). As for Hyd-3, in generation of a putative second FHL complex, termed FHL-2, the Hyd-4 might either associate with formate dehydrogenase or the FdhF homologue YdeP (Fig 1.3B) (Sargent 2016). So far, together with the poor levels of transcription normally observed, the ability to clearly demonstrate Hyd-4 activity in *E. coli* proved to be a

challenge, suggesting this is a silent cryptic operon without physiological or biochemical activity (Sargent 2016).

2.1.5. [NiFe]-hydrogenases from *Ralstonia eutropha* H16

The β-proteobacterium *Ralstonia eutropha* H16 (also *Cupriavidus necator*) is capable of growing at the boundary between aerobic and anaerobic conditions, as well as in heterotrophy and autotrophy. Under autotrophic conditions, the use of H_2 as the sole energy source is enabled by four different O_2-tolerant [NiFe]-hydrogenases: membrane-bound hydrogenase (MBH), soluble NAD+-reducing hydrogenase (SH), regulatory hydrogenase (RH) and actinobacterial hydrogenase (AH) (Fig 1.4), all of which are encoded on the megaplasmid pHG1 (Tran-Betcke et al. 1990; Lenz and Friedrich 1998; Bernhard et al. 2001; Schwartz et al. 2003).

The MBH is categorized to a group of the H_2-uptake [NiFe]-hydrogenases and anchored to the membrane via a membrane-integral cytochrome b (HoxZ), thereby facing the periplasm (Kortluke et al. 1992; Bernhard et al. 1997; Radu et al. 2014). Electrons from H_2 cleavage are transferred directly via the cytochrome and quinol pool into the electron transport chain (Fritsch et al. 2013). At this end, O_2 is reduced and the proton gradient built up in parallel at the membrane during electron transport is used for ATP synthesis (Schink and Schlegel 1979; Walker 2013). The large subunit HoxG containing the active site is analogous to standard [NiFe]-hydrogenases coordinated by two CN and one CO ligands, whilst the small subunit HoxK is occupied by a chain of three [FeS]-clusters (proximal [4Fe3S]-, medial [3Fe4S]-, distal [4Fe4S]-cluster) which are spaced about 10 Å apart, thus forming a electron transfer pathway (Saggu et al. 2010). While the medial [3Fe4S]-cluster is paramagnetic, the distal [4Fe4S]-cluster is cubic as observed in the standard [NiFe]-hydrogenases and usually diamagnetic in the oxidized state with EPR-silent signal (Saggu et al. 2009, 2010).

The SH, located in the cytoplasm of the cell, catalyzes H_2 cleavage to release electrons directly used for NAD^+ reduction, thus supplying the cell with the reduction equivalent NADH. It is categorized to group 3d of the bidirectional [NiFe]-hydrogenases. The SH consists mainly of an NAD^+ reductase heterodimer HoxFU, which contains [FeS]-clusters including [2Fe2S]-cluster, FMN-b (flavin mononucleotide), and a heterodimer of the small and large subunits HoxHY harboring

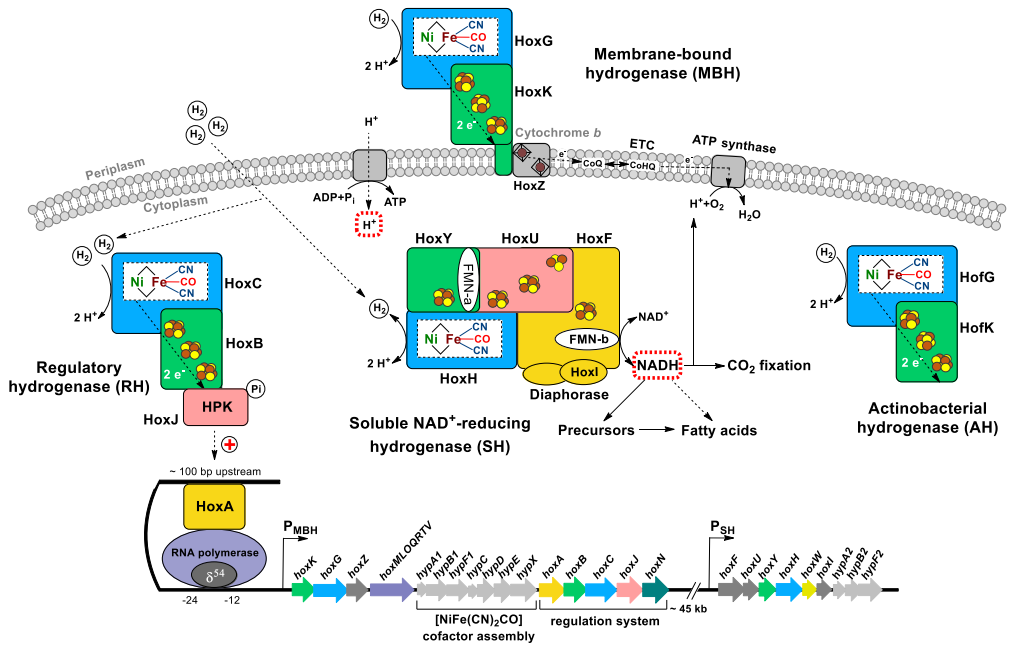

Figure 1.4 [NiFe]-hydrogenases from *R. eutropha* H16.
Subunit composition, cofactors and cellular location of those hydrogenases (top), and RH-mediated regulation of gene expression as well as gene clusters encoding MBH, RH and SH in the megaplasimd pHG1 (bottom) are depicted.

the catalytic active [NiFe]-center, the proximal [4Fe4S]-cluster and FMN-a (Schneider and Schlegel 1976; Burgdorf et al. 2005).

The RH is a dimer of the heterodimer of the small and large subunits $(HoxBC)_2$. Spectroscopic studies reveal that the RH harbors a standard-like $[NiFe(CN)_2CO]$ active site with one CO and two CN ligands on HoxC and three canonical [4Fe4S]-clusters on HoxB (Pierik et al. 1998; Kleihues et al. 2000; Buhrke et al. 2001). It is coupled with the homotetrameric histidine kinase HoxJ that communicates with the DNA-binding protein HoxA constituting a two-component regulatory system (Lenz et al. 2002; Buhrke et al. 2004; Friedrich et al. 2005). The RH recognizes H_2 in the environment and transmits the signal to a response regulator, which in turn control transcription of the energy-converting MBH and SH operons (Fig 1.5). HoxJ phosphorylates itself in an autocatalytic reaction and subsequently transfer of the phosphate group to the cognate response regulator HoxA can take place. Unlike "conventional" two-component regulatory systems (Fig 1.5A), however, phosphorylation of HoxA has a negative effect on transcription of the hydrogenase

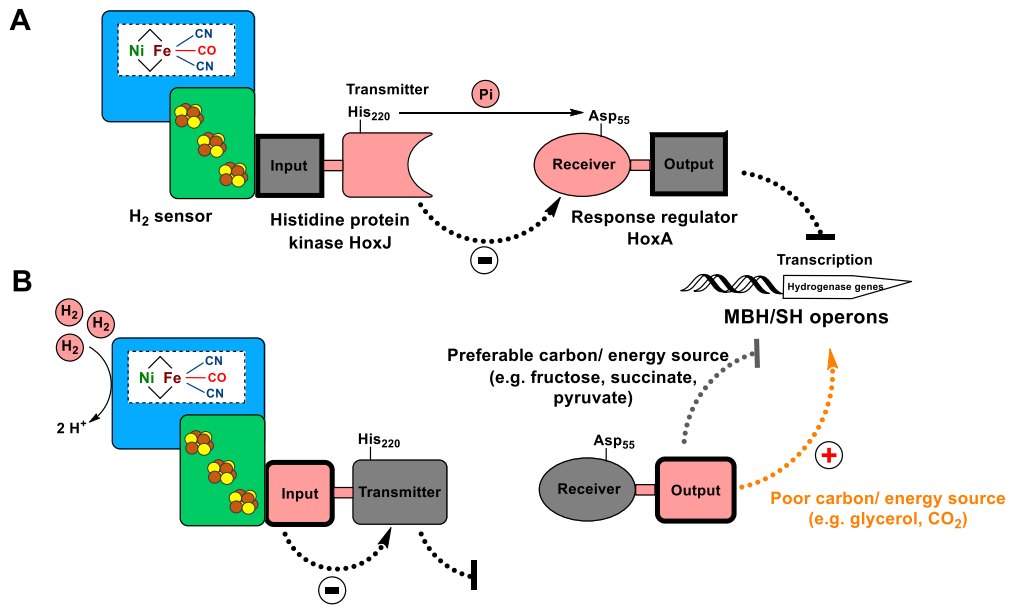

Figure 1.5 Proposed regulation process of hydrogenase gene expression in *R. eutropha*.
(A) In the absence of H_2, the kinase HoxJ plays a negative effect on hydrogenase gene expression by transferring a phosphoryl group to the response regulator HoxA. (B) In the presence of H_2, transferring the phosphoryl group from HoxJ to HoxA is blocked by the H_2-sensing RH that inhibits kinase activity of HoxJ and unphosphorylated HoxA functions as a transcription activator. In addition, the level of hydrogenase gene expression also directly correlates with the quality of nutrients (grey & orange dashed arrows). Domains that are responsible for the biological response of the system under the respective conditions are shown in pink. The solid arrow symbolizes the phosphotransfer reaction, while bold dashed arrows indicate positive (+) or negative (-) control.

genes (Lenz et al. 1997; Lenz and Friedrich 1998). In the absence of H_2, HoxJ mediates phosphotransfer to HoxA, rendering it inactive (Burgdorf et al. 2005). When H_2 molecules enter the cell, they react with the RH, unleashing a specific interaction of currently unknown nature between it and HoxJ. The latter interaction may involve the transfer of electrons between the RH and the PAS domain in the input module of HoxJ (Buhrke et al. 2004). Thus, the RH blocks the phosphoryl transfer from HoxJ to HoxA and ultimately is a positive regulator on H_2-dependent transcription (Fig 1.5B). Furthermore, it has been proposed that the reduction of the HoxB [FeS]-clusters somehow causes a conformational change in the RH-HoxJ complex, which affects the phosphorylation activity of HoxJ (Buhrke et al. 2005b).

Interestingly, the signal transduction pathway is cryptic in *R. eutropha* grown in the natural habitat, as control of hydrogenase expression is exerted by additional carbon and energy sources (Lenz et al. 1997). Monitoring hydrogenase gene expression in the presence of both H_2 and organic substrates reveals a significant correlation between substrate quality and expression levels: Expression is high when poor substrates like glycerol or CO_2, are available in addition to H_2, while expression declines when preferentially used nutrients, such as pyruvate, succinate or fructose, are present (Fig 1.5B). This global carbon catabolite control is superimposed onto the H_2-responsive signaling and also indicates that energy deficiency is a key driver for the induction of hydrogenase expression in *R. eutropha* (Friedrich et al. 1981; Friedrich 1982; Schwartz et al. 2013; Jugder et al. 2015). In this case, the substrate quality is judged by the corresponding growth rate, however, the underlying regulatory mechanism is still unknown. Moreover, unlike the most [NiFe]-hydrogenases, maturation of RH does not require a proteolytic cleavage of the C-terminal peptide from the large subunit HoxC (Lenz and Friedrich 1998; Kleihues et al. 2000). The small subunit HoxB lacks both a signal peptide for membrane translocation and a C-terminal hydrophobic domain that normally anchors the protein to the membrane, indicating a cytoplasmic location for H_2-sensors (Menon et al. 1990; Bernhard et al. 1997; Gross et al. 1999). Instead of a hydrophobic domain, HoxB carries a conserved peptide that is essential for the formation of a double dimer $(HoxBC)_2$ and its interaction with the histidine kinase HoxJ (Kleihues et al. 2000; Buhrke et al. 2004). Taken together, these features make RH the simplest [NiFe]-hydrogenases in case of maturation process.

The fourth hydrogenase AH, which has similarity to the [NiFe]-hydrogenases common in actinobacteria, has been recently assigned to group 1h of the [NiFe]-hydrogenases (Greening et al. 2016). It displays remarkable features with high tolerance to O_2, pH and temperature, which allow the organism to support basic metabolism especially in resting cells under challenging conditions like starvation and stress (Constant et al. 2010; Schäfer et al. 2016). Like group 1 “standard” hydrogenases, the AH consists of a large subunit harboring the catalytic center and a small subunit that presumably contains three [FeS]-clusters, but its H_2-oxidizing activity is three orders of magnitude lower than the activities of the energy-conserving group 1 hydrogenases (Schäfer et al. 2013). The SH composition resembles the cofactor content of the RH, however, the proximal [4Fe4S]-cluster in the AH seems to be ligated by three cysteine residues and one aspartate in contrast to that of the RH

coordinated by four cysteine residues. Furthermore, the shape of the gas channel in the AH seems to be rather standard-like compared to the situation in the RH (Lenz et al. 2015; Schäfer et al. 2016). Thus, the electron-withdrawing effect of the aspartate-derived carboxyl-O_2 may have the ability to increase the potential of this specific proximal [4Fe4S]-cluster, consequently conferring O_2-tolerance of AH, which remains to be elucidated.

2.1.6. Proposed catalytic cycling of [NiFe]-hydrogenases

The [NiFe]-center undergoes several redox states during reactivation and catalysis, which can be well studied using protein crystallography, electrochemistry, EPR (Electron paramagnetic resonance) and IR spectroscopy (Fontecilla-Camps et al. 2007; Vincent et al. 2007; Lubitz et al. 2014). These redox states of the [NiFe]-center can be divided into two groups of EPR-inactive Ni(II) silent and EPR-active Ni(III) detectable states (Fig 1.6). So far, the H_2-catalytic clycing of [NiFe]-hydrogenases is proposed to include four redox species: active Ni_a-S, Ni_a-SR, Ni_a-C and Ni_a-L states (Fig 1.7). Firstly, cleavage of H_2 leads to the transition of the oxidized Ni_a-S to the fully reduced Ni_a-SR state. Secondly, Ni_a-C is produced by one-electron oxidation of Ni_a-SR and then oxidized to restore protonation of the protein fold resulting in the formation of Ni_a-L state. Finally, one-eletron oxidation of Ni_a-L restores Ni_a-S, accompanied by the release of a proton from the protein (Lill and Siegbahn 2009; Ogata et al. 2009; Pandelia et al. 2010; Ash et al. 2017; Tai et al. 2018, 2019). Since spectral signals from the active site are usually otherwise superimposed by [FeS]-cluster-derived bands, recent studies approached to investigate the [FeS]-cluster-free HoxC, showing two additional resting intermediates (Ni_r-SI and Ni_r-SII) at low-temperature IR (Caserta et al. 2020a, 2021). Upon addition of the small subunit HoxB *in vitro*, the HoxBC complex is formed, which possesses the typical catalytic active states similar to the native RH (Caserta et al. 2020b).

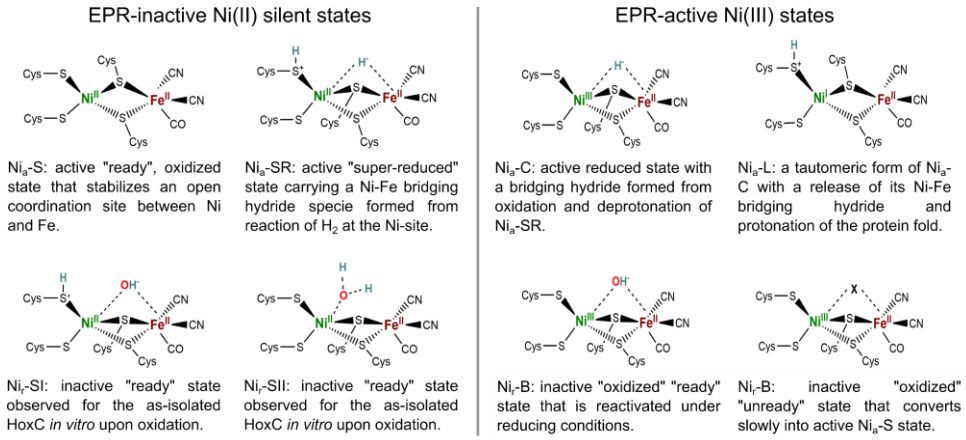

Figure 1.6 Intermediates of the [NiFe]-cofactor upon exposure to the H_2 or O_2.
During H_2 conversion at the active site, the iron atom remains in a Fe(II) "low spin" configuration, whereas the nickel atom is redox active species with the active states Ni(II), Ni(III) and presumably Ni(I) in response to treatment of the enzymes with natural or artificial oxidants/reductants. The bridging ligand X of the Ni$_u$-A is still unknown, which is most likely OOH^- or OH^- species.

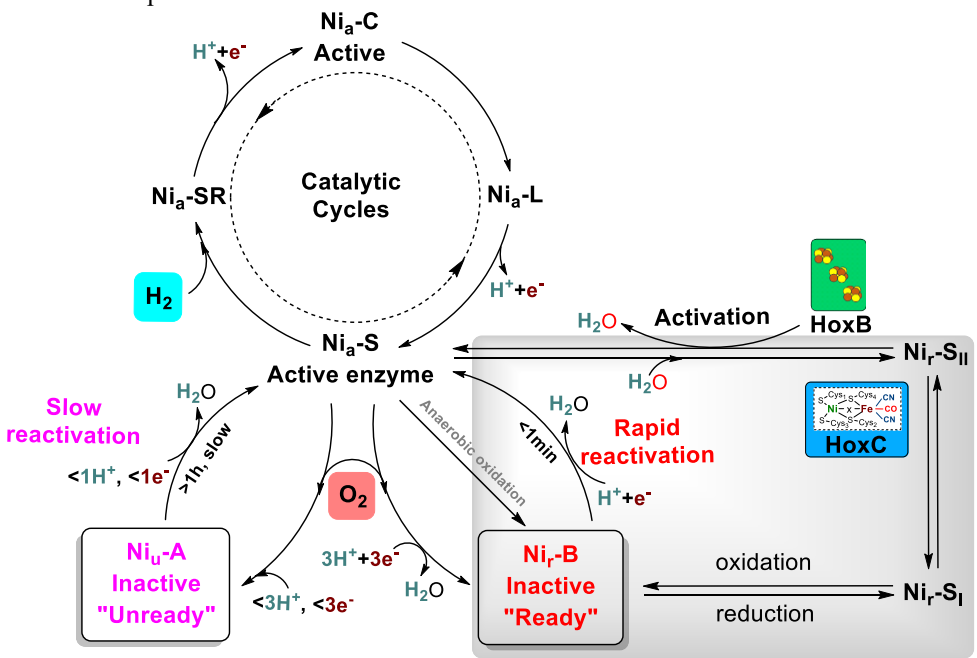

Figure 1.7 The proposed general catalytic cycles and oxidative inactivation of the active site of [NiFe]-hydrogenases as well as additional states of HoxC.
Catalytic intermediates Ni$_a$-S, Ni$_a$-SR, Ni$_a$-C and Ni$_a$-L of the active site constitute for the H_2-uptake/evolution reactions (top cycle), The inactivation and reactivation of the active center is based on the availability of the electrons (bottom cycels). While the inactive "ready" Ni$_r$-B state can be reactivated rapidly under reducing conditions, more time is required for reactivation of the inactive "unready" Ni$_u$-A state. The grey box comprises the interconvertible states (Ni$_r$-SI, Ni$_r$-SII) observed for the as-isolated HoxC (blue) and upon addition of HoxB (green), active state Ni$_a$-S is restored *in vitro*.

2.1.7. O_2-tolerance of [NiFe]-hydrogenases

While O_2 binds to the active site of an [NiFe]-hydrogenase, it does not induce irreversible degradation of the enzyme, at least for those so-called O_2-tolerant hydrogenases which can resume function in a far shorter time (within minutes). Instead, O_2 is quickly reduced into a H_2O molecule using three protons and electrons. Thus, a hydroxyl group is bridged to the Ni and Fe at the active site, and then removed by consumption of a set of proton and electron forming another H_2O molecule (Fig 1.7) (Goris et al. 2011; Wulff et al. 2016). Exposure to O_2 usually results in formation of inactive "super-oxidized" states: Ni_u-A and Ni_r-B, which can be reactivated by reduction with different reaction kinetics (Fig 1.7) (Ogata et al. 2005; Lubitz et al. 2014). The Ni_u-A state is differentiated from the Ni_r-B state on the basis of slower reaction kinetics for reactivation (Lamle et al. 2004; Vincent et al. 2007). Hydrogenases that do not form Ni_u-A and maintain catalytic activity under aerobic conditions, are characterized as O_2-tolerant hydrogenases (Volbeda et al. 2005; Pandelia et al. 2010; Saggu et al. 2010; Fritsch et al. 2013). Compared to the proximal [4Fe4S](Cys)$_4$-cluster of standard O_2-sensitive [NiFe]-hydrogenases, an unusual [4Fe3S] proximal cluster that was observed in O_2-tolerant [NiFe]-hydrogenases, e.g., *E. coli* Hyd-1, *R. eutropha* MBH and *H. marinus* MBH, plays a crucial role in the O_2-tolerance of those enzymes. In this case, owing to having an extra hyper-oxidized state of this unique [FeS]-cluster, two successive electrons can be rapidly provided to the active site for O_2 reduction into harmless H_2O. Another molecular mechanism proposed also involves the proximal [FeS]-cluster, where the significant coordination rearrangement occurs in the [NiFe] center to shield it from O_2. Those two insights have presented new functions of the proximal [FeS]-cluster not only as a component of the electron transfer unit, but also as the redox regulator that protects the [NiFe] center from O_2 damage (Cracknell et al. 2009; Ogata et al. 2009; Fritsch et al. 2011; Shomura et al. 2011; Roessler et al. 2012; Flanagan and Parkin 2016; Shomura 2019). These results have prompted researchers to mutate amino acids around proximal [FeS]-cluster to further improve O_2-tolerance and thus broaden their applications (Mouesca et al. 2013; Volbeda et al. 2015, 2018). Even through, the differences in kenetic activation between Ni_u-A and Ni_r-B on the structural level remain elusive. As such, the corresponding molecular mechanism is yet unclear.

In the *R. eutropha* SH, these extra cysteines are not present. The SH is maintained in inactive state during aerobic purification, but can be reactivated under NAD^+-linked

aerobic conditions to generate NADH. The low redox potential obtained by coupling with the NAD^+/NADH pool is proposed to largely prevent the inactivation by O_2 exposure under physiological conditions. This is attributed to the selectively releasable cofactor FMN-a bound to HoxY (Schneider and Schlegel 1976; Van Der Linden et al. 2004; Lauterbach et al. 2011a, 2011b, 2013; Lauterbach and Lenz 2013). Furthermore, a previous model proposed the presence of an additional cyanide ligand coordinated to the Ni and Fe in *R. eutropha* SH that are claimed to sterically prevent O_2 attack, however, this has been recently disproven (Happe et al. 2000; Bleijlevens et al. 2004; Van Der Linden et al. 2004; Horch et al. 2010; Lauterbach et al. 2011a). SH has been experimentally shown to exhibit oxidase activity in addition to hydrogenase activity, by which oxygen is catalytically detoxified with intermediate formation of cysteine sulfenates. A comparison of the conversion rates for H_2 and O_2 reveals that in the presence of 40% O_2, up to 3% of the electrons generated by H_2 oxidation serve as "protection" and are reused for O_2 reduction (Lauterbach and Lenz 2013; Horch et al. 2015). Hence, the occurrence of two catalytic activities, H_2 conversion and O_2 reduction, at the same time cofactor of SH may inspire the design of novel biomimetic catalysts performing H_2-conversion even in the presence of O_2.

A different adaptation to confer O_2-tolerance of RH in *R. eutropha* (HoxBC) and *Rhodobacte capsulatus* (HupUV) is the modification of the gas channels connecting the active site and the large subunit protein surface. The presence of relatively large hydrophobic amino acid residues as side-chains contributes to the steric hindrance of movement of larger molecules, e.g., O_2 and CO, but not H_2 towards the active site (Buhrke et al. 2005a; Duché et al. 2005; Volbeda et al. 2005). The replacement of the relatively large phenylalanine and isoleucine residues of RHs of *R. eutropha* and *Rh. capsulatus* with the smaller valine and leucine, which are found at the same positions in the O_2-sensitive [NiFe]-hydrogenase from *D. gigas*, results in RHs that are sensitive and inhibited by O_2 and CO (Buhrke et al. 2005a; Duché et al. 2005). In contrast, O_2 diffusion to the active site has been reduced by replacement of valine and leucine with residues containing larger side-chains or with higher polarity in the normal O_2-sensitive [NiFe]-hydrogenase of *D. fructosovorans*, thus gaining greater O_2-tolerance. Moreover, O_2-tolerance has been enhanced by replacing two methionine residues, which allow inactivating slower and reactivating quicker on O_2 exposure (Liebgott et al. 2011). When the [NiFe]-active center of RH is exposed to O_2 or CO, its interaction with the active site results in the loss of activity of RH. However, the activity of RH variants containing replacement of bulky amino acids could be restored

by reduction with dithionite, indicating that the inactive oxidized states are responsible for the loss of activity after O_2 exposure (Buhrke et al. 2005a; Ash et al. 2015). Together, these features of *R. eutropha* RH provide a protective mechanism against O_2 that differs from the O_2-tolerant *R. eutropha* MBH and *E. coli* Hyd-1 (Goris et al. 2011; Roessler et al. 2012), and modifying gas channels may be an attractive strategy for engineering O_2-tolerant derivatives to protect the normal O_2-sensitive [NiFe]-hydrogenases from O_2.

2.1.8. Requirements for cofactor biosynthesis of [NiFe]-hydrogenases

Biosynthesis of [NiFe(CN)$_2$CO] cofactor at the active center. At least a set of seven maturation proteins including six so-called Hyp ("hydrogenase pleiotropic") proteins and a specific endopeptidase that completes the maturation process by C-terminal processing of the large subunit, is required for the synthesis and incorporation of the [NiFe]-active center into the most [NiFe]-hydrogenases (Fig 1.8) (Casalot and Rousset 2001; Böck et al. 2006; Forzi and Sawers 2007). In proteobacteria, the *hyp* genes are typically tightly clustered with their respective hydrogenase structural genes, whereas in archaea they are often found isolated and distributed throughout the genome (Vignais and Billoud 2007; Thauer et al. 2010). So far, the best studies of Hyp proteins are present in *E. coli* and *R. eutropha*, particularly due to the pioneering work achieved on the maturation system (Jacobi et al. 1992; Dernedde et al. 1996).

The CN ligands are synthesized from carbamoyl phosphate by HypF in an ATP-dependent manner (Forzi et al. 2007). The carbamoyl group is then transferred to the thiol group of the C-terminal cysteine in HypE and dehydrated, thereby forming a HypE thiocyanate. Subsequently, the cyano groups are transferred to the iron-containing HypCD-complex (Reissmann et al. 2003; Blokesch et al. 2004a, 2004b; Watanabe et al. 2007; Petkun et al. 2011). HypC and HypD serve as a scaffold for the assembly and insertion of the [Fe(CN)$_2$CO] moiety and its transfer to the empty large subunit apoprotein (Bürstel et al. 2012). Due to the presence of an oxidation-sensitive [4Fe4S]-cluster in HypD, transfer of CN ligands is thought to involve a HypD-dependent redox-responsive step (Blokesch et al. 2004a; Watanabe and Oikawa 2007; Soboh et al. 2012). More recently, in vitro reconstitution system indicates that the [Fe(CN)$_2$CO] cofactor is incorporated as a whole unit into the large subunit precursor of Hyd-1 and Hyd-2 based on the specific molecular interactions between the HybG-HypD complex, while the HypCD complex is specifically

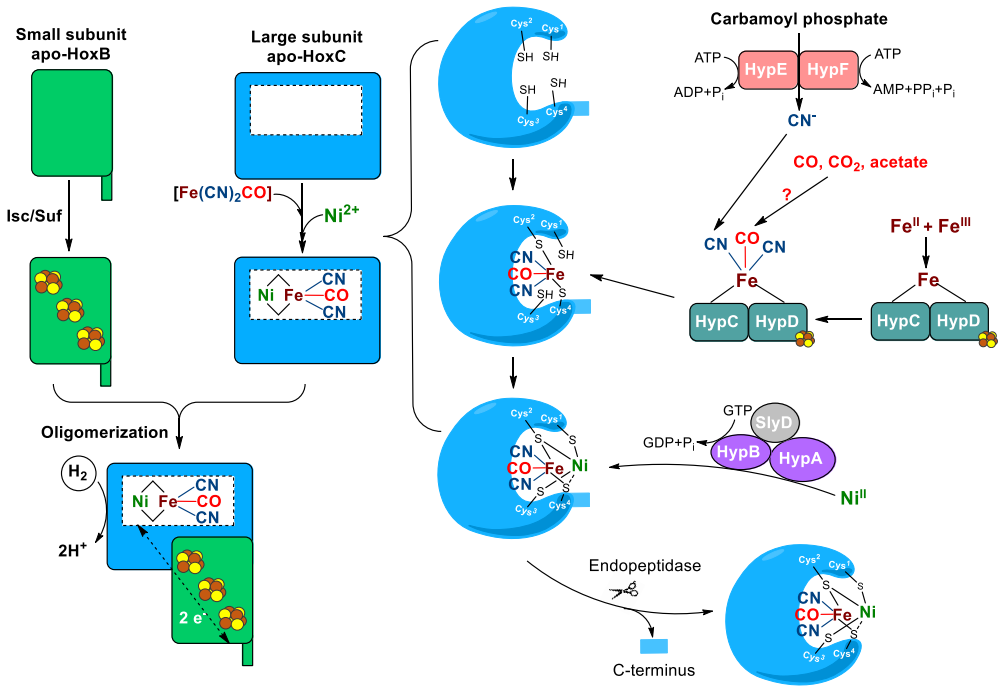

Figure 1.8 Proposed maturation model of the regulatory [NiFe]-hydrogenase of *R. eutropha* and biosynthesis of the [NiFe]-active site in *E. coli* (right).
The incorporation of the $Fe(CN)_2CO$ cofactor into the large subunit empty apo-HoxC, is mediated by the accessory proteins HypCDEF followed by Ni^{2+} incorporation mediated by HypAB complex, in addition to the action of SlyD (*sensitive to lysis D*) in case of *E. coli*. Whilst the RH maturation lacks a proteolysis step, maturation of the holoprotein large subunit is completed followed by the proteolytic removal of a C-terminal peptide catalyzed by a specific endoprotease which is dedicated specifically encoded by *hyaD*, *hybD*, *hycI* genes for *E. coli* Hyd-1, Hyd-2, and Hyd-3 respectively (HoxM and HoxW in case of the *R. eutropha* MBH and SH respectively). Upon cofactor insertion, the mature large subunit HoxC oligomerizes with the mature small subunit HoxB processed by assembly of [FeS]-clusters via the universal Isc/Suf to form function RH.

responsible for Hyd-3 maturation. These findings well support a model in which HypD is a central component during synthesis, whereas HybG or its homolog HypC but not HypD binds specifically and deliverys the $[Fe(CN)_2CO]$ cofactor to the large subunit precursor of the corresponding hydrogenases of *E. coli* (Blokesch et al. 2001; Stripp et al. 2013, 2021; Arlt et al. 2021; Soboh et al. 2022). To date, the source of the Fe and the CO ligand remains elusive, however, it has been proposed to originate from free CO (Lenz et al. 2007), CO_2 (Soboh et al. 2013), acetate (Roseboom et al. 2005), or some other metabolic precursors instead of acetate (Bürstel et al. 2011). The CO ligand is probably formed under anaerobic conditions by a variety of metabolic

pathways, whereas under aerobic conditions it is first synthesized from formyl-tetrahydrofolate by HypX and then binds to the Fe-HypCD complex (Bürstel et al. 2016; Schulz et al. 2020). HypX also plays a positive role in the H_2-uptake activity of *R. eutropha* MBH and SH (50% in *hypX*-deleted strains) (Buhrke and Friedrich 1998). Nevertheless, the anaerobic biosynthesis route of the CO ligand in [NiFe]-hydrogenases still awaits to be elucidated. The $[Fe(CN)_2CO]$-cofactor insertion into the O_2-tolerant *R. eutropha* MBH requires two additional auxiliary proteins, HoxV and HoxL, functioning as a scaffold protein and a specific chaperone respectively, both of which are supposed to be involved in protection of the active site from O_2 (Ludwig et al. 2009).

After successful incorporation of the $[Fe(CN)_2CO]$ fragment, nickel is inserted via four cysteines into the large subunit (Blokesch et al. 2002). According to the available crystal structures of [NiFe]-hydrogenases, the nickel ion is covalently bound to the protein scaffold via four conserved cysteine residues (Cys^1-Cys^4), while two of them (Cys^2, Cys^4) serve as bridging ligands coordinating also the iron ion (Fig 1.8) (Volbeda et al. 1996; Pierik et al. 1999; Kwon et al. 2018; Albareda et al. 2019). Notably, Cys^4 has been shown not to be required for nickel coordination in the large subunits of *E. coli* Hyd-3, the RH, SH and MBH of *R. eutropha* (Massanz and Friedrich 1999; Magalon and Böck 2000; Winter et al. 2004). In *E. coli*, nickel incorporation appears to be possible spontaneous under high nickel concentrations, as their absence e.g., in Δ*hypAB* mutants can be partially compensated by an increase in extracellular nickel concentrations (Wolf et al. 1998; Olson et al. 2001; Hube et al. 2002). Thus, the nickel metallochaperones HypA/HybF, HypB and SlyD which deliver nickel to the waiting hydrogenases, are redundant under high nickel concentrations (Waugh and Boxer 1986; Leach et al. 2007; Pinske et al. 2015b). However, the maturases HypAB significantly accelerate the GTP-dependent nickel insertion due to the GTPase activity of HypB (Gasper et al. 2006). Following insertion of the [NiFe]-center, a sequence of approx. 30 amino acids is cleaved from the C-terminus of the large subunit by a highly specific endoprotease, for example, HoxM, HoxW and HycI in the case of *R. eutropha* SH, MBH and *E. coli* Hyd-3, respectively, in order to allow oligomerization with the small subunit (Rossmann et al. 1995; Thiemermann et al. 1996; Massanz et al. 1997; Theodoratou et al. 2005).

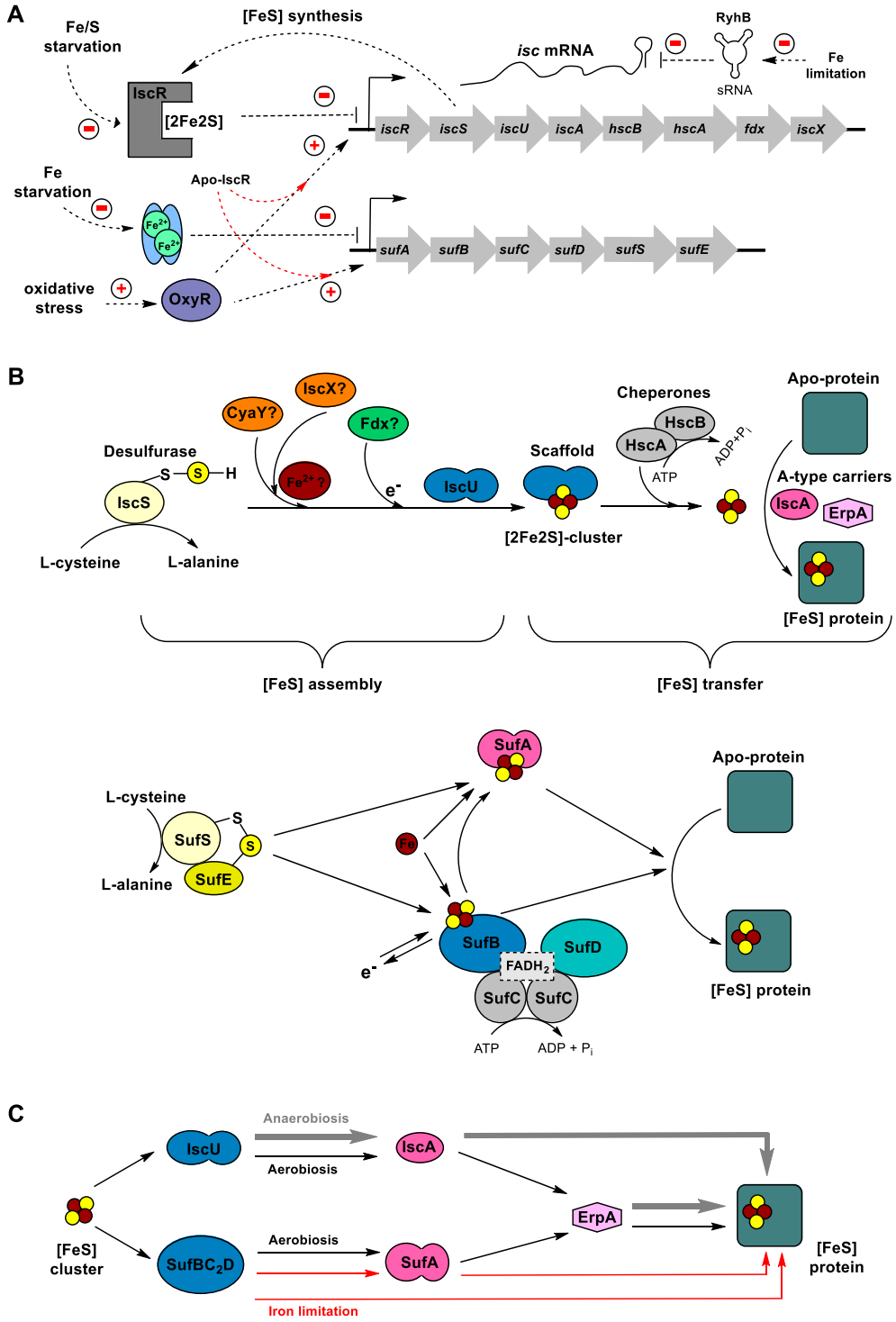

Figure 1.9 Regulation of [FeS]-cluster assembly pathways (A) and proposed [FeS]-cluster assembly on the IscU/SufB scaffolds (B) as well as [FeS]-cluster delivery routes in *E. coli* under different growth conditions (C).

Holo-IscR and apo-IscR will be present in an equilibrium that is dependent on the amount of Isc proteins available for cluster synthesis. Holo-IscR will repress *isc* operon transcription when there is sufficient cluster assembly capacity. Under normal growth conditions *suf* operon transcription will be low due to repression by Fur-Fe^{2+} complex. [FeS]-cluster assembly is performed on the scaffold protein IscU, which receives the sulfur from the L-cysteine desulfurase IscS. CyaY is believed to stabilize a conformation of the IscS-IscU complex. The role of IscX is unclear. Ferredoxin (Fdx) is proposed to participate in the reductive coupling of two [2Fe2S]-clusters to form a single [4Fe4S]-cluster on IscU in eukaryotes or in the last release step in prokaryotes. Release of the clusters is catalyzed by the chaperones HscAB. The A-type carrier (ATC) proteins IscA, ErpA and SufA are required to deliver the formed FeS-clusters to a specific apoprotein. In the Suf-dependent [FeS]-cluster assembly, SufS and SufE mobilize sulfur for donation to SufB and SufA. An [FeS]-cluster can form on both SufA and SufB. An apoprotein can get its [FeS]-cluster in different routes probably as a function of the growth conditions and might be specific to different target proteins. The [FeS]-cluster on SufA can be directly or indirectly via ErpA transferred to an apoprotein under aerobic growth or iron limitation conditions respectively, while the SufB [FeS]-cluster could be directly transferred to an apoprotein particularly for the apo-IscR or could participate in redox processes during cluster assembly. The direct iron donor is still unknown so far. The cofactor $FADH_2$ within the $SufBC_2D$ complex is likely to provide electrons, but its function in [FeS]-cluster assembly is still unclear.

Biosynthesis of [FeS]-clusters. While the large subunit of [NiFe]-hydorgenases necessitates the assembly of the [NiFe]-active site for proper function, the small subunit (SSU) also requires insertion of [FeS]-clusters which are responsible for electron relay to/from the active site. In *E. coli*, [FeS]-cluster biosynthesis and insertion into apoproteins proceeds via two separate pathways: the “Isc” (iron-sulfur-cluster) and “Suf” (sulfur formation) pathways. The required proteins are encoded by the *iscRSUA-hscBA-fdx-iscX* and *erpA*, and *sufABCDSE* respectively (Fig 1.9A) (Roche et al. 2013). Interestingly, in some bacteria, archaea and plant plastids, only the Suf system is present by serving as the sole [FeS]-cluster biosynthesis pathway (Py and Barras 2010; Boyd et al. 2014; Mettert and Kiley 2015; Wayne Outten 2015). Nevertheless, the Suf-dependent biosynthesis machinery is defect in *E. coli* BL21 derivatives due to an in-frame deletion between *sufA* and *sufB* within the *suf* operon (Daegelen et al. 2009; Jeong et al. 2009; Studier et al. 2009; Corless et al. 2020). Expression of *isc* operon is inhibited by an active holo-IscR hosting a [2Fe2S]-cluster. Under unfavorable [FeS]-cluster biosynthesis conditions, such as iron/sulfur starvation or oxidative stress conditions, accumulation of apo-IscR activates the expression of *isc* and *suf* operons (Outten et al. 2004; Gyaneshwar et al.

2005; Lee et al. 2008). This is also reflected by a positive effect of improving iron-sulfur supply, like addition of ferric ammonium citrate or ferrous sulfate, to the growth medium on overexpression of [FeS]-cluster proteins in *E. coli* (Nakamura et al. 1999; Jaganaman et al. 2007; Kuchenreuther et al. 2010; Birrell et al. 2016; Jagilinki et al. 2020). Aerobic conditions that increase the [FeS]-demand, reduce holo-IscR levels and elevate apo-IscR levels, accordingly increasing upregulation of expression of both operons (Giel et al. 2006, 2013). Furthermore, the Suf machinery is also upregulated in response to oxidative stress and iron limitation through other regulators Fur and OxyR (Patzer and Hantke 1999; Outten et al. 2004; Saini et al. 2010; Wollers et al. 2010). Under normal growth conditions, the Isc pathway is thought to play the major role in [FeS]-cluster biosynthesis, whereas under conditions of oxidative stress or iron starvation, the Suf pathway is reported to play a greater role. However, despite these features, even high levels of the Suf system have failed to fully mature some [FeS] proteins in the absence of the Isc machinery (Ezraty et al. 2013). Although Suf machinery functions more efficiently than Isc during stress, the broadened specificity of the Isc pathway makes it the referable system for housekeeping [FeS] biogenesis. [FeS]-cluster is formed on the scaffold IscU or SufB and then transferred to the apoproteins by the A-type carrier (ATC) proteins, e.g. IscA, ErpA or SufA (Fig 1.9B) (Loiseau et al. 2007; Py et al. 2011; Pinske and Sawers 2012; Pinske et al. 2013). Under aerobic growth conditions, it has been revealed that the [FeS]-cluster is transferred first to IscA/SufA, then to ErpA, and finally to the target apo-protein (Fig 1.9C). However, under anaerobic conditions or iron limitation conditions, alternative routes may be used in which the cluster travels from the IscU scaffold to IscA or from SufB scaffold to SufA, respectively, and then directly to the substrates (Vinella et al. 2009, 2013). As such, substrates may acquire clusters from different routes as a function of the growth conditions. Taken together, the [FeS]-cluster delivery proteins are highly versatile, ensuring efficient [FeS] maturation under different growth conditions.

Nickel transport and regulation system. The nickel required for biosynthesis of the active site of [NiFe]-hydrogenases is delivered by a specific ATP-binding cassette (ABC) transporter NikABCDE encoded by the *nikABCDER* genes (Fig 1.10) (Eitinger and Mandrand-Berthelot 2000). Expression of the *nik* operon is modulated by the global transcription factor FNR under anaerobic conditions (Wu et al. 1989). NikA is a periplasmic Ni-binding protein, whereas NikBC comprise the membrane channel

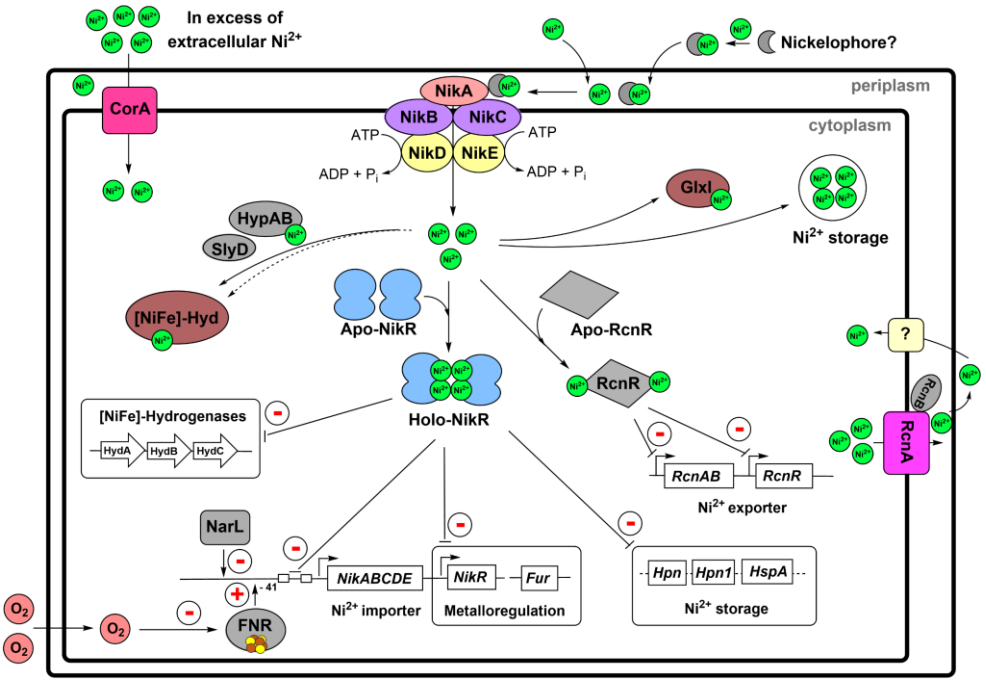

Figure 1.10 The nickel transport systems and nickel-dependent regulation in *E. coli*. As nickel is toxic at elevated concentrations, the acquisition and distribution of intracellular nickel ions is a highly-controlled process. The nickel homeostasis network in *E. coli* contains a nickel importer and exporter NikABCDE and RcnAB respectively, nickel-dependent transcription regulators NikR and RcnR, the nickel metallochaperones HypA/HybF, HypB and SlyD responsible for delivery of nickel to the hydrogenase enzyme precursors and nickel enzyme glyoxalase I GlxI.

subunits. NikDE encompass the ATP-binding domains to enforce the nickel import. Holo-NikR represses the NikABCDE synthesis in the presence of excess intracellular nickel (De Pina et al. 1999). Additionally, at high extracellular nickel concentrations, nickel can be non-specifically imported by the magnesium transport system CorA (Hausinger 1987; Wu et al. 1989). However, magnesium as preferable substrate of the CorA, can completely suppress the non-specific nickel uptake even at very low magnesium concentrations (10 µM) (Wu et al. 1989; Navarro et al. 1993).

Despite nickel being essential, at high concentrations, nickel can be toxic to the cell, as it can bind to other metalloproteins and displace the cognate metals resulting in an inactive metalloproteins (Macomber and Hausinger 2011; Higgins et al. 2012; Higgins 2019). Recently, the nickel export proteins RcnAB have been identified in

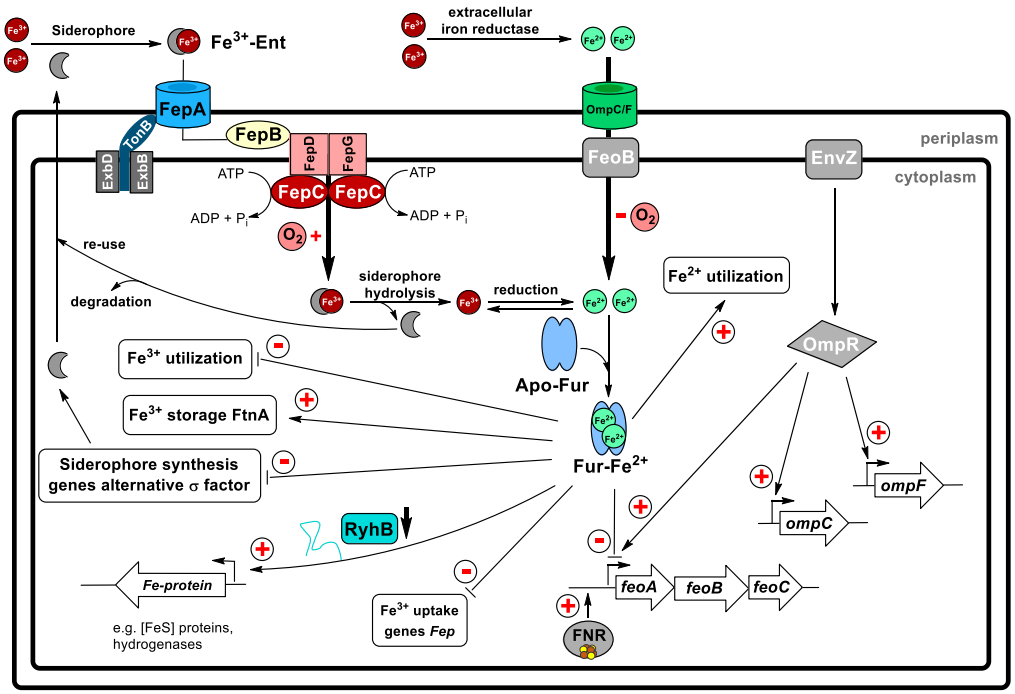

Figure 1.11 The ferric Fe^{3+} (Fep) and ferrous Fe^{2+} (Feo) uptake systems and Fe^{2+}-dependent regulation in *E. coli*.
Iron acquisition is assumed to be performed by the siderophore-based ferric Fep uptake system (FepABCDG proteins) under aerobic conditions or the ferrous Feo transport system containing (FeoB, OmpC/F) under low O_2 and anaerobic conditions. The Feo transport system is the main delivery route of iron for [NiFe]-hydrogenase cofactor biosynthesis in *E. coli*.

E. coli (Rodrigue et al. 2005; Blériot et al. 2011). RcnAB expression is controlled by a newly identified nickel-dependent regulator RcnR. Surprisingly, at low extracellular nickel concentrations, *rcnA* deletion results in reduced nickel accumulation, whereas *nikR* deletion restores *E. coli* Hyd-3 activity. These results indicate that NikR-dependent repression of *nik* transcription is sensitive to the presence of RcnA (Rowe et al. 2005; Iwig et al. 2006; Iwig and Chivers 2010). Therefore, both NikR and RcnR activities are modulated by the nickel requirements of the cell, thereby affecting nickel assembly and hydrogense activity.

Iron transport and regulation system. In addition to nickel requirement for hydrogenase activity, iron is essential for metal cofactor formation of hydrogenases. Due to toxic effects and oxidative damage induced by excessive iron in bacterial cells, the intracellular level of free catalytically active iron is typically kept low based on

the intricate balance between transport, utilization and storage of iron. Most bacteria possess mechanisms to import iron as its oxidized ferric iron (Fe^{3+}), reduced ferrous iron (Fe^{2+}) or both (reviewed in (Ã et al. 2003; Grass 2006)). Fe^{3+} is generally transported by various siderophore-mediated uptake systems, e.g. FecA-E, FepA-G, FhuA-D, whereas Fe^{2+} is transported by the high-affinity uptake system FeoABC (Fig 1.11) (Hantke, 2003, Andrews et al., 2003, Cartron et al. 2006). Under microaerobic or anaerobic growth conditions, iron is predominantly imported in its soluble reduced Fe^{2+} state, while under aerobic growth conditions, iron is oxidized to the insoluble ferric Fe^{3+} state ready for uptake (Braun and Hantke 2011; Kosman 2013; Lau et al. 2016). Expression of genes encoding proteins for iron metabolism is controlled by the ferric-uptake regulator Fur, which uses Fe^{2+} as a cofactor and functions as a repressor. However, the expression of the *E. coli* Fur regulon is influenced by O_2 availability, as it affects the oxidation state of iron and the way in which cells acquire iron (Beauchene et al. 2015, 2017). When the level of available intracellular Fe^{2+} increases, it drives more Fur-Fe^{2+} formation and correspondingly increases its affinity for DNA by nearly 1.000-fold (Ã et al. 2003). Under anaerobic conditions, a more active Fur-Fe^{2+} complex leads to reduced expression of the iron import systems. In contrast, under aerobic conditions, low intracellular iron levels induce Fe^{3+} uptake and utilization (Massé and Arguin 2005). Furthermore, the negative effect of Fur-Fe^{2+} on *feoABC* expression can be overcome by the presence of OmpR, thus favoring Fe^{2+} over Fe^{3+} transport (Gerken et al. 2020). Overall, the iron uptake systems are more diverse in *E. coli*, which allows for sufficient intracellular availability and the maintaince of iron homeostasis under aerobic and anaerobic conditions.

2.2. Metabolism of *E. coli* and microbial bioprocess

2.2.1. Central carbon metabolism in *E. coli*

The central carbon metabolism in *E. coli* under fermentative conditions typically including the mixed-acid fermentation (a mixture of succinate, formate, acetate, lactate and ethanol), overflow metabolism and amino acid biosynthesis was extensively summerized in the previous master thesis (Fan 2017). Under oxic conditions, pyruvate is converted to CO_2 and acetyl-CoA that is further processed within the citric acid cycle to produce more ATP and reducing equivalents, by the pyruvate dehydrogenase complex which is downregulated under anaerobic conditions

and controlled by the NADH/NAD^+ ratio and the pyruvate concentration (Quail et al. 1994; de Graef et al. 1999).

2.2.2. The global regulator FNR controls switch of *E. coli* oxic and anoxic metabolism

The most important global regulator fumarate-nitrate-reduction (FNR) controls gene expression involved in anaerobic fermentation and respiration at the transcriptional level in *E. coli*, whilst it causes a downregulation of genes essential for aerobic respiration (Spiro and Guest 1990; Kiley and Beinert 1998; Förster and Gescher 2014). Expression of *fnr* is not coupled to growth condition, consequently equal amounts of FNR are available in the cell under oxic and anoxic conditions (Unden and Schirawski 1997). Three different forms of FNR occur within the cell: apoenzyme (apoFNR), a monomeric FNR with a [2Fe2S]-cluster, and the homodimer with a [4Fe4S]-cluster per monomer (Fig 1.12) (Jervis et al. 2009; Tolla and Savageau 2010). Among these three forms, only the homodimer is able to bind to target DNA-sites and globally induce expression of many genes (over 100) in response to O_2 starvation (Mazoch and Kučera 2002). Increased intracellular O_2 availability leads to monomerization of the homodimer and decomposition of the [4Fe4S]-cluster to the [2Fe2S]-cluster (Khoroshilova et al. 1997; Popescu et al. 1998; Unden et al. 2002). After prolonged incubation with O_2, the [2Fe2S]-cluster further dissociates and apo-FNR is formed devoid of Fe and sulfide (Lazazzera et al. 1996). However, active [4Fe4S]·FNR can be reformed from apo-FNR by the absence of O_2 or under reducing conditions by adding a reductant, such as glutathione or thiol proteins and cofactors (Tran et al. 2000; Unden et al. 2002). Furthermore, an *in vitro* study suggests the cluster interconversion of active dimer and inactive monodimer of FNR is a reversible process (Zhang et al. 2012). Nevertheless, FNR prefers to be either the [4Fe4S]·FNR dimer or the apo-FNR under anaerobic or aerobic growth conditions. So far, [4Fe4S]-cluster assembly on FNR *in vivo* has been clearly demonstrated by the function of the Isc system, but not the Suf system in *E. coli* (Schwartz et al. 2000; Mettert et al. 2008). In summary, the function of FNR *in vivo* depends on the ratio of active ([4Fe4S]·FNR) to inactive FNR ([2Fe2S]·FNR, apo-FNR) and on the rates of formation and dissociation of active FNR.

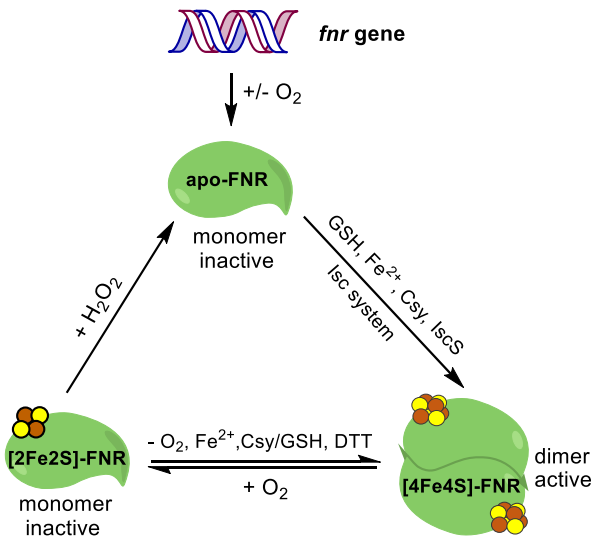

Figure 1.12 Summary of the *in vivo* and *in vitro* [FeS]-clusters and oligomeric states of FNR regulated by oxygen in *E. coli*.

2.2.3. Microbial fermentation bioprocess and consistent bioprocess development

Since high cell densities are a requirement for maximized volumetric yields of recombinant proteins in *E. coli*, the main purpose of microbial cultivations is to increase the biomass yields into high cell densities linked to a high yield of desired recombinant proteins (Riesenberg and Guthke 1999; Sommer et al. 2011). The common method to obtain high cell densities is the use of the substrate-limited fed-batch cultivation strategy, where one substrate component is growth rate limiting and the growth rate can be controlled to match the oxygen transfer rate allowing for the cultivation to be run in aerobic conditions (Jung et al. 1988; Shiloach and Fass 2005). By this method, it is also possible to reduce the metabolic overflow from pyruvate to acetate, as the accumulated acetate has a negative effect on cell growth and production of target protein (Shimizu et al. 1988; Jensen and Carlsen 1990; Luli and Strohl 1990). Nevertheless, early-stage product development can practically only be performed as batch-type processes for initial rapid optimization of parameters. A key issue in product development is how to transfer a batch strategy to a fed-batch operation in a large process. Thus, in the early production development phase, it is necessary to directly introduce fed-batch technologies and industrial cultivation

modes that need to be simple but targeted and provide major benefits for the bioprocess development (Neubauer and Winter 2001; Neubauer et al. 2013).

Typically, early process development is mainly focused on miniaturization and yield maximization at the expense of monitoring and control of the cultivations (Junker and Wang 2006). Currently, different automated high-throughput screening approaches are conducted in microwell plates (MWPs), or in modified MWPs for up to 48 parallel cultivations with feeding, online monitoring and pH control via microfluidic addition of fluids (Horinouchi et al. 2014; Blesken et al. 2016; Dörr et al. 2016). Nevertheless, the big difference in environments between cultivation in MWPs and biomanufacturing in large fed-batch bioreactors is a major limitation in the bioprocess development from early screening to final production (Neubauer et al. 2013, 2020). To reduce the risk of failure during scale-up, it is essential to keep conditions comparable to the production scale in performing strain and process engineering (from microliter to liter systems), as cultivation regimes have a significant impact on the physiological metabolism of the producer strain (Hemmerich et al. 2018). For a robust scale-up, the physiological conditions inside the cell and the space-time dynamics of the environmental parameters have to be investigated by performing dynamic experiments and high-frequency data to understand the behavior of a biological process (Neubauer and Cruz-Bournazou 2017). In a consistent bioprocess development, a major bottleneck is the performance of fed-batch operations during parallel screening at milliliter scale. In parallel, laboratory liter-scale bioreactors are highly material intensive and require manual intervention. Therefore, the use of parallelized miniaturized bioreactor systems for both screening and upstream process development will greatly relieve this bottleneck (Bareither and Pollard 2011; Velez-Suberbie et al. 2018). By this approach, it is possible to ensure that a potential bioprocess reaches production within the earliest possible times. Additionally, in combination with automated liquid-handling systems, it offers a good opportunity to increase the high-throughput and parallelization of microbial cultivations in small-scale STR systems. Instead of micropumps, the fed-batch-like EnBase® technology uses a catalytic glucose delivery system that enzymatically controls the glucose feeding rate in situ and consequently control microbial metabolism (Panula-Perälä et al. 2008; Krause et al. 2016). This controlled microbial growth system comprises several benefits such as aerobic metabolism to high cell densities and lower production of acidifying side-products and thus a stable pH over long cultivation times. Also, the growth at a constant volumetric growth rate, i.e. an approximately

linear increase in OD, offers advantages in terms of robustness and reproducibility in comparison with exponentially growing cultures (Krause et al. 2010). As a result, this technology that can offer controlled cultivation conditions has been successfully applied in bioprocess developments for different recombinant proteins (Šiurkus et al. 2010; Glazyrina et al. 2012; Li et al. 2015; Ongey et al. 2019). Furthermore, an automated platform should be established for a faster and effective bioprocess development, which requires a fully automated process handling, at-line sample analysis, closed-loop process control, advanced feeding strategies similar to industrial processes, as well as the integration into a model-based operation algorithm (Neubauer et al. 2013; Haby et al. 2019). This smart platform could be applied for optimal experimental designs, model-based screenings and scale-down experiments, thereby significantly increasing the reliability and transferability of data throughout process development in advanced bioprocess developments (Schmid and Aschoff 2017; Anane et al. 2019; Hans et al. 2020).

Summarizing, these technologies available for modeling biological systems, combined with on-line process analytical techniques and advanced robotic experimental facilities, can not only accelerate the development of new process and optimization of existing ones, but also ensure a consistent and efficient cultivation process development by taking into account all the possible cultivation conditions that may be encountered upon process scale-up.

3. Objectives of this work

In view of global warming and depletion of natural resources, scientists are struggling to look for renewable and environmentally friendly alternative energy systems. Hydrogenases can serve a valuable model system for these tasks. They are metalloenzymes capable of catalyzing hydrogen oxidation and/or evolution. To meet human demands on clean energy, synthetic biology and modern biotechnology are needed to achieve economically efficient and large amount production of active hydrogenases. However, understanding of these highly complex enzymes is severely hampered by low production yields, thus extremely limiting their biochemical investigations and potential biotechnological applications. Heterologous production of these hydrogenases in a robust and genetically tractable expression host is an attractive strategy to make these enzymes more accessible.

In the present work, oxygen-tolerant regulatory [NiFe]-hydrogenase (RH) from *Ralstonia eutropha* due to its relatively simple structure and extensive use in spectroscopic studies, was chosen as a model hydrogenase to develop a general heterologous production system in *Escherichia coli*. From the construction of plasmid expression to the consistent bioprocess development, various attempts have been approached in this cumulative thesis and distributed into four manuscript papers assigned as **Paper I-IV** in the text. These manuscripts deal with the investigations in protein yield, activity and spectroscopic properties of cofactors. The specific objectives of this work were:

1. Optimization of heterologous *Re*RH production in *E. coli* aided by *E. coli* indigenous maturation system (**Paper I/II**)
    - Expression vector construction
    - Optimization of culture conditions for soluble RH production in *E. coli*
    - Scalability test over different shake flask scales
    - Process improvement using a fed-batch based autoinduction system

2. Spectroscopic characterization of heterologous produced *Re*RH subunits (**Paper I**)
    - UV-visible spectroscopic detection of [FeS]-clusters on HoxB
    - EPR detection of [4Fe4S]-clusters on HoxB and RH

- IR detection of CN and CO ligands at the catalytic [NiFe]-center of HoxC and RH

3. Towards production of catalytically active *Re*RH in *E. coli* by metabolic engineering and co-expression of maturation genes (**Paper III**)
   - Comparison of strain and culture conditions
   - Co-expression of *R. eutropha hyp* genes
   - Metal ion additions on EnPresso B medium
   - Investigation of the correlation between active RH production profiles and duration time
   - Co-production of additional maturases HoxN and HypX
   - Facilitation of active RH production by integrating fed-batch based lactose autoinduction

4. Scale-up of active RH production in fed-batch bioreactor fermentation (**Paper IV)**
   - Screening the metal effect on cell growth and active RH production in glucose mineral salt medium (MSM) cultures
   - Implementation of a high cell density bioreactor cultivation with 2 L MSM

4. Results and discussion

The broad aim of the work is focused on the efficient and rapid heterologous production of *R. eutropha* RH in a soluble and active form in *E. coli*, yielding high concentrations and its biochemical characterization. Thus, based on the principles of bioprocess engineering, protein yields including volumetric, specific and space-time yield, specific activity (per mg of purified protein), absolute activity (per L of culture) and space-time activity yield were the main concern in this thesis. The biochemical properties for the heterologously produced RH were studied to assess their ability to catalyze electrochemical oxidation of H_2 to electrons and protons as well as to perform spectroscopic analysis compared to the native form isolated from *R. eutropha*. The conceptual ideas and results of this dissertation were contributed to four individual papers including published articles. **Paper I-II** focused on the soluble RH production, while **Paper III-IV** payed attention to the RH activity with active production yield. To give the reader a brief overview of this work, the results and discussion of each paper were shortly summarized below, but the points raised for each specific topic are discussed in more detail in the full texts of the corresponding publications and manuscripts, which are attached at the end of this thesis.

4.1. Optimization of heterologous *Re*RH production in *E. coli* aided by *E. coli* indigenous maturation system (Paper I/II)

The RH functions as H_2 sensor regulating the expression of energy-converting hydrogenases including MBH and SH proteins in the presence of H_2 (Lenz et al. 1997, 2010). In addition to the HoxBC heterodimer, the H_2-sensing two-component regulatory system includes the histidine kinase HoxJ and the response regulator HoxA (Lenz and Friedrich 1998) (Fig 2.1A, left). Decades agao, a version comprised of HoxC and a truncated HoxB has been designed, the so-called RH_{stop} (Fig 2.1A, right). The truncated RH possesses the ability to oxidize H_2 *in vitro*, and can be isolated as single HoxBC heterodimer. However, due to the replacement of the 55 amino acids at the C-terminus of HoxB with a Strep-tag, it can no longer interact with the kinase HoxJ (Bernhard et al. 2001; Buhrke et al. 2005b). Based on this RH_{stop} version, in the first article (**Paper I**) a synthetic biology approach was used to design and construct the RH production plasmid pQF8. The plasmid expresses the genes for the large

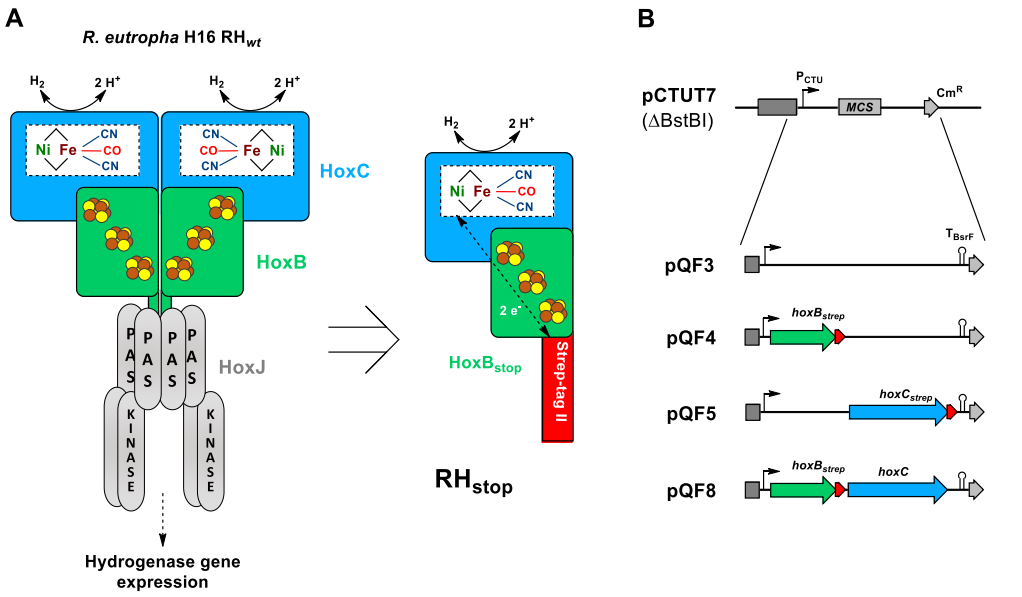

Figure 2.1 Schematic representation of the RH and expression plasmid constructed in this chapter.
The heterotetrameric native RH hydrogenase associated with the histidine kinase HoxJ (A, left) and the truncated heterodimeric RH_{stop} used in this study (A, right) as well as the plasmid pQF8 encoding RH structural subunits HoxBC (B). The [NiFe(CN)$_2$CO] active site is bound to the large subunit HoxC (blue) via four cysteine residues, while the small subunit (green) hosts three almost linearly arranged [4Fe4S]-clusters. pQF4 and pQF5 encoded the *hoxB* and *hoxC* genes with C-terminal Strep-tag, respectively.

subunit HoxC and the small subunit $HoxB_{strep}$ under control of the IPTG inducible $P_{lac\text{-}CTU}$ promoter. Additionally, plasmids pQF4 and pQF5 were designed to produce a single RH subunit, HoxC and HoxB, respectively (Fig 2.1 B).

After transferring the plasmid into appropriate *E. coli* cells, screening experiments in 24 deep-well plates with 3 mL working volume were conducted to investigate relevant cultivation parameters, including production strain, inducer concentration, temperature and expression time in TB-based batch system. Compared to wildtype K-12 strains (e.g., TG1 and W3110), higher total and more stable RH yields were observed in *E. coli* BL21 Gold cells, which might be attributed to the absence of the OmpT and Lon proteases in this strain (Grodberg and Dunn 1989; Gottesman 1996). As expected, increasing IPTG concentrations resulted in higher total RH production, however, 50 µM IPTG were sufficient to produce more than 80% of the maximum yield obtained with 1 mM IPTG. Although the highest expression of the RH genes

was induced with 1 mM IPTG in the screening experiments, low IPTG concentrations of 50 μM favoured the solubility of the RH (14 mg L^{-1}). Similarly, a decrease of the cultivation temperature from 37 ℃ to 30 ℃ proved to be beneficial for the solubility of heterologous RH. These conditions for soluble RH production seems to have the lowest risk of protein misfolding or aggregation e.g., inclusion body formation, as lower protein production rates increase the likelihood of proper protein folding (Neubauer et al. 2006; Evans et al. 2019).

Subsequently, the enzyme-based automated in situ glucose-release EnPresso growth system including steadily boosting the nutrient at the induction point to prolong cell growth and elevate cell densities was used. Not surprisingly, the booster had a positive effect on cell densities and subsequently soluble RH yields compared to non-boosted cultures. When switching to EnPresso-based fed-batch like cultures, the initial modest soluble RH yield was increased by 10-fold to 125 mg L^{-1}. Generally, prior to scale-up of a bioprocess, the parameters are initially optimized in small-scale batch cultivations, however, the optimized parameters could not be transferred directly from a small batch cultivation to a large fed-batch bioreactor cultivation, because different cultivation modes are typically used. Here, the EnPresso B technology was chosen as it enables easy scalability from microwell plates to glucose-limited fed-batch larger bioreactor fermentations with consistent conditions and it has been earlier used to produce different recombinant proteins (Krause et al. 2010; Li et al. 2015; Ongey et al. 2019). To investigate the reproducibility of fed-batch like cultivations during scale-up, the shake flask cultures in 2.5-L UYF with a broth volume of 500 mL (20% *v/v*) under optimized conditions of inducer concentration, temperature and production strain were performed. In comparison of 250-mL UYF cultivations, soluble RH yields in terms of the volumetric and specific protein yields were increased by >2-fold in 2.5-L UYF cultivations (255 mg L^{-1} and 6 mg g^{-1}), indicating a good scalability of RH production in *E. coli* over shake-flask scales. To this end, based on the use of fed-batch-like EnPresso system, the results from **Paper I** are an important basis for further improving the yield and activity of RH production in *E. coli*.

Compared to standard single-shot IPTG induction, autoinduction can provide a simple and fast way to achieve high protein yields, as there is no need to monitor cell growth or add inducer at the appropriate time after culture growth. Usually, the induction effect by lactose in glycerol-based autoinduction is highly sensitive to the glucose concentration as catabolite repression results in reduced lactose uptake rates at excess

glucose (Görke and Stülke 2008; Wurm et al. 2017a, 2017b). However, recent studies using a combination of lactose and glucose-limited EnPresso B fed-batch like medium successfully addressed this glucose-dependent inducer exclusion problem (Hoffman et al. 1995; Gombert and Kilikian 1998; Pei et al. 2011). From this system, the slow glucose release does not prevent lactose autoinduction and the lactose only serves as inducer without being catabolized as carbon source consequently reducing the oxygen sensitivity of lactose autoinduction, which is strongly associated with protein production in glycerol-based autoinduction cultures (Blommel et al. 2007; Li et al. 2011; Ukkonen et al. 2013; Mayer et al. 2014). Therefore, in order to simplify the process of heterologous RH production and to improve soluble RH production, a combined approach comprising the autoinduction technique and fed-batch-like EnPresso B growth system was used (**Paper II**).

Autoinducing media often contain glucose that is initially used as the preferred carbon source and prevents target protein expression during early growth phase due to catabolite repression, it is thus necessary to find out the minimal glucose concentration added to the autoinduction cultures. In the used fed-batch like EnPresso growth system, RH production already started within the first 2 h after inoculating a culture if 0.5 g L^{-1} glucose was used, indicating the absence of an induction delay which is typically present in conventional glycerol-based autoinduction medium (Blommel et al. 2007). This is well in line with a previous report detecting that protein synthesis started when glucose concentrations drop below 0.3 g L^{-1} (Mayer et al. 2014). At low IPTG concentrations (<100 μM), the inducer is actively transported into the cell by lactose permease LacY, whereas at higher IPTG concentrations used for normal induction (200-1000 μM) the inducer enters the cell by passive diffusion (Marbach and Bettenbrock 2012; Faust et al. 2015). For RH production, although 10 μM IPTG was sufficient to induce expression, 50 μM IPTG seems to be required for full induction, which is well supported by previous studies that IPTG concentrations below 40 μM caused only partial induction. This is likely due to the fact that either the amount of IPTG is not sufficient to remove all repressor molecules from the operator site in the induced cells, or that only a subpopulation could be induced by the limited amount of externally available IPTG (Fernández-Castané et al. 2012a, 2012b). Similarly, a minimal lactose concentration of 0.5 g L^{-1} was enough for induction of recombinant RH production, probably due to the reduced need of lactose for slow growth provided by the enzymatic glucose feeding EnPresso system (Mayer et al. 2014). By screening the inducer concentrations, the optimal RH production level was

reached using 2 g L^{-1} lactose or 50 µM IPTG. Moreover, RH synthesis was stable and gradually accumulated throughout the whole production phase up to 36 h.

Compared to the classic single-shot IPTG induction, IPTG autoinduction resulted in comparable final cell densities and soluble RH yields, however, the space-time yields increased about 2-fold due to the shorter cultivation time. Similarly, autoinduction with 2 g L^{-1} lactose resulted in a 3-fold increase in volumetric and specific RH yield (278 mg L^{-1} and 7.5 mg g^{-1}) and even a 4-fold increase in space-time yield of nearly 12 mg $(L\ h)^{-1}$. Since the positive effect of booster on RH production was observed in both classic and autoinduction, repeated boosting significantly enhanced both specific and volumetric RH yields (220 mg L^{-1} for classic single-shot IPTG induction, 366 mg L^{-1} for lactose autoinduction) due to increased cell densities, which highlights the strong dependence of RH production yields on the biomass. The fed-batch autoinduction system ultimately improved the RH production yields on the basis of a similar biomass compared to standard IPTG induction, probably due to an increased or maximized metabolic capacity of individual cells in favor of target protein production. This is an essential advantage over previous extensively studied autoinduction systems, which enable higher final yields of target proteins by increasing final biomass (Kotik et al. 2004; Grabski et al. 2005; Li et al. 2011). Here, the results confirm the general applicability of the developed fed-batch based autoinduction system for efficient recombinant protein production in *E. coli* and provide an alternative possibility to conventional IPTG induction system for enhancing the heterologous RH production.

4.2. Spectroscopic characterization of heterologous produced *Re*RH subunits* (Paper I)

After optimization of apo-RH production, RH purified from *E. coli* showed no *in vitro* H_2-oxidation activity (**Paper I**). In order to figure out the lack of activity, different spectroscopic methods were used to study the cofactor content in both Hox proteins (see section 8.3). In the **Paper I**, the IR spectra of heterologously produced HoxC and RH in *E. coli* clearly indicated that the absence of catalytic [NiFe]-cofactor is the reason for the lack of RH activity. Moreover, the lack of [NiFe]-center in the isolated HoxC was also supported by UV-visible spectroscopy, showing the absence of

* UV-visible spectroscopy was performed by Q.F. and G.C., while IR and EPR measurements and data evaluation were performed by G.C. and C.L.

characteristic [NiFe]-site-related absorption bands rencently observed in the native HoxC isolated from *R. eutropha* (Caserta et al. 2020a). Regarding the purification process, a color change of the *Strep*-tactin column from colorless to dark brownish occurred after loading HoxB- or RH-containing clarified *E. coli* crude extracts (Fig 4.2A), but not in HoxC-containing extract. This dark brownish color is attributed to the [FeS]-clusters present in these proteins as reported by *in vitro* reconstitution of [FeS]-clusters (Py and Barras 2010; Wollers et al. 2010). In addition to the peak at 280 nm associated with the protein backbone due to the absorption of aromatic amino acid residues of the protein, apparent signals recorded by a broad shoulder around 410 nm and 550 nm were detected (Fig 2.2A/B). These signals were vanished completely upon reduction of as-isolated HoxB with excess sodium dithionite (Fig 2.2A), indicating the presence of [FeS] clusters, which is in line with previously reported observations in native RH isolated from *R. eutropha* (Buhrke et al. 2005b). Next, to gain insight into the composition of [FeS] clusters, EPR spectroscopy was used to analyze the HoxB (Fig 2.2C) and RH samples (**Paper I**). The as-isolated HoxB (oxidized) sample seemed to be mainly EPR-silent with minor contributions of $[3Fe4S]^{+}$ clusters (Fig 2.2C, top), consistent with the data of partially damaged [4Fe4S]-clusters as reported in native RH (Roncaroli et al. 2015; Caserta et al. 2020b). Reduction of HoxB with sodium dithionite produced an intense rhombic EPR signal ascribed to the reduced $[4Fe4S]^{+}$ cluster (Fig 2.2C, bottom), similar to the data reported for RH purified from *E. coli* (**Paper I**) and HoxB subunit isolated from *R.eutropha* (Caserta et al. 2020b).

Previous Mössbauer and EPR studies have proven to the presence of three [4Fe4S] clusters in the small subunit HoxB of native RH and demonstrated reduction of almost all three [4Fe4S]-clusters to the $[4Fe4S]^{1+}$ state (2.7 clusters of three) upon treatment with sodium dithionite (Roncaroli et al. 2015). However, the spectral signature of $[4Fe4S]^{+}$-cluster detected in HoxB purified in *E. coli* is somewhat different to the case of wildtype or HoxB isolated from *E. coli* (Caserta et al. 2020b), presumably related to the incomplete cluster incorporation in all these individually isolated HoxB proteins from *E. coli*. This suggests that the stabilization of all [FeS]-clusters, at least at the proximal position is accomplished by a mature HoxC assembled with a full [NiFe]-cofactor. Furthermore, there are indications for through-space dipolar interactions, consequently suggesting that at least two reduced [4Fe4S]-clusters contribute to the purified HoxB protein in *E. coli*. In contrast to other classical [NiFe]-hydrogenases including O_2-tolerant membrane-bound hydrogenases due to the

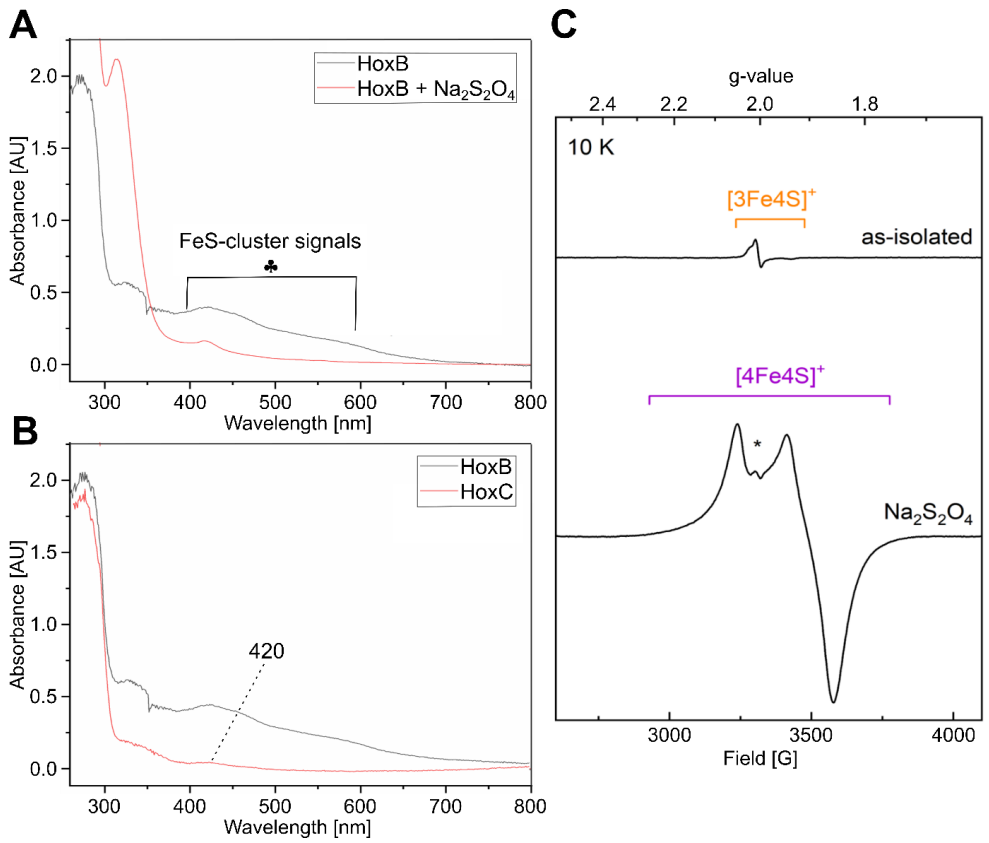

Figure 2.2 Spectroscopic characterization of HoxB and HoxC purified from *E. coli*. (A) UV-visible absorption spectra of 0.2 mM as-isolated HoxB (grey line) and reduced HoxB by sodium dithionite ($Na_2S_2O_4$) (red line) in 100 mM Tris/HCl pH 8.0, 150 mM NaCl. Signals of as-isolated HoxB (♣) was vanished upon treatment with an excess of sodium dithionite, indicating the presence of [FeS]-clusters. (B) Comparison of UV-visible absorption spectra of as-isolated HoxB (grey line) and HoxC (red line) produced from *E. coli*. The spectra of *E. coli* HoxB and HoxC show minor absorptions around 420 nm, presumably related to heme-containing protein contaminants copurified with Hox proteins. (C) EPR spectra recorded at 10 K with a microwave power of 1 mW of as-isolated HoxB (0.2 mM) from *E. coli* (top trace), containing minor contributions of a $[3Fe4S]^+$ cluster species, in agreement with data reported in native RH purified from *R. eutropha* and N-terminally Strep-tagged HoxB purified from *E. coli* (Caserta et al. 2020b), whereas EPR spectra of reduced HoxB treated with an excess of sodium dithionite (bottom trace) contain rhombic signals attributed to a $[4Fe4S]^+$ cluster. The asterisk (*) represents a weak signal probably derived from a [2Fe2S] cluster subspecies that originates either from partial [4Fe4S] cluster degradation or from protein contaminants copurified with HoxB, consistent with data recently reported in RH_{stop} purified from *E. coli* (**Paper I**).

geometric arrangement of the clusters relative to the active site, the proximal [4Fe4S]-cluster of RH does not become reduced upon H_2 incubation, supporting the

assumption of fast discharging of the proximal [4Fe4S]-cluster and rapid electron transfer to the neighboring [4Fe4S]-cluster (medial and then distal) (Roncaroli et al. 2015). Thus, the presence of catalytic [NiFe]-center in the large subunit seems to be capable of promoting the complete insertion of the iron-sulfur cofactors in the small subunit and protecting them from ambient oxidation, in addition to the ability to split electrons from the ambient H_2.

Metalloprotein often contain metal ions or metal-associated cofactors required for proper catalytic or protein activity, signal transducers or charged components that stabilize the protein (Banci and Bertini 2013). In fact, the cofactors of RH or HoxB/C subunits precipitated at high protein concentrations, actually above approx. 3.5 mg L^{-1} of purified protein measured by NanoDrop when stored under air at -20 °C or 4 °C for several days (Fig 4.2B). This is a general problem of hydrogenases thereby resulting in loss of their activity. Although the hydrogenase is of high stability in its isolated oxidized inactive state, its activity can markedly decrease during storage of cells, storage of the purified proteins as well as during the purification process (Fan et al. 2020). For example, previous studies introduce modifications of the hydrogenase purification protocol e.g., flushing with pure H_2 at the end of the cultivation, to prevent oxidative damage of the protein during cell storage, consequently increasing the specific activities in a range of 16- to 130-fold after modification of the purification procedure (Girbal et al. 2005; Demuez et al. 2007). Thus, the purified RH preparation should be flash-frozen in liquid nitrogen and stored at -80 °C ready for further activity measurements or spectroscopic analaysis.

Taken together, the biochemical characterization indicates the lack of the [NiFe]-center in heterologouly produced HoxC and RH, however, HoxB and RH appear to contain native-like [4Fe4S]-clusters in the HoxB subunit.

4.3. Towards production of catalytically active *Re*RH in *E. coli* by metabolic engineering and co-expression of maturation genes (Paper III)

Inactive RH produced in aerated *E. coli* cultures suggests the absence of indigenous *E. coli* Hyp maturases, as their FNR-dependent expression requires anaerobiosis (Lutz et al. 1991; Jacobi et al. 1992; Messenger and Green 2003). Althrough RH maturation in the presence of O_2 or CO should in principle be possible, due to the O_2 tolerance of the RH activity (Bernhard et al. 2001; Buhrke et al. 2005a; Ash et al. 2015), a comparison of different *E. coli* strains grown under aerobic or O_2-limited microaerobic cultivation conditions showed that active RH was only produced under O_2-limited microaerobic conditions in *E. coli* K-12 strains (Fig 2.7A). This indicates that microaerobic/anaerobic growth conditions are required for the cofactor maturation of the RH using the indigenous *E. coli* maturation proteins. However, the specific activities correspond to only approx. 3%-0.5% of the native RH isolated from *R. eutropha* (1.0-4.5 U mg^{-1}), indicating that the *E. coli* Hyp proteins are not capable of maturing the RH cofactor effectively (Bernhard et al. 2001; Buhrke et al. 2005a, 2005b; Caserta et al. 2020b). In *R. eutropha*, six specific auxiliary proteins (HypA1B1F1CDE) are required for proper maturation of the [NiFe]-cofactor (Buhrke et al. 2001). Thus, the native 6 *hyp* genes (*hyp1* operon) were co-expressed with structural *hoxBC* genes, resulting in a 1.5-3.5-fold increase in specific RH activities in *E. coli* K-12 strains W3110 and MC4100 (Fig 2.7B). However, still no activity was detectable in *E. coli* BL21 Gold strains, probably due to major defects in anaerobic metabolism and nickel transport system (Daegelen et al. 2009; Pinske et al. 2011). This clearly demonstrates the specificity of the maturation proteins and the need of co-expression of native maturases to ensure efficient maturation of active RH. The highest specific RH activity was produced in *E. coli* MC4100 cultures which was used for further improvement of active RH production.

The standard-like HypF protein from *E. coli* usually contains three strongly conserved functional domains including an N-terminal acetyl transferase module, a central zinc finger region and a C-terminal region with a histidine-rich motif found in several *O*-carbamoyl transferases (Paschos et al. 2001, 2002). Since the *R. eutropha* HypF1 is an unusually truncated version of the standard-like *E. coli* HypF (<~50%) only containing one of three strongly conserved domains (Wolf et al. 1998; Paschos et al. 2002; Jones et al. 2004), active RH was produced without co-expression of

R. eutropha hypF1, consistent with the consensus in the literature of the necessity of endogenous *E. coli* HypF for full RH cofactor maturation (Lenz et al. 2007). It is likely that the *E. coli* HypF homologue can take over the function of *R. eutropha* HypF1 under anaerobic/microaerobic conditions (Wolf et al. 1998; Lenz et al. 2007). Although the truncated HypF1 is sufficient for hydrogenase maturation in *R. eutropha* but active only under aerobic conditions, no RH activity was observed in the absence of *E. coli*-type HypF under anaerobic conditions (Wolf et al. 1998; Lenz et al. 2007; Winter et al. 2010). These studies suggest that the binding of *R. eutropha* HypF1 to HypE renders a non-functional complex responsible for CN cofactor maturation under anaerobic conditions. Similarly, lower RH activity was observed in the presence of both HypF homologs compared to the presence of only *E. coli* HypF (Fig 2.7B, C). Both HypF homologs appear to compete with each other under anaerobic conditions. Interestingly, this competition almost disappeared at lower temperature of 18 °C, consequently resulting in comparable specific activities of RH purified from strains with and without *hypF1* gene, respectively (Fig 2.7D). Probably, at least at 18 °C, the truncated *R. eutropha* HypF1 either has a comparable RH maturation efficiency as the *E. coli* HypF during an extended process with sufficient substrate produced or is completely inactive under this condition. In this study the former seems to be more convincing. While canonical HypF proteins synthesize cyanide (CN) residue from carbamoyl phosphate and ATP, while the truncated HypF1 likely requires carbamoyl adenylate for CN synthesis (Reissmann et al. 2003; Blokesch et al. 2004b). It is possible that carbamoyl adenylate is produced in sufficient quantities in living cells only under aerobic conditions. Since low temperatures increase dissolved oxygenation levels of the liquid medium, at 18 °C, the dissolved oxygen concentration is certainly higher than at 30 °C, consequently resulting in the higher RH activities obtained at lower induction temperature. Furthermore, low temperatures might prevent misfolding of the essential maturation proteins, giving rise to higher availability of functional maturases and thus higher maturation efficiency. Taken together, the results indicate that not only the presence of specific and efficient maturation system but also the appropriate culture conditions are essential for the success of [NiFe]-cofactor maturation at levels sufficient for active RH production in *E. coli*.

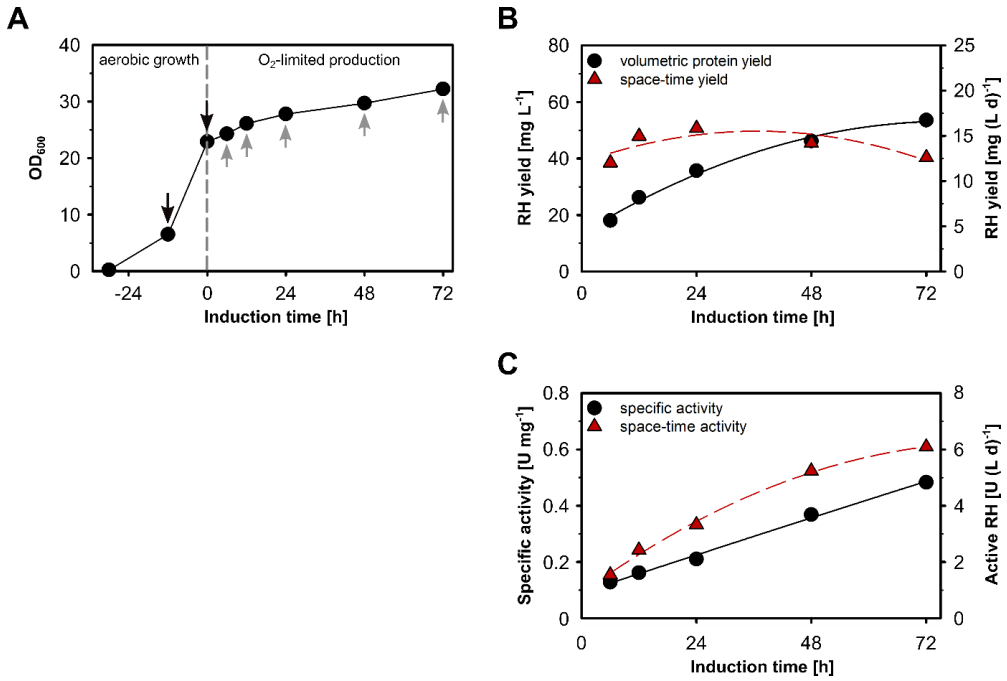

Figure 2.3 Production profile of active RH in relation to production time.
Strain *E. coli* MQF8RH2 was cultivated in 2.5 L UYF with 250 mL boosted EnPresso B medium at 30 °C, 250 rpm. After 18 h a 1st dose of booster was added and the cultivation continued for 12 h. At the induction point a 2nd dose of booster and 0.1 mM $NiCl_2$ were added and RH production induced by addition of 50 µM ITPG. Immediately, the culture was equally distributed on five 125 mL PreSens flasks (40 % *v/v*) and RH production performed under O_2-limited conditions at 18°C. One of each of the parallel cultures were harvested 6, 12, 24, 48 or 72 h of post-induction. The cell growth is shown in **(**A**)**. Black arrows indicate addition of booster and grey arrows harvesting points. RH protein was purified with affinity chromatography (B) and specific activities measured from the purified RH samples (C). Space-time yields **(**B**)** and space-time activity **(**C**)** were calculated using the entire process time from inoculation until cell harvest.

However, in spite of slightly increased total activity yields, only 75% of soluble RH yield produced in 30 °C was achieved in 18 °C cultures, suggesting that RH precursor biosynthesis is somewhat different in time and space from cofactor maturation. To improve the efficiency of RH production process, the correlations between production time, cell growth, RH synthesis and activity were investigated. After induction the OD_{600} did not increase significantly, but the cells continued to grow slowly during the 72-hour induction to a final OD_{600} of about 32, indicating that the nutrients in the medium were sufficient for cell growth and biosynthesis of recombinant proteins under O_2-limited conditions (Fig 2.3A). Not surprisingly, RH was gradually produced

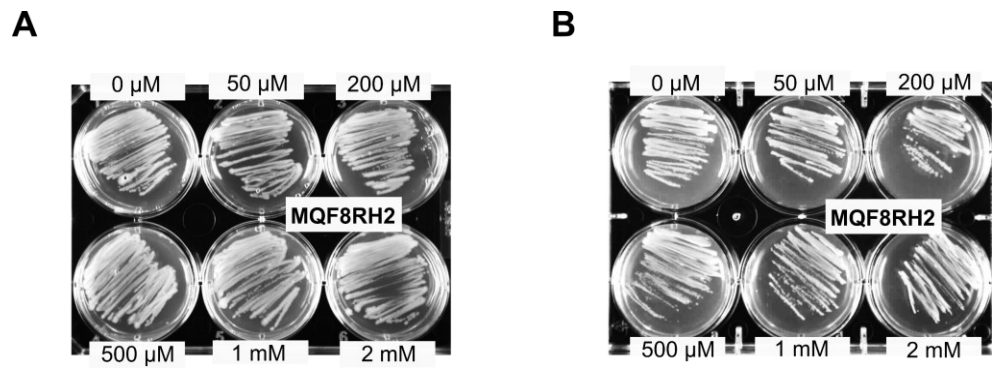

Figure 2.4 Tolerance of cell fitness to different metal ion concentrations on complex rich medium cultures.
Strain *E. coli* MQF8RH2 was cultured in solid agar complex TY medium supplemented with different $NiCl_2$ (A) or $FeCl_3$ concentrations ranged from 0 to 2 mM and incubated overnight at 37 °C.

within a range of 18 mg L^{-1} to 54 mg L^{-1} during the whole induction process, whereas the space-time RH yield (mg per L culture and per day process time) increased steadily in the first 24 h of induction followed by a slight decrease of about 7% per day (Fig 2.3B), suggesting an optimal production period from 24 to 48 h of induction in terms of protein yield. Interestingly, the specific RH activity increased almost linearly and continuously with increasing induction time, indicating ongoing active site maturation (Fig 2.7E). The highest activity was reached at 72 h of induction with 0.5 U mg^{-1} (Fig 2.3C). Similarly, the space-time activity showed an increasing trend approaching a maximum of about 6 U $(L\ d)^{-1}$ after 72 h of induction. This increase is attributed to the increase in both the specific activity and the total RH yield. Obviously, the process duration is obviously important for RH cofactor maturation and thus its activity. Overall, it can be noted that in terms of protein production alone, the process can be stopped 24-48 hours after induction, as the slight increase in protein quantity observed from this point on cannot any longer economically justify the costs of extending the production time. In contrast, with regard to the activity of the RH, a prolongation of the process is valuable to improve the quality of highly active RH, as it provides sufficient time for the slower maturation of the RH so that an increase in total and space-time activity can be observed throughout the entire induction phase.

The biosynthesis of active site cofactor of [NiFe]-Hydrogenase enzymes requires nickel and iron in addition to multiple accessory proteins. Sufficient availability of these metal ions is a key factor for the production of active hydrogenase. Thus, the

low activity observed might be due to an insufficient supply of those metal ions, as demonstrated by the first attempt to increase RH activity by the addition of high nickel concentration (500 μM) to the growth cultures (Fig 2.7C). In general, *E. coli* cells are grown in the extracellular environment present at very low nickel or iron concentration, e.g., 1 μM (Grass 2006; Macomber and Hausinger 2011; de Reuse et al. 2013). First, these were assayed using a growth test run under conditions supplemented with varied nickel or iron concentrations ranging from 0 to 2 mM in complex medium to evaluate the cell fitness of *E. coli* (Fig 2.4). Surprisingly, nickel or iron levels did not affect the cell fitness of *E. coli* in complex rich media (Fig 2.4), as typically they might be toxic to *E. coli* cells at high concentrations. This indicates a considerably high cell growth tolerance to nickel or iron concentrations on complex rich medium. This unchanged cell growth behavior upon addition of metals is likely due to the presence of chelation character on metal ions in the growth medium, which limits the availability of these metal ions (Rathnayake et al. 2013). Next, the highest RH activity was achieved upon addition of 100 μM $NiCl_2$ whilst a negligible effect on RH activity was observed with $FeSO_4$ addition up to 500 μM, indicating that sufficient iron but insufficient nickel is present in the used EnPresso B medium for active RH production. It is possible more diversity of iron uptake systems in *E. coli*, which allows sufficient intracellular availability and maintains iron homeostasis under aerobic and anerobic conditions (Braun 2003; Braun and Hantke 2011; Kosman 2013; Lau et al. 2016). Furthermore, the results obtained with different ratios of nickel and iron (0:0, 100:0, 0:100, 100:100, [μM:μM]) supplemented EnPresso medium demonstrate the nickel dependence for RH activity, since in the absence of additional nickel very little *in vitro* RH activity can be detected. In contrast to iron, nickel is much less abundant and might be limiting in case of the overproduction of nickel-containing proteins such as [NiFe]-hydrogenase. In *E. coli*, nickel is taken up via the specific nickel uptake Nik system, which is synthesized only under anaerobic conditions and downregulated by the transcriptional repressor NikR at high intracellular nickel concentrations (Fig 2.5) (Wu et al. 1989; Rowe et al. 2005; Iwig and Chivers 2010). In excessive nickel concentrations or in Nik-deficient strains (e.g., *E. coli* BL21), nickel can be non-specifically taken up by the magnesium transport system. However, the specificity and capacity of this system for nickel is much lower than that of the Nik transport system, as it can be fully inhibited when its natural substrate, magnesium, is present in the culture above 10 μM (Kehres et al. 1998; Smith and Maguire 1998; Eitinger and Mandrand-Berthelot 2000). It is possible that the low

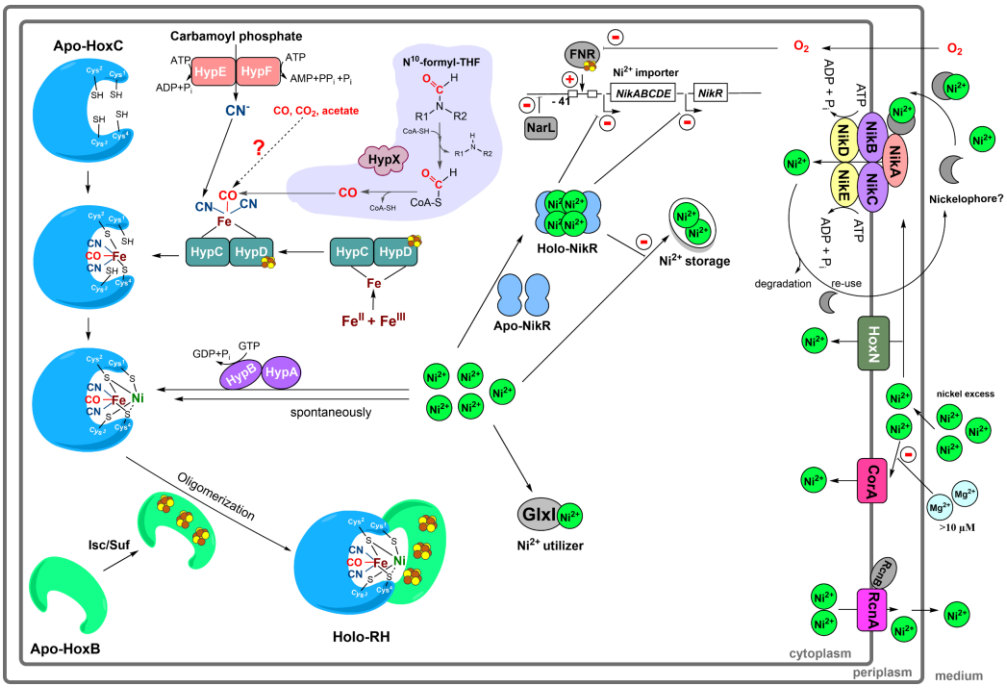

Figure 2.5 Schematic representation of maturation enzymes and metabolic pathways involved in heterologous active RH production in recombinant *E. coli* used in this study.

[FeS]-cluster assembly in the small subunit is mediated by the *E. coli* Isc/Suf machinery, while the [NiFe(CN)$_2$CO] cofactor is synthesized by at least six auxiliary proteins, namely HypA-F. A seventh maturase, HypX, is required for aerobic CO ligand biosynthesis. Using N^{10}-formyltetrahydrofolate (N^{10}-formyl-THF) as the substrate to release CO from HypX, two consecutive reactions are proposed: The formyl group of N^{10}-formyl-THF is first transferred to coenzyme A (CoA) producing formyl-CoA in the N-terminal domain of HypX, and then decarbonylation of formyl-CoA results in free CoA and carbon monoxide in the C-terminal domain. Fe(CN)$_2$CO insertion precedes Ni insertion. Nickel can be taken up into *E. coli* by the specific Nik system under anaerobic conditions or by the non-specific CorA transport system under aerobic conditions or by the co-expressed high affinity nickel permease HoxN of *R. eutropha*. In addition to delivering intracellular nickel to hydrogenase enzyme precursor, nickel can be used by other nickel enzymes, e.g. glyoxalase I (GlxI), or delivered to NikR-dependent storages, or exported via the nickel exporter RcnAB system, in order to maintain the nickel homeostasis in *E. coli*.

nickel uptake efficiency of *E. coli* is the major limiting factor in heterologous RH production developed so far, with only 15% of the activity purified from native *R. eutropha* (0.6 U mg^{-1} v.s. 4.5 U mg^{-1}) (Caserta et al. 2020b). Therefore, to improve the effectiveness of nickel uptake systems, the high-affinity nickel transporter HoxN of *R. eutropha* which allows the nickel uptake independent of regulations via FNR

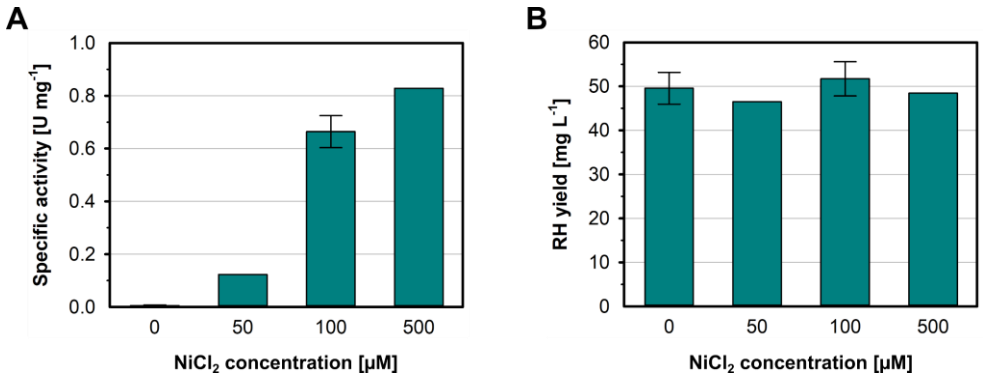

Figure 2.6 Nickel dependence of [NiFe]-cofactor biosynthesis in the presence of HoxN and HypX.
Strain *E. coli* MQF8RH8 was cultivated in 50 mL boosted EnPresso B medium under aerated growth conditions. After induction, different $NiCl_2$ concentrations were added and RH production lasted for 48 h at 18 °C. (A) Specific RH activities measured from the purified RH samples, (B) Soluble RH titers calculated from Coomassie stained gels after affinity purification.

and NikR, was introduced with all native Hyp proteins (see section 8.1). The co-production of HoxN resulted in a substantial increase in RH activity both under anaerobic and aerobic growth conditions (Fig 2.7F). Furthermore, the results clearly show that HoxN is functional in nickel uptake in the presence of high O_2, thus allowing RH maturation.

As described above, the highest RH activity was observed when the RH was isolated from O_2-limited *E. coli* cultures. However, the RH protein yield was only 3-times lower compared to aerobic cultivations (see section 4.1, ~40 v.s 125 mg L^{-1}). In addition to the limitation of nickel supply under aerated conditions, the availability of CO is a limiting factor for the maturation of [$NiFe(CN)_2CO$] cofactor (Bürstel et al. 2011). To overcome this CO limitation barrier, a further auxiliary maturase encoding gene *hypX* from *R. eutropha* was introduced. The gene encodes a CoA-dependent formyl-tetrahydrofolate (formyl-THF) decarbonylase (Bürstel et al. 2016; Schulz et al. 2020). As expected, this improved the RH activity by 3-fold compared to a strain producing the HoxN permease alone with *Hyp1* operon (Fig 2.7F). Remarkably, co-production of HoxN and HypX in aerobically grown cells resulted in RH activities that were about 2-fold higher than those measured for RH isolated from anaerobically grown cells. Interestingly, no toxic effect of increasing nickel concentrations was observed in EnPresso B cultures (up to 0.5 mM $NiCl_2$) with HoxN (Fig 2.6), indicating

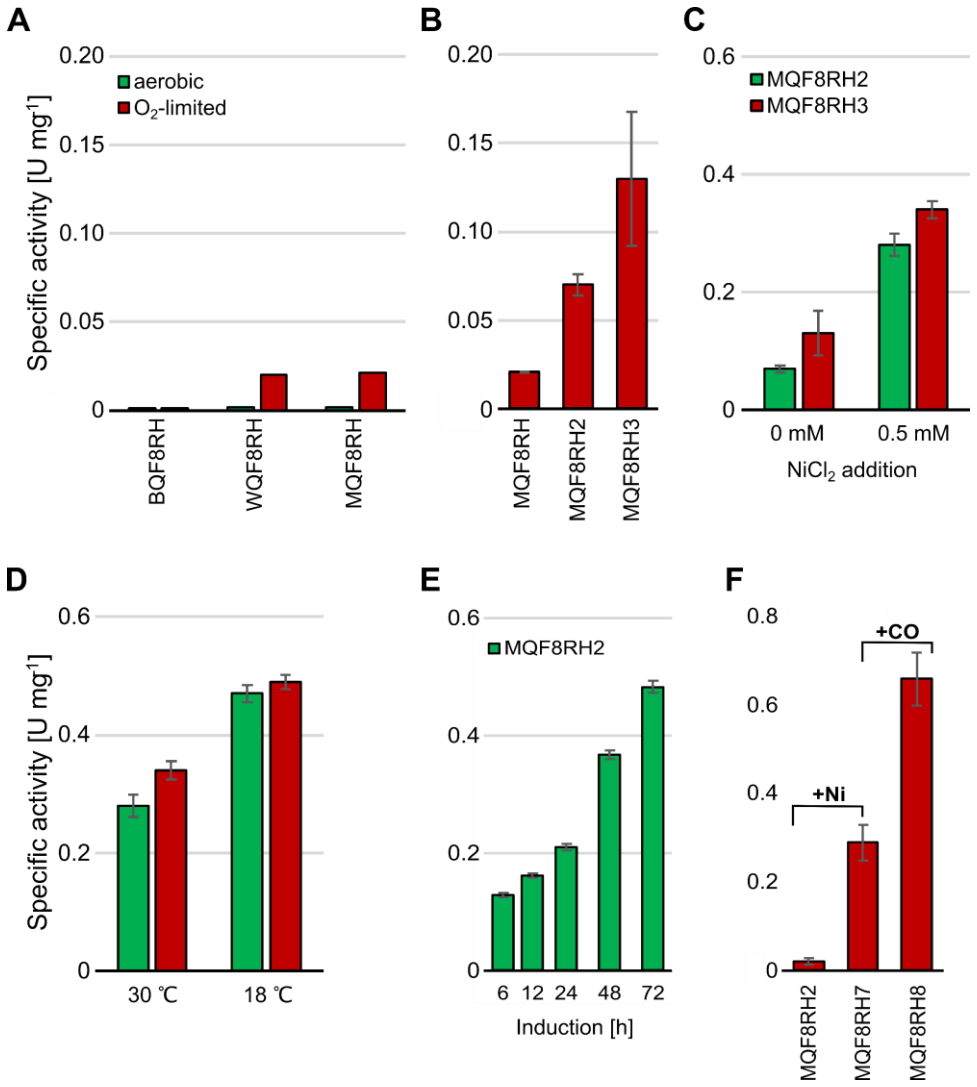

Figure 2.7 Improvement of RH activity heterologously produced in *E. coli*.
All *E. coli* cultivations were performed in 50 mL boosted EnPresso B medium with induction of 50 µM IPTG under different culture conditions (see details in **Paper III**). Different factors such as production mode and strains (A), co-expression of *R. eutropha hyp1* operon (B), nickel ion supply (C), production temperature (D) and time (E), co-production of high-affinity nickel permease HoxN and additional specific maturase HypX (F) were investigated and effects on RH activity were determined.

a relatively wide tolerance of the cultures to nickel concentration. This is unusual to the previous data obtained for HoxN, showing a reduction in the activity of nickel-containing proteins and cell growth at nickel concentration only above 1 µM (Friedrich et al. 1981; Wolfram et al. 1995; Schiffels et al. 2013). On the one hand, it

is likely due to the rapid incorporation of intracellular nickel into the apo-RH based on high RH expression levels, consequently preventing accumulation of free intracellular nickel to toxic levels. On the other hand, it is probably due to the chelating properties of organic compounds of the growth medium, e.g., peptone, which restrict the availability of free extracellular nickel. Nevertheless, based on the results (Fig 2.7), possible factors affecting the heterologous production of catalytically active hydrogenase in *E. coli*, in addition to the parameters of culture conditions and process regarding protein yield, could be clearly summarized as follows:

- Selection of appropriate production strains and suitable culture condtions
- Co-expression of specific & efficient maturation system for cofactor assembly
- Requirement of sufficient metal ions as substrates for cofactor formation
- Introduction of effective uptake systems for metal ions, particularly nickel (e.g. HoxN)
- Temperature-dependent availability of functional maturases
- Induction time-dependent cofactor maturation efficiency & activity
- Available substrates for cofactor maturation in aerated cultures (e.g. HypX)

Finally, a functional *R. eutropha* RH could be produced by the introduction of HoxN and HypX under aerated growth conditions, and somewhat surprisingly, even in the *E. coli* BL21 strains, which are known to be defective in hydrogenase biosynthesis (Pinske et al. 2011). Compared to standard single shot IPTG induction, lactose autoinduction significantly increased the volumetric RH yield by more than 2.5-fold and the space-time yield by 4-fold, respectively (**Paper II**). As expected, lactose autoinduction yielded 1.5-fold higher soluble RH yield in both strains with a similar final cell density and a comparable specific RH activity in contrast to standard IPTG induction (Fig 2.8A-C). Due to the shorter total process time and higher soluble protein yield, lactose autoinduction resulted in a 2.3-fold increase in the space-time yield of active RH reaching 38 U (L d)$^{-1}$ (Fig 2.8D). Moreover, active RH productivity obtainied from lactose autoinduced aerated EnPresso cultures was even 6-fold higher than that of O_2-limited cultures (Fig 2.3C). Therefore, the results herein confirm that

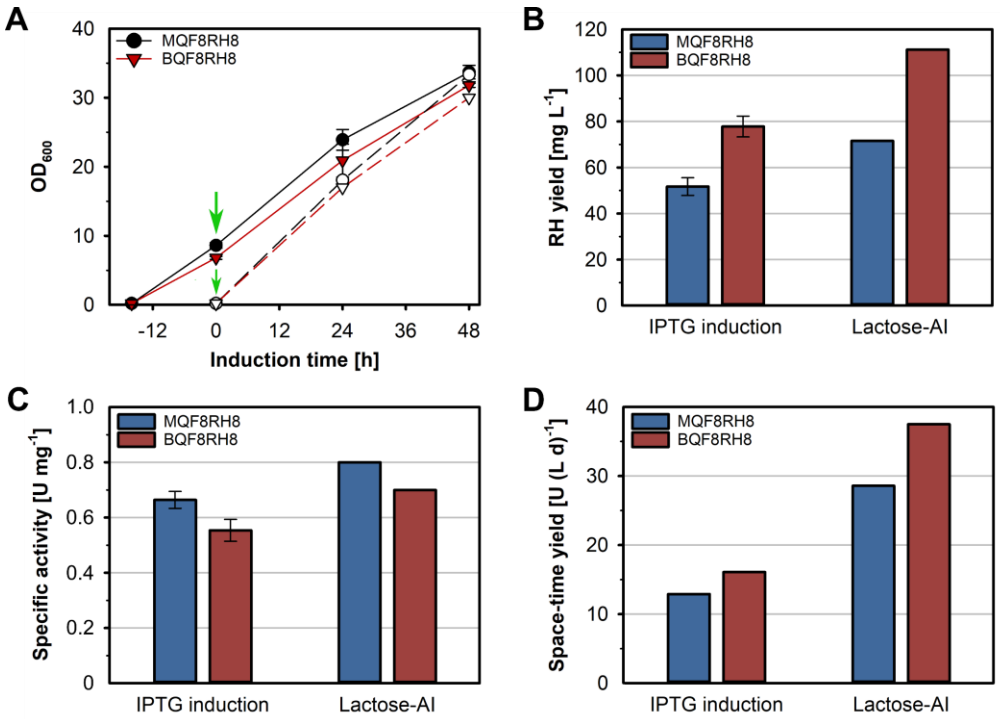

Figure 2.8 Improved soluble active RH production with lactose autoinduction in aerated EnPresso B cultures.
Strain *E. coli* MQF8RH8 and BQF8R8 were cultured in 50 mL boosted EnPresso B medium at 18 °C under aerated growth conditions. For autoinduction, 2 g L^{-1} lactose was added to induce RH production at the beginning of the cultivation. For comparison, standard single shot IPTG induction (50 µM IPTG) was performed. At the induction point, all cultures were supplemented with 0.1 mM $NiCl_2$ and cells were harvested 48 h after induction. The induction time points are inducated by green arrows. White symbols represent growth of *E. coli* cells with lactose autoinduction, while filled symbols represent growth with standard single shot IPTG induction. (A) Cell growth curves, (B) Soluble volumetric RH yields calculated from Coomassie stained gels after affinity purification, (C) Specific RH activities measured from the purified RH samples, (D) Space-time yields of active RH calculated from the results in (B) and (C), averaged over the process time.

the fed-batch autoinduction system can provide an alternative way to simplify the production process and thereby improve the active RH production. Overall, the modifications of the production process herein achieved soluble RH titers of 40-110 mg L^{-1} in shake flask cultivations with a maximal activity yield of 120 U L^{-1} and a maximal specific activity of 3 U mg^{-1}, corresponding to a several 100-fold increase in active RH production from native *R. eutropha* (0.4-1 U L^{-1} with 1-4.5 U mg^{-1}) (Bernhard et al. 2001; Caserta et al. 2020b).

4.4. Scale-up of active *Re*RH production in fed-batch bioreactor fermentation (Paper IV)

The main achievement of this thesis is the bioprocess development of a universal heterologous hydrogenase production system in *E. coli*. It is capable to be successfully employed to economically produce large quantities of difficult-to-produce metalloenzymes, subsequently facilitating the basic and applied research of those proteins. To determine the reproducibility and robustness of this optimization process for active RH production, a rationally designed fed-batch bioreactor fermentation at laboratory bench-top-scales was developed (**Paper IV**).

Before moving forward to bioreactor cultivations, however, the correlations between the nickel or iron concentrations, cell growth and active RH production in glucose mineral salt medium (MSM) cultures had to be determined, as previous studies have shown that cell growth is severely negatively influenced by higher nickel concentrations in mineral salt media (Rowe et al. 2005; Macomber and Hausinger 2011; Schiffels et al. 2013). In MSM cultures, cell growth and soluble RH production were not significantly affected by iron concentrations (up to 1 mM), but negatively impacted at nickel concentrations above 0.1 mM as indicatd by prolonged cellular adaptation. However, RH activity had a strong dependency on both metals at increasing concentrations, which ceased to increase when exceeding 0.1 mM $NiSO_4$ or 0.5 mM $FeCl_3$. The results demonstrate that the importance of glucose MSM culture supplementation with metals is required for cofactor synthesis, as in their absence no *in vitro* activity can be detected. Interestingly, the *E. coli* strain grown in glucose MSM cultures showed a relatively high tolerance to nickel concentrations up to 0.1 mM for cell growth and RH activity. This is in contrast to previous reports that the toxic nickel concentration was 1-30 µM for enzyme activity and cell growth in modified MSM cultures (Wolfram et al. 1995; Rowe et al. 2005; Kim et al. 2010, 2011; Sun et al. 2010; Schiffels et al. 2013). Taken together, the results concluded that the nickel concentration should not exceed 0.1 mM, while due to additional [4Fe4S]-cluster synthesis iron concentration should not be below 0.5 mM supplemented to the glucose MSM cultures.

To scale up the cultures to higher volumetric cell densities, two parallelized independent repeated cultivations were performed in a 3.7 L lab-scale bioreactor filled with 2 L of mineral salt medium. Here, a glucose-limited fed-batch cultivation mode

was applied, consisting of three phases: (i) an usual glucose-based batch phase, (ii) a fed-batch phase with external glucose feeding with glucose concentration as the growth limiting factor, and (iii) a production phase. 8.5 g L^{-1} glucose was used as the sole carbon source in the initial batch phase. After exhaustion of the initially added glucose (~18 h, μ_{max} of 0.25 h^{-1}), indicating the end of batch phase, external feeding of a highly concentrated glucose solution (600 g L^{-1}) started with an exponentially increasing rate over the time to ensure a targeted specific growth rate of 0.18 h^{-1}. After 29 h reaching an OD_{600} of 75, the feeding was gradually switched from exponential to a reduced constant feed, while induction of RH expression started. Additionally, the levels of glucose were below the detection limit and the acetate was below 2 g L^{-1} to avoid overflow metabolism during the entire fed-batch phase. The fermentation was supplemented with $MgSO_4$ at each increase of OD_{600} of 20 and stopped after 161 h of cultivation. The final biomass concentration was determined to be 66 g L^{-1} CDW (an OD_{600} of 150), and corresponded to a reduction in the average biomass yield $Y_{X/S}$ from 0.5 g g^{-1} to 0.3 g g^{-1} by shifting the cultivation from batch to fed-batch phase, which is within the range of the most *E. coli* strains (0.3-0.48 g g^{-1}) (Fahnert et al. 2004). A constant value of respiration quotient (RQ) around 1 and a k_La value of 1200 h^{-1} was determined in both independent fed-batch bioreactor cultivations, showing a good reproducibility of the developed high cell density fed-batch bioreactor cultivation.

RH was stably produced and gradually accumulated to a final total concentration of approx. 320 mg L^{-1} during the fed-batch bioreactor cultivations, even at specific growth rates below 0.01 h^{-1}. Stronger expression levels of RH were observed during the first 48 h of induction than during the later production phase, consequently resulting in a substantial increase in total specific concentrations followed by maintaining a constant value until the end of cultivation. The soluble RH yield and specific activity also gradually increased up to 130 mg L^{-1} and 1.23 U mg^{-1}, respectively, corresponding to a 130-fold increase in soluble RH yield (1.3-fold higher specific activity) obtained from native producer in 10 L fermenter cultivation (Bernhard et al. 2001), and even 4-fold higher than the shake-flask cultivations (**Paper III**). The results clearly indicate that the process developed herein is highly reproducible and productive. Additionally, the soluble protein yield obtained from is even several thousand-times higher than that of the *P. furiosus* [NiFe]-hydrogenase heterologously produced in *E. coli* (Sun et al. 2010), further demonstrating the value of the developed cultivation strategy.

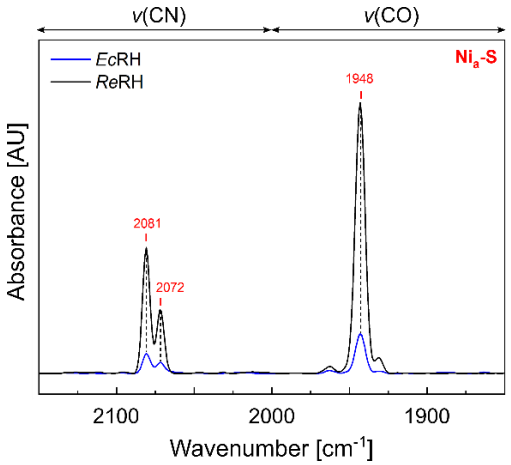

Figure 2.9 Comparison of IR spectra of RH samples purified from *E. coli* and *R. eutropha.**
The as-isolated RH samples produced from *E. coli* fed-batch bioreactor cultivation at 72 h of induction (blue line) and from *R. eutropha* (black line) were compared with IR spectroscopy. The signals indicate the presence of CO and CN ligands at the active site of RH showing the active site Nia-S state (2081, 2071, 1948 cm^{-1}).

Notably, the volumetric RH titer declined after 48 h of induction in the shake flask cultures, which was not observed in the fed-batch bioreactor cultures. It is possible that the continuous glucose feed avoids nutrient limitations. Nevertheless, the specific activity decreased by 2.5-fold compared to the maximum obtained in the shake flask cultures (**Paper III**), while the cofactor content observed by IR detection was only about 25% of that reported for the native form with a maximal specific activity of 4.5 U mg^{-1} (Fig 2.9) (Caserta et al. 2020b). It can be assumed that the RH apoprotein cannot receive cofactors as efficiently as the enzyme produced in shake flask cultures, probably due to different medium used or insufficient nickel being delivered to the cells based on high cell densities. Nevertheless, the production of soluble RH is significantly higher in the bioreactor, thus compensating for the lower specific activity compared to the shake flasks.

Interestingly, insoluble RH concentration produced always remained to 50% under high cell density glucose-limited MSM conditions, which was not observed in the previous EnPresso B-based shake flask cultivations (**Paper I-III**). It may be remarked that this negative effect on correctly folded RH solubility is significantly restricted by the cellular stress triggered by nutrient depletion in pure glucose-based MSM compared to semi-complex rich EnPresso medium (Kopito 2000; Mogk et al. 2015).

The difference may be related to the much higher cell densities and time of cultivation, which affect the adaptation of the cellular system in connection to the protein synthesis system and the stress responses. It may be hypothesized that the extracellular cAMP level could be one of the key factors, which would impact the expression strength and thus the balance between correctly folding and aggregation of target protein (Lin et al. 2004). Furthermore, the results confirm that the pure glucose-based mineral salt media are beneficial for recombinant RH produced as soluble and insoluble inclusion bodies in lab-scale high cell density cultivations, latter of which is well supported by previous studies (Fahnert et al. 2004; Neubauer et al. 2006). Besides product formation at high cell densities, expression at low growth rates may offer a positive effect by an increased stress resistance, which could be important in response to environment changes caused by high cell densitiy cultivations (Neubauer and Winter 2001). Nevertheless, measurements of the stringent response ppGpp level indicate the segregation of a part of the cell population into viable but nonculturable cells at very slow growth rates (<0.02 h-1), during the very slow growth for both recombinant and non-recombinant *E. coli* fed-batch processes (Neubauer et al. 1995; Teich et al. 1999). Thus, those may serve as analytical focus points for further improvements in terms of RH activity and solubility in larger scale high cell density bioreactor cultivations.

In summary, the first scale-up attempt is promising as shown that heterologous RH production is not distributed by effects caused by different cultivation scales, and therefore the cultivation process should be robust when providing reproducible growth conditions at different scales.

5. Conclusions

In the present work, the O_2-tolerant regulatory [NiFe]-hydrogenase from *R. eutropha* was chosen as a model to develop a general heterologous hydrogenase production system in *E. coli* towards productivity enhancement. To achieve heterologous biosynthesis of active RH, several expression plasmids encoding the RH structural subunits HoxBC and maturation proteins required for [NiFe(CN)$_2$CO]-cofactor assembly were constructed and co-expressed in different *E. coli* strains with compatible promoters.

Cultivation-relevant parameters e.g., temperature, inducer concentration and expression time significantly affected soluble RH production on TB batch cultivations. By switching from a batch to an enzyme-based fed-batch-like cultivation in shake flask scales, the initial modest soluble RH yield increased significantly by 10-fold (125 mg L^{-1}) and even by 20-fold in larger shake flask cultivations (255 mg L^{-1}, 6 mg g^{-1}), indicating a good scalability of the RH production over different shake flask scales. Accordingly, the enzyme-based fed-batch-like EnPresso B cultivation system was used for process optimization.

A combination of autoinduction and enzymatic glucose release EnProsso growth system could successfully address the glucose-dependent inducer exclusion problem, which is typically caused by the induction effect of lactose in glycerol-based autoinduction cultivation. The results showed that the fed-batch autoinduction system had a significantly positive effect on soluble RH productivity (3-fold higher than standard IPTG induction), and particularly increased the space-time yields (11.5 v.s 3 mg $(L\ h)^{-1}$) by shortening the cultivation time. Further investigations suggested that repeated boosting considerably enhanced both specific and volumetric RH yields (220 mg L^{-1} and 6 mg g^{-1} for classic single-shot IPTG induction, 366 mg L^{-1} and 7 mg g^{-1} for lactose autoinduction) due to increased cell densities, highlighting the strong dependence of RH yields on the biomass in fed-batch-like cultivations. Nevertheless, the fed-batch autoinduction system developed herein is essential advantageous as it may favor the production of target proteins by increasing or maximizing the metabolic capacity of individual cells compared to standard IPTG induction, ultimately giving rise to higher RH yields on a similar biomass basis.

Co-expression of the native Hyp maturation enzymes resulted in active RH in wildtype strains of *E. coli* grown under O_2-limited microaerobic conditions. The cofactor maturation efficiency and specific activity were obviously increased by prolonging production duration at lower temperatures. Further investigations suggested that the sufficient availability of nickel and iron ions depends on their concentration in the culture medium and on the presence and effectiveness of the necessary cellular uptake systems. Therefore, the high-affinity nickel transporter HoxN from *R. eutropha* was introduced, which allows the nickel uptake independent of regulations via FNR and NikR, thus enabling the production of functional *R. eutropha* RH under aerated growth conditions. Surprisingly, in this study, the best active RH production was achieved by introducing HoxN and HypX in *E. coli* BL21 strains which are known to be defective in hydrogenase biosynthesis. Overall, the modifications herein resulted in soluble titers of 40-110 mg L^{-1} in shake flask cultivations with an activity yield of 120 U L^{-1} and a specific activity of 3 U mg^{-1}, corresponding to a production performance for active RH that is several 100-fold better than that from native *R. eutropha* (0.1-1 mg L^{-1} with 1-4.5 U mg^{-1}).

Finally, high cell density fed-batch cultivation in lab-scale bioreactors confirmed that the RH production titers and activity yield of 130-320 mg L^{-1} and 160 U L^{-1} respectively are also possible in pure glucose-based mineral salt medium, accordingly demonstrating the scalability and robustness of the optimized heterologous RH production process from small scale cultivations to lab-scale bioreactors. The heterologous production system developed herein provides irrefutable benefits over the native producer *R. eutropha*, since the successful achievement of scale-up studies and economically feasible production are reachable. Furthermore, this work offers a good opportunity to readily supply such difficult-to-produce complex metalloproteins at large quantities efficiently and rapidly to meet the demand in basic and applied studies.

To sum up, the data obtained in this thesis advance knowledge on how to achieve high-yield heterologous production of [NiFe]-hydrogenases in *E. coli* and the current associated bottlenecks. The hydrogenase production bioprocess developed here, although complex, can provide valuable strategies for the future production bioprocess development of new complex hydrogenases. Based on the knowledge obtained from this work, a rational bioprocess strategy could be proposed to simplify the upstream bioprocess development for heterologous hydrogenase production in

E. coli (Fig 3.1). Prior to transferring the expression plasmid encoding hydrogenase subunits into *E. coli*, the metabolic issues of *E. coli* as a production host, i.e. the nickel uptake or aerobic metabolism responsible for the ability of *E. coli* to express an active [NiFe]-hydrogenase, should be addressed first. Rational strain engineering efforts on *E. coli* metabolism would provide new insights into the host's own expression level, particularly for [NiFe]-hydrogenase deficient strains, and could be considered as a possible advantageous prerequisite for future [NiFe]-hydrogenase production in *E. coli*. Afterwards, by directly targeting protein yield and activity, it can be realized for development and optimization of heterologous production of a soluble and active [NiFe]-hydrogenase in *E. coli* and process scale up based on the robust and consistent bioprocess development approaches. Accordingly, this proposed strategy can not only substantially reduce the time and material costs by avoiding unnecessary steps, but also facilitate the process development by merging the high-throughput expression optimization methods and a parallel automation platform that is integrated with the latest computational tools, modeling and process engineering, advanced controlled growth strategies and at-line process analytical techniques.

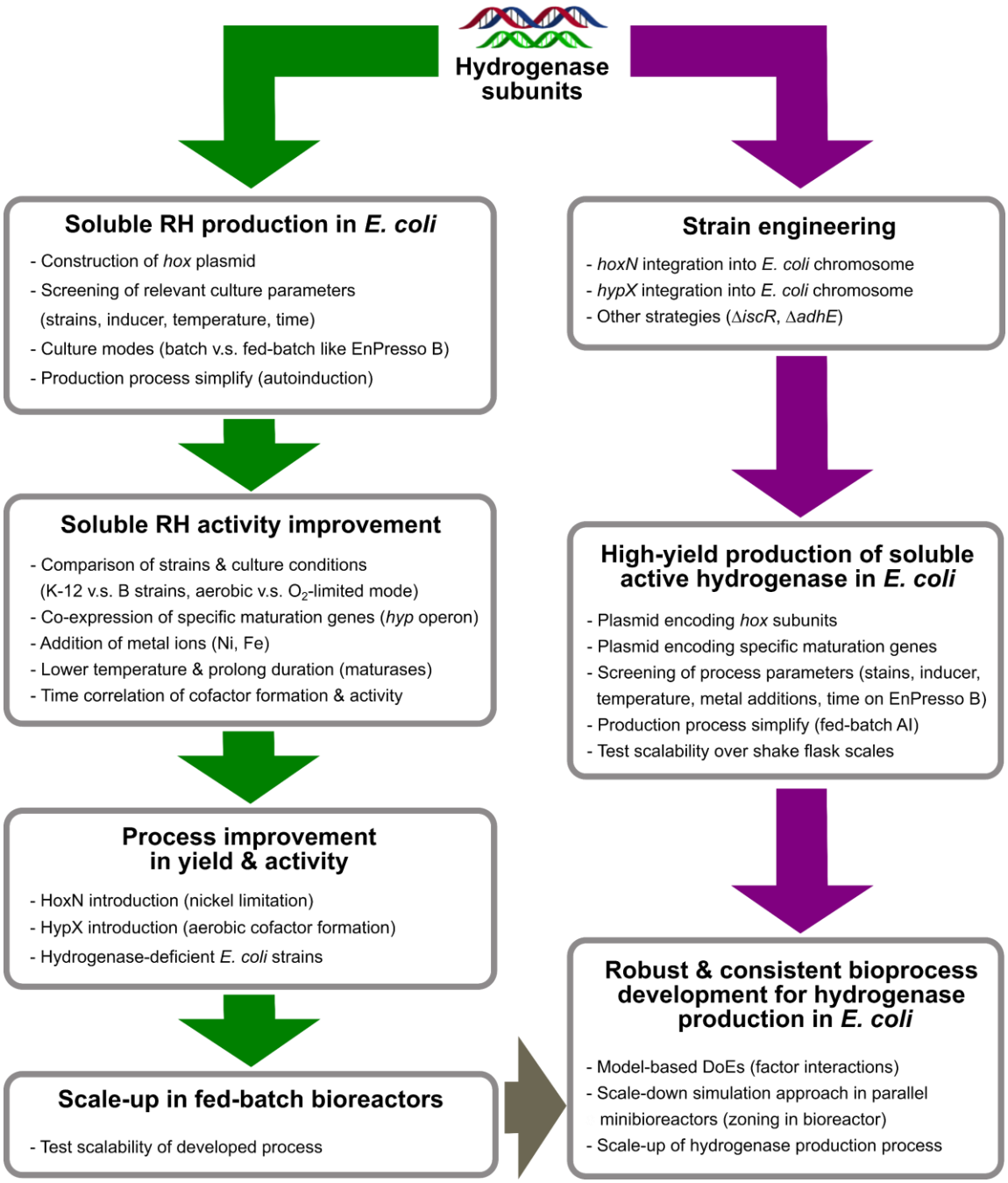

Figure 3.1 Overview of heterologous regulatory hydrogenase production process developed (green arrows) and further work of this thesis (gray) and a proposed process strategy for the production of other [NiFe]-hydrogenases from *R. eutropha* in *E. coli* (purple arrows).

6. Outlook

The heterologous production system developed in this work has successfully achieved a reasonablly high RH productivity in soluble and active form in the production host *E. coli* through approaches from gene construction to bioprocess optimization. The preliminary production levels in laboratory-scale fed-batch bioreactor cultivation appear to be very encouraging to open a solid basis for the possibility of scale-up studies to larger industrial scale production. Therefore, it would be interesting to further investigate and optimize the scalability of production processes to figure out which stressed conditions may affect the formation of the product (RH solubility) and its activity in larger scale. Further possible modifications can be done by combining an initial starter Enbase culture with a subsequent fed-batch of external glucose feeding, or providing further complex additives into the mineral salt medium like casamino acids or peptone and yeast extract, capable of improving RH production in terms of protein quality and quantity as EnPress B medium preferred RH production in a soluble form in shake flask cultures.

Alternatively, since higher biomass significantly increased RH production in shake flask cultures, a high cell density fed-batch process has to be developed in the future in order to improve the RH production. This could be implemented in the Infors Multifors (Infors HT) bioreactor system, which allow cultivations in parallel stirred tank bioreactors with a final volume of up to 1 L for investigating relevant process parameters, feeding strategies and supplementation with trace elements (mainly nickel and iron). Since autoinduction combined with fed-batch-like EnPresso growth system had a positive effect on soluble active RH yields in shake flask cultures, the use of this autoinduction approach would be of greater benefit for optimization of a scalable RH production process.

Moreover, future work will concentrate on optimizing this synthetic system to further improve the cofactor biosynthesis efficiency and RH activity based on high RH protein yields. Since introducing the nickel transporter HoxN (an intracellular membrane protein) and the specific maturase HypX (aerobic CO ligand delivery) has a stimulating effect on active site formation and RH activity, the gene fragments of HoxN and HypX could be integrated into the chromosome of *E. coli*, thus ensuring that each individual cell has the ability to take up sufficient nickel amounts and to biosynthesize sufficient CO ligand under aerated conditions. Although in this study

HoxN was co-produced with other required Hyp maturation proteins on a single plasmid in *E. coli* cells together with a structural RH expression plasmid, this may limit the HoxN expression at low concentrations of IPTG as well as the integration process into intracellular membrane of individual cells, ultimately affecting the nickel uptake capability of each cell.

RH is the first model for the development of a bioprocess for heterologous hydrogenase production in *E. coli*. However, the hydrogenase activity of RH is several orders of magnitutde lower than that of common energy-converting [NiFe]-hydrogenases, such as about 70-fold lower compared to SH from the same native host *R. eutropha*. Compared to other [NiFe]-hydrogenases from *R. eutropha*, RH is significantly less processive, which limits its biotechnological applicability. Also, SH has been extensively investigated for laboratory-scale biotechnological applications such as NAD(P)H generation, CO_2 conversion and H_2 production. Therefore, in order to demonstrate the general usefulness of the developed production strategy with RH as a model protein for production of hydrogeneases in *E. coli*, it is necessary to transfer the knowledge obtained to the production of SH from *R. eutropha* with much higher activity and applicability.

Generally, scaling a bioprocess is underestimated problem. The formation of different zones, e.g. inhomogeneous glucose and oxygen distribution in the bioreactor increases with increasing reactor size. In order to enable to produce active hydrogenase on a larger scale, it is necessary to investigate what extent these conditions affect the formation of the product and its activity. Ideally, recombinant protein production methods can be adaptable to a broad range of workflows and culture volumes, from high-throughput screening approaches in microtiter plates to larger scale production in instrumented bioreactors. In the last years, the use of high-throughput miniaturized bioreactor systems for strain screening and bioprocess development, significantly reduces the time spans from product discovery to biomanufacturing and thus the cost required for early bioprocess development. Thus, to determine the robustness of the production process, the expected stressed conditions due to zoning in the bioreactor can be simulated on a small scale using the automated high-throughput 2mag mini-bioreactor system that is integrated into a parallel automation platform for faster and effective bioprocess development. To confirm the simulated results, the production process can be afterwards gradually scaled up from 1 L to 10 L bioreactor scale.

7. Publications

Paper I

Optimization of Culture Conditions for Oxygen-Tolerant Regulatory [NiFe]-Hydrogenase Production from *Ralstonia eutropha* H16 in *Escherichia coli*

Qin Fan, Giorgio Caserta, Christian Lorent, Oliver Lenz, Peter Neubauer and Matthias Gimpel

***Microorganisms* 9, 1195**

microorganisms

MDPI

Article

Optimization of Culture Conditions for Oxygen-Tolerant Regulatory [NiFe]-Hydrogenase Production from *Ralstonia eutropha* H16 in *Escherichia coli*

Qin Fan [1], Giorgio Caserta [2], Christian Lorent [2], Oliver Lenz [2], Peter Neubauer [1] and Matthias Gimpel [1,*]

[1] Institute of Biotechnology, Technische Universität Berlin, Chair of Bioprocess Engineering, Ackerstraße 76, D-13355 Berlin, Germany; qin.fan@campus.tu-berlin.com (Q.F.); peter.neubauer@tu-berlin.de (P.N.)
[2] Department of Chemistry, Technische Universität Berlin, Straße des 17. Juni 135, D-10623 Berlin, Germany; giorgio.caserta@tu-berlin.de (G.C.); christian.lorent@tu-berlin.de (C.L.); oliver.lenz@tu-berlin.de (O.L.)
* Correspondence: matthias.gimpel@tu-berlin.de; Tel.: +49-(0)30-314-79471

Abstract: Hydrogenases are abundant metalloenzymes that catalyze the reversible conversion of molecular H_2 into protons and electrons. Important achievements have been made over the past two decades in the understanding of these highly complex enzymes. However, most hydrogenases have low production yields requiring many efforts and high costs for cultivation limiting their investigation. Heterologous production of these hydrogenases in a robust and genetically tractable expression host is an attractive strategy to make these enzymes more accessible. In the present study, we chose the oxygen-tolerant H_2-sensing regulatory [NiFe]-hydrogenase (RH) from *Ralstonia eutropha* H16 owing to its relatively simple architecture compared to other [NiFe]-hydrogenases as a model to develop a heterologous hydrogenase production system in *Escherichia coli*. Using screening experiments in 24 deep-well plates with 3 mL working volume, we investigated relevant cultivation parameters, including inducer concentration, expression temperature, and expression time. The RH yield could be increased from 14 mg/L up to >250 mg/L by switching from a batch to an EnPresso B-based fed-batch like cultivation in shake flasks. This yield exceeds the amount of RH purified from the homologous host *R. eutropha* by several 100-fold. Additionally, we report the successful overproduction of the RH single subunits HoxB and HoxC, suitable for biochemical and spectroscopic investigations. Even though both RH and HoxC proteins were isolated in an inactive, cofactor free apo-form, the proposed strategy may powerfully accelerate bioprocess development and structural studies for both basic research and applied studies. These results are discussed in the context of the regulation mechanisms governing the assembly of large and small hydrogenase subunits.

Keywords: [NiFe]-hydrogenase; *Ralstonia eutropha*; heterologous protein production; cofactor assembly; difficult-to-express protein; *Escherichia coli*

Citation: Fan, Q.; Caserta, G.; Lorent, C.; Lenz, O.; Neubauer, P.; Gimpel, M. Optimization of Culture Conditions for Oxygen-Tolerant Regulatory [NiFe]-Hydrogenase Production from *Ralstonia eutropha* H16 in *Escherichia coli*. *Microorganisms* **2021**, *9*, 1195. https://doi.org/10.3390/microorganisms9061195

Academic Editors: Hiroya Yurimoto and Dietmar Haltrich

Received: 26 April 2021
Accepted: 28 May 2021
Published: 31 May 2021

1. Introduction

Hydrogenases can be found in many bacteria and archaea as well as in a few unicellular eukaryotes [1]. According to the metal composition of the active site, they are classified as [Fe]-, [FeFe]-, and [NiFe]-hydrogenases [1]. Among the members of [NiFe]-hydrogenases, O_2-tolerant enzymes are particularly attractive as they remain catalytically active under oxic conditions, unlike all other hydrogenases [2]. This facilitates their biotechnological application in the areas of biohydrogen production, cofactor regeneration, and fuel cells [3–5]. All so-far isolated [NiFe]-hydrogenases consist of at least two subunits; a large subunit (LSU) of approximately 60 kDa housing the catalytic center and a small subunit (SSU) of approximately 30 kDa hosting one to three iron-sulfur (Fe–S) clusters [6]. The Fe–S clusters serve as an electron relay transferring reducing power towards or away from the catalytic center [7]. The catalytic center carries the heterobimetallic [NiFe] site, in which a nickel and an iron ion are bridged by two cysteines. Two further cysteines act as terminal

ligands to Ni, while one CO and two CN^- ligands participate in the coordination of the Fe [8]. The highly complicated [$NiFe(CN)_2CO$]-cofactor assembly of hydrogenases requires a dedicated set of at least six maturation Hyp proteins and a specific endopeptidase [2,9].

The β-proteobacterium *Ralstonia eutropha* H16 (also named *Cupriavidus necator*) harbors four different O_2-tolerant [NiFe]-hydrogenases; the membrane-bound hydrogenase (MBH), the soluble NAD^+-reducing hydrogenase (SH), the actinobacterial-like hydrogenase (AH), and the regulatory hydrogenase (RH) [10]. Here, we focus on the RH that functions as H_2 sensor regulating the expression of energy-converting MBH and SH proteins [2]. In addition to the RH heterodimer, consisting of the HoxB and HoxC subunits, the H_2-sensing two-component regulatory system includes the histidine kinase HoxJ and the response regulator HoxA [11] (Figure 1). Considering the high complexity of the RH system depicted in Figure 1, many in vitro studies, e.g., EPR [12], IR [13–15], Mössbauer [16], resonance Raman (RR) [17], and nuclear resonance vibrational (NRVS) [18] spectroscopy, have been carried out on a truncated version of the protein (RH_{stop}, Figure 1 right side), which allows for the isolation of the single HoxBC heterodimer [19,20]. Nevertheless, relatively low protein yields of 0.01–0.1 mg of purified enzyme per L of culture have been reported for both homologous (*R. eutropha)* [13,19,20] and heterologous (*E. coli*) [21] RH_{stop} production.

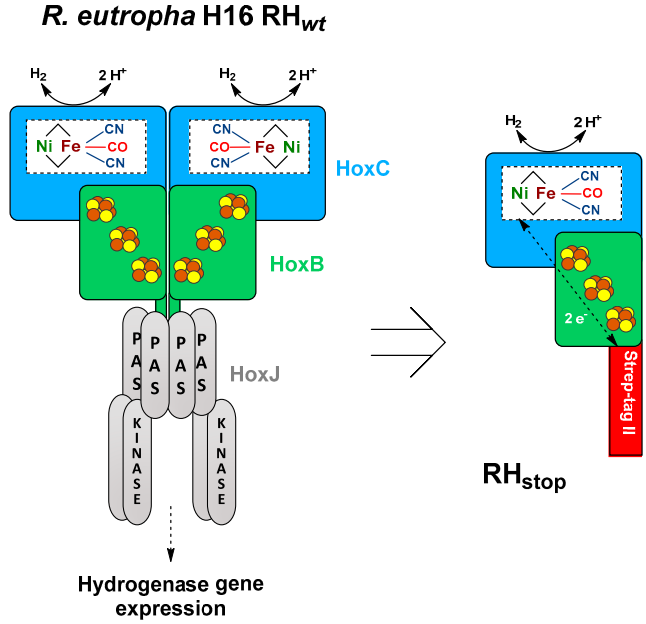

Figure 1. Schematic representation of the heterotetrameric native RH hydrogenase associated with the histidine kinase HoxJ (**left**) and the truncated heterodimeric RH_{stop} used in this study (**right**) adapted from the review of Lenz et al. [10]. The $NiFe(CN)_2(CO)$ active site is bound to the large subunit (blue) via four cysteine residues, while the small subunit (green) hosts three [4Fe–4S] clusters.

The heterologous production of hydrogenases is a challenging task [22]. However, the relatively simple architecture of the RH compared to other [NiFe]-hydrogenases and its utilization as a model system for the investigation of the catalytic cycle of [NiFe]-hydrogenases [14,23,24], prompted us to develop new strategies for heterologous high-yield productions of RH_{stop} in *E. coli* as a model for bioprocess development of heterologous [NiFe]-hydrogenase production.

Here, we report on determining parameters for improved RH overproduction resulting in the isolation of high amounts of soluble RH_{stop} protein as well as its isolated large subunit HoxC and small subunit HoxB. We used the enzyme-based glucose-release strategy (EnBase®) for high-yield RH production under small-scale fed-batch like conditions and,

subsequently, for the successful overproduction of the RH single subunits HoxB and HoxC, suitable for biochemical and spectroscopic investigations. Surprisingly, the large and small subunit hydrogenase assembly was observed in the absence of the catalytic [NiFe]-center. These results are discussed in the context of the still unknown maturation mechanism and the regulation factors governing the assembly of large and small hydrogenase subunits.

2. Materials and Methods

2.1. Bacterial Strains and Growth Conditions

E. coli TG1 (Table S1) [25] was used for cloning. For HoxBC overproduction, we used *E. coli* BL21-Gold (Agilent, Waldbronn, Germany). Unless stated otherwise, *E. coli* cultivations were performed at 30 °C in an incubation shaker at 250 rpm. Terrific broth (TB) [26] was used for batch cultivations. EnPresso B (EnPresso GmbH, Berlin, Germany) was used for fed-batch-like cultivations [27]. For all *E. coli* cultivations, 25 µg/mL chloramphenicol were added.

2.2. Plasmid Design and Construction

For the construction of a *hox* gene expression plasmid, we first removed the unique *BstBI* site of plasmid pCTUT7 (Table S2) [28] by integration of the oligonucleotides MG0034 and MG035 (Table S3) into BstBI-cut pCTUT7, yielding plasmid pQF1. Subsequently, the *Bacillus subtilis bsrF* transcription terminator [29] was integrated between the unique HindIII and BamHI sites using the annealed oligonucleotides MG0051 and MG0052, yielding plasmid pQF3. To generate a *hoxB* version that encodes a Strep-tag II sequence instead of the C-terminal HoxJ-binding domain, two subsequent PCR reactions were performed, the first on plasmid pCH594 [23] and primer pair MG0038/MG0039. The resulting fragment served as template for a second PCR reaction using the primer pair MG0038/MG0040. The resulting 0.9 kb fragment was digested with XbaI and HindIII and ligated into the corresponding pQF3 vector yielding plasmid pQF4. The primer pair MG0043/MG0044 and plasmid pCH594 as template were used to PCR-amplify a 1.5 kb fragment encoding the C-terminally Strep-tagged HoxC. The fragment was digested with XbaI and HindIII and ligated into pQF3, resulting in plasmid pQF5. For co-production of both RH subunits, an additional plasmid was constructed. To this end, a PCR was performed with plasmid pQF5 as the template and primer pair MG0041/MG0042 to generate a fragment encoding untagged HoxC. The amplicon was digested with BstBI and HindIII, and the resulting fragment was integrated into the likewise cut plasmid pQF4, yielding plasmid pQF8 (encoding $HoxB_{Strep}C$). The correctness of all constructs was verified by sequencing (LGC Genomics, Berlin, Germany).

2.3. Deepwell Plate Cultivation

Small-scale expression screenings were carried out in square-bottom 24-deepwell plates (24xDWP; Thomson Instrument Company, Oceanside, CA, USA) with a working volume of 3 mL at 37 °C in an orbital shaker. For optimal gas exchange, plates were covered with the Duetz System sandwich cover and clamp system (Enzyscreen, Er Haarlem, The Netherlands). Cultures were inoculated to an initial OD_{600} of 0.2 from a fresh overnight preculture in an Ultra Yield Flasks™ (UYF; Thomson Instrument Company, Oceanside, CA, USA) shaken at 37 °C and 250 rpm. As OD_{600} reached 0.8–1.0, 3 mL of respective cultures were transferred into the 24xDWP and expression was induced with varying concentrations of IPTG inducer (0, 5, 20, 50, 100, 500 µM, and 1 mM). Cells were harvested 5 h after induction by centrifugation for 10 min at 16,000× *g* at 4 °C and subjected to SDS-PAGE and Western blot analysis immediately. When using EnPresso B culture medium, for each well, boosting nutrients and a second dose of 1.5 U/L Reagent A were added at the induction time according to the manufacturer's instructions. Cells were cultivated for 24 h after induction in the shaker (Infor HT, 25 mm offset, Switzerland) at 30 °C, 250 rpm. Then, 0.5 mL samples were taken 6 and 24 h after induction by centrifugation for 10 min at 16,000× *g* at 4 °C. The cell pellets were stored at −20 °C until further use. Optical densities

(OD_{600}) of the cultures were determined after manually diluting 50–200 µL of the culture with 0.9% (*v*/*v*) NaCl solution and measuring the absorption at 600 nm using a Ultrospec 2100 pro spectrophotometer (Amersham Bioscience, Switzerland).

2.4. Shake-Flask Cultivation

Expression in the shake flask scale was carried out in baffled UYFs with TB or EnPresso B medium (filled to 20% of their maximum volume). All UY-flasks were sealed with adhesive air-permeable membranes (AirOTop; Thomson Instrument, Oceanside, CA, USA), and incubated with orbital shaking at 30 °C, 250 rpm. EnPresso B medium was used for fed-batch-like cultivation according to the manufacturer's recommended procedure (EnPresso GmbH, Berlin, Germany). Cultivations were performed in 50 mL or 500 mL EnPresso B medium in 250 mL or 2.5 L UY-flasks. A dose of 1.5 U/L glucose-releasing biocatalyst Reagent A was added to the medium immediately followed by inoculation to an OD_{600} of 0.2 from a log-phase LB culture. After overnight cultivation (15–18 h), target gene expression was induced by IPTG addition. If required, a booster and a second dose of 4.5 U/L Reagent A were added at the induction point. After induction, cells were cultivated for another 24 h and were then harvested by centrifugation for 10 min with 8000× *g* at 4 °C. Similarly, batch cultivations in 500–1000 mL complex TB medium were performed using 2.5 L UYF. Here, target gene expression was induced by addition of IPTG at OD_{600} of approximately 0.8. After induction, cells were cultivated for another 18–24 h and harvested as stated above. In all cases, 0.1 mL/L Antifoam 204 (0.01% *v*/*v*; Sigma-Aldrich, Steinheim, Germany) was added to prevent foam formation during UYF cultivations and OD_{600} was measured as described above.

2.5. Purification of Strep-Tagged Hox Proteins

Purification of the Strep-tagged proteins using high-capacity Strep-Tactin Superflow (IBA, Göttingen, Germany) was performed according to the manufacturer's instructions. Briefly, cell pellets were resuspended in washing buffer A (100 mM Tris-HCl, pH 8.0, 150 mM NaCl) (4 mL per g wet cell weight) supplemented with 1 mg/mL lysozyme and 1 mM PMSF and subsequently disrupted by sonication (8–10 min for each 20 mL of suspension; 30 s on/off, sonotrode with 7 mm diameter, 60% amplitude). Crude extracts were centrifuged for 30 min at 16,000× *g* at 4 °C and the soluble fraction was loaded onto a Gravity flow Strep-Tactin column. The column was washed with five bed volumes of washing buffer A, and the proteins were eluted with six bed volumes of buffer A containing 2.5 mM D-desthiobiotin. If required, eluates were concentrated by ultra-filtration (14,000× *g*, 4 °C) using Amicon Ultra Ultracel 30 kDa cut-off concentrators (Merk Millipore, Darmstadt). The final concentrate was flash-frozen in liquid nitrogen and stored at −80 °C. SDS-PAGE and subsequent quantification of the bands with ImageJ was used for determination of protein concentrations. A solution of bovine serum albumin served as the standard. All gels were visualized by staining with modified colloidal Coomassie blue G250 as reported elsewhere [30].

2.6. Western Blot Analysis

Proteins were separated in 12% SDS-PAGE gels. Semi-dry Western blotting was performed as described previously [31]. To prevent nonspecific binding of antibodies, the PVDF membrane was blocked with 2% *v/v* BSA in PBST buffer (137 mM NaCl, 2.7 mM KCl, 10.2 mM Na_2HPO_4, pH 7.4, 0.2% Tween 20). Strep-tagged proteins were immunologically detected using specific antibodies against the Strep tag (Iba GmbH, Germany) in a 1:2500 dilution and alkaline phosphatase-conjugated goat anti-mouse IgG (Sigma-Aldrich, Germany) in a 1:8000 dilution. Visualization of the membranes was achieved via the AP catalyzed reaction of the chromogenic BCIP/NBT substrates [80 µL BCIP (20 mg/mL BCIP in 100% DMF) plus 60 µL NBT (50 mg/mL NBT in 70% DMF) in 10 mL reaction buffer]. Blots were digitized with a Scan-Prisa 640U scanner and quantified with ImageJ.

2.7. Spectroscopic Analysis and Activity Assays of RH

H_2-mediated reduction of methylene blue was measured spectrophotometrically as previously described [32]. The reaction was performed in a 3-mL glass cuvette (1 cm path length) with a rubber septum at 30 °C. The methylene blue was added to the cuvette containing the reaction buffer (50 mM K_2HPO_4/KH_2PO_4, pH 7.0) to a final concentration of 200 μM. After saturating the reaction mixture with H_2, the protein samples (50–300 μM) were injected. The specific H_2-dependent reduction of methylene blue was monitored at 570 nm using a Cary 50 UV-vis spectrophotometer (Varian, Agilent) and a molar extinction coefficient of 13.1/(mM cm). Hydrogenase activity is expressed in Units (U, corresponding to 1 μmol of H_2 oxidized per min) per mg of protein. Each activity measurement lasted 20–30 min.

UV-vis absorption spectra were recorded on a Cary 300 UV-vis spectrophotometer (Varian, Agilent). The spectra were recorded between 250 nm and 800 nm using buffer A as reference. UV-vis spectra of HoxC were recorded using 200 μM and 20 μM protein solutions, respectively. Buffer A was used to adjust the protein concentrations.

EPR of RH was performed at a concentration of 0.2 mM. The measurements were carried out as previously described [13,14].

HoxC and RH proteins (0.2–0.4 mM) were transferred into a gas-tight, temperature-controlled (10 °C), transmission cell (volume ca. 7–10 μL) equipped with two sandwiched CaF_2 windows, separated by a Teflon spacer (50 μm path length). Spectra with a 2/cm resolution were recorded on a Tensor 27 Fourier-transform spectrometer from Bruker equipped with a liquid nitrogen cooled mercury cadmium telluride (MCT) detector as previously described [14]. A buffer spectrum was used as a reference to calculate the corresponding absorbance spectra. The Bruker OPUS software 7.5 package (Bruker Optics) was used for data acquisition and evaluation.

3. Results

3.1. Construction of Expression Vectors for Heterologous Hydrogenase Production in E. coli

Because of their complex structure and the sophisticated biosynthesis process, development of a bioprocess for heterologous production of [NiFe]-hydrogenase is a quite challenging task. For construction of the required expression plasmids, the pBR322 derivative pCTUT7 [28] was chosen as the basis. The plasmid carries the strong P_{lac} promoter derivative $P_{lac\text{-}CTU}$ [28] that allows IPTG-inducible hydrogenase gene expression. Plasmid pQF8 (Figure S1) harbors the RH structural genes *hoxB* and *hoxC* arranged as an operon under control of the $P_{lac\text{-}CTU}$ promoter. A Strep-tag II replaces the C-terminal domain of HoxB responsible for interaction with the histidine kinase HoxJ [33] and allows facile purification of the RH_{Stop} by affinity chromatography. The HoxC protein remained untagged. In addition, we constructed plasmids pQF4 and pQF5 (Figure S1), which encoded the single structural hydrogenase subunits HoxB and HoxC, respectively, each with a C-terminal Strep tag II sequence.

First expression experiments using *E. coli* strains TQF4B, TQF5C, or TQF8RH (*E. coli* TG1 carrying plasmids pQF4, pQF5, or pQF8, respectively) were performed at 37 °C in shake flasks containing TB complex medium. In all cases, the *hoxB* and *hoxC* genes were overexpressed and the corresponding proteins could be purified by affinity chromatography (Figure S2), demonstrating the functionality of these plasmids. The bands corresponded to the calculated theoretical molecular masses of 32 kDa, 54 kDa, and 52 kDa for $HoxB_{Strep}$, $HoxC_{Strep,}$ and untagged HoxC, respectively. In case of HoxB, however, the yield was comparatively low and a second band directly below HoxB was detected in the preparation from TQF4B, which might indicate proteolytic degradation of HoxB as recently shown (Figure S2) [34]. This was confirmed by immunoblotting, as both bands reacted with the anti-Strep-tag antibody. Nonetheless, the second HoxB band was not observed in RH samples purified from stain TQF8RH, possibly due to the presence of HoxC that might help to protect HoxB from degradation. Moreover, in all samples of purified Hox proteins, a prominent additional band with a size of approximately 60 kDa was visible.

3.2. Screening of Inducer Concentrations for HoxBC Overproduction in E. coli

The low HoxB yields and the presence of contaminating proteins in purifications from strain *E. coli* TG1 prompted us to evaluate the performance of *E. coli* strain BL21-Gold, which is frequently used for heterologous protein production. We carried out batch cultivations with 3 mL TB medium in square bottom deep-well plates and induced *hox* gene expression in strains BQF4B, BQF5C and BQF8RH by the addition of different IPTG concentrations (see Materials and Methods). As expected, increasing IPTG concentrations resulted in higher total Hox protein production (Figure 2). However, in all three cases, 50 µM IPTG were sufficient to produce more than 80% of the maximum yield obtained with 1 mM IPTG (Figure 2). Moreover, the additional HoxB band observed when using *E. coli* TG1 for overproduction (see above and Figure S2) was not detectable in HoxB preparations from strains BQF4B or BQF8RH (Figure 2), indicating higher stability of the recombinant protein in the B-strains, which might be attributed to the absence of the OmpT and Lon proteases [35,36]. Consequently, this condition was used for the following scale-up experiments in Ultra Yield flasks (UYF).

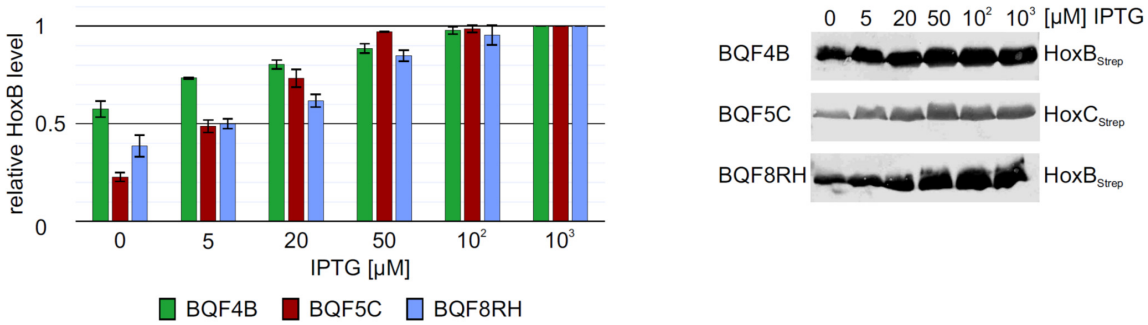

Figure 2. Heterologous overproduction of Hox proteins from plasmids pQF4, pQF5, or pQF8 in *E. coli* BL21-Gold (BQF4B, BQF5C, or BQF8RH). Cells were cultivated in TB medium in deep-well plates at 37 °C as described in Materials and Methods. RH production was induced with varying IPTG concentrations. HoxB production was analyzed by Western blotting (normalized to OD_{600}) with Strep-tag antibodies (right part) and subsequent quantification of the bands using ImageJ. For each strain, protein amounts were calculated relative to the amount of protein at a maximum inducer concentration of 1 mM IPTG.

3.3. Low Inducer Concentrations and Low Temperatures Support Production of Soluble RH

Based on the promising screening results, we moved on to process upscaling. To this end, we performed experiments with strain BQF8RH cultivated in a TB medium in UYFs. Expression of the RH genes was induced by 1 mM IPTG as this resulted in the highest RH production in the previous screening experiments (see above). SDS-PAGE analysis of the RH subunits purified by affinity chromatography revealed that the yield of both HoxB and HoxC was relatively low compared to that of cultures induced with 50 µM IPTG (Figure S3A,B). This low yield might be attributed to a loss of soluble protein due to the formation of inclusion bodies under the conditions used, which in turn might be due to an unsuitable cultivation temperature [37] or an inducer concentration that was too high [38]. To investigate the temperature effect, we reduced the cultivation temperature from 37 °C to 30 °C. In fact, we observed about 3.5-fold higher protein levels (Figure 3A) upon cultivation at 30 °C. Even growth temperatures below 30 °C could be applied to facilitate soluble protein production [39,40]. However, a further decrease of the expression temperature from 30 °C to 20 °C did not increase the yield of soluble RH protein (Figure S4). While the growth time at 20 °C reaching the same final OD_{600} increased by almost 1.5-fold compared to 30 °C, the space-time yield of purified RH decreased by almost half (Figure S4).

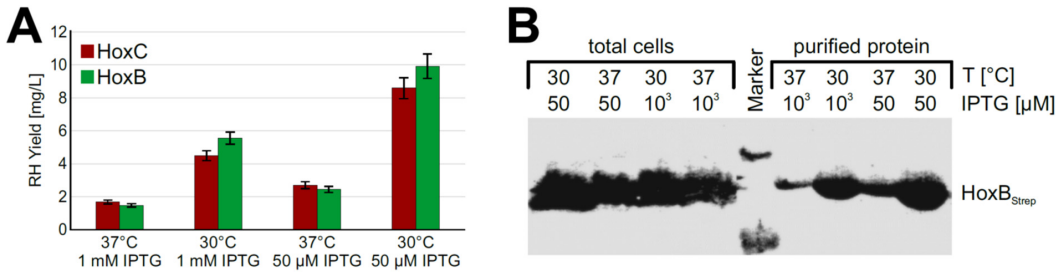

Figure 3. RH production in *E. coli* BQF8RH cultivated in 50 mL TB medium in UYF at 37 °C and 30 °C. RH production was induced with IPTG as indicated for 5 h. Soluble RH was purified by affinity chromatography and subsequently analyzed by SDS-PAGE and Western blotting. (**A**) Calculated amounts of purified RH after quantification of the stained gels in Figure S3 with ImageJ; (**B**) Western blot of total protein and soluble protein with antibodies against the Strep-tag at HoxB.

Next, we investigated the impact of the inducer concentration on the yield of soluble recombinant RH. To this end, we induced protein production with either 1 mM or 50 µM IPTG. Interestingly, the lower inducer concentration improved the yield of soluble RH about 2-fold at both 30 °C and 37 °C (Figure 3A). Similar amounts of $HoxB_{Strep}$ were produced in whole cells irrespective of the temperature and the inducer concentration (Figure 3B). However, significantly higher yields were obtained when RH_{Stop} was purified from cells grown at a lower temperature and a lower inducer concentration. Similarly, the two single RH subunits HoxB and HoxC could be produced in soluble form under these conditions using strains BQF4B and BQF5C, respectively (Figure S5).

Taken together, our results indicate that the RH as well as their single subunits can be recombinantly produced in *E. coli* and the purification of soluble RH succeeds better at lower growth temperatures and lower inducer concentrations, which seem to lower the formation of inclusion bodies.

3.4. Optimization of Expression Time

The determination of the optimal expression time is also important to increase the overall productivity of the process. To address this question, the Hox protein production levels were investigated in TB batch cultures of strains BQF4B, BQF5C, and BQF8RH, respectively. Hox protein production was induced by addition of 50 µM IPTG at OD_{600} of approximately 0.8, and the amount of produced Hox protein at different time points was analyzed by Western blotting (Figure 4). As expected, the Hox protein level increased during the first 10 h after induction for all three strains. The highest amount of total Hox protein was reached after 10 h of induction (Figure 4). No further increase in protein level was detected in TB batch cultivations upon prolonged induction for 23 h at the time when the cell growth also stopped (Figure 4). Consequently, the way to obtain high cell densities by prolonged cell growth, rather than prolonged induction time, is to increase HoxBC production, which is the subsequent aim of this study.

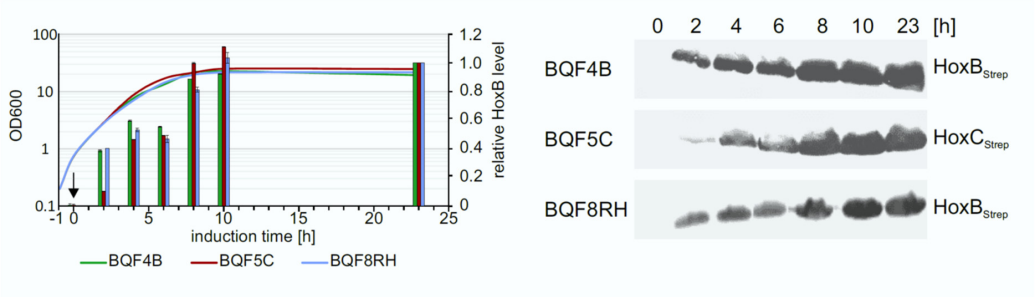

Figure 4. Time-dependent overproduction of $HoxB_{Strep}$, $HoxC_{Strep}$ and RH. Strains BQF4B, BQF5C, and BQF8RH were cultivated in 50 mL TB medium at 30 °C in UYF. Samples normalized to OD_{600} of 5 were taken at the indicated time points after the addition of 50 µM IPTG (t = 0 h). Production of Hox proteins was analyzed by Western blotting. Growth curves of the different strains and relative Hox protein levels (**left**) as quantified from the Western blot (**right**). The individual protein levels after 23 h of induction were set to 1.

3.5. Fed-Batch Like Cultivation for Heterologous RH Production in E. coli

Growth of *E. coli* in conventional complex media does not result in high cell densities [41–43]. Therefore, we applied the enzyme-based glucose delivery EnBase technology for growing our recombinant strains [27]. In this cultivation process, the continuous and automated gradual release of glucose into the medium, catalyzed by a glucoamylase, and the presence of pH-stabilizing substituents, result in high cell densities (OD_{600} = 20–50), which generally leads to higher yields of recombinant protein in small-scale shake flasks [44–46]. In addition, this technology is easy to scale-up to real, high-cell-density, fed-batch cultivations.

To improve the RH production performance of strain BQF8RH, we used the EnPresso B growth system [44,45] with or without addition of booster tablet and a second dose of glucoamylase (EnPresso GmbH, Germany) prior to induction. After growth for 18 h, gene expression was induced trough IPTG addition in concentrations ranging from 0–1 mM. Equal amounts of cells were harvested after 24 h of induction, and the individual HoxB levels were determined by Western blotting (Figure 5A). In both boosted and non-boosted cultures, respectively, increasing inducer concentrations resulted in increasing HoxB levels (Figure 5B), as already observed in TB complex medium (Figure 2). As illustrated in Figure 5B, both the boosted and the non-boosted cultures show comparable maximum HoxB yields at the highest inducer concentration. Interestingly, about 90% of the maximum HoxB yield was already attained with 50 µM IPTG in the boosted Enpresso B culture, whereas only about 45% of the maximum HoxB yield was reached in the non-boosted culture upon induction with 50 µM IPTG, indicating a positive effect of the booster on RH production at lower inducer concentration. In contrast to the batch cultivation, less leaky expression was observed in the EnPresso cultures without induction (compare Figures 2 and 5). Not surprisingly, due to the glucose-limited growth, the non-boosted cultures reached final OD_{600}s that were approximately 1.5-fold lower compared to the boosted cultures (Figure 5C). Consequently, the volumetric RH yield was about 2-fold higher in the boosted compared to non-boosted cultures (Figure 5D). A similar result of an about 2-fold increase in cell density was observed in 50-mL UYF cultures with and without booster (Figure 5D). In contrast to non-boosted cultures, the soluble RH yield per cell was slightly increased in boosted cultures, whereas approximately 2-fold higher volumetric RH yield was obtained largely due to the overall increase in the cell density (Figure 5E,F). Our results indicate that the fed-batch like growth system is suitable for inducer-dependent RH production in *E. coli* through an automated, enzyme-based glucose-release into the cultures.

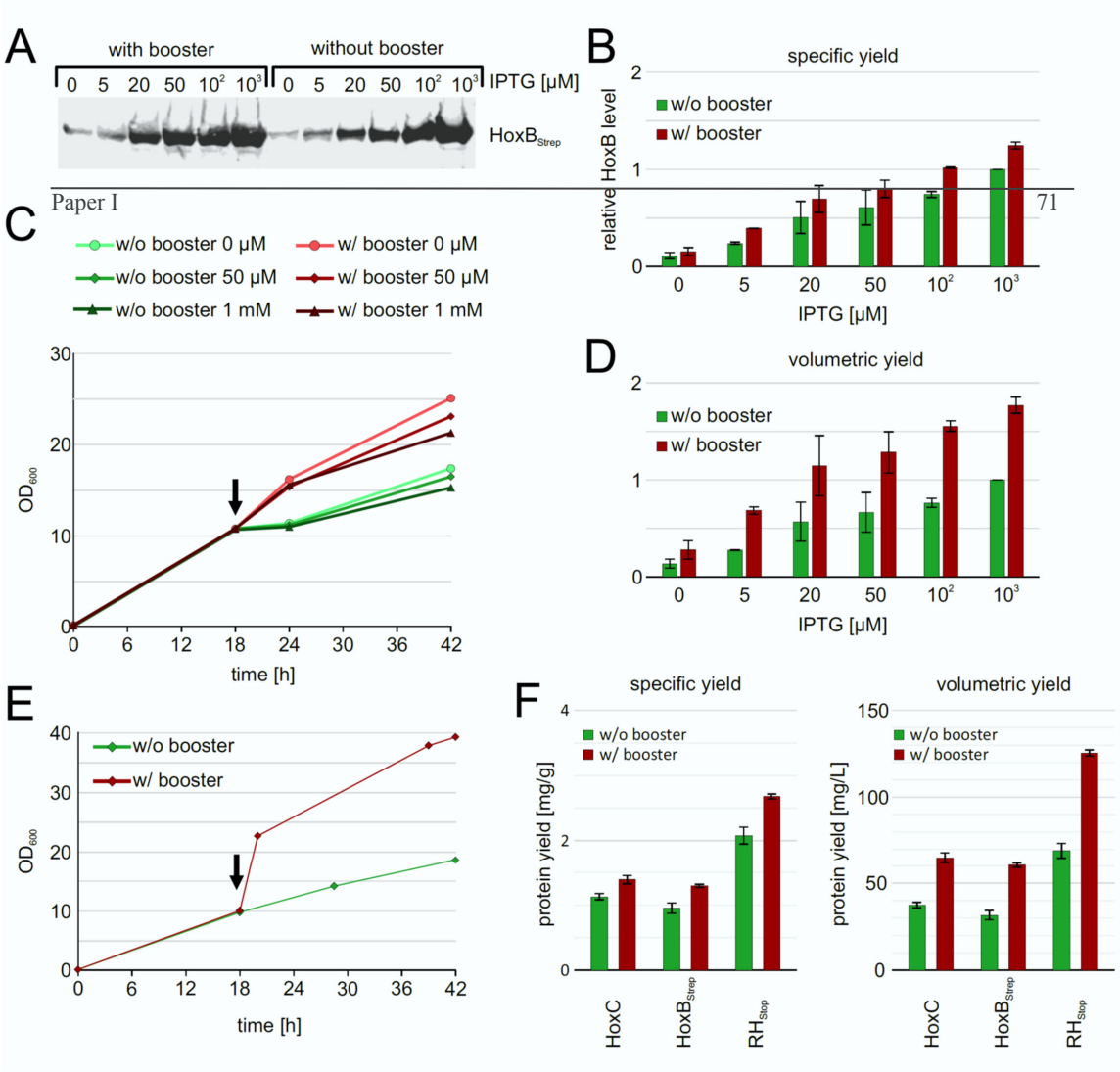

Figure 5. Heterologous production of RH by strain BQF8RH grown in EnPresso B medium with or without addition of booster. Cells were cultivated in deepwell plates at 30 °C as described in Materials and Methods. RH production was induced with varying IPTG concentrations. (**A**) Analysis of HoxB production by Western blotting with anti-Strep-tag antibodies. (**B**) Calculation of the specific HoxB yield normalized to the yield in non-boosted cultures induced with 1 mM IPTG. (**C**) Growth curve of representative cultures. The black arrow indicates the induction point. (**D**) Calculation of the volumetric HoxB yield normalized as in **B**. (**E**) Growth curves of strain BQF8RH in 50 mL EnPresso medium with or without booster in UYF. (**F**) Calculation of specific and volumetric RH yield from strain BQF8RH as grown in **E**.

3.6. Upscalable RH Production in Shake Flask in Batch and Fed-Batch Cultivations

To investigate the reproducibility of the batch und fed-batch like cultures during scale-up, we performed shake flask cultures in 2.5-L UYF with a broth volume of 500 mL (20% *v*/*v*) under optimized conditions of inducer concentration, temperature, and production strain. At the end, the cells grew slower in 2.5-L UYFs most likely due to lower oxygen transfer coefficient (K_La) values (at least 3.5-times lower) than that in 250-mL UYFs [47]. Interestingly, the slower growth positively affected RH production in both media. We were

able to achieve RH yields of 4 mg/g cell wet weight in TB and even 6 mg/g in boosted EnPresso medium (Figure 6B). The final titer was increased up to approximately 255 mg/L in EnPresso cultivations, which represents a 2-fold higher yield compared to the 500 mL TB batch culture (Figure 6) and a 2-fold increase compared to the 50 mL EnPresso cultures (Figure 5F). From these results, we conclude that a good scalability of RH production could be achieved over the shake-flask scales (250 mL vs. 2.5 L shake flasks) in terms of the volumetric and specific protein yields. A lower K_{La} value may seem to be advantageous for scale-up and facilitate RH production.

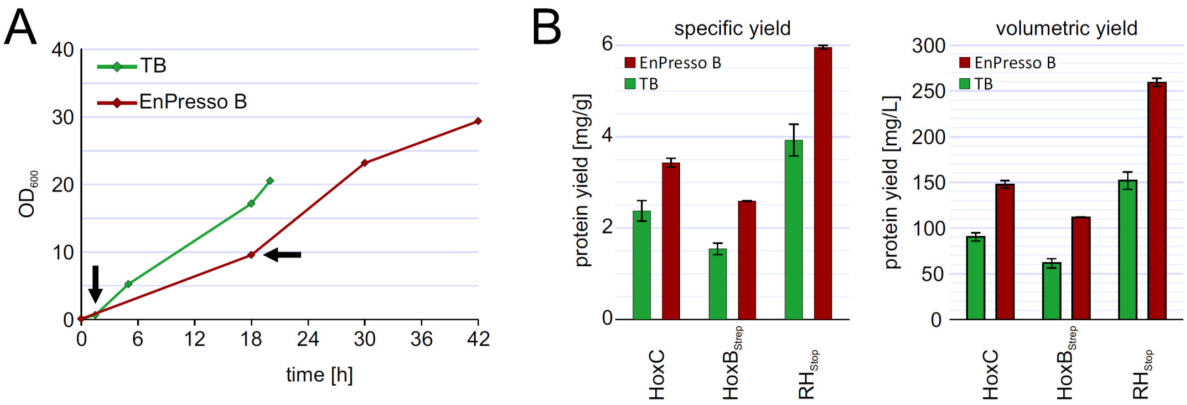

Figure 6. Up-scaling of RH production to 500 mL culture volume in 2.5 L UYF (**A**) growth curve of strain BQF8RH in complex TB or boosted EnPresso. (**B**) Calculation of specific and volumetric RH yield from strain BQF8RH as grown in **A**.

Taken together, switching from a batch to a fed-batch like system with an enzyme-based automated in situ glucose-release including steadily boosting the nutrient at the induction point to prolong cell growth and elevate cell densities greatly benefits the heterologous production of soluble RH in *E. coli*. As it has been demonstrated earlier that EnPresso-based results can be easily scaled to real glucose-limited fed-batch fermentations, the results provided should be an important basis for the design of a bioreactor-based process in larger volumes.

3.7. Biochemical and Spectroscopic Characterization of the Recombinant HoxBC and HoxC Proteins

The heterologously produced soluble $HoxC_{Strep}$ and RH_{stop} proteins from TB batch and EnPresso cultures were analyzed by SDS-PAGE (Figure S6) and subsequently assayed for hydrogenase activity. However, no H_2-mediated reduction of methylene blue was detected. The lack of activity prompted us to investigate the metal cofactor content in both proteins. Infrared (IR) spectroscopy was used to probe the ν(CO) (1870–2020/cm) and ν(CN) (2030–2150/cm) stretching modes of the CO and CN^- ligands of the [NiFe] catalytic center, which are observed in a spectral region devoid of protein contribution. Homologously produced HoxC exhibits two CO bands at 1941/cm and 1952/cm and broad CN^- signals at 2066/cm and 2084/cm, which are related to the two Ni_r-$S_{I/II}$ resting states of the catalytic center (Figure 7A) [14,18]. The IR spectrum of native RH_{stop}, on the other hand, exhibits a dominant CO band at 1943/cm and two CN^- absorptions at 2070/cm and 2081/cm, which have been previously assigned to the catalytic Ni_a-S intermediate (Figure 7B) [34]. The IR spectra of the heterologously produced HoxC and RH_{stop} proteins, however, revealed signals that are exclusively related to the protein backbone, i.e., amide II bands at 1548/cm. Thus, the IR data indicate that the lack of hydrogenase activity is related to the absence of the catalytic center. The lack of the catalytic center in the isolated HoxC protein was also supported by UV-visible spectroscopy, revealing the absence of

characteristic [NiFe] site-related absorption bands previously observed in the homologously produced HoxC protein (Figure 7C) [14].

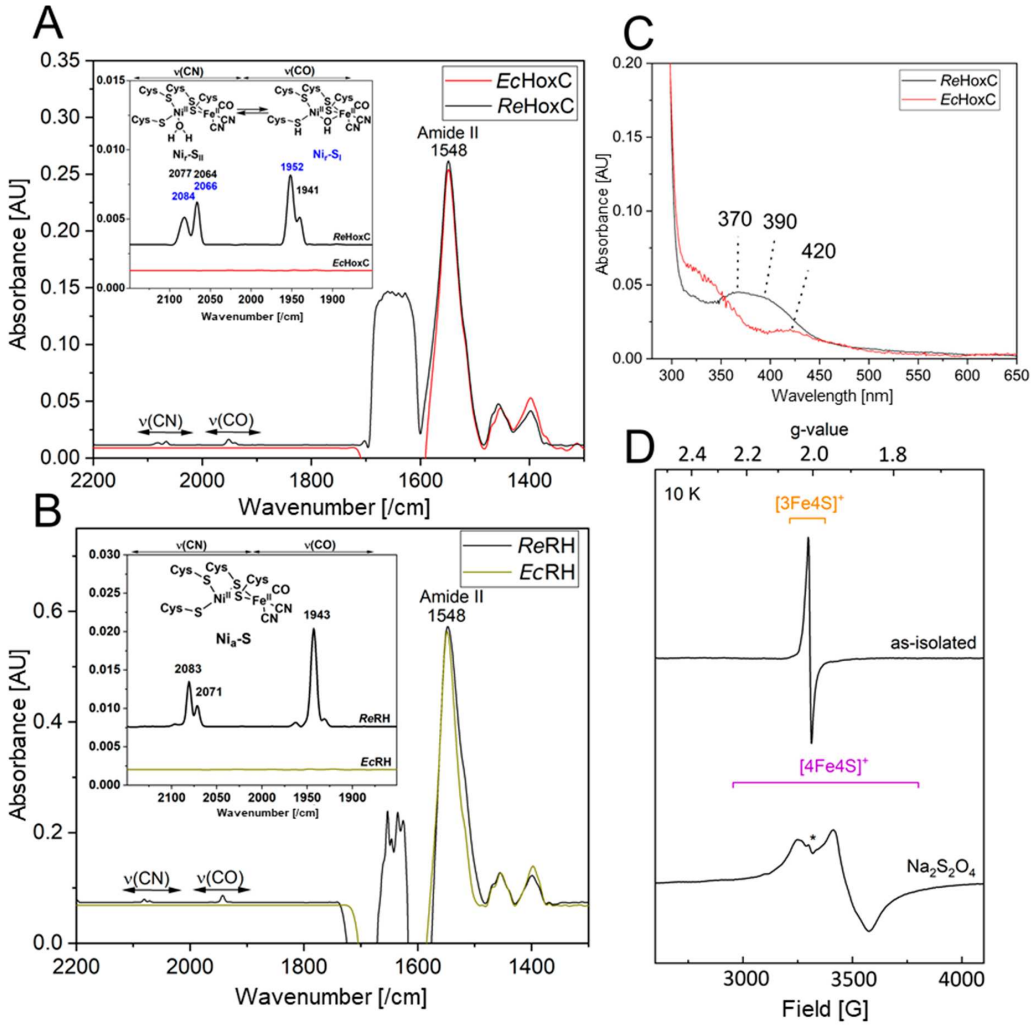

Figure 7. Comparative spectroscopic characterization of RH and isolated HoxC purified from *R. eutropha* and *E. coli*. (**A**) Comparison of IR spectra of as-isolated HoxC produced from *E. coli* (*Ec*HoxC, red line) and *R. eutropha* (*Re*HoxC, black line). (**B**) Comparison of IR spectra of as-isolated RH_{stop} produced from *E. coli* (dark yellow line) and *R. eutropha* (black line). (**C**) Comparison of UV-vis absorption spectra of 20 μM as-isolated HoxC produced from *E. coli* (red line) and *R. eutropha* (black line). The spectrum of *E. coli*-derived HoxC shows only minor absorptions around 420 nm, probably related to heme-containing protein contaminants copurified with the large subunit. HoxC from *R. eutropha* shows active site contributions characterized by two absorption bands at 370 and 390 nm [14]. (**D**) EPR spectra recorded at 10 K with a microwave power of 1 mW of as-isolated RH_{stop} (0.2 mM) from *E. coli* (top trace), containing minor contributions of a $[3Fe–4S]^+$ cluster species, in line with data recorded of native RH [34]. The bottom trace represents reduced RH_{stop} treated with an excess of sodium dithionite. The spectrum contains rhombic signals attributed to a $[4Fe–4S]^+$ cluster. The asterisk (*) denotes a weak signal, deriving presumably from a [2Fe–2S] cluster subspecies originating either from partial [4Fe–4S] cluster degradation or from protein contaminants. Spectra in **A**, **B** are normalized to the amide II band intensity at 1548/cm.

Although RH_{stop} isolated from *E. coli* showed neither detectable hydrogenase activity nor CO/CN-related bands in the IR spectrum, the protein preparations were characterized by a dark brownish color, suggesting the presence of iron-sulfur-clusters in the HoxB

subunit. To gain insight into the FeS cluster composition, we performed EPR spectroscopy on as-isolated (oxidized) as well as reduced RH_{stop} samples. Reduction was accomplished through anaerobic incubation of RH_{stop} with an excess of sodium dithionite. While as-isolated RH_{stop} (Figure 7D, top) displayed only minor signals attributed to $[3Fe\text{-}4S]^+$ clusters [34], the reduced sample (bottom) exhibited clear signals of $[4Fe\text{-}4S]^+$ clusters ($g_x = 2.043$, $g_y = 1.917$, $g_z = 1.858$), similar to those that were previously reported for the HoxB subunit isolated from *R. eutropha*. The EPR spectrum did not contain any signals related to the catalytic center, underling the fact that RH preparations originating from cultivation in *E. coli* lack the catalytic center.

In summary, the biochemical and spectroscopic characterization indicate the lack of the [NiFe] catalytic center in heterologously produced HoxC and RH_{stop}. RH_{stop}, however, seems to contain native-like iron-sulfur clusters in the HoxB subunit.

4. Discussion

In the present study, *R. eutropha* RH and its isolated HoxC and HoxB subunits were successfully produced in *E. coli* and purified from the soluble extract using a single-step affinity chromatography. In the case of RH overproduction, untagged HoxC was co-purified with Strep-tagged HoxB, indicating formation of the heterodimeric RH protein in *E. coli*, which is in good agreement with RH_{stop} forming a heterodimer in *R. eutropha* [33]. To improve RH production in *E. coli* BL21-Gold, experiments were conducted to identify optimal process parameters. Our results suggest that RH production is best upon induction of *hoxBC* gene expression with an IPTG concentration of 50 μM at a growth temperature of 30 °C. Lower culture temperatures decrease the risk of protein aggregation, because smaller protein production rates increase the likelihood of proper protein folding. In contrast, at a higher growth temperature such as 37 °C, recombinant proteins tend to form inclusion bodies [39,48,49]. Additionally, misfolded or aggregated proteins often induce the σ^H-dependent stress response which, in turn, leads to an increased activity of heat-shock proteases and subsequently to an increased degradation of the aggregated proteins [50,51]. By contrast, the activity of heat shock proteases is reduced at lower temperatures resulting in a more stable protein production [52]. However, even after lowering the cultivation temperature to 20 °C, the most prominent contaminating band in our RH preparations was still present (Figure S4B), indicating that a further decrease of the temperature would not improve the purity of the RH preparations.

Although the yield of overproduced RH_{stop} increased with increasing inducer concentration, our results showed that higher inducer concentrations negatively affect the solubility of the target protein. The use of higher inducer concentrations and the concomitant faster translation rates can exhaust the bacterial protein quality control systems and lead to improper folding of the newly translated proteins, resulting in inclusion bodies, as shown before in many studies (see e.g., p22 tailspike protein, amyloid, interleukin-1β) [53]. Consequently, IPTG-induced soluble RH production is most efficient at a low concentration of 20–50 μM in TB batch and fed-batch-like cultivation. Furthermore, we successfully applied the enzyme-based EnPresso system to produce difficult-to-express metalloproteins. Here, we achieved approximately 255 mg/L of purified RH, which is 18-times higher than that obtained in the initial batch cultures. Additionally, the production of RH in *E. coli* had a good scalability in shake-flask scales (250 mL- and 2.5 L-scale).

Surprisingly, no activity was detected in all RH_{stop} and HoxC samples purified from *E. coli*, although the proteins were soluble. This was due to the absence of the $NiFe(CN)_2(CO)$ cofactor, as confirmed by IR, EPR, and UV-vis spectroscopic data. However, these findings are not unexpected, as previous studies have demonstrated that active RH_{stop} can be heterologously produced in *E. coli* only under anaerobic cultivation conditions and upon co-production of the maturation proteins (HypA-F) from *R. eutropha* [19–21]. Moreover, expression of *E. coli hyp* genes and the specific nickel uptake system is controlled by the global transcriptional activator FNR (fumarate nitrate regulator) under anaerobic conditions [54,55]. Thus, the absence or a low level of active FNR under aerobic condi-

tions [56] might contribute to the inactivity of the RH produced in aerobically grown *E. coli*. Furthermore, the absence of the [NiFe]-cofactor in the HoxC subunit is fully in line with the observed defect in hydrogen metabolism in the biotechnologically important model bacterium *E. coli* BL21 [57].

Nevertheless, our data are in support of the fact that the RH small subunit HoxB acquires its Fe–S clusters during synthesis in *E. coli* BL21. Interestingly, the mature HoxB subunit seems to form a complex with the [NiFe] cofactor-free HoxC subunit, revealing a partially mature RH. These data are quite surprising as it was previously believed that the RH possess an intrinsic proofreading mechanism preventing the complex formation of premature subunits [58]. The RH from *R. eutropha* belongs to the [NiFe]-hydrogenases lacking the C-terminal peptide extension of the large subunit. Most [NiFe]-hydrogenase large subunits carry such a C-terminal extension [1], which is cleaved off by an endopeptidase once the $NiFe(CN)_2(CO)$ catalytic center has been incorporated into the apo-protein [9]. The presence of this peptide sequence is supposed to prevent oligomerization of the small and large hydrogenase subunits [59–61]. However, a few [NiFe]-hydrogenases are naturally devoid of a C-terminal extension, yet they seem to employ the standard Hyp apparatus to synthesize the [NiFe] catalytic center. The RH from *R. eutropha* is one of them [23]. Both RH and the isolated catalytic HoxC are fully equipped with an intact $NiFe(CN)_2(CO)$ cofactor when purified from their original host *R. eutropha* [14]. Thus, a C-terminal extension is not required for either the subunit assembly or for the interaction with the Hyp apparatus [58]. Our data on the heterologously produced RH_{stop} suggest that HoxBC assembly is not triggered by the presence of the [NiFe] cofactor. Previous data have shown that the absence of the native Hyp proteins of *R. eutropha* results in a significantly lowered amount of both the HoxB and HoxC subunits in soluble *R. eutropha* extracts, suggesting a larger instability of at least the cofactor-free large subunit and thus preventing its proper interaction with the small RH subunit [62]. Surprisingly, this control mechanism seems to not function when the RH is overproduced in *E. coli* BL21. This obvious difference between the two hosts, *R. eutropha* and *E. coli*, was quite unexpected and deserves further investigation.

Taken together, compared to previous reports [19,20], our production system can provide excellent yields of soluble apo RH and HoxC proteins, suitable for structural and functional characterizations. The overall production yield obtained with our strategy exceeds the amount of RH gained in the purification of native RH from *R. eutropha* by several 100-fold [19,20]. Even though these proteins are only produced without [NiFe] cofactor, the availability of large quantities of recombinant precursors would allow to develop new artificial semisynthetic H_2-producing catalysts in vitro, without the requirement of the canonical maturation machinery. This strategy has been proven successful in case of [FeFe]- and [Fe]-hydrogenases [22,63,64], where the incorporation of synthetic complexes contributed to the flourishing artificial enzymology.

Supplementary Materials: The following are available online at https://www.mdpi.com/article/10.3390/microorganisms9061195/s1, Figure S1: Plasmids used in this study; Figure S2: Analysis of Hox protein production in *E. coli* TG1; Figure S3: RH production in *E. coli* BQF8RH; Figure S4: Comparison of RH production at 20 °C and 30 °C; Figure S5: Production of single Hox proteins in *E. coli* BL21-Gold; Figure S6: SDS-PAGE analysis of purified HoxC and RH used for spectroscopic characterization; Table S1: Strains used in this study; Table S2: Plasmids used in this study; Table S3: Oligonucleotides used in this study.

Author Contributions: M.G. and Q.F. designed experiments together with P.N. and O.L. Q.F. carried out all molecular biological and biochemical experiments. G.C. and C.L. performed the spectroscopic IR and EPR measurements and the data evaluation. All authors analyzed the data with major contributions from Q.F. and M.G. Q.F. prepared the original draft. M.G., P.N., G.C., and O.L. revised the manuscript. All authors have read and agreed to the published version of the manuscript.

Funding: This work was supported by the Cluster of Excellence "Unifying Systems in Catalysis" (UniSysCat) coordinated by the Technische Universität Berlin and its graduate school, Berlin International Graduate School of Natural Sciences and Engineering (BIG-NSE), funded by the Deutsche

Forschungsgemeinschaft (DFG) under Germany's Excellence Strategy (EXC 2008/1-390540038). Q.F. obtained a grant from the China Government Scholarship program, 2017. G.C. and O.L. are grateful for EU financial support (Article 38.1.2, GA) within the European Union's Horizon 2020 research and innovation program under grant agreement No 810856.

Institutional Review Board Statement: Not applicable.

Informed Consent Statement: Not applicable.

Acknowledgments: The authors appreciate Ingo Zebger and Peter Hildebrandt for use of spectroscopic facilities and Janna Schoknecht for excellent technical assistance in activity measurements.

Conflicts of Interest: The authors declare no conflict of interest.

References

1. Greening, C.; Biswas, A.; Carere, C.R.; Jackson, C.J.; Taylor, M.C.; Stott, M.B.; Cook, G.M.; Morales, S.E. Genomic and metagenomic surveys of hydrogenase distribution indicate H_2 is a widely utilised energy source for microbial growth and survival. *ISME J.* **2016**, *10*, 761–777. [CrossRef]
2. Fritsch, J.; Lenz, O.; Friedrich, B. Structure, function and biosynthesis of O_2-tolerant hydrogenases. *Nat. Rev. Microbiol.* **2013**, *11*, 106–114. [CrossRef]
3. Friedrich, B.; Fritsch, J.; Lenz, O. Oxygen-tolerant hydrogenases in hydrogen-based technologies. *Curr. Opin. Biotechnol.* **2011**, *22*, 358–364. [CrossRef] [PubMed]
4. Preissler, J.; Reeve, H.A.; Zhu, T.; Nicholson, J.; Urata, K.; Lauterbach, L.; Wong, L.L.; Vincent, K.A.; Lenz, O. Dihydrogen-Driven NADPH Recycling in Imine Reduction and P450-Catalyzed Oxidations Mediated by an Engineered O_2-Tolerant Hydrogenase. *ChemCatChem* **2020**, *12*, 4853–4861. [CrossRef]
5. Lu, Y.; Koo, J. O_2 sensitivity and H_2 production activity of hydrogenases—A review. *Biotechnol. Bioeng.* **2019**, *116*, 3124–3135. [CrossRef]
6. Vignais, P.M.; Billoud, B. Occurrence, Classification, and Biological Function of Hydrogenases: An Overview. *Chem. Rev.* **2007**, *107*, 4206–4272. [CrossRef]
7. Lubitz, W.; Ogata, H.; Rüdiger, O.; Reijerse, E. Hydrogenases. *Chem. Rev.* **2014**, *114*, 4081–4148. [CrossRef]
8. Peters, J.W.; Schut, G.J.; Boyd, E.S.; Mulder, D.W.; Shepard, E.M.; Broderick, J.B.; King, P.W.; Adams, M.W.W. [FeFe]- and [NiFe]-hydrogenase diversity, mechanism, and maturation. *Biochim. Biophys. Acta-Mol. Cell Res.* **2015**, *1853*, 1350–1369. [CrossRef]
9. Lacasse, M.J.; Zamble, D.B. [NiFe]-hydrogenase maturation. In *Biochemistry*; American Chemical Society: Washington, DC, USA, 2016; pp. 1689–1701.
10. Lenz, O.; Lauterbach, L.; Frielingsdorf, S.; Friedrich, B. Oxygen-tolerant hydrogenases and their biotechnological potential. In *Biohydrogen*; De Gruyter: Berlin, Germany; München, Germany; Boston, MA, USA, 2015; pp. 61–96.
11. Lenz, O.; Friedrich, B. A novel multicomponent regulatory system mediates H_2 sensing in *Alcaligenes eutrophus*. *Proc. Natl. Acad. Sci. USA* **1998**, *95*, 12474–12479. [CrossRef]
12. Brecht, M.; van Gastel, M.; Buhrke, T.; Friedrich, B.; Lubitz, W. Direct detection of a hydrogen ligand in the [NiFe] center of the regulatory H_2-sensing hydrogenase from *Ralstonia e utropha* in its reduced state by HYSCORE and ENDOR spectroscopy. *J. Am. Chem. Soc.* **2003**, *125*, 13075–13083. [CrossRef]
13. Buhrke, T.; Brecht, M.; Lubitz, W.; Friedrich, B. The H_2-sensor of *Ralstonia eutropha*: Biochemical and spectroscopic analysis of mutant proteins modified at a conserved glutamine residue close to the [NiFe] active site. *JBIC J. Biol. Inorg. Chem.* **2002**, *7*, 897–908. [CrossRef]
14. Caserta, G.; Lorent, C.; Ciaccafava, A.; Keck, M.; Breglia, R.; Greco, C.; Limberg, C.; Hildebrandt, P.; Cramer, S.P.; Zebger, I.; et al. The large subunit of the regulatory [NiFe]-hydrogenase from *Ralstonia eutropha*—A minimal hydrogenase? *Chem. Sci.* **2020**, *11*, 5453–5465. [CrossRef]
15. Ash, P.A.; Liu, J.; Coutard, N.; Heidary, N.; Horch, M.; Gudim, I.; Simler, T.; Zebger, I.; Lenz, O.; Vincent, K.A. Electrochemical and infrared spectroscopic studies provide insight into reactions of the NiFe regulatory hydrogenase from *Ralstonia eutropha* with O_2 and CO. *J. Phys. Chem. B* **2015**, *119*, 13807–13815. [CrossRef]
16. Roncaroli, F.; Bill, E.; Friedrich, B.; Lenz, O.; Lubitz, W.; Pandelia, M.-E. Cofactor composition and function of a H_2-sensing regulatory hydrogenase as revealed by Mössbauer and EPR spectroscopy. *Chem. Sci.* **2015**, *6*, 4495–4507. [CrossRef]
17. Horch, M.; Schoknecht, J.; Mroginski, M.A.; Lenz, O.; Hildebrandt, P.; Zebger, I. Resonance Raman Spectroscopy on [NiFe] hydrogenase provides structural insights into catalytic intermediates and reactions. *J. Am. Chem. Soc.* **2014**, *136*, 9870–9873. [CrossRef]
18. Caserta, G.; Pelmenschikov, V.; Lorent, C.; Tadjoung Waffo, A.F.; Katz, S.; Lauterbach, L.; Schoknecht, J.; Wang, H.; Yoda, Y.; Tamasaku, K.; et al. Hydroxy-bridged resting states of a [NiFe]-hydrogenase unraveled by cryogenic vibrational spectroscopy and DFT computations. *Chem. Sci.* **2021**, *12*, 2189–2197. [CrossRef]
19. Bernhard, M.; Buhrke, T.; Bleijlevens, B.; De Lacey, A.L.; Fernandez, V.M.; Albracht, S.P.J.; Friedrich, B. The H_2 Sensor of *Ralstonia eutropha*. *J. Biol. Chem.* **2001**, *276*, 15592–15597. [CrossRef]

20. Buhrke, T.; Löscher, S.; Lenz, O.; Schlodder, E.; Zebger, I.; Andersen, L.K.; Hildebrandt, P.; Meyer-Klaucke, W.; Dau, H.; Friedrich, B.; et al. Reduction of unusual iron-sulfur clusters in the H_2-sensing regulatory Ni-Fe hydrogenase from *Ralstonia eutropha* H16. *J. Biol. Chem.* **2005**, *280*, 19488–19495. [CrossRef] [PubMed]
21. Lenz, O.; Zebger, I.; Hamann, J.; Hildebrandt, P.; Friedrich, B. Carbamoylphosphate serves as the source of CN^-, but not of the intrinsic CO in the active site of the regulatory [NiFe]-hydrogenase from *Ralstonia eutropha*. *FEBS Lett.* **2007**, *581*, 3322–3326. [CrossRef]
22. Fan, Q.; Neubauer, P.; Lenz, O.; Gimpel, M. Heterologous hydrogenase overproduction systems for biotechnology—An overview. *Int. J. Mol. Sci.* **2020**, *21*, 5890. [CrossRef]
23. Kleihues, L.; Lenz, O.; Bernhard, M.; Buhrke, T.; Friedrich, B. The H_2 sensor of *Ralstonia eutropha* is a member of the subclass of regulatory [NiFe] hydrogenases. *J. Bacteriol.* **2000**, *182*, 2716–2724. [CrossRef]
24. Winter, G.; Buhrke, T.; Lenz, O.; Jones, A.K.; Forgber, M.; Friedrich, B. A model system for [NiFe] hydrogenase maturation studies: Purification of an active site-containing hydrogenase large subunit without small subunit. *FEBS Lett.* **2005**, *579*, 4292–4296. [CrossRef]
25. Baer, R.; Bankier, A.T.; Biggin, M.D.; Deininger, P.L.; Farrell, P.J.; Gibson, T.J.; Hatfull, G.; Hudson, G.S.; Satchwell, S.C.; Séguin, C.; et al. DNA sequence and expression of the B95-8 Epstein-Barr virus genome. *Nature* **1984**, *310*, 207–211. [CrossRef] [PubMed]
26. Sambrook, J.; Fritsch, E.F.; Maniatis, T. *Molecular Cloning: A Laboratory Manual*, 2nd ed.; Cold Spring Harbor Laboratory Press: New York, NY, USA, 1989.
27. Neubauer, P.; Šiurkus, J.; Panula-Perälä, J.; Neubauer, A.; Ukkonen, K.; Krause, M.; Meyer, D.; Pelzer, S.; Eck, J.; Tegel, H.; et al. EnBase™–MTP based high-cell-density fermentation for high-throughput and high-content screening. *New Biotechnol.* **2009**, *25*, S161. [CrossRef]
28. Kraft, M.; Knüpfer, U.; Wenderoth, R.; Kacholdt, A.; Pietschmann, P.; Hock, B.; Horn, U. A dual expression platform to optimize the soluble production of heterologous proteins in the periplasm of *Escherichia coli*. *Appl. Microbiol. Biotechnol.* **2007**, *76*, 1413–1422. [CrossRef]
29. Preis, H.; Eckart, R.A.; Gudipati, R.K.; Heidrich, N.; Brantl, S. CodY activates transcription of a small RNA in *Bacillus subtilis*. *J. Bacteriol.* **2009**, *191*, 5446–5457. [CrossRef]
30. Kang, D.; Gho, Y.S.; Suh, M.; Kang, C. Highly sensitive and fast protein detection with Coomassie brilliant blue in sodium dodecyl sulfate-polyacrylamide gel electrophoresis [5]. *Bull. Korean Chem. Soc.* **2002**, *23*, 1511–1512.
31. Gimpel, M.; Heidrich, N.; Mäder, U.; Krügel, H.; Brantl, S. A dual-function sRNA from B. subtilis: SR1 acts as a peptide encoding mRNA on the *gapA* operon. *Mol. Microbiol.* **2010**, *76*, 990–1009. [CrossRef]
32. Lenz, O.; Lauterbach, L.; Frielingsdorf, S. O_2-tolerant [NiFe]-hydrogenases of *Ralstonia eutropha* H16: Physiology, molecular biology, purification, and biochemical analysis. In *Methods in Enzymology*; Elsevier Inc.: Amsterdam, The Netherlands, 2018; Volume 613, pp. 117–151.
33. Buhrke, T.; Lenz, O.; Porthun, A.; Friedrich, B. The H_2-sensing complex of *Ralstonia eutropha*: Interaction between a regulatory [NiFe] hydrogenase and a histidine protein kinase. *Mol. Microbiol.* **2004**, *51*, 1677–1689. [CrossRef]
34. Caserta, G.; Lorent, C.; Pelmenschikov, V.; Schoknecht, J.; Yoda, Y.; Hildebrandt, P.; Cramer, S.P.; Zebger, I.; Lenz, O. In Vitro Assembly as a Tool to Investigate Catalytic Intermediates of [NiFe]-Hydrogenase. *ACS Catal.* **2020**, *10*, 13890–13894. [CrossRef]
35. Grodberg, J.; Dunn, J.J. OmpT encodes the *Escherichia coli* outer membrane protease that cleaves T7 RNA polymerase during purification. *J. Bacteriol.* **1988**, *170*, 1245–1253. [CrossRef]
36. Gottesman, S. Proteases and their targents in *Escherichia coli*. *Annu. Rev. Genet.* **1996**, *30*, 465–506. [CrossRef]
37. Catherine, H. Schein; Mathieu, H.M. Noteborn. Formation of soluble recombinant proteins in *Escherichia Coli* is favored by lower growth temperature. *Nat. Biotechnol.* **1988**, *6*, 291–294.
38. Carrió, M.M.; Villaverde, A. Localization of chaperones DnaK and GroEL in bacterial inclusion bodies. *J. Bacteriol.* **2005**, *187*, 3599–3601. [CrossRef] [PubMed]
39. Vasina, J.A.; Baneyx, F. Recombinant protein expression at low temperatures under the transcriptional control of the major *Eschenchia coli* cold shock promoter *cspA*. *Appl. Environ. Microbiol.* **1996**, *62*, 1444–1447. [CrossRef]
40. Yamanaka, K. Cold shock response in *Escherichia coli*. *J. Mol. Microbiol. Biotechnol.* **1999**, *1*, 193–202.
41. Warnecke, T.; Gill, R.T. Organic acid toxicity, tolerance, and production in *Escherichia coli* biorefining applications. *Microb. Cell Factories* **2005**, *4*, 25. [CrossRef]
42. Sezonov, G.; Joseleau-Petit, D.; D'Ari, R. *Escherichia coli* physiology in Luria-Bertani broth. *J. Bacteriol.* **2007**, *189*, 8746–8749. [CrossRef]
43. Losen, M.; Frölich, B.; Pohl, M.; Büchs, J. Effect of oxygen limitation and medium composition on *Escherichia coli* fermentation in shake-flask cultures. *Biotechnol. Prog.* **2004**, *20*, 1062–1068. [CrossRef]
44. Panula-Perälä, J.; Šiurkus, J.; Vasala, A.; Wilmanowski, R.; Casteleijn, M.G.; Neubauer, P. Enzyme controlled glucose auto-delivery for high cell density cultivations in microplates and shake flasks. *Microb. Cell Factories* **2008**, *7*, 31. [CrossRef]
45. Krause, M.; Ukkonen, K.; Haataja, T.; Ruottinen, M.; Glumoff, T.; Neubauer, A.; Neubauer, P.; Vasala, A. A novel fed-batch based cultivation method provides high cell-density and improves yield of soluble recombinant proteins in shaken cultures. *Microb. Cell Fact.* **2010**, *9*, 11. [CrossRef]

46. Ongey, E.L.; Giessmann, R.T.; Fons, M.; Rappsilber, J.; Adrian, L.; Neubauer, P. Heterologous Biosynthesis, Modifications and Structural Characterization of Ruminococcin-A, a Lanthipeptide From the Gut Bacterium *Ruminococcus gnavus* E1, in *Escherichia coli*. *Front. Microbiol.* **2018**, *9*, 1688. [CrossRef]
47. Glazyrina, J.; Materne, E.; Hillig, F.; Neubauer, P.; Junne, S. Two-compartment method for determination of the oxygen transfer rate with electrochemical sensors based on sulfite oxidation. *Biotechnol. J.* **2011**, *6*, 1003–1008. [CrossRef]
48. Strandberg, L.; Enfors, S.O. Factors influencing inclusion body formation in the production of a fused protein in *Escherichia coli*. *Appl. Environ. Microbiol.* **1991**, *57*, 1669–1674. [CrossRef]
49. Baneyx, F.; Mujacic, M. Recombinant protein folding and misfolding in *Escherichia coli*. *Nat. Biotechnol.* **2004**, *22*, 1399–1407. [CrossRef]
50. Guisbert, E.; Yura, T.; Rhodius, V.A.; Gross, C.A. Convergence of Molecular, Modeling, and Systems Approaches for an Understanding of the *Escherichia coli* Heat Shock Response. *Microbiol. Mol. Biol. Rev.* **2008**, *72*, 545–554. [CrossRef]
51. Evans, C.R.; Fan, Y.; Ling, J. Increased mistranslation protects *E. coli* from protein misfolding stress due to activation of a RpoS-dependent heat shock response. *FEBS Lett.* **2019**, *593*, 3220–3227. [CrossRef]
52. Chesshyre, J.A.; Hipkiss, A.R. Low temperatures stabilize interferon a-2 against proteolysis in *Methylophilus methylotrophus* and *Escherichia coli*. *Appl. Microbiol. Biotechnol.* **1989**, *31*, 158–162. [CrossRef]
53. Neubauer, P.; Fahnert, B.; Lilie, H.; Villaverde, A. Protein inclusion bodies in recombinant bacteria. In *Inclusions in Prokaryotes*; Springer: Berlin/Heidelberg, Germany, 2006; pp. 237–292.
54. Messenger, S.L.; Green, J. FNR-mediated regulation of *hyp* expression in *Escherichia coli*. *FEMS Microbiol. Lett.* **2003**, *228*, 81–86. [CrossRef]
55. Eitinger, T.; Mandrand-Berthelot, M.A. Nickel transport systems in microorganisms. *Arch. Microbiol.* **2000**, *173*, 1–9. [CrossRef]
56. Unden, G.; Achebach, S.; Holighaus, G.; Tran, H.Q.; Wackwitz, B.; Zeuner, Y. Control of FNR function of Escherichia coli by O2 and reducing conditions. *J. Mol. Microbiol. Biotechnol.* **2002**, *4*, 263–268.
57. Pinske, C.; Bönn, M.; Krüger, S.; Lindenstrauß, U.; Sawers, R.G. Metabolic deficiences revealed in the biotechnologically important model bacterium *Escherichia coli* BL21(DE3). *PLoS ONE* **2011**, *6*, e22830. [CrossRef]
58. Hartmann, S.; Frielingsdorf, S.; Caserta, G.; Lenz, O. A membrane-bound [NiFe]-hydrogenase large subunit precursor whose C-terminal extension is not essential for cofactor incorporation but guarantees optimal maturation. *Microbiologyopen* **2020**, *9*, 1197–1206. [CrossRef]
59. Theodoratou, E.; Paschos, A.; Mintz-Weber, S.; Böck, A. Analysis of the cleavage site specificity of the endopeptidase involved in the maturation of the large subunit of hydrogenase 3 from *Escherichia coli*. *Arch. Microbiol.* **2000**, *173*, 110–116. [CrossRef] [PubMed]
60. Senger, M.; Stripp, S.T.; Soboh, B. Proteolytic cleavage orchestrates cofactor insertion and protein assembly in [NiFe]-hydrogenase biosynthesis. *J. Biol. Chem.* **2017**, *292*, 11670–11681. [CrossRef] [PubMed]
61. Thomas, C.; Muhr, E.; Sawers, R.G. Coordination of synthesis and assembly of a modular membrane-associated [NiFe]-hydrogenase is determined by cleavage of the C-terminal peptide. *J. Bacteriol.* **2015**, *197*, 2989–2998. [CrossRef] [PubMed]
62. Buhrke, T.; Bleijlevens, B.; Albracht, S.P.J.; Friedrich, B. Involvement of *hyp* gene products in maturation of the H_2-sensing [NiFe] hydrogenase of *Ralstonia eutropha*. *J. Bacteriol.* **2001**, *183*, 7087–7093. [CrossRef] [PubMed]
63. Shima, S.; Chen, D.; Xu, T.; Wodrich, M.D.; Fujishiro, T.; Schultz, K.M.; Kahnt, J.; Ataka, K.; Hu, X. Reconstitution of [Fe]-hydrogenase using model complexes. *Nat. Chem.* **2015**, *7*, 995–1002. [CrossRef] [PubMed]
64. Artero, V.; Berggren, G.; Atta, M.; Caserta, G.; Roy, S.; Pecqueur, L.; Fontecave, M. From enzyme maturation to synthetic chemistry: The case of hydrogenases. *Acc. Chem. Res.* **2015**, *48*, 2380–2387. [CrossRef] [PubMed]

Paper II

Production of soluble regulatory hydrogenase from *Ralstonia eutropha* in *Escherichia coli* using a fed-batch-based autoinduction system

Qin Fan, Peter Neubauer and Matthias Gimpel

***Microb. Cell Fact.* 20, 1–22**

Fan *et al. Microb Cell Fact* (2021) 20:201
https://doi.org/10.1186/s12934-021-01690-4

Microbial Cell Factories

RESEARCH Open Access

Production of soluble regulatory hydrogenase from *Ralstonia eutropha* in *Escherichia coli* using a fed-batch-based autoinduction system

Qin Fan, Peter Neubauer and Matthias Gimpel*

Abstract

Background: Autoinduction systems can regulate protein production in *Escherichia coli* without the need to monitor cell growth or add inducer at the proper time following culture growth. Compared to classical IPTG induction, autoinduction provides a simple and fast way to obtain high protein yields. In the present study, we report on the optimization process for the enhanced heterologous production of the *Ralstonia eutropha* regulatory hydrogenase (RH) in *E. coli* using autoinduction. These autoinduction methods were combined with the EnPresso B fed-batch like growth system, which applies slow in situ enzymatic glucose release from a polymer to control cell growth and protein synthesis rate.

Results: We were able to produce 125 mg L^{-1} RH corresponding to a productivity averaged over the whole process time of 3 mg $(L\ h)^{-1}$ in shake flasks using classic single-shot IPTG induction. IPTG autoinduction resulted in a comparable volumetric RH yield of 112 mg L^{-1} and due to the shorter overall process time in a 1.6-fold higher productivity of 5 mg $(L\ h)^{-1}$. In contrast, lactose autoinduction increased the volumetric yield more than 2.5-fold and the space time yield fourfold reaching 280 mg L^{-1} and 11.5 mg $(L\ h)^{-1}$, respectively. Furthermore, repeated addition of booster increased RH production to 370 mg L^{-1}, which to our knowledge is the highest RH concentration produced in *E. coli* to date.

Conclusions: The findings of this study confirm the general feasibility of the developed fed-batch based autoinduction system and provide an alternative to conventional induction systems for efficient recombinant protein production. We believe that the fed-batch based autoinduction system developed herein will favor the heterologous production of larger quantities of difficult-to-express complex enzymes to enable economical production of these kinds of proteins.

Keywords: Regulatory hydrogenase, Difficult-to-express protein, *Ralstonia eutropha*, *Escherichia coli*, IPTG autoinduction, Lactose autoinduction, Fed-batch like cultivation, EnPresso B

Background

Recombinant protein production in *Escherichia coli* is most extensively performed under the control of lactose-inducible promoter systems [1]. Alternative to manual IPTG induction of gene expression from these P_{lac}-derived promoters, autoinduction is a simple method for induction of recombinant protein synthesis.

*Correspondence: matthias.gimpel@tu-berlin.de
Chair of Bioprocess Engineering, Technische Universität Berlin, Straße des 17. Juni 135, 10623 Berlin, Germany

Cultures can be simply inoculated into autoinducing medium and grown to saturation without the need to follow the growth of the culture and add the inducer at an appropriate time. This provides huge advantages in high-throughput applications and time scheduling of shake-flask experiments. Lactose can be used as the potent and cheap replacement of IPTG as inducer for recombinant protein synthesis [2–6]. In principle, the *lac* operon is induced when allolactose derived from lactose by the active intracellular β-galactosidase, binds and inactivates the LacI repressor, thereby as a consequence of lactose uptake into the cells [7]. Autoinduction is based on the glucose catabolite repression and inducer exclusion phenomenon which is initiated by the presence of glucose [8–11]. When carbon substrate mixtures of glucose, lactose or glycerol are used, glucose is preferentially consumed followed by glycerol and lactose that also acts as inducer of P_{lac} controlled genes [12]. Studier and colleagues have explored and optimized autoinduction media. They have been successfully applied for production of target proteins in small and large scale using T7 expression systems [5, 13–15]. Interestingly, these lactose autoinduction media provided higher cell densities and target protein yields compared to manual IPTG induction in commonly used media [5, 16, 17]. Unlike IPTG, lactose is taken up by the *lacY*-encoded lactose permease and metabolized to the actual inducer allolactose in *E. coli*, resulting in a delayed induction effect [7]. Moreover, the induction effect by lactose is highly sensitive to the glucose concentration as catabolite repression results in reduced lactose uptake rates at excess glucose [7, 18, 19]. Furthermore, several defined autoinduction media including various amino acid and vitamin supplements have been successfully applied to label target proteins with isotopes or selenomethionine [5, 20–23]. Generally, glycerol as a growth-supporting carbon and energy source in lactose autoinduction media supports high cell density [24, 25]. However, in such system, recombinant protein production is highly dependent on the oxygenation level, particularly reduced production at high aeration rates due to an altered order of carbon source preference from lactose to glycerol has been observed [12]. This strong oxygen-sensitivity of protein production complicates scalability and reproducibility of autoinduction cultures or restricts the protein yields at low oxygenation level due to lower cell densities [26, 27].

Recently, the use of a combination of lactose and glucose-limited EnPressoB fed-batch medium demonstrated that glucose limitation rather than glucose starvation is important for *E. coli*, consequently protein expression works well with a continuous biocatalytic glucose release from dextrins [28–31]. Unlike in glycerol-based autoinduction media, in EnPresso-based medium lactose only serves as inducer but is not catabolized as carbon source thereby reducing the oxygen sensitivity of lactose autoinduction [31, 32]. The slow glucose release does not prevent lactose autoinduction and the lactose concentration stays approximately constant at reasonable high cell densities (OD_{600} > 20) during 24 h cultivation [32].

[NiFe]-hydrogenases are generally heterogeneous, multicomplex, metalloenzymes [33, 34]. According to their physiological function, composition and localization in the organism, [NiFe]-hydrogenases have so far been classified into five distinct groups, including membrane-bound uptake hydrogenases (MBH), cytoplasmic uptake hydrogenases and H_2 sensors (cyanobacterial, H_2-sensing hydrogenases), bidirectional hydrogenases containing additional subunits for binding soluble substrates (NAD^+ and/or $NADP^+$, MV, F420), membrane associated H_2-evolving hydrogenases and high affinity H_2-oxidizing hydrogenases [35, 36]. However, the functional core of the [NiFe]-hydrogenases is basically a heterodimeric protein with a large and a small subunit, although additional subunits are present in many of these enzymes [35, 37]. Interestingly, a few [NiFe]-hydrogenases are tolerant to O_2 which is a prerequisite for their industrial application [35, 38, 39]. The O_2-tolerant regulatory hydrogenase (RH) from *Ralstonia eutropha* H16 which is composed of the large subunit HoxC and the small subunit HoxB, together with the histidine kinase HoxJ they form the H_2-sensing complex $(HoxBC)_2HoxJ_4$ [40–42]. More recently, the single HoxBC heterodimer isolated from *R. eutropha* has been shown to maintain its catalytic activity and its tertiary structure similar to the classic hydrogenases and was widely used in a number of in vitro spectroscopic studies [41, 43–47]. From structural and functional points of view, RH is superior to other hydrogenases and considered as valuable and simplest model system for studying multicomplex hydrogenases.

We have recently reconstituted the synthesis of the RH subunits HoxBC from *R. eutropha* in *E. coli* BL21 Gold under control of a P_{lac}-derived promoter [48]. Using classical IPTG induction soluble RH was produced in batch cultivations at a modest yield of 14 mg L^{-1}. When switching to EnPresso-based fed-batch like shake-flask cultures the yield was increased more than 18-fold to approx. 255 mg L^{-1} [48], corresponding to several 100-folds increase in the RH amount purified from *R. eutropha* [44]. In this study, we aimed to examine the general applicability of autoinduction in combination with the EnPresso B glucose release growth system and the potential advantages of such a combined approach for the improvement of recombinant protein production compared to the classical single-shot IPTG induction. Using screening experiments in deepwell plates we investigated optimal IPTG and lactose concentrations for

autoinduced RH production under fed-batch like conditions. Compared to classical IPTG induction about twofold higher volumetric yields and even fourfold higher space–time yields were obtained with lactose autoinduction. Finally, the heterologous RH production in *E. coli* achieved using fed-batch based lactose autoinduction showed a good scalability in shake flask scales and can be applied to rationally designed bioreactor cultivations.

Results

Effect of concentrations of glucose/lactose ratio on RH production in EnPresso B-based autoinduction

Derivatives of the *lac* promoter are widely used in biotechnological processes for the controlled regulation of gene expression. Usually production of the recombinant protein is induced by a single shot addition of the artificial inducer IPTG at a certain point of the cultivation. In contrast, lactose-based autoinduction is a simple and rapid way to obtain high yields of a recombinant protein. In an autoinduction medium, the presence of glucose inhibits induction by lactose through catabolite repression and inducer exclusion [5]. To evaluate the suitability of autoinduction for heterologous production of the *R. eutropha* RH, we used *E. coli* BL21-Gold derivative BQF8RH (*E. coli* BL21-Gold transformed with plasmid pQF8 carrying the RH structural genes *hoxB* and *hoxC* under control of the $P_{lac\text{-}CTU}$ promoter) that allows IPTG-inducible RH gene expression [48]. Cultures were performed in 24-deepwell plates (3 mL working scale) containing non-boosted EnPresso B medium supplemented with different amounts of glucose (0.5 or 1 g L^{-1}) and lactose (0.5, 1 or 2 g L^{-1}). Similar cell growth of the *E. coli* strain was observed with all glucose and lactose combinations added (Fig. 1A). The highest cell density with OD_{600} of 12.5 was reached with addition of 1 g L^{-1} glucose and 2 g L^{-1} lactose (Fig. 1A). Thus, despite the addition of higher amounts of glucose and lactose, no noticeable effect on growth was observable. The specific production of HoxB was detected by Western blotting. As expected, no hydrogenase was produced without addition of lactose, while $HoxB_{Strep}$ was detectable in all other samples (Fig. 1B), indicating that lactose based autoinduction is feasible for RH production in *E. coli*. The highest RH level was observed in EnPresso supplemented with 0.5 g L^{-1} glucose and 2 g L^{-1} lactose.

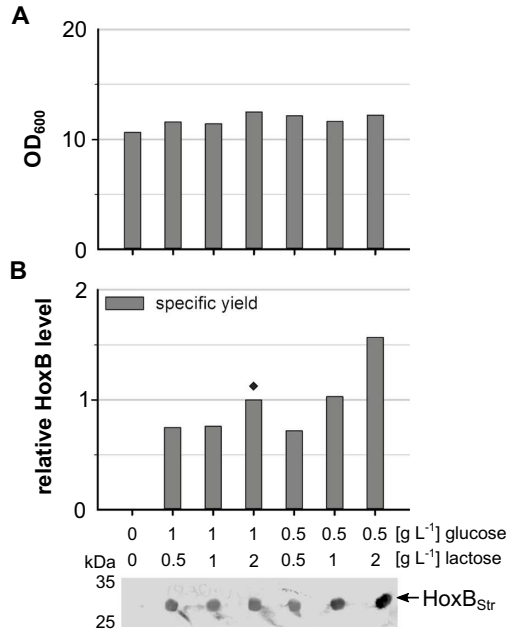

Fig. 1 Effect of glucose and lactose on cell growth and HoxB production with autoinduction. *E. coli* BQF8RH was cultivated in 3 mL non-boosted EnPresso B medium on a 24-deepwell plate at 30 °C, 250 rpm for 24 h. Different concentrations of lactose and glucose were added as indicated to trigger RH production. **A** Final cell densities. **B** Samples normalized to OD_{600} of 5 were taken and HoxB detected by Western blotting. Specific HoxB yields were calculated relative to the HoxB yield reached in autoinduction with 1 g L^{-1} glucose and 2 g L^{-1} lactose (indicated by ♦)

Screening of lactose concentrations for autoinduction of RH production

To further investigate the role of lactose autoinduction we compared RH production induced by different concentrations of lactose (0.5, 2 or 4 g L^{-1}) during growth in boosted and non-boosted EnPresso as above. Again 0.5 g L^{-1} glucose was added to the cultivations to inhibit protein expression at the beginning. As expected, the boosted cultures reached final OD_{600}s of approx. 45 after 30 h which is about threefold higher compared to the non-boosted cultures (Fig. 2A). At indicated time points samples normalized to OD_{600} of 5 were taken and $HoxB_{Strep}$ production analysed by Western blotting with Strep-tag specific antibodies. The specific HoxB level steadily increased over the cultivation time in all cultures indicating that lactose based autoinduction of RH expression is feasible (Fig. 2B, C). In both boosted and non-boosted cultures, approx. 80% of the maximum specific RH level was already reached after 6 h with all inducer concentrations tested. Interestingly, HoxB was already detectable within 2 h of cultivation, indicating that the initial glucose concentration (0.5 g L^{-1}) is low enough to allow lactose to trigger RH production during the early stage of cultivation. Furthermore, our results show that 2 g L^{-1} lactose is optimal for autoinduction, as this resulted in a slightly higher RH level relative to 0.5 or 4 g L^{-1} lactose. In addition, cultures with booster

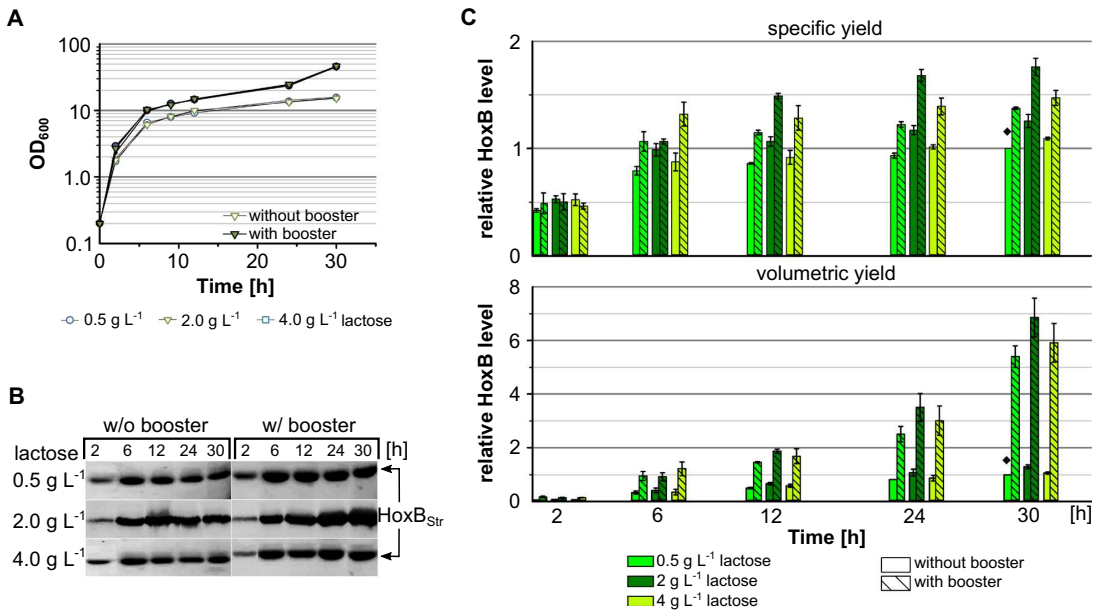

Fig. 2 RH production with autoinduction by varying concentrations of lactose. *E. coli* BQF8RH was cultivated in 3 mL EnPresso B medium with/out booster on 24-deepwell plate at 30 °C, 250 rpm for 30 h. Autoinduction was achieved by addition of different lactose concentrations as indicated and 0.5 g L^{-1} glucose. Samples normalized to OD_{600} of 5 were taken at the indicated time points and used for detection of HoxB levels by Western blotting (WB) **A** growth curve, **B** WB for detection of HoxB yields, **C** specific HoxB yield (top) and volumetric HoxB yield (bottom). Both specific and volumetric yield were calculated relative to the HoxB yield reached after 30 h in non-boosted EnPresso induced with 0.5 g L^{-1} lactose (indicated by ♦)

added from the beginning of the cultivation show a 1.4-fold higher specific RH level compared to non-boosted cultures (Fig. 2B, C) which is in good agreement with the previously observed positive effect of the booster [48]. Nevertheless, due to the higher cell density addition of booster resulted in a 4.5-fold higher final volumetric HoxB yield.

Screening of IPTG concentrations for autoinduction of RH production

The conventional induction protocol for gene expression using P_{lac} derivatives is the single shot IPTG induction which is commonly performed after reaching a certain cell density. Recently, we have demonstrated that the single shot IPTG induction of the EnPresso B cultures with IPTG concentrations between 50 and 1000 µM provided fairly similar yields of recombinant RH protein whilst low IPTG concentrations proofed beneficial for the solubility of the recombinant protein [48]. To investigate the effect of IPTG autoinduction in EnPresse B medium on cell growth and RH production, we compared RH expression induced by different concentrations of IPTG (0, 10, 20, 50, 80 or 150 µM) performed in 24-deepwell plates. Analogous to autoinduction with lactose, 0.5 g L^{-1} glucose was supplied to the media to inhibit the IPTG uptake and subsequent *hox* gene expression at the beginning of the cultivation. As before, addition of booster facilitated cell growth and resulted in final OD_{600}s above 40 which is threefold higher compared to the non-boosted cultures (Fig. 3A).

However, interestingly the strength of induction did not influence the growth neither boosted and nor for non-boosted cultures (Fig. 3A). HoxB was already detectable after 2 h of cultivation and the specific HoxB level steadily increased until 24 h of cultivation independent from booster and inducer concentration (Fig. 3C). Compared to induction with 10 or 150 µM IPTG, slightly higher RH titers were obtained by induction with 50 µM IPTG. Regardless of the inducer concentration, boosted cultures showed an approx. 1.5-fold higher HoxB level, which is in good accordance with previous results [48]. Again, the higher cell densities in boosted cultures resulted in about 5 to 6-fold higher volumetric yields compared to non-boosted cultures.

In summary, all cultures demonstrated a seemingly stable RH expression profile and steady RH accumulation

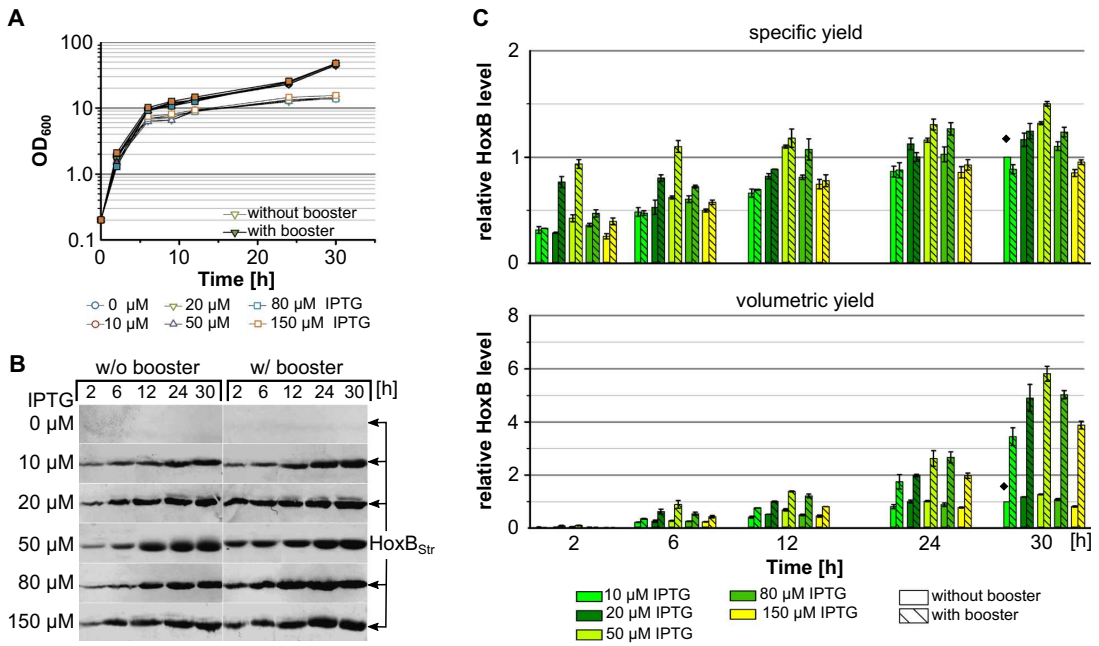

Fig. 3 RH production with autoinduction by varying concentrations of IPTG. *E. coli* BQF8RH was cultivated in 3 mL EnPresso B medium with/out booster on 24-deepwell plate at 30 °C, 250 rpm for 30 h. Autoinduction was achieved by addition of different IPTG concentrations as indicated and 0.5 g L^{-1} glucose. Samples normalized to OD_{600} of 5 were taken at the indicated time points and used for detection of HoxB levels by Western blotting (WB). **A** Growth curve, **B** WB for detection of HoxB yields, **C** specific HoxB (top) and volumetric HoxB yield (bottom). Both specific and volumetric yield were calculated relative to the HoxB yield reached after 30 h in non-boosted EnPresso induced with 0.5 g L^{-1} lactose (indicated by ♦)

during the whole cultivations. Here, the optimal concentrations for autoinduction seem to be 50 µM IPTG and 2 g L^{-1} lactose, respectively. Thus, autoinduction with lactose or IPTG can be used for recombinant RH production in fed-batch like EnPresso cultures.

Effect of glucose polymer feeding on RH production

Addition of glucose polymer to boost the EnPresso fed-batch like cultures improved final cell density and RH productivity in both classical IPTG induction [48] and autoinduction (see above). To further investigate the effect of the booster on RH production, we performed cultivation of *E. coli* BQF8RH in 24-DWPs with addition of different booster amounts. In all cases RH production was induced by either lactose or IPTG autoinduction. As expected, increasing amounts of booster gradually increased cell growth (Fig. 4A; Additional file 1: Fig. S1). Thus, this underlines the obvious influence of boosting concentrations on cell growth. Similarly, analysis of final RH levels using Western blotting (Fig. 4B) corroborates that RH production is positively affected by increased booster amounts. However, the highest specific yield is reached with 1 × booster and addition of 2 × booster did not significantly increase the specific RH yield further (Fig. 4C). Nevertheless, a slight increase in cell density with 2 × booster resulted in a slightly higher volumetric RH yield compared to the 1 × boosting. The same booster effect could be observed for both IPTG and lactose autoinduction. Moreover, comparable specific RH levels were observed independent from the autoinducer (Fig. 4B). Hence, lactose autoinduction according to the higher cell density (Fig. 4C) resulted in higher RH production titers which is consistent with the results described above.

RH production with IPTG/lactose autoinduction in shake flasks

After initial screening trials in 24-deepwell plates the cultures were scaled up to a broth volume of 50 mL cultivated in 250 mL Ultra Yield shake flasks as described in "Materials and methods". Protein production was induced for 24 h with 50 µM IPTG or 2 g L^{-1} lactose which were added into the medium together with 0.5 g L^{-1} glucose at the beginning of the cultivations. RH was purified by affinity chromatography and analysed by SDS-PAGE.

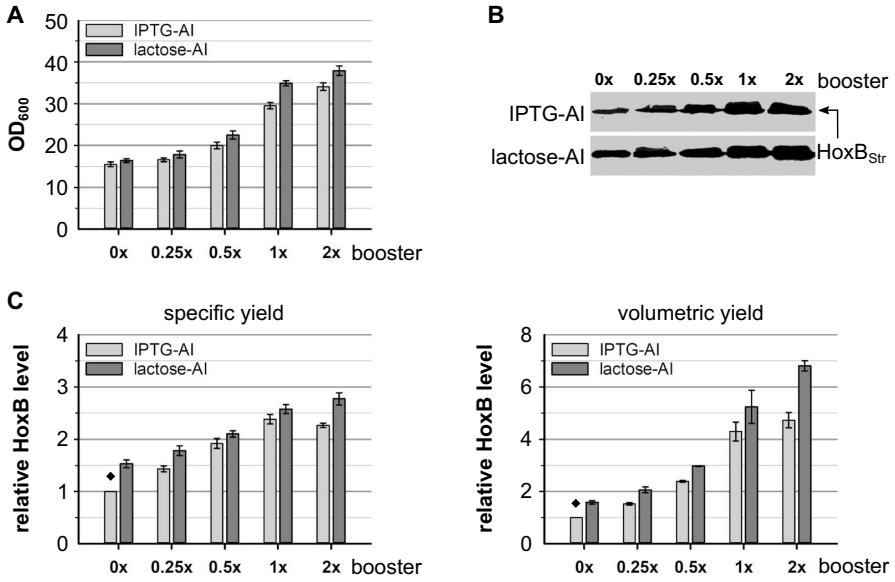

Fig. 4 Effect of glucose polymer boosting on cell growth and RH production. *E. coli* BQF8RH was cultivated in 3 mL EnPresso B medium with varying booster concentrations (0 ×, 0.25 ×, 0.5 ×, 1 ×, 2×) on 24-deepwell plate at 30 °C, 250 rpm for 30 h. RH expression was autoinduced by 50 µM IPTG or 2 g L^{-1} lactose in the presence of 0.5 g L^{-1} glucose. Samples normalized to OD_{600} of 5 were taken at the end of cultivation and used for detection of HoxB levels by Western blotting (WB). **A** Cell growth, **B** WB for detection of HoxB yields, **C** specific HoxB yield and volumetric HoxB yield. Both specific and volumetric yield were calculated relative to the HoxB yield reached in 0 × boosted IPTG-autoinduced EnPresso culture (indicated by ♦)

While the final OD_{600}s after 24 h induction did not differ significantly between IPTG and lactose autoinduction cultures, compared to single shot induction with IPTG the final OD_{600} was about 1.5-fold lower (Fig. 5A). This is probably attributed to the significantly longer cultivation time when performing single shot induction, since induction is carried out after 18 h by which time the cultures have already reached an OD_{600} of about 10. Compared to classical single shot induction with IPTG, slightly lower volumetric yields were achieved with IPTG autoinduction, whereas specific yields were slightly higher (Fig. 5B). As a consequence of the shorter total process duration when using IPTG autoinduction, the space–time yield could be elevated about 1.6-fold.

By using 2 g L^{-1} lactose for autoinduction, the results of IPTG autoinduction could be significantly exceeded. Furthermore, higher volumetric yields were obtained both in EnPresso cultures with and without booster using lactose autoinduction compared to classical IPTG induction. In particular, in boosted EnPresso cultures, a final RH production titre of 278 mg L^{-1} could be achieved. The positive effect of lactose autoinduction on RH production is also reflected in the specific yield and the space–time yield of approx. 11.5 mg $(L\ h)^{-1}$ in connection with the shorter process time, corresponding to fourfold increase compared to standard IPTG induction. As expected, for lactose and IPTG based autoinduction, booster addition improved the final volumetric and specific RH production by approximately 2- and 3-fold, respectively, compared to without booster. Therefore, it can be assumed that autoinduction provides an alternative way to enhance recombinant RH production yields.

Enhanced RH production by repeated glucose polymer feeding

The continued glucose release by supply of additional polymer booster to the medium had a positive effect on cell growth and RH production as described above. Thus, we attempted to improve the RH production by repeated continued glucose supply. Parallel cultivations in shake flasks were carried out based on classic single-shot IPTG induction with 50 µM IPTG and lactose autoinduction using 2 g L^{-1} lactose (Fig. 6). The 1st dose of booster and biocatalyst was added at the induction point and a 2nd dose of booster and biocatalyst (4.5 U L^{-1} for IPTG induction, 3 U L^{-1} for lactose-autoinduction) was added after 12 h of induction. Without glucose polymer feeding, cells reached a final OD_{600} of 18–21 after 36 h of

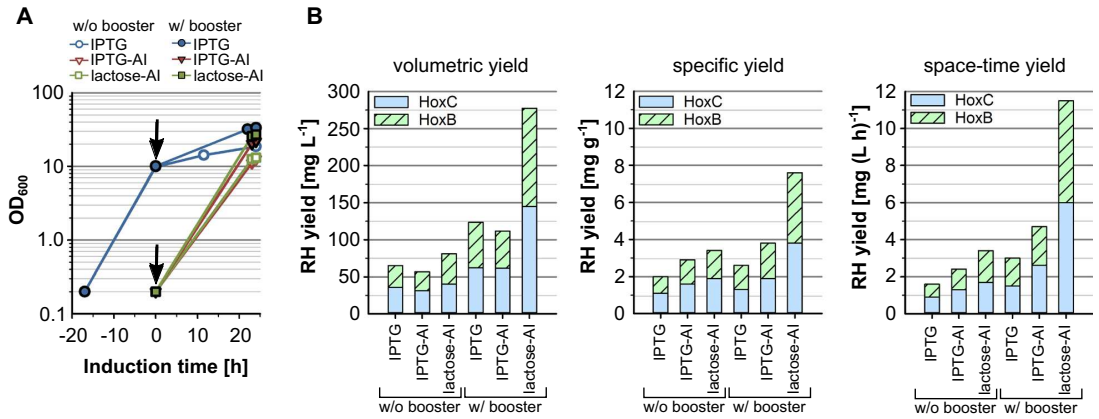

Fig. 5 Soluble RH production in EnPresso B-based UYF shake flask cultivations. *E. coli* BQF8RH was cultivated in 50 mL EnPresso B medium with/out boosting in 250 mL UYF at 30 °C. For autoinduction 50 µM IPTG or 2 g L^{-1} lactose were added to induce RH production at the beginning of the cultivation. For comparison classic single shot IPTG induction was performed. For IPTG or lactose autoinduction cultures were induced from the beginning of the cultivation and cells harvested after 24 h of growth. For classic IPTG induction cells were cultivated for 18 h without inducer. Subsequently, RH production was induced by addition of 50 µM IPTG and finally cells were harvested after 24 h of induction resulting in a total process time of 42 h. The induction time points are indicated by black arrows. **A** Growth curve, **B** Specific, volumetric and space–time yield of RH calculated from Coomassie stained gels after affinity purification and quantification with ImageJ as described in "Materials and methods"

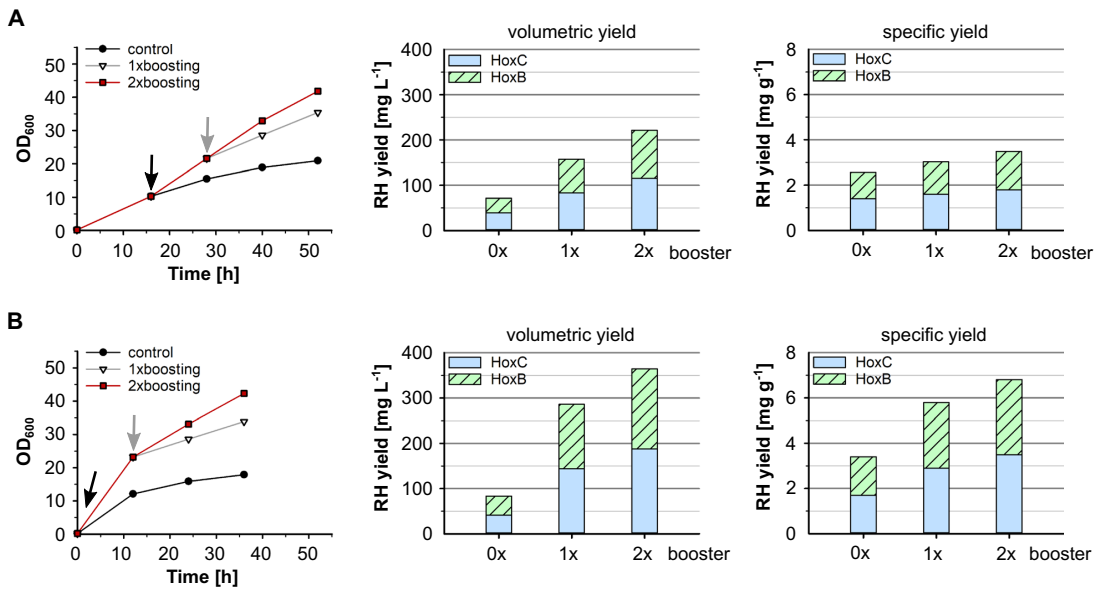

Fig. 6 Glucose polymer boosting for soluble RH production. *E. coli* BQF8RH was cultivated in 50 mL EnPresso B medium with/without boosting in 250 mL UYF at 30 °C. Growth curves, specific and volumetric RH yield are presented. The RH yields were calculated from Coomassie stained gels after affinity purification and quantification with ImageJ as described in "Materials and methods". **A** RH production using classic single-shot IPTG induction. **B** RH production using lactose-autoinduction. Black arrow: addition of booster and induction point; Grey arrow: addition of a second dose of booster

induction with IPTG or lactose, respectively. With glucose polymer feeding, the final cell density was remarkably increased in both cultivations up to an OD_{600} of 35 with single polymer feeding and even approx. 42 with repeated, two-times glucose polymer feeding. As before the addition of booster resulted not only in an increased biomass production but also in a higher specific RH yield. Consequently, the volumetric RH yield obtained with lactose autoinduction increased to 366 mg L^{-1}. Overall, a nearly twofold increase in specific RH yields could be obtained with lactose autoinduction compared to IPTG induction with a maximum of 7 mg g^{-1} using lactose autoinduction with two-times glucose polymer feeding.

Scalability of the RH production

To further evaluate the use of lactose autoinduction for RH production, cell densities and final RH yields obtained in deepwell plate and in 125 mL or 250 mL shake flask cultures were compared after 24 h of cultivation. In all three cultivation scales, comparable cell densities could be achieved regardless of the addition of the booster (Additional file 2: Table S1). However, cultivation in the 250 ml UYF resulted in slightly higher cell densities most likely due to the higher K_La values in the larger shake flask [49]. Similarly, increasing the size of the shake flask cultures had no significant negative effect on specific and volumetric RH yields (Additional file 2: Table S1). Thus, these results demonstrate the good scalability of the RH production process using fed-batch based lactose autoinduction over the shake flask and deepwell plate scales.

Discussion

Recently, we demonstrated the functionality of the enzyme-based fed-batch like EnPresso system for the heterologous production of hydrogenases in *E. coli* using the regulatory hydrogenase from *R. eutropha* as a model [48]. With a classical IPTG induction, RH titers of 130–260 mg L^{-1} could be achieved in shake flask scale. Here, low IPTG concentrations of 50 µM favour the solubility of the RH and the use of the booster increases the specific as well as the volumetric yield [48]. Based on this, in the present work we wanted to evaluate the possibility of enhancing RH production using autoinduction. Initial experiments in deepwell plates indicated that heterologous RH production in *E. coli* using autoinduction with lactose is possible (Figs. 1 and 2). The comparison of different lactose amounts used for autoinduction indicated that an intermediate lactose concentration of 2 g L^{-1} is optimal for RH production. Even though 4 g L^{-1} lactose resulted in slightly higher final OD_{600}, the highest specific and even volumetric RH yield was obtained after autoinduction with 2 g L^{-1} lactose (Fig. 2). This is in good accordance with the work of Ali [50] who proposed that low lactose concentrations (0.1—2.0 g L^{-1}) would be more profitable for autoinduction in EnPresso B-based fed-batch like cultures, as high lactose concentrations (˃2 g L^{-1}) would lead to a longer batch phase consequently resulting in more biomass but less protein production [50]. Likewise, the faster growth in the presence of high lactose concentrations could lead to oxygen limitation, which further reduces protein synthesis [50]. On the contrary, higher lactose concentrations have been reported to provide an additional benefit for better induction of prolonged protein expression in the autoinduction systems [51, 52]. However, the use of the EnBase fed-batch like system with slow gradual glucose feeding enables slow protein synthesis with slowly growing cells [53, 54]. Previously, 0.3 g L^{-1} have been calculated as the lowest external lactose concentration sufficient for induction of recombinant protein production in *E. coli* growing at the minimal growth rate, whereas 4.1 g L^{-1} lactose is essential to ensure induction at any growth rate [55]. The sufficiency of relatively low lactose concentrations for successful autoinduction in enzymatic glucose supply systems might be attributed to the constant lactose concentration observed during 24 h of cultivation [32]. In such systems, the continuous glucose release prevents an diauxic growth shift and consequently lactose consumption while the product is slowly but steadily produced in a correctly folded form [32]. In our case, 2 g L^{-1} lactose seems to be optimal for autoinduction of soluble RH production in EnPresso B fed-batch like cultured *E. coli*. Nevertheless, the minimal lactose concentration of 0.5 g L^{-1} was enough for induction of recombinant RH synthesis which is perfectly supported by the result of Mayer et al., who proposed that slow growth might contribute to reduce the need of lactose [32].

Recently, it had been reported that IPTG can replace lactose in the classic lactose-based autoinduction system to enhance protein production in batch cultures [52]. At low IPTG concentrations (< 100 µM) the inducer is actively transported into the cell by the lactose permease LacY, while at higher IPTG concentrations used for normal induction (200–1000 µM) the inducer enters the cell by passive diffusion [52, 56]. Thus, the expression level is controlled by the IPTG uptake while the excessive inducer remains in the culture medium [57, 58]. Here, our results show that IPTG-based autoinduction is also suitable for heterologous production of RH. Although 10 µM IPTG was sufficient for the induction of RH expression, the highest yield was achieved with 50 µM IPTG (Fig. 3) which is in clear line with previous studies that only partial induction was achieved at IPTG concentrations below 40 µM. This is probably due to the fact that either the amount of IPTG is not sufficient to remove all repressor molecules from the operator site

in the induced cells, or that only a subpopulation could be induced by the limited amount of externally available IPTG. [57, 58]. In our case, 50 µM IPTG seems to be enough for full induction of RH expression under control of the bistable *lac*-derived operon. RH production started already within the first 2 h of cultivation, indicating the absence of an induction delay which typically occurs in conventional glycerol-based autoinduction medium [12]. Our observations are in clear line with recent findings that protein synthesis occurs under conditions where the glucose concentration drops below 0.3 g L^{-1} in fed-batch like cultures [32]. Thus, we estimate that the initial glucose concentration of 0.5 g L^{-1} seems to be low enough to allow the uptake of IPTG or lactose and consequently inducing P_{lac}-controlled gene expression in EnPresso-based cultures.

When the cultures were scaled up from squared deepwell plates to different UYF scales no significant difference in cell growth was observed. Despite 4 times higher K_La values in the 250 ml UYF compared to the deepwell plate [59, 60], similar final cell densities were achieved. This suggests that the availability of oxygen is not a limiting factor which is well supported by previous work showing a reduced sensitivity to the oxygenation level by lactose autoinduction [31]. Our results indicate that the process can be scaled up or down very well. Thus, the fed-batch based lactose autoinduction is suitable for automated high-throughput screenings as a starting point for the development of analogue bioprocesses aimed at the production of difficult to express proteins, e.g. hydrogenases. Additionally, the good scalability of the RH production process in the current shake flask scales (125 mL- and 250 mL-scale) the fed-batch based lactose autoinduction can be applied to rationally designed bioreactor cultivations. Recent studies have shown that the lactose autoinduction concept coupled with an enzymatic glucose release system, compared with glycerol-based systems, is more widely applicable to shaken and stirred bioreactor cultivations with different scales and different aeration capabilities [31, 32].

Compared to non-boosted EnPresso B cultures, booster supplementation increased the volumetric RH production by 2 to 3-fold, as glucose released from the booster provided an additional carbon source for cell growth and protein production resulting in higher protein yields. The importance of the booster is indicated by higher cell densities as well as higher specific RH yields (Fig. 4C) that could be reached with increasing booster concentrations. However, specific RH production did not significantly increase further when using 2 × booster (Figs. 4 and 6) indicating a crucial limit of the booster effect on the RH production capability of individual cells. Nevertheless, repeated boosting improved both specific and volumetric RH yield by 1.3-fold compared to single boosting and even by fourfold compared to non-boosted cultivation, which confirms the positive influence of the booster on RH production and is in good agreement with previous findings [61]. Here, our results highlight the high dependence of RH production yields on the cell densities under both classic single shot IPTG induction and autoinduction of EnPresso fed-batch like cultures.

A comparison of RH yields obtained from cultures in UYFs induced with either classical single shot IPTG induction or autoinduction further corroborated the use of autoinduction for hydrogenase production in *E. coli*. While no significant differences in the specific yield could be observed between both IPTG induction protocols, a fourfold increase in volumetric and specific RH yield was obtained by autoinduction with 2 g L^{-1} lactose compared to optimized single-shot IPTG induction, pointing out an alternative possibility of recombinant protein production in *E. coli*. Furthermore, the similar volumetric yields together with the shorter cultivation time resulted in a space time yield of nearly 12 mg $(L\ h)^{-1}$ with lactose autoinduction in EnPresso B medium which is fourfold higher compared to standard IPTG induction.

Our results presented in this study reconfirm the applicability of such fed-batch lactose autoinduction and the use of IPTG in fed-batch like autoinduction for the production of recombinant proteins in general and of difficult-to-express proteins such as hydrogenases in particular. To date, despite extensive studies on autoinduction systems, all of them using optimized defined media have generally achieved higher final yields of target proteins by increasing final biomass compared to standard IPTG induction [14, 16, 47]. However, our fed-batch autoinduction system ultimately resulted in higher protein yields based on a similar biomass, probably due to an increased or maximized metabolic capacity of individual cell in favor of target protein production. Therefore, this interesting finding renders our developed system potentially advantageous over previous autoinduction systems and of practical implications in terms of improvement of recombinant protein production in the future.

Conclusion

Here, we combined the autoinduction concept with the fed-batch like enzymatic glucose release technology to improve heterologous regulatory hydrogenase production in *E. coli*. Taken together, the findings of this study lay a foundation for using this developed approach for efficient production of other similar proteins in future studies of structural and functional characterization as well as biotechnological applications.

Materials and methods

Bacterial strain and culture medium

For all cultivations *E. coli* BQF8RH (BL21-Gold [*E. coli* B F^- *ompT hsdS*(r_B^- m_B) dcm^+ Tet^R *gal endA Hte*] harbouring plasmid pQF8) [48], was used. The plasmid allows production of both HoxC and C-terminally strep-tagged HoxB under control of the strong P_{lac} derivative $P_{lac\text{-}CTU}$ [48]. If not stated otherwise all cultivations were carried out in EnPresso B medium according to the manufactures (EnPresso GmbH, Germany) and 25 µg mL^{-1} chloramphenicol were added.

Cultivation in 24-deepwell plates

Screening of conditions for autoinduction of *hox* gene expression was performed in square-shaped 24-deepwell plates (24-DWP; Thomson Instrument Company) covered with sterile Breathable Film seal (Starlab, Hamburg, Germany) using EnPresso B with or without addition of booster in a working volume of 3 mL per well. In both cases 3 U L^{-1} biocatalyst were used to catalyse glucose release. In deviation from the manufacturer's instructions, the booster was added directly at inoculation. Cultures were inoculated to OD_{600} of 0.2 and incubated at 30 °C and 250 rpm with orbital shaking (25 mm offset, Infor HT, Switzerland). Cell density and target protein level were analysed at five time points during the cultivation (2, 6, 12, 24 and 30 h). For optimization of the inducer concentration varying concentrations of either IPTG (0, 10, 20, 50, 80 or 150 µM) or lactose (0.5, 2 or 4 g L^{-1}) were added at the inoculation time. Additionally, different combinations of glucose (0.5 or 1 g L^{-1}) and lactose (0.5, 1 or 2 g L^{-1}) were used for autoinduction in non-boosted cultures.

Improvement of the booster concentration was performed in cultures induced with 50 µM IPTG or 2 g L^{-1} lactose. At the time of inoculation, different booster concentrations (0 ×, 0.25 ×, 0.5 ×, 1 ×, 2 ×) were added with 1 × booster corresponding to the manufacturer's recommendation (EnPresso GmbH, Germany). In all cases, glucose release was controlled by addition of 3 U L^{-1} biocatalyst at inoculation according to the manufacturer's instructions. Cell density and target protein level were analysed after 30 h of cultivation. Optical densities (OD_{600}) of the cultures were determined as described previously [48].

Cultivation in shake-flasks

Cultivation in the shake-flask scale was carried out in 250-mL Ultra Yield Flasks (UYFs) sealed with a sterile porous membrane seal (AirOtop™) (Thomson Instrument Company) filled with 20% v/v EnPresso B medium with or without booster. For autoinduction, 50 µM IPTG or 2 g L^{-1} lactose were added. The shake-flask cultures supplemented with 0.01% v/v antifoam 204 (Sigma-Aldrich) were inoculated to OD_{600} of 0.2 and incubated at 30 °C and 250 rpm (25 mm offset, Infors HT, Switzerland). If required a second dose of booster and biocatalyst were added after 12 h of induction.

Protein purification and SDS-PAGE analysis

Cells were harvested by centrifugation for 10 min at 8000 × *g* at 4 °C and pellets frozen at − 20 °C overnight. After thawing the pellets were resuspended in washing buffer A (100 mM Tris–HCl, pH 8.0, 150 mM NaCl) supplemented with 1 mg mL^{-1} lysozyme and 1 mM PMSF. Here, 4 mL of washing buffer were used per 1 g of wet cell weight. Subsequently, cells were disrupted by sonification (30 s on/off, sonotrode with 7 mm diameter, 60% amplitude) for 8–10 min. The resulting crude extract was centrifuged for 30 min at 16,000 × *g* at 4 °C to yielding the soluble protein extract. The clarified cell lysates were applied to *Strep*-Tactin® Gravity Superflow® columns (IBA GmbH, Germany) and processed according to the manufacturer's instructions. For 10 mL of soluble extract, a 300 µL bed volume was used. The column was washed with 6 bed volumes of washing buffer, and the Hox proteins were eluted 6 times with 0.5 bed volume of elution buffer containing 2.5 mM D-desthiobiotin. Subsequently, elution fractions were analysed by SDS-PAGE using 12% PAA gels. BSA served as a standard for quantification. After staining with colloidal Coomassie solution the gels were scanned and subsequently bands quantified using Image J.

For total protein analysis 0.2 mL broth samples were collected at the selected time points, centrifuged at 16,000 × *g* and 4 °C for 10 min and pellets stored at − 20 °C. The pellets were resuspended in 2 × SDS sample buffer normalized to an OD_{600} of 5 and heated for 20 min at 95 °C. After centrifugation 20 µL of the SDS-denatured samples were loaded on 12% PAA gels as above.

Western blotting

Western blotting was performed as described recently [48]. Briefly, after SDS-PAGE proteins were transferred onto a PVDF membrane (0.45 µm pore size, Carl Roth, Germany) by semi-dry blotting in a Transblot Turbo Transfer system (Bio-Rad, Germany) at 1.3 A/25 V for 30 min. Strep-tagged HoxB was detected using monoclonal anti-*Strep*-tag®II mouse antibody (1:2500 dilution) (iba GmbH, Germany). As a secondary antibody, alkaline phosphatase (AP)-conjugated goat anti-Mouse IgG antibody (Sigma-Aldrich, Germany) was used (1:8000 dilution). Bands were visualized via the AP-catalysed reaction of the chromogenic BCIP/NBT substrates as described recently [48]. Blots were digitized with a ScanPrisa 640U and quantified with ImageJ.

Supplementary Information

The online version contains supplementary material available at https://doi.org/10.1186/s12934-021-01690-4.

Additional file 1: Figure S1. Cell growth with different amounts of booster in IPTG and lactose autoinduction cultivations

Additional file 2: Table S1. Comparison of cell densities and volumetric RH production yields obtained from deepwell plate (DWP) to UltraYield flask (UYF) cultures (125 mL or 250 mL of flask volume) after 24 h of cultivation using lactose autoinduction.

Acknowledgements
Not applicable.

Authors' contributions
QF, MG and PN participated in experiment design and interpretation of the results. QF carried out all laboratory experiments, QF and MG analysed the data. QF drafted the manuscript. MG and PN revised the manuscript. All authors read and approved the final manuscript.

Funding
This work was supported by the Cluster of Excellence "Unifying Systems in Catalysis" (UniSysCat) coordinated by the Technische Universität Berlin and its graduate school, Berlin International Graduate School of Natural Sciences and Engineering (BIG-NSE), funded by the Deutsche Forschungsgemeinschaft (DFG) under Germany's Excellence Strategy (EXC 2008/1–390540038). QF appreciates the support of China Scholarship Council by obtaining a grant from the Chinese Government Scholarship program, 2017.

Availability of data and materials
All data generated or analysed during this study are included in this published article [and its additional information files].

Declarations

Ethics approval and consent to participate
Not applicable.

Consent for publication
Not applicable.

Competing interests
The authors declare that they have no competing interest.

Received: 25 June 2021 Accepted: 27 September 2021
Published online: 18 October 2021

References

1. Rosano GL, Ceccarelli EA. Recombinant protein expression in *Escherichia coli*: advances and challenges. Front Microbiol. 2014;5:172.
2. Neubauer P, Wolff C, Hecker M, Hofmann K, Meyer L, Kruschke P, Heinrich HW. Introduction of the tac-promoter by lactose under fermentation conditions. Acta Biotechnol. 1991;11:23–9.
3. Neubauer P, Hofmann K, Holst O, Mattiasson B, Kruschke P. Maximizing the expression of a recombinant gene in *Escherichia coli* by manipulation of induction time using lactose as inducer. Appl Microbiol Biotechnol. 1992;36:739–44.
4. Neubauer P, Hofmann K. Efficient use of lactose for the lac promoter controlled overexpression of the main antigenic protein of the foot and mouth disease virus in *Escherichia coli* under fed-batch fermentation conditions. FEMS Microbiol Rev. 1994;14:99–102.
5. Studier FW. Protein production by auto-induction in high density shaking cultures. Protein Expr Purif. 2005;41:207–34.
6. Wu PH, Nair GR, Chu IM. Wu WT High cell density cultivation of *Escherichia coli* with surface anchored transglucosidase for use as whole-cell biocatalyst for α-arbutin synthesis. J Ind Microbiol Biotechnol. 2008;35:95–101.
7. Görke B, Stülke J. Carbon catabolite repression in bacteria: many ways to make the most out of nutrients. Nat Rev Microbiol. 2008;6:613–24.
8. Fischer D, Teich A, Neubauer P, Hengge-Aronis R. The general stress sigma factor σ(S) of *Escherichia coli* is induced during diauxic shift from glucose to lactose. J Bacteriol. 1998;180:6203–6.
9. Stülke J, Hillen W. Carbon catabolite repression in bacteria. Curr Opin Microbiol. 1999;2:195–201.
10. Kremling A, Bettenbrock K, Laube B, Jahreis K, Lengeler JW, Gilles ED. The organization of metabolic reaction networks. Metab Eng. 2001;3:362–79.
11. Bettenbrock K, Fischer S, Kremling A, Jahreis K, Sauter T, Gilles E-D. A Quantitative approach to catabolite repression in *Escherichia coli*. J Biol Chem. 2006;281:2578–84.
12. Blommel PG, Becker KJ, Duvnjak P, Fox BG. Enhanced bacterial protein expression during auto-Induction obtained by alteration of Lac repressor dosage and medium composition. Biotechnol Prog. 2007;23:585–98.
13. Grabski A, Mehler M, Drott D. Unattended high-density cell growth and and induction of protein expression with the overnight express autoinduction system. Innovations. 2003;17:3–8.
14. Grabski A, Mehler M, Drott D. The overnight express autoinduction system: High-density cell growth and protein expression while you sleep. Nat Methods. 2005;2:233–5.
15. Kunze M, Huber R, Gutjahr C, Müllner S, Büchs J. Predictive tool for recombinant protein production in *Escherichia coli* shake-flask cultures using an on-line monitoring system. Biotechnol Prog. 2012;28:103–13.
16. Li Z, Kessler W, van den Heuvel J, Rinas U. Simple defined autoinduction medium for high-level recombinant protein production using T7-based *Escherichia coli* expression systems. Appl Microbiol Biotechnol. 2011;91:1203–13.
17. Gordon E, Horsefield R, Swarts HGP. de Pont JJHHM, Neutze R, Snijder A: Effective high-throughput overproduction of membrane proteins in *Escherichia coli*. Protein Expr Purif. 2008;62:1–8.
18. Wurm DJ, Hausjell J, Ulonska S, Herwig C, Spadiut O. Mechanistic platform knowledge of concomitant sugar uptake in *Escherichia coli* BL21(DE3) strains. Sci Rep. 2017;7:45072.
19. Wurm DJ, Herwig C, Spadiut O: How to determine interdependencies of glucose and lactose uptake rates for heterologous protein production with *Escherichia coli*. In: *Methods in Molecular Biology*. Humana Press Inc., 2017; Vol. 1586, pp 397–408.
20. Tyler RC, Sreenath HK, Singh S, Aceti DJ, Bingman CA, Markley JL, Fox BG. Auto-induction medium for the production of [U-15N]- and [U-13C, U-15N]-labeled proteins for NMR screening and structure determination. Protein Expr Purif. 2005;40:268–78.
21. Fox BG, Blommel PG. Autoinduction of protein expression. Curr Protoc Protein Sci. 2009;56:1–18.
22. Sivashanmugam A, Murray V, Cui C, Zhang Y, Wang J, Li Q. Practical protocols for production of very high yields of recombinant proteins using Escherichia coli. Protein Sci. 2009;18:936–48.
23. Sreenath HK, Bingman CA, Buchan BW, Seder KD, Burns BT, Geetha HV, Jeon WB, Vojtik FC, Aceti DJ, Frederick RO, Phillips GN, Fox BG. Protocols for production of selenomethionine-labeled proteins in 2-L polyethylene terephthalate bottles using auto-induction medium. Protein Expr Purif. 2005;40:256–67.
24. Lin ECC. Glycerol Dissimilation and its Regulation in Bacteria. Annu Rev Microbiol. 1976;30:535–78.
25. Kopp J, Slouka C, Ulonska S, Kager J, Fricke J, Spadiut O, Herwig C. Impact of glycerol as carbon source onto specific sugar and inducer uptake rates and inclusion body productivity in *Escherichia coli* BL21(DE3). Bioengineering. 2017;5:1.
26. Soini J, Ukkonen K, Neubauer P. High cell density media for *Escherichia coli* are generally designed for aerobic cultivations – consequences for large-scale bioprocesses and shake flask cultures. Microb Cell Fact. 2008;7:26.
27. Zimmermann H, Anderlei T, Büchs J. Oxygen limitation is a pitfall during screening for industrial strains. Appl Microbiol Process enignnering. 2006;72:1157–60.
28. Hoffman BJ, Broadwater JA, Johnson P, Harper J, Fox BG, Kenealy WR. Lactose fed-batch overexpression of recombinant metalloproteins in *Escherichia coli* BL21(DE3): Process control yielding high levels of metal-incorporated, soluble protein. Protein Expr Purif. 1995;6:646–54.

29. Gombert AK, Kilikian BV. Recombinant gene expression in *Escherichia coli* cultivation using lactose as inducer. J Biotechnol. 1998;60:47–54.
30. Pei XL, Wang QY, Li CL, Qiu XF, Xie KL, Huang LF, Wang AM, Zeng ZW, Xie T. Efficient production of a thermophilic 2-Deoxyribose-5-Phosphate aldolase in glucose-limited fed-batch cultivations of escherichia coli by continuous lactose induction strategy. Appl Biochem Biotechnol. 2011;165:416–25.
31. Ukkonen K, Mayer S, Vasala A, Neubauer P. Use of slow glucose feeding as supporting carbon source in lactose autoinduction medium improves the robustness of protein expression at different aeration conditions. Protein Expr Purif. 2013;91:147–54.
32. Mayer S, Junne S, Ukkonen K, Glazyrina J, Glauche F, Neubauer P, Vasala A. Lactose autoinduction with enzymatic glucose release: characterization of the cultivation system in bioreactor. Protein Expr Purif. 2014;94:67–72.
33. Fontecilla-Camps JC, Volbeda A, Cavazza C, Nicolet Y. Structure/function relationships of [NiFe]- and [FeFe]-hydrogenases. Chem Rev. 2007;1:4273–303.
34. Lubitz W, Ogata H, Ru O, Reijerse E. Hydrogenases. Chem Rev. 2014;114:4081–148.
35. Vignais PM, Billoud B. Occurrence, classification, and biological function of hydrogenases: an overview. Chem Rev. 2007;107:4206–72.
36. Constant P, Chowdhury SP, Hesse L, Pratscher J, Conrad R. Genome data mining and soil survey for the novel group 5 [NiFe]-hydrogenase to explore the diversity and ecological importance of presumptive high-affinity H_2-oxidizing bacteria. Appl Environ Microbiol. 2011;77:6027–35.
37. Lauterbach L, Idris Z, Vincent KA, Lenz O. Catalytic properties of the isolated diaphorase fragment of the NAD^+-reducing [NiFe]-hydrogenase from *Ralstonia eutropha*. PLoS ONE. 2011;6:25939–51.
38. Burgdorf T, Lenz O, Buhrke T, Van Der Linden E, Jones AK, Albracht SPJ, Friedrich B. [NiFe]-hydrogenases of *Ralstonia eutropha* H16: Modular enzymes for oxygen-tolerant biological hydrogen oxidation. J Mol Microbiol Biotechnol. 2005;10:181–96.
39. Friedrich B, Fritsch J, Lenz O. Oxygen-tolerant hydrogenases in hydrogen-based technologies. Curr Opin Biotechnol. 2011;22:358–64.
40. Lenz O, Bernhard M, Buhrke T, Schwartz E, Friedrich B. The hydrogen-sensing apparatus in *Ralstonia eutropha*. J Mol Microbiol Biotechnol. 2002;4:255–62.
41. Buhrke T, Lenz O, Porthun A, Friedrich B. The H_2-sensing complex of *Ralstonia eutropha*: Interaction between a regulatory [NiFe] hydrogenase and a histidine protein kinase. Mol Microbiol. 2004;51:1677–89.
42. Buhrke T, Lenz O, Krauss N, Friedrich B. Oxygen tolerance of the H_2-sensing [NiFe] hydrogenase from *Ralstonia eutropha* H16 is based on limited access of oxygen to the active site. J Biol Chem. 2005;280:23791–6.
43. Volbeda A, Charon M-H, Piras C, Hatchikian EC, Frey M, Fontecilla-Camps JC. Crystal structure of the nickel–iron hydrogenase from *Desulfovibrio gigas*. Nature. 1995;373:580–7.
44. Bernhard M, Buhrke T, Bleijlevens B, De Lacey AL, Fernandez VM, Albracht SPJ, Friedrich B. The H_2 Sensor of *Ralstonia eutropha*. J Biol Chem. 2001;276:15592–7.
45. Buhrke T, Löscher S, Lenz O, Schlodder E, Zebger I, Andersen LK, Hildebrandt P, Meyer-Klaucke W, Dau H, Friedrich B, Haumann M. Reduction of unusual iron-sulfur clusters in the H_2-sensing regulatory NiFe hydrogenase from *Ralstonia eutropha* H16. J Biol Chem. 2005;280:19488–95.
46. Horch M, Schoknecht J, Mroginski MA, Lenz O, Hildebrandt P, Zebger I. Resonance raman spectroscopy on [NiFe] Hydrogenase provides structural insights into catalytic intermediates and reactions. J Am Chem Soc. 2014;136:9870–3.
47. Roncaroli F, Bill E, Lenz O. Cofactor composition and function of a H_2 -sensing regulatory hydrogenase as revealed by Mössbauer and EPR spectroscopy. Chem Sci. 2015;6:4495–507.
48. Fan Q, Caserta G, Lorent C, Lenz O, Neubauer P, Gimpel M. Optimization of culture conditions for oxygen-tolerant regulatory [NiFe]-Hydrogenase production from *Ralstonia eutropha* H16 in *Escherichia coli*. Microorganisms. 2021;9:1195.
49. Glazyrina J, Materne E, Hillig F, Neubauer P, Junne S. Two-compartment method for determination of the oxygen transfer rate with electrochemical sensors based on sulfite oxidation. Biotechnol J. 2011;6:1003–8.
50. Ali BA: Application of the enzyme controlled glucose feeding for the production of recombinant proteins. *Tech Univ Berlin* 2018.
51. Studier FW: Stable expression clones and au-toinduction for protein production in *Escherichia coli*. *Structural Genomics*; Humana Press: Totowa, NJ, 2014; Vol. 1091.
52. Faust G, Stand A, Weuster-Botz D. IPTG can replace lactose in auto-induction media to enhance protein expression in batch-cultured *Escherichia coli*. Eng Life Sci. 2015;15:824–9.
53. Panula-Perälä J, Šiurkus J, Vasala A, Wilmanowski R, Casteleijn MG, Neubauer P. Enzyme controlled glucose auto-delivery for high cell density cultivations in microplates and shake flasks. Microb Cell Fact. 2008;7:31.
54. Krause M, Ukkonen K, Haataja T, Ruottinen M, Glumoff T, Neubauer A, Neubauer P, Vasala A. A novel fed-batch based cultivation method provides high cell-density and improves yield of soluble recombinant proteins in shaken cultures. Microb Cell Fact. 2010;9:11.
55. Yildirim N, Mackey MC. Feedback regulation in the lactose operon: A mathematical modeling study and comparison with experimental data. Biophys J. 2003;84:2841–51.
56. Marbach A, Bettenbrock K. Lac operon induction in *Escherichia coli*: Systematic comparison of IPTG and TMG induction and influence of the transacetylase LacA. J Biotechnol. 2012;157:82–8.
57. Fernández-Castané A, Vine CE, Caminal G, López-Santín J. Evidencing the role of lactose permease in IPTG uptake by *Escherichia coli* in fed-batch high cell density cultures. J Biotechnol. 2012;157:391–8.
58. Fernández-Castané A, Caminal G, López-Santín J. Direct measurements of IPTG enable analysis of the induction behavior of *Escherichia coli* in high cell density cultures. Microb Cell Fact. 2012;11:1–9.
59. Duetz WA, Witholt B. Oxygen transfer by orbital shaking of square vessels and deepwell microtiter plates of various dimensions. Biochem Eng J. 2004;17:181–5.
60. Ukkonen K, Vasala A, Ojamo H, Neubauer P. High-yield production of biologically active recombinant protein in shake flask culture by combination of enzyme-based glucose delivery and increased oxygen transfer. Microb Cell Fact. 2011;10:107.
61. Li J, Jaitzig J, Hillig F, Süssmuth R, Neubauer P. Enhanced production of the nonribosomal peptide antibiotic valinomycin in *Escherichia coli* through small-scale high cell density fed-batch cultivation. Appl Microbiol Biotechnol. 2014;98:591–601.

Publisher's Note

Paper III

High-yield production of catalytically active regulatory [NiFe]-hydrogenase from *Cupriavidus necator* in *Escherichia coli*

Qin Fan, Giorgio Caserta, Christian Lorent, Ingo Zebger, Peter Neubauer, Oliver Lenz and Matthias Gimpel

***Front. Microbiol.* 13, 1525**

frontiers | Frontiers in Microbiology

ORIGINAL RESEARCH
published: 29 April 2022
doi: 10.3389/fmicb.2022.894375

High-Yield Production of Catalytically Active Regulatory [NiFe]-Hydrogenase From *Cupriavidus necator* in *Escherichia coli*

Qin Fan[1], Giorgio Caserta[2], Christian Lorent[2], Ingo Zebger[2], Peter Neubauer[1], Oliver Lenz[2] and Matthias Gimpel[1]*

[1] Chair of Bioprocess Engineering, Department of Biotechnology, Technische Universität Berlin, Berlin, Germany,
[2] Department of Chemistry, Technische Universität Berlin, Berlin, Germany

OPEN ACCESS

Edited by:
Constanze Pinske,
Martin Luther University of Halle-Wittenberg, Germany

Reviewed by:
Hideaki Ogata,
Nara Institute of Science and Technology (NAIST), Japan
Simone Morra,
University of Nottingham, United Kingdom

***Correspondence:**
Matthias Gimpel
matthias.gimpel@tu-berlin.de

Specialty section:
This article was submitted to Microbial Physiology and Metabolism, a section of the journal Frontiers in Microbiology

Received: 11 March 2022
Accepted: 08 April 2022
Published: 29 April 2022

Citation:
Fan Q, Caserta G, Lorent C, Zebger I, Neubauer P, Lenz O and Gimpel M (2022) High-Yield Production of Catalytically Active Regulatory [NiFe]-Hydrogenase From Cupriavidus necator in Escherichia coli. Front. Microbiol. 13:894375. doi: 10.3389/fmicb.2022.894375

Hydrogenases are biotechnologically relevant metalloenzymes that catalyze the reversible conversion of molecular hydrogen into protons and electrons. The O_2-tolerant [NiFe]-hydrogenases from *Cupriavidus necator* (formerly *Ralstonia eutropha*) are of particular interest as they maintain catalysis even in the presence of molecular oxygen. However, to meet the demands of biotechnological applications and scientific research, a heterologous production strategy is required to overcome the low production yields in their native host. We have previously used the regulatory hydrogenase (RH) from *C. necator* as a model for the development of such a heterologous hydrogenase production process in *E. coli*. Although high protein yields were obtained, the purified enzyme was inactive due to the lack of the catalytic center, which contains an inorganic nickel-iron cofactor. In the present study, we significantly improved the production process to obtain catalytically active RH. We optimized important factors such as O_2 content, metal availability, production temperature and time as well as the co-expression of RH-specific maturase genes. The RH was successfully matured during aerobic cultivation of *E. coli* by co-production of seven hydrogenase-specific maturases and a nickel permease, which was confirmed by activity measurements and spectroscopic investigations of the purified enzyme. The improved production conditions resulted in a high yield of about 80 mg L^{-1} of catalytically active RH and an up to 160-fold space-time yield in *E. coli* compared to that in the native host *C. necator* [<0.1 U (L d) $^{-1}$]. Our strategy has important implications for the use of *E. coli* K-12 and B strains in the recombinant production of complex metalloenzymes, and provides a blueprint for the production of catalytically active [NiFe]-hydrogenases in biotechnologically relevant quantities.

Keywords: regulatory hydrogenase, difficult-to-express protein, *Escherichia coli*, [NiFe]-hydrogenase, *Cupriavidus necator*

INTRODUCTION

[NiFe]-hydrogenases are metalloenzymes that catalyze the reversible oxidation of molecular hydrogen (H_2) into protons and electrons, which makes them very attractive from both scientific and applied perspectives (Fontecilla-Camps et al., 2007; Lubitz et al., 2014). Their core module is composed of a large subunit harboring the catalytic nickel-iron [NiFe] center and a small subunit hosting one to three iron-sulfur clusters that mediates electron transfer between the active site and the physiological electron acceptor/donor (Ogata et al., 2016). The inorganic [NiFe] center is coordinated to the protein *via* four cysteine-derived thiolates, two of which are terminal nickel ligands whereas the other two serve as bridging ligands between the nickel and the iron. The iron is further coordinated by one carbonyl (CO) group and two cyanide (CN^-) residues (Fontecilla-Camps et al., 2007; Lubitz et al., 2014; Peters et al., 2015). Synthesis and incorporation of the [NiFe] cofactor into the apo-hydrogenase is a highly complex process that requires a set of at least six maturation proteins, named HypABCDEF (Forzi and Sawers, 2007; Lacasse and Zamble, 2016). The HypCD complex serves as central scaffold for the assembly of the $Fe(CN)_2CO$ moiety (Blokesch et al., 2004a; Bürstel et al., 2012; Watanabe et al., 2012). The cyanide ligands are synthesized from carbamoyl phosphate by a concerted action of HypE and HypF (Casalot and Rousset, 2001; Reissmann et al., 2003; Blokesch et al., 2004b; Rangarajan et al., 2008; Lacasse and Zamble, 2016). The source of the CO ligand in anaerobic hydrogenase biosynthesis is still unknown (Bürstel et al., 2011). Among others (Lenz et al., 2007), acetate (Roseboom et al., 2005) and CO_2 (Soboh et al., 2013) have been suggested as precursors, but compelling evidence is lacking. Under aerobic conditions, however, formyl-tetrahydrofolate serves as the CO precursor (Bürstel et al., 2016). The preformed $Fe(CN)_2CO$ fragment is then transferred from the HypCD complex into the apo-form of the large hydrogenase subunit (Arlt et al., 2021). Subsequently, the nickel is incorporated by HypA and HypB complex (Lacasse and Zamble, 2016). In *E. coli*, the SlyD protein is also involved in nickel insertion (Leach et al., 2007; Kaluarachchi et al., 2012; Pinske et al., 2015). Upon insertion of the complete [NiFe] cofactor, the hydrogenase large subunit usually undergoes proteolytic cleavage, in which the C-terminal extension is cleaved off (Senger et al., 2017; Pinske et al., 2019; Hartmann et al., 2020). This cleavage step allows oligomerization of the cofactor-containing large subunit with the small subunit, whose Fe-S clusters are incorporated by the universal Isc/Suf machinery.

Due to the complex maturation process, recombinant production of [NiFe]-hydrogenases is challenging, especially in heterologous systems, and makes scalability difficult (Fan et al., 2020). We have chosen the regulatory [NiFe]-hydrogenase (RH) from *Cupriavidus necator* (formerly *Ralstonia eutropha*) as a model for the development of a heterologous hydrogenase production system in *E. coli*. *C. necator* actually possesses four different [NiFe]-hydrogenases, all of which are O_2-tolerant, i.e., they perform H_2 conversion even in the presence of molecular oxygen (Fritsch et al., 2013; Schwartz et al., 2013; Lenz et al., 2015). The RH functions as H_2 sensor in the context of H_2-dependent transcriptional regulation of the genes encoding the two energy-conserving [NiFe]-hydrogenases of *C. necator* (Lenz et al., 1997, 2010). Like typical [NiFe]-hydrogenases, the RH consists of two subunits, a large subunit HoxC (52 kDa) containing the $NiFe(CN)_2CO$ center and a small subunit HoxB (36 kDa) harboring three [4Fe-4S] clusters (Pierik et al., 1998; Kleihues et al., 2000). Its H_2-oxidizing activity is absolutely insensitive to O_2 (Buhrke et al., 2005a; Ash et al., 2015). The maturation proteins required for cofactor assembly of the RH are encoded by the *hyp1* operon (*hypA1B1F1CDE*) of *C. necator* (Buhrke et al., 2001). In contrast to most other [NiFe]-hydrogenases, the RH large subunit HoxC does not undergo C-terminal processing, making RH a relatively simple [NiFe]-hydrogenase model. Recently, we succeeded to produce the RH heterologously in *E. coli* in a soluble form and purified the protein by a single affinity chromatography step (Fan et al., 2021a). By using an EnPresso B-based fed-batch-like growth mode, we obtained up to 250 mg L^{-1} of RH in shake flask cultures. This RH yield was about 250-fold higher than that from the native producer (Bernhard et al., 2001; Fan et al., 2021a). The productivity has been further improved using IPTG or lactose autoinduction (Fan et al., 2021b). Regrettably, the purified RH turned out to be inactive. While the small subunit appeared to be fully equipped with Fe-S clusters, the large subunit lacked the [NiFe] cofactor, indicating malfunctioning maturation in the heterologous host.

In this study, we aimed at the heterologous production of RH with catalytic activity by testing different *E. coli* strains with various genetic backgrounds and by varying the process conditions. By co-expression of the *hyp1* operon from *C. necator* and the supplementation of the growth medium with $NiCl_2$ we obtained RH with catalytic activity. The successful incorporation of the $NiFe(CN)_2CO$ cofactor was confirmed by IR and EPR spectroscopy. By co-expression of the *hoxN* and *hypX* genes, encoding a nickel permease and a dedicated maturase, respectively, catalytically active RH was also purified from aerobically grown *E. coli* BL21.

MATERIALS AND METHODS

Bacterial Strains, Media and Growth Conditions

While *E. coli* TG1 (Baer et al., 1984) was used for plasmid maintenance, the *E. coli* B strain BL21 Gold (Stratagene, Germany) and the K-12 strains W3110 (Bachmann, 1972) and MC4100 (Casadaban and Cohen, 1979) were used for RH production. Plasmid pQF8 (Fan et al., 2021a) was used for overproduction of structural RH subunits, $HoxB_{Strep}$ and HoxC, under control of the IPTG inducible $P_{lac-CTU}$ promoter. All strains and plasmids are listed in **Supplementary Tables 1, 2**.

Transformations and plasmid propagations were performed on solid and liquid TY medium (16 g L^{-1} tryptone, 10 g L^{-1} yeast extract, 5 g L^{-1} NaCl, for solid medium 2% agar-agar). The fed-batch-like EnPresso® B medium (EnPresso GmbH, Berlin, Germany) was used for RH production. The EnPresso B medium is based on a typical *E. coli* mineral salt medium supplemented with trace elements and Na_2SeO_3, Na_2MoO_4 and $Ni(NO_3)_2$ as

described previously (Soini et al., 2008). In this medium, glucose is enzymatically released from a non-metabolizable polymer contained therein. For preparation of a pre-culture, *E. coli* cells were inoculated from a single colony in 10 mL LB medium (10 g L^{-1} tryptone, 5 g L^{-1} yeast extract, 10 g L^{-1} NaCl) and shaken for 6–8 h at 37°C, 250 rpm (Infors HT, 25 mm offset, Switzerland). For main cultures, 50 mL EnPresso® B medium was inoculated to an OD_{600} of 0.2 in 250 mL baffled Ultra Yield® shake flask (Thomson Instrument Company, Oceanside, CA, United States) (20% v/v) supplemented with 25 μL of reagent A (1.5 U L^{-1}) for overnight cultivation at 30°C, 250 rpm (Infor HT, Switzerland). At the induction point booster and 75 μl reagent A (4.5 U L^{-1}) were added according to the manufacturer's instructions (EnPresso GmbH, Berlin, Germany) and RH production triggered by addition of 50 μM IPTG. The cells were cultivated under the same conditions for 24 h at 30°C or for 48 h/72 h at 18°C. If required all media were supplemented with 25 μg mL^{-1} chloramphenicol and 25 μg mL^{-1} kanamycin for selection.

For induction under O_2 limited conditions the cultivation protocol was altered as follows. To ensure a high cell density before, a first dose of booster and 75 μl reagent A (4.5 U L^{-1}) were added after overnight cultivation and growth continued for 12 h under the same conditions. After 12 h of boosted growth, cultures were transferred into 125 mL baffled PreSens shake flask (40% v/v) which was placed on an SFR shake flask reader (PreSens Precision Sensing GmbH, Regensburg, Germany) in a Kuhner LTX orbital shaker (50 mm offset, Adolf Kühner AG, Basel, Switzerland) with online monitoring of dissolved oxygen (DO) and pH. The oxygen level was controlled by manually reducing the shaking speed from 250 rpm to 100 rpm until a DO value almost close to 0% was reached to ensure O_2-limited (microaerobic) conditions. A 2nd dose of booster and reagent A was added together with 50 μM IPTG to induce RH production and cultivation continued at 30°C for 36 h or at 18°C for 48 h/66 h/72 h as indicated. Finally, cells were harvested by centrifugation at 8,000 × *g*, 4°C for 10 min. The cell pellets were frozen in liquid nitrogen and stored at −80°C until further use. To investigate an effect of metal ion addition on active RH production, appropriate concentrations of $NiCl_2$ or $FeSO_4$ were added to the cultures at the induction point and 8 mL boosted cultures were distributed onto the Deep Well OxoDish® OD24-DW deepwell plates with DO online monitoring and cultivated in an SDR SensorDish® Reader (both from PreSens Precision Sensing GmbH, Regensburg, Germany) which was placed in a Duetz plate holder (EnzyScreen BV, Heemstede, Netherlands) and placed and cultivated in the Kuhner LTX shaker (50 mm offset, Adolf Kühner AG, Basel, Switzerland). After 24 h of induction under O_2-limited cultivation conditions at 30°C cells were harvested from the 8 mL culture suspension as described above.

RH Purification, Spectroscopic Characterization and Activity Assay

RH purification has been described in detail previously (Fan et al., 2021a,b). All elution fractions were concentrated by ultra-filtration (14,000 × g, 4°C) using Amicon Ultra Ultracel 30 kDa cut-off concentrators (Merk Millipore, Germany). An aliquot of the final concentrate was used for SDS-PAGE. The gels were stained with colloidal Coomassie blue G250 solution and subsequently bands were quantified with ImageJ for determination of protein concentrations. A defined solution of bovine serum albumin served as standard. H_2-oxidizing activity of RH was measured spectrophotometrically using a Cary50 UV-vis spectrophotometer (Varian, Agilent, Santa Clara, California), and the H_2 uptake assay using methylene blue as an electron acceptor was used as described previously (Lenz et al., 2018). Measurements were performed with two biological replicates and the standard deviation was calculated from at least two independent technical replicates. For screening experiments of optimal nickel or iron concentrations, the H_2-oxidation activity was measured in soluble extract of the cell lysates separated from solid cell debris and insoluble fraction after sonication (3 min, 30 s on/off, sonotrode with 3 mm diameter, 30% amplitude) (UP200S, Hielscher GmbH, Germany). The reaction was started by the addition of 200 μl soluble extract to 1.8 mL reaction buffer followed by 100% H_2 gas saturation as described previously (Fan et al., 2021a). The RH concentration in the soluble extract was quantified in Western blot analysis using known concentration of HoxC as a control. Infrared (IR) and electron paramagnetic resonance (EPR) spectroscopy of RH were measured as described previously (Fan et al., 2021a).

Construction of Plasmids for *hyp* Gene Expression

Plasmid pGK16, a derivative of the medium copy plasmid pGK14 (Brantl, 1994) carrying a kanamycin resistance gene instead of the erythromycin resistance gene (Gimpel, unpublished) was used as basis for the construction of the *hyp* gene expression plasmids. First, the 267 bp *Sal*I/*Bgl*II fragment from plasmid pGW2 (Schollmeyer, 2020) harboring the P_{tac} promoter, a multiple cloning site and a transcription terminator was cloned into the corresponding pGK14 vector, yielding plasmid pQF11. Next, using Q5 DNA polymerase (New England Biolabs), PCR amplification of the complete *hyp1* operon from pRH-Hyp (Lenz et al., 2007) and *hyp1 (ΔF1)* operon from pRH-Hyp(ΔF1) (Lenz et al., 2007) was performed with oligonucleotides MG0164 (5′-TCATCTAGACGGAGTCTTTGGGAGATACTG-3′) and MG0168 (5′-ACTGCGGCCGCTTAACAAATGCGCGGAAGCT G-3′). The PCR products were digested with *Xba*I and *Not*I and cloned into the pQF11 cut with the same enzymes yielding pQF12 and pQF13. The plasmid pQF12, which contains the complete *hyp1* operon, was used as the basis for the integration of further maturation enzymes. The high-affinity nickel permease encoding *C. necator hoxN* gene was PCR amplified using primers MG0226 (ATCGCGGCCGCACAGGAGACTTCCAGCATGTTCCA) and MG0227 (ACTGCGGCCGCTTAACATGAACTTGTCGGCCAG GA) and plasmid pCH231 (Wolfram et al., 1995) as template. The resulting 0.9 kb fragment was digested with *Not*I and subsequently ligated into the corresponding pQF12 vector yielding plasmid pQF17. The primer pair MG0243 (AGTTCTAGAGCGAGTCGGCTATGCGCATATTGC)/MG024

4 (ATGTCTAGATCAAGATCGTTTCCCCGCAAGTGC) and plasmid pGE771 (Lauterbach and Lenz, 2013) as template were used to PCR-amplify a 1.8 kb fragment encoding the *C. necator* aerobic maturase HypX. The resulting fragment was digested with *Xba*I and ligated into the corresponding pQF17 vector, resulting in plasmid pQF18. The correctness of the amplified sequences was confirmed by sequencing (LGC Genomics, Berlin). A schematic map of all plasmids can be found in **Supplementary Figure 1**. Expression plasmids were introduced sequentially.

RESULTS

Heterologous Production of Catalytically Active RH in O_2-Limited *E. coli* Cultures

In a previous study we showed that high RH yields can be obtained with *E. coli* BL21 Gold carrying the RH overproduction plasmid pQF8 (strain BQF8RH; Fan et al., 2021a). However, the purified RH did not contain any [NiFe] cofactor (Fan et al., 2021a), which is consistent with major defects of *E. coli* BL21 in metal ion transport and metalloprotein biosynthesis (Pinske et al., 2011). This phenotype has been attributed to a non-sense mutation in the *fnr* gene whose gene product regulates nickel transport and *hyp* gene expression. Global deficiencies in anaerobic metabolism and metal ion transport seem to be common for *E. coli* B derivatives (Pinske et al., 2011). To overcome this obstacle, we transformed the two *E. coli* K-12 derivatives *E. coli* W3110 and *E. coli* MC4100 with plasmid pQF8, resulting into the recombinant strains WQF8RH and MQF8RH, respectively. All strains were cultivated under both aerobic and O_2-limiting conditions in shake-flasks containing EnPresso B medium, as described in section "Materials and Methods." O_2 limitation (DO value close to 0%) was initiated by reducing the shaking speed from 250 to 100 rpm after induction (**Supplementary Figure 3**). After 24 h of IPTG induction, cells were collected, disrupted, and the RH was purified by affinity chromatography. Furthermore, the H_2-oxidizing activity of all RH samples was determined.

Regardless of the aeration, similar RH protein yields were obtained (data not shown). However, considering the higher final cell densities (**Supplementary Figure 2A**), the obtained volumetric yields were 1.5–2.5-fold higher under aerobic conditions (**Figure 1A**). Interestingly, among the three strains tested, BQF8RH performed best under aerobic conditions but worst under O_2-limiting conditions (**Figure 1A** and **Supplementary Figure 2C**), suggesting that anaerobic conditions might be suboptimal for RH production in *E. coli* BL21. Presumably, the lack of certain anaerobic respiration-related proteins and/or enzymes in the B strains prevents rapid adaptation to anaerobic stress (Pinske et al., 2011) and leads to slower growth and lower protein production (Kim et al., 2014). However, the RH purified from BQF8RH showed no activity regardless of the growth conditions (**Figure 1B**). In contrast, RH preparations from both *E. coli* K-12 derivatives grown under O_2-limiting conditions exhibited a specific activity of 0.02 U mg^{-1}, while RH purified from aerobically grown cells was inactive (**Figure 1B**). The latter could be due to either the lack of the hydrogenase maturation apparatus or insufficient uptake of nickel ions under aerobic cultivation, both of which are modulated by the transcriptional regulator FNR under anaerobic conditions (Wu et al., 1989; Lutz et al., 1991; Messenger and Green, 2003). Thus, the lack of FNR in *E. coli* B-strains, as well as the reduced FNR levels in the presence of O_2, might prevent nickel uptake, [NiFe] cofactor assembly, and consequently the synthesis of catalytically active RH. Nevertheless, the RH activities obtained from both *E. coli* K-12 derivatives were quite low and corresponded to only 0.5–1% of those reported for the RH protein isolated from *C. necator,* which is in the range of 1.6–4.5 U mg^{-1} (Buhrke et al., 2005a,b; Caserta et al., 2020). This indicates that the hydrogenase maturation apparatus of *E. coli* K-12 is only able to mature *C. necator* RH to a very limited extent.

Co-expression of the *C. necator hyp* Genes Improves RH Maturation in *E. coli*

It has been reported previously that co-expression of the *C. necator hyp* genes markedly improve the activity of heterologously produced RH (Lenz et al., 2007). Thus, we constructed plasmids pQF12 and pQF13 carrying the entire *C. necator hyp1* operon [*hypA1B1(F1)CDE*] with or without *hypF1*, respectively, under control of the IPTG-inducible P_{tac} promoter. The plasmids were transferred into strains BQF8RH, WQF8RH, and MQF8RH, resulting in BQF8RH2 and BQF8RH3, WQF8RH2 and WQF8RH3, MQF8RH2 and MQF8RH3, respectively. The strains were cultivated under O_2-limiting conditions, RH was purified, and its H_2-oxidation activity was measured. Co-expression of the maturase genes did not significantly affect the RH yield, indicating that the cells tolerate the higher metabolic load (**Figures 1A,C**). RH purified from strains BQF8RH2 and BQF8RH3 still showed no activity, whereas co-expression of the maturase genes significantly increased the RH activity in the K12 derivatives (**Figure 1D**). RH purified from WQF8RH2 and MQF8RH2 displayed a specific activity of 0.03 U mg^{-1} and 0.07 U mg^{-1} (**Figure 1D**), which corresponds to a 1.5 and 3.5-fold increase, respectively, compared to the parental strains, which did not express the *C. necator hyp* genes. Remarkably, the strains WQF8RH3 and MQF8RH3, which co-express the *hyp1* operon without *hypF1*, showed even higher RH activities with a 2.5- and 6-fold increase, respectively (**Figure 1D**). These data highlight the positive effect of the co-expressed *C. necator* maturase genes on the catalytic activity of RH and underscore the previously observed requirement of the *hypF* gene of *E. coli* for RH maturation under anaerobic conditions (Lenz et al., 2007). Furthermore, *E. coli* MQF8RH3 was found to be most suitable for production of active RH as it showed the highest specific RH activity among the strains discussed so far. However, despite co-expression of the *C. necator hyp* genes, the activity of the heterologously produced RH remained very low.

Addition of Nickel Improves the RH Activity in *E. coli*

The comparatively low activity of the heterologously produced RH might result from an insufficient supply of nickel by the

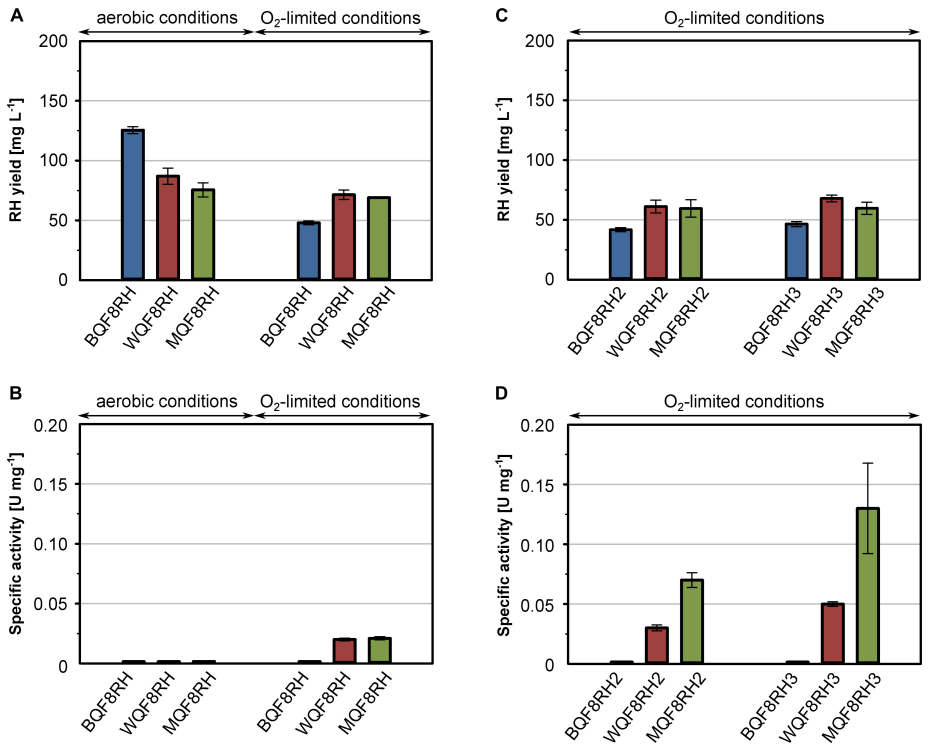

FIGURE 1 | Comparison of production strains, cultivation mode and *hyp* gene co-expression for heterologous RH production. *E. coli* strains BQF8RH, WQF8RH and MQF8RH (derivatives of *E. coli* strains BL21 Gold, W3110 and MC4100, respectively) carry plasmid pQF8 encoding the two RH subunits were used. For co-expression of the maturation genes of *C. necator*, strains BQF8RH, MQF8RH and WQF8RH were transformed with either plasmid pQF12 (encoding the entire *hyp1* operon) or plasmid pQF13 (encoding the modified *hyp1(ΔF1)* operon lacking *hypF1*) yielding strains BQF8RH2, WQF8RH2 or MQF8RH2 and BQF8RH3, WQF8RH3 or MQF8RH3, respectively. All strains were cultivated in 50 mL EnPresso B medium as described in section "Materials and Methods." For aerobic production, cultivation was performed in 250-mL Ultra Yield flasks (20% V/V) shaken at 250 rpm, whereas O_2-limited production was performed in 125-mL PreSens flasks (40% V/V) adjusted to a DO near 0% by manually decreasing the shaking speed. RH protein was purified by affinity chromatography **(A,C)** and specific activities measured from the purified samples **(B,D)**.

EnPresso B medium used for strain cultivation. Similar to LB, EnPresso B medium is a rich medium that most likely has a chelating effect on metal ions, thereby reducing their bioavailability (Rathnayake et al., 2013). To test this hypothesis, we added 500 μM nickel to the medium and cultivated the *E. coli* strains MQF8RH, MQF8RH2 and MQF8RH3 under microaerobic conditions. $NiCl_2$ supplementation did neither affect the bacterial growth nor the yield of the purified RH (**Figure 2A**), excluding toxic effects of the additional nickel. In contrast, the extra nickel resulted in a significant increase in RH activity when the *C. necator hyp* machinery was co-expressed (**Figure 2B**). In fact, we observed an increase from 0.07 U mg^{-1} to 0.28 U mg^{-1} for the RH isolated from MQF8RH2 and from 0.13 U mg^{-1} to 0.34 U mg^{-1} for the RH isolated from strain MQF8RH3 cultivated at 30°C (**Figure 2B**). An even higher activity of 0.5 U mg^{-1} was obtained when the same strains were cultured at 18°C for an extended time period of 66 h after IPTG induction (see section "Materials and Methods"), although the lower temperature decreased the volumetric RH yield (**Figure 2A**). Remarkably, the RH proteins isolated from strains MQF8RH2 and MQF8RH3 cultivated at 18°C had similar specific activities, suggesting that the presence of the *C. necator hypF1* gene no longer impacted enzyme maturation (**Figures 1D**, **2B**). The lower cultivation temperature is accompanied by an increased oxygen concentration, which could be the reason for the acquired functionality of HypF1. In conclusion, lowering the cultivation temperature and nickel supplementation markedly improved the specific activity of RH isolated from *E. coli* MC4100.

Escherichia coli BL21 Gold is known to be deficient in nickel uptake (Pinske et al., 2011). We thus tested whether the addition of $NiCl_2$ improves the activity of the RH purified from strains BQF8RH, BQF8RH2, and BQF8RH3 cultivated at 30°C. Indeed, we detected a low activity of 0.09 U mg^{-1} for the RH purified from strain BQF8RH3 (**Figure 2D**). Thus, nickel availability appears to be the major impediment to [NiFe] cofactor assembly

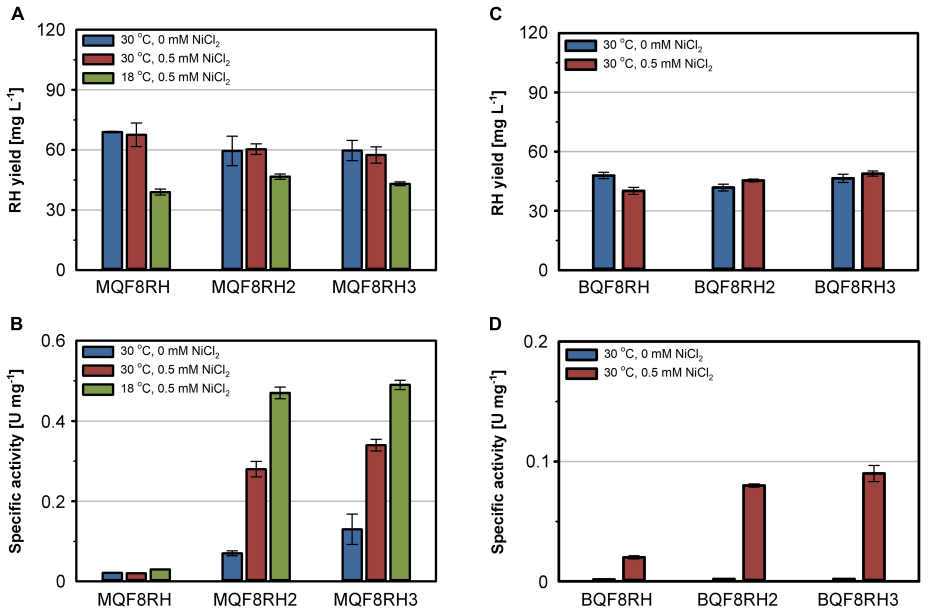

FIGURE 2 | Effect of $NiCl_2$ addition and cultivation temperature on RH yield and activity. Strains *E. coli* MQF8RH, MQF8RH2, MQF8RH3, BQF8RH, BQF8RH2 and BQF8RH3 were cultivated in 125 mL PreSens flask with 50 mL boosted EnPresso B medium under O_2-limited conditions. After induction, the temperature was either maintained at 30°C or shifted to 18°C. $NiCl_2$ (0.5 mM) was supplemented at the time point of the induction of RH gene expression as indicated. RH protein was purified by affinity chromatography **(A,C)** and specific activities measured from the purified samples **(B,D)**.

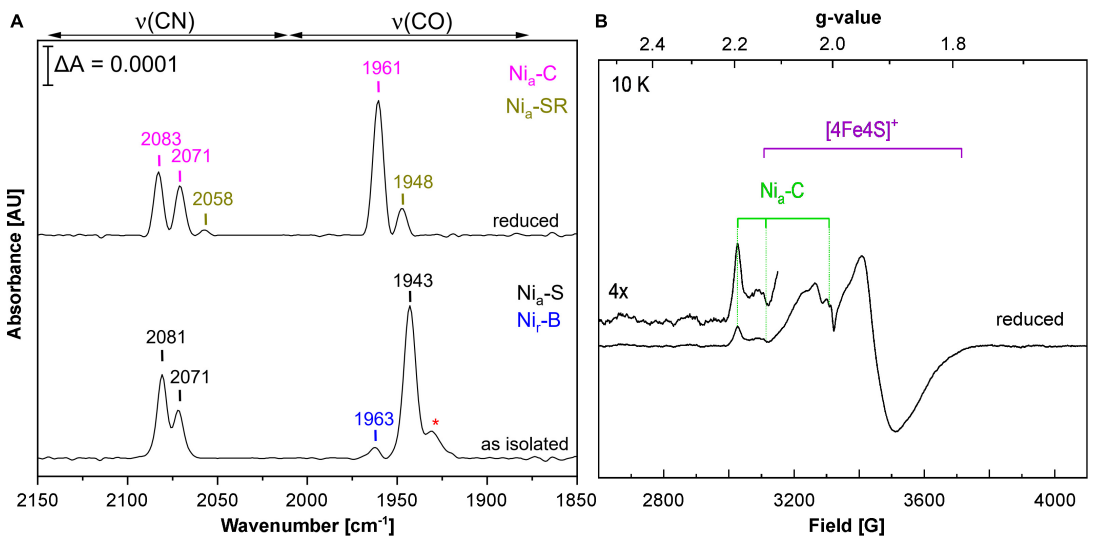

FIGURE 3 | Spectroscopic characterization of RH heterologously produced in *E. coli.* Spectroscopic data were recorded on RH purified from MQF8RH2 (30°C/0.5 mM $NiCl_2$). **(A)** IR spectra of as-isolated and H_2-reduced RH. The signals indicate the presence of CO and CN ligands of the $NiFe(CN)_2CO$ active site. Bands are labeled according to the different redox states of the RH (Ash et al., 2015; Roncaroli et al., 2015; Caserta et al., 2020), i.e., Ni_a-S (2,081, 2,071, 1,943 cm^{-1}), Ni_r-B (2,097, 2,089, 1,963 cm^{-1}), Ni_a-SR (2,073, 2,058, 1,948 cm^{-1}), and Ni_a-C (2,083, 2,071, 1,961 cm^{-1}). The red asterisk most likely indicates traces of Ni_r-S species (1,931 cm^{-1}). **(B)** EPR spectrum of sodium dithionite ($Na_2S_2O_4$)-reduced RH. The spectrum was recorded at 10 K and a microwave power of 1 mW.

in *E. coli* BL21 Gold. However, the RH activity was approximately fourfold lower than that of the K-12 strain MQF8RH3 cultivated under the same conditions.

Heterologously Produced RH Contains the Native NiFe $(CO)(CN)_2$ Cofactor

Using *E. coli* MC4100 as host, we obtained RH activities that were about half of those reported for the first RH preparations from *C. necator* (Bernhard et al., 2001). This prompted us to spectroscopically investigate the cofactor content of purified RH from *E. coli* strain MQF8RH3, which was cultivated under O_2-limiting conditions at 30°C and elevated nickel concentrations. By infrared spectroscopy, we monitored the CO and CN stretching vibrations of the CO and CN^- ligands of the $NiFe(CN)_2(CO)$ cofactor, which appear in a spectral region, in which no other protein-specific vibrations occur (De Lacey et al., 2007; Lubitz et al., 2014). The IR spectrum of the as-isolated, oxidized RH protein was dominated by the typical bands of the so-called Ni_a-S state, characterized by a CO stretching band at 1,943 cm^{-1} and two cyanide stretchings at 2,071 and 2,081 cm^{-1}. The IR signal amplitudes suggested a cofactor occupation of 5–10%. Treatment with H_2 gas resulted in reduced RH, whose IR spectrum is dominated by the Ni_a-C state with a CO stretching band at 1,961 cm^{-1} and two CN stretchings at 2,071 and 2,083 cm^{-1} (**Figure 3A**; Bernhard et al., 2001; Buhrke et al., 2005b; Roncaroli et al., 2015; Caserta et al., 2020). EPR spectroscopy, which allows the detection of paramagnetic states, confirmed the presence of signals related to the Ni_a-C-state (g_x = 2.19, g_y = 2.13, g_z = 2.01) as well as $[4Fe\text{-}4S]^{1+}$ cluster(s) signals in reduced RH treated with an excess of sodium dithionite (**Figure 3B**), which is in line with previous results obtained from RH isolated from *C. necator* (Roncaroli et al., 2015). These results demonstrate that the RH isolated from *E. coli* contains a canonical $NiFe(CN)_2(CO)$ cofactor that shares the same spectroscopic properties as the native RH isolated from *C. necator*.

Optimal Metal Ion Supplementation for RH Activity in *E. coli*

The nickel supplementation experiments described above were performed with a nickel concentration of 500 μM. To determine the optimal metal content in the growth medium, we devised a screening experiment with *E. coli* MQF8RH3 cultivated in 24-deepwell plates filled with EnPresso B medium containing different concentrations of nickel and iron. The cells were harvested, and the RH activity in crude cell extracts was determined as described in material and methods. The addition of up to 2 mM of either $NiCl_2$ or $FeSO_4$ had no effect on cell growth, as the final OD did not vary significantly (**Figure 4A**). As expected, $NiCl_2$ addition led to an increase of RH activity in the crude extracts. The highest activity of 0.5 U mg^{-1} was observed upon addition of 100 μM $NiCl_2$, which corresponds to an approximately threefold increase compared to the sample without nickel addition (**Figure 4B**). Further increase in nickel concentration diminished the RH activity (**Figure 4B**). In contrast, the addition of up to 500 μM $FeSO_4$ had only a negligible effect on the RH activity in the crude extract. A further increase even reduced the RH activity below 50% of the level achieved without iron addition. Thus, metal concentrations higher than 100 μM Ni and 500 μM Fe had a negative effect on RH activity and were avoided in subsequent experiments. Based on these screening experiments, we investigated the effect of nickel and iron on RH production and activity in larger medium volumes. *E. coli* MQF8RH3 was cultivated at 18°C in EnPresso B supplemented with different nickel:iron ratios [0:0, 100:0, 0:100, 100:100 (μM:μM)]. RH was purified and its activity was measured (**Figure 5**). The RH yield was the same under all conditions (**Figure 5A**). An activity of approx. 0.13 U mg^{-1} was observed without the addition of nickel or iron (**Figure 5B**), which is consistent with our data at 30°C (**Figure 2B**). The activity did not vary significantly upon addition of 100 μM $FeSO_4$, indicating that sufficient iron is present in the EnPresso B medium. In contrast, the addition of 100 μM $NiCl_2$ resulted in a fourfold increase of specific activity of 0.55 U mg^{-1}, which was similar to the value measured in the presence of 100 μM $NiCl_2$/100 μM $FeSO_4$ (0.57 U mg^{-1}, **Figure 5B**). Based on these results, we added 100 μM $NiCl_2$ but not further iron source to the growth media.

Improved RH Maturation by Co-production of HoxN and HypX From *C. necator*

The results described above clearly show a significant activity increase when the RH is isolated from O_2-limited *E. coli* cultures. Aerobic cultivation, by contrast, led to higher protein yields (**Figure 1A**). Therefore, we aimed to improve RH activity under aerobic conditions. Nickel supply is limited particularly under aerobic conditions as the endogenous nickel uptake system in *E. coli* in FNR-dependent and functional only under anaerobic conditions (Wu et al., 1989). Thus, we considered the gene encoding the high-affinity nickel permease HoxN, which mediates nickel uptake in *C. necator* under aerobic conditions (Eberz et al., 1989; Eitinger and Friedrich, 1991; Wolfram et al., 1995). Consequently, we extended plasmid pQF12 by adding *hoxN* gene from *C. necator* resulting into plasmid pQF17 (*hypA1B1F1CDE-hoxN)* (**Supplementary Figure 1**).

Additionally, we also considered that under aerobic conditions the formyltetrahydrofolate decarbonylase HypX from *C. necator* is responsible for the biosynthesis of the CO ligand of the $NiFe(CN)_2(CO)$ site (Bürstel et al., 2016; Schulz et al., 2020). Thus, we further extended plasmid pQF17 by implementing the *hypX* gene, yielding plasmid pQF18 (*hypA1B1F1CDEX-hoxN)*. The plasmids pQF17 and pQF18 were transferred to *E. coli* MQF8RH, resulting in strains MQF8RH7 and MQF8RH8, respectively. The new strains were grown in addition to strain MQF8RH2 in $NiCl_2$-supplemented (100 μM) and boosted EnPresso B medium under both aerobic and O_2-limited conditions. Cells were harvested after 48 h of IPTG induction, proteins purified and their specific activities quantified. While the presence of the new genes did not significantly affect the RH yield in the new strains (**Figure 6A**), the introduction

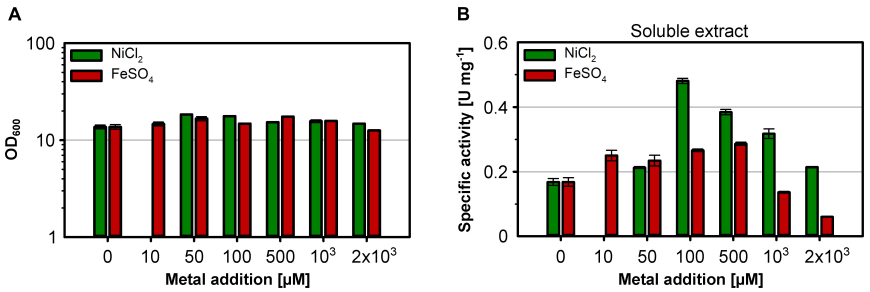

FIGURE 4 | Effect of the Ni and Fe concentration on cell growth and RH activity. *E. coli* strain MQF8RH3 was cultivated in 24-deepwell plates with 8 mL boosted EnPresso medium at 30°C under O_2-limited conditions. $NiCl_2$ or $FeSO_4$ were supplemented using the indicated concentrations varying from 0 to 2.0 mM. Cells were harvested 24 h after induction with 50 µM IPTG. **(A)** Optical density of the cell culture just before harvesting. **(B)** Soluble extracts were obtained by sonication and RH activity was measured. The specific RH activity was calculated based on the RH concentrations determined in the crude extracts by Western blotting (**Supplementary Figure 4**).

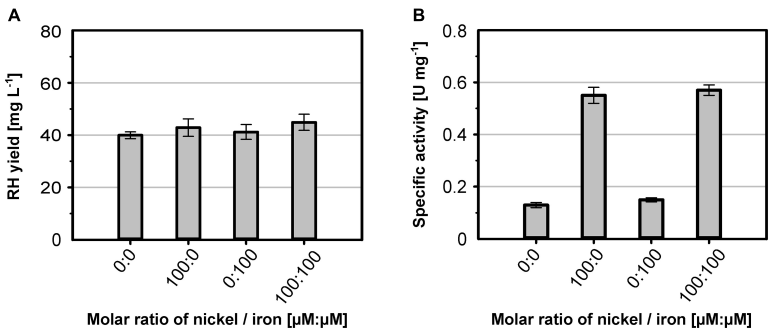

FIGURE 5 | Metal effect on soluble RH yield and activity. *E. coli* strain MQF8RH3 was cultivated in 125 mL PreSens flasks with 50 mL boosted EnPresso B medium at 18°C. The medium was supplemented with different molar ratios of $NiCl_2$ and $FeSO_4$ as indicated. **(A)** RH protein was purified by affinity chromatography, and the yield was quantified. **(B)** Specific activities measured from the purified RH samples.

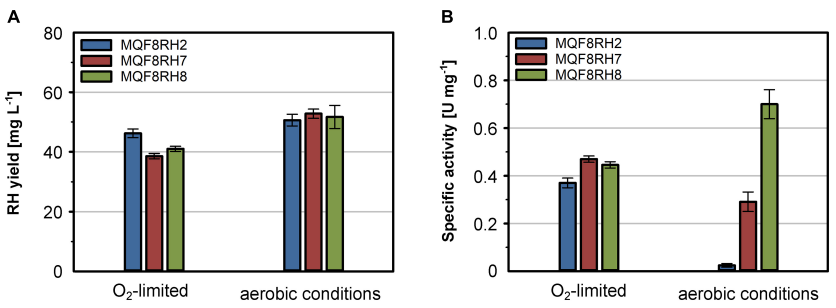

FIGURE 6 | Effect of *hoxN1* and *hypX* genes on the production of active RH. *E. coli* strains MQF8RH2 (RH-Hyp1), MQF8RH7 (RH-Hyp1-HoxN1) and MQF8RH8 (RH-Hyp1-HoxN1-HypX) were cultivated at 18°C in 50 mL boosted EnPresso B medium supplemented with 0.1 mM $NiCl_2$. After induction with 50 µM IPTG, RH production lasted for 48 h under either aerobic or O_2-limited conditions. **(A)** RH protein was purified by affinity chromatography, and the yield was quantified. **(B)** Specific activities measured from the purified RH samples.

of HoxN led to a slight increase of RH activity under O_2-limited conditions and about 12-fold higher activity under aerobic conditions (**Figure 6B**). These data clearly indicate that HoxN is functional in nickel uptake in the presence of high O_2 concentrations. The introduction of *hypX* did not improve the RH activity obtained from cells grown under O_2-limiting conditions, in line with a so far elusive HypX-independent CO ligand synthesis (Soboh et al., 2013; Arlt et al.,

2021). In contrast, the RH isolated from the aerobically grown strain MQF8RH8 showed a twofold higher specific activity (0.7 U mg^{-1}) than the RH purified from strain MQF8RH7 (**Figure 6B**). These data, surprisingly, evidenced the successful implementation of HypX in *E. coli* strains able to synthesize the active site CO ligand under aerobic conditions. Taken together, these findings demonstrate that co-expression of HypX and HoxN in addition to the *C. necator hyp1* operon enables biosynthesis of active RH even under aerobic conditions. Additionally, we successfully increased the space-time yield of catalytically active RH by a factor of about 27 compared to strain MQF8RH2 cultivated under the same conditions (12.5 *vs.* 0.45 U (L d) $^{-1}$). The reported RH activity under aerobic conditions represents the highest activity for a heterologous produced RH so far.

Production of Catalytically Active RH in *E. coli* BL21 Gold

The successful heterologous production of active RH through co-expression of the *hyp* and *hoxN* genes under aerobic conditions prompted us to revisit strain BQF8RH that so far showed the highest RH yield, although inactive (**Figure 1A**). Hence, we transformed strain BQF8RH with plasmid pQF18 and investigated the RH production in the resulting strain BQF8RH8 using the MC4100 derivative MQF8RH8 for comparison. Both strains were cultivated under aerobic conditions with or without the addition of $NiCl_2$. The added $NiCl_2$ neither affected cell growth (**Figure 7A**) nor the RH yield of the two strains (**Figure 7B**). As expected, the *E. coli* BL21 derivative BQF8RH8 showed an about 50% higher RH yield compared to the K12 derivative MQF8RH8. However, the prolongation of the aerobic induction period from 48 h to 72 h resulted in a twofold decrease in RH yield for both strains (**Figure 7B**). Clearly, nickel supplementation is necessary for production of catalytically active RH (**Figure 7C**) when the strains are cultivated under aerobic conditions. After 48 h of induction, the specific activities of the RH preparations from both MQF8RH8 and BQF8RH8 ranged similarly at about 0.6 U mg^{-1}. Despite the marked decrease in RH yield (**Figure 7B**), extension of the production period from 48 h to 72 h resulted in a threefold and fivefold increase in the specific RH activities of the samples isolated from strains MQF8RH8 and BQF8RH8 to 2 U mg^{-1} and even 3 U mg^{-1}, respectively (**Figure 7C**). Accordingly, the specific RH activity of strain BQF8RH8 was almost as high as that of RH isolated from the native host *C. necator* (Caserta et al., 2020). Considering protein yield and specific activity, the yield of active RH was similar (40 U L^{-1} of culture) for both

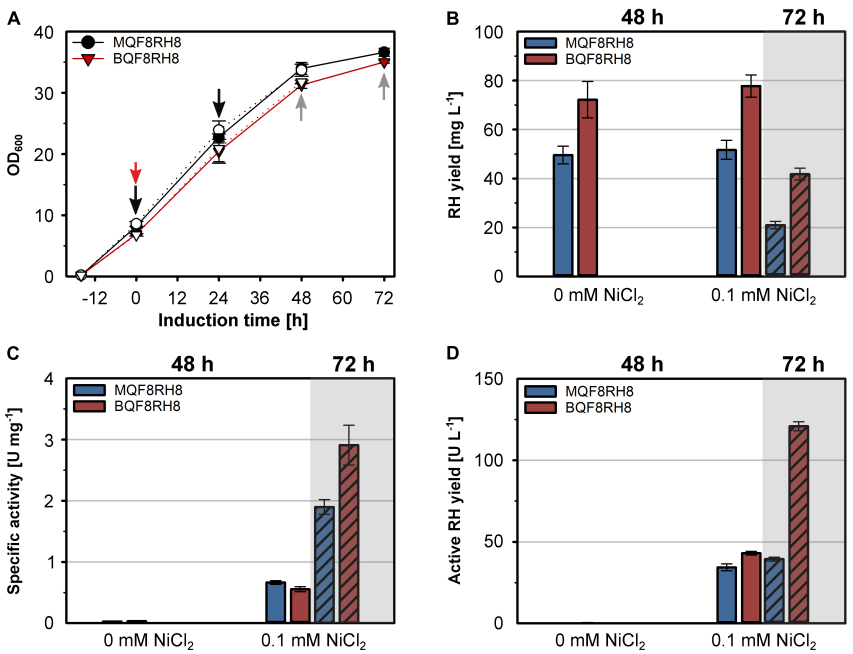

FIGURE 7 | Production of active RH in aerated cultures of *E. coli* BL21 Gold. *E. coli* strains MQF8RH8 and BQF8RH8 were cultured in 50 mL boosted EnPresso B medium at 18°C under aerobic conditions. RH gene expression was induced with 50 μM IPTG and cells harvested 48 h or 72 h (hatched columns) after induction. $NiCl_2$ was added at the time point of induction of gene expression as indicated. **(A)** Cell growth. The time point of induction is indicated by a red arrow, while the time points of booster addition and cell harvest are indicated by black and gray arrows, respectively. Open and filled symbols represent growth of *E. coli* with or without 0.1 mM $NiCl_2$, respectively. **(B)** RH protein was purified by affinity chromatography, and the yield was quantified. **(B)** specific activities measured from the purified RH samples. **(D)** Volumetric yield of RH calculated from the results in panels **(B,C)**.

induction periods of MQF8RH8 and for BQF8RH8 after 48 h of induction (**Figure 7D**). Remarkably, after an induction time of 72 h, we obtained an unprecedented yield of active RH of 120 U L^{-1} (**Figure 7D**) for strain BQF8RH8.

DISCUSSION

Here, we present a major improvement in the heterologous hydrogenase production in *E. coli* exemplified by the purification of catalytically active RH from *C. necator*. We optimized important factors such as the cultivation mode (anaerobic/aerobic), Ni and Fe content in the medium, production temperature, and co-expression of specific maturation genes, thereby systematically increasing the H_2-oxidizing activity. The RH activities as well as the protein yields obtained from all experiments conducted are summarized in **Supplementary Table 3**. Even though the RH is synthesized in an active form in its native host, *C. necator*, under aerobic conditions (Bernhard et al., 2001; Buhrke et al., 2005a; Ash et al., 2015), no active RH could be purified from aerobically grown *E. coli* strains without further genetic amendments. Under microaerobic/anaerobic growth conditions, however, little RH activity was observed, consistent with the fact that the hydrogenase maturation apparatus of *E. coli* is functional only under anaerobiosis (Messenger and Green, 2003; Forzi and Sawers, 2007; Lenz et al., 2007). Nevertheless, the very low activity suggests that the *E. coli* Hyp maturases are inefficient in outfitting the RH with the $NiFe(CN)_2CO$ cofactor. Indeed, the co-expression of the *hyp1* operon encoding the HypA1, B1, F1, C, D, and E proteins from *C. necator* further increased RH activity in *E. coli* (**Figure 1**). Although the Hyp proteins of *E. coli* and *C. necator* show an amino acid sequence identity of 18–45% (Wolf et al., 1998; Böck et al., 2006; Vignais and Billoud, 2007), this observation clearly demonstrates that they are not generally interchangeable with each other. The HypF protein plays an interesting role here. HypF1 from *C. necator* seems to be inactive under anaerobic conditions, and the *E. coli* HypF ortholog of *E. coli* takes over its function, consistent with a previous report (Lenz et al., 2007). Moreover, both HypF versions seem to compete with each other, as there is an increase in RH activity under anaerobic conditions in the absence of HypF1 of *C. necator*. The likely reason is that the inactive version of *C. necator* interferes with the interaction of the HypE protein with the *E. coli* HypF. Notably, the HypF1 of *C. necator* comprises only one of three domains present in canonical HypF proteins, such as that from *E. coli* (Wolf et al., 1998; Paschos et al., 2002). While canonical HypF proteins synthesize cyanide (CN) residue from carbamoyl phosphate and ATP, the truncated HypF likely requires carbamoyl adenylate for CN synthesis (Reissmann et al., 2003; Blokesch et al., 2004b). It is possible that carbamoyl adenylate is produced in sufficient quantities in living cells only under aerobic conditions. This assumption is supported by the higher RH activities obtained at lower temperature (**Figure 2**) which can be explained by a higher oxygenation of the medium compared to higher temperatures. Furthermore, lower temperatures might prevent misfolding of both the RH subunits and the maturases.

As nickel and iron are essential for RH activity, both metal ions must be provided in sufficient quantities. The availability of the metal ions depends both on their concentration in the medium, their bioavailability and the presence of specific cellular uptake systems. In *E. coli*, Fe^{2+} is predominantly transported across the membrane by the Feo system under microaerobic and anaerobic growth conditions, while Fe^{3+}, occurring predominantly under aerobic conditions, is taken up by the Fec system (Braun and Hantke, 2011; Kosman, 2013; Lau et al., 2016). Thus, the versatile iron uptake systems in *E. coli* allow for sufficient intracellular availability and iron homeostasis under both aerobic and anaerobic conditions. Kim et al. (2010, 2011) reported that iron rather than nickel needs to be added for the production of active *E. coli* hydrogenase 1 and *Hydrogenovibrio marinus* [NiFe]-hydrogenase in *E. coli* in a modified minimal medium. In the case of EnPresso B, the addition of iron had a negligible effect on the RH activity (**Figures 4**, **5**), indicating that this medium already contains sufficient iron. In contrast to iron, nickel is much less abundant and might be limiting in case of the overproduction of nickel-containing proteins such as [NiFe]-hydrogenase. In *E. coli*, nickel is taken up *via* the specific Nik system, which is synthesized only under anaerobic conditions. In Nik-deficient strains, such as *E. coli* BL21, nickel can be taken up by the magnesium transport system, which, however, has much lower specificity for nickel than the Nik transporter (Eitinger and Mandrand-Berthelot, 2000). In line with previous results that a high concentration (0.5 mM) of $NiCl_2$ added to the medium restores the activity of *E. coli* hydrogenases in strains with defects in nickel uptake (Waugh and Boxer, 1986; Wu et al., 1989), the activity of the RH improves significantly in all tested strains upon nickel addition (**Figures 2–5**). Interestingly, not only the Nik-deficient BL21 derivatives but also the MC4100 derivatives showed nickel dependence, indicating that the chelating properties of the medium limit the availability of nickel. The co-production of the high-affinity nickel permease HoxN from *C. necator* resulted in a substantial increase in RH activity both under anaerobic and aerobic growth conditions. Moreover, the presence of HoxN enables RH maturation even in the presence of molecular oxygen (**Figure 6**). Notably, the addition of up to 0.1 mM $NiCl_2$ to our EnPresso B medium had no effect on cell growth, even in the presence of HoxN.

It has been previously shown that under aerobic conditions the availability of CO is limiting for maturation of the $NiFe(CN)_2CO$ cofactor of hydrogenase (Bürstel et al., 2011). To address this potential problem in case of the production of hydrogenase in aerobically grown *E. coli*, we co-expressed the auxiliary *hypX* gene from *C. necator*, which is known to encode a CoA-dependent formyl-tetrahydrofolate (THF) decarbonylase (Schulz et al., 2020). This strategy improved the RH activity by threefold compared to a strain producing the HoxN permease alone (**Figure 6**). Remarkably, co-expression of *hoxN* and *hypX* genes in aerobically grown cells resulted in RH activities that were above those measured for RH isolated from anaerobically grown cells (**Figure 7**). Here, prolonged cultivation time from 48 h to 72 h significantly improved the specific RH activity, suggesting that the active site formation seems to be clearly dependent

on post-induction time. It is possible that the biosynthesis and incorporation of active site is a slow process, as it requires the involvement of multiple active maturases. This assumption is supported by the linear and continuous increase in specific RH activities with increasing induction time upon induction from 6 h to 72 h. Therefore, prolonging the induction time might serve as a further alternative strategy to maximize the cofactor occupancy in the active center and increase hydrogenase activity.

CONCLUSION

Commercial use of [NiFe]-hydrogenases is limited by the difficulty of producing these biocatalysts in scalable quantities. With some important exceptions, [NiFe]-hydrogenases are usually isolated from their native hosts (Fan et al., 2020). This is due to the fact that these complex metalloenzymes require a sophisticated maturation machinery. With this study we demonstrated that it is possible to produce a non-native [NiFe]-hydrogenase recombinantly in *E. coli* with high yield and a catalytic activity that—most importantly—is equivalent to that of hydrogenase purified from the native host. We purified the O_2-tolerant regulatory hydrogenase from *C. necator* from three *E. coli* derivatives with different genetic backgrounds under various growth conditions. Whereas Bernhard et al. and Caserta et al. obtained approx. 1 U L^{-1} (1.1 mg L^{-1} of RH with an activity of 1 U mg^{-1}) (Bernhard et al., 2001) and 0.4 U L^{-1} (0.1 mg L^{-1}, 4.5 U mg^{-1}) (Caserta et al., 2020), respectively, of purified RH from the native host, *C. necator*, our heterologous production process achieved 120 U L^{-1} (40 mg L^{-1} with 3 U mg^{-1}). This corresponds to an 100–300-fold higher yield of catalytically active RH. The highest yield was obtained from aerobically cultivated of *E. coli*, which significantly shortens the process time compared to the production in *C. necator*. Through strain improvement, i.e., the co-expression of specific maturation genes, and process optimization, we were even able to produce a catalytically active metalloprotein in the metabolically deficient *E. coli* BL21. Through optimally controlled expression of the required genes and optimized production conditions, the combinational strategy developed in this work offers a clear advantage over the native producer. Our strategy provides a useful roadmap for biotechnologically relevant production of [NiFe]-hydrogenases and can be applied in scale-up studies to achieve commercial feasibility of complex, difficult-to-produce metalloenzymes.

DATA AVAILABILITY STATEMENT

The raw data supporting the conclusions of this article will be made available by the authors, without undue reservation.

AUTHOR CONTRIBUTIONS

MG, QF, and OL participated in experimental design and interpretation of the results. QF carried out all molecular biological and biochemical experiments, and prepared the original draft. GC, CL, and IZ performed the spectroscopic IR and EPR measurements and the data evaluation. GC, CL, IZ, PN, and OL analyzed the data with major contributions from QF and MG. MG, PN, and OL revised the manuscript. All authors read and approved the final manuscript.

FUNDING

This work was supported by the Cluster of Excellence "Unifying Systems in Catalysis" (UniSysCat) coordinated by the Technische Universität Berlin and its graduate school, Berlin International Graduate School of Natural Sciences and Engineering (BIG-NSE), funded by the Deutsche Forschungsgemeinschaft (DFG) under Germany's Excellence Strategy (EXC 2008/1-390540038). QF obtained a grant from the China Government Scholarship program, 2017. GC and OL are grateful for EU financial support (Article 38.1.2, GC) within the European Union's Horizon 2020 Research and Innovation Program under grant agreement no 810856.

ACKNOWLEDGMENTS

We would like to appreciate Peter Hildebrandt for use of spectroscopic facilities and Janna Schoknecht for excellent technical assistance in activity measurements. We would also like to acknowledge support by the German Research Foundation and the Open Access Publication Fund of TU Berlin.

SUPPLEMENTARY MATERIAL

The Supplementary Material for this article can be found online at: https://www.frontiersin.org/articles/10.3389/fmicb.2022.894375/full#supplementary-material

REFERENCES

Arlt, C., Nutschan, K., Haase, A., Ihling, C., Tänzler, D., Sinz, A., et al. (2021). Native mass spectrometry identifies the HybG chaperone as carrier of the $Fe(CN)_2CO$ group during maturation of *E. coli* [NiFe]-hydrogenase 2. *Sci. Rep.* 11:24362. doi: 10.1038/s41598-021-03900-w

Ash, P. A., Liu, J., Coutard, N., Heidary, N., Horch, M., Gudim, I., et al. (2015). Electrochemical and infrared spectroscopic studies provide insight into reactions of the NiFe regulatory hydrogenase from *Ralstonia eutropha* with O_2 and CO. *J. Phys. Chem. B* 119, 13807–13815. doi: 10.1021/acs.jpcb.5b04164

Bachmann, B. J. (1972). Pedigrees of some mutant strains of *Escherichia coli* K-12. *Bacteriol. Rev.* 36, 525–557. doi: 10.1128/MMBR.36.4.525-557.1972

Baer, R., Bankier, A. T., Biggin, M. D., Deininger, P. L., Farrell, P. J., Gibson, T. J., et al. (1984). DNA sequence and expression of the B95-8 Epstein-Barr virus genome. *Nature* 310, 207–211. doi: 10.1038/310207a0

Bernhard, M., Buhrke, T., Bleijlevens, B., De Lacey, A. L., Fernandez, V. M., Albracht, S. P. J., et al. (2001). The H_2 sensor of *Ralstonia eutropha*. *J. Biol. Chem.* 276, 15592–15597. doi: 10.1074/jbc.M009802200

Blokesch, M., Albracht, S. P. J., Matzanke, B. F., Drapal, N. M., Jacobi, A., and Böck, A. (2004a). The complex between hydrogenase-maturation proteins HypC and

HypD is an intermediate in the supply of cyanide to the active site iron of [NiFe]-hydrogenases. *J. Mol. Biol.* 344, 155–167. doi: 10.1016/j.jmb.2004.09.040

Blokesch, M., Paschos, A., Bauer, A., Reissmann, S., Drapal, N., and Böck, A. (2004b). Analysis of the transcarbamoylation-dehydration reaction catalyzed by the hydrogenase maturation proteins HypF and HypE. *Eur. J. Biochem.* 271, 3428–3436. doi: 10.1111/j.1432-1033.2004.04280.x

Böck, A., King, P. W., Blokesch, M., and Posewitz, M. C. (2006). Maturation of hydrogenases. *Adv. Microb. Physiol.* 51, 1–71. doi: 10.1016/S0065-2911(06)51001-X

Brantl, S. (1994). The *copR* gene product of plasmid p1P501 acts as a transcriptional repressor at the essential *repR* promoter. *Mol. Microbiol.* 14, 473–483. doi: 10.1111/j.1365-2958.1994.tb02182.x

Braun, V., and Hantke, K. (2011). Recent insights into iron import by bacteria. *Curr. Opin. Chem. Biol.* 15, 328–334. doi: 10.1016/j.cbpa.2011.01.005

Buhrke, T., Bleijlevens, B., Albracht, S. P. J., and Friedrich, B. (2001). Involvement of *hyp* gene products in maturation of the H_2-sensing [NiFe] hydrogenase of *Ralstonia eutropha*. *J. Bacteriol.* 183, 7087–7093. doi: 10.1128/JB.183.24.7087-7093.2001

Buhrke, T., Lenz, O., Krauss, N., and Friedrich, B. (2005a). Oxygen tolerance of the H_2-sensing [NiFe] hydrogenase from *Ralstonia eutropha* H16 is based on limited access of oxygen to the active site. *J. Biol. Chem.* 280, 23791–23796. doi: 10.1074/jbc.M503260200

Buhrke, T., Löscher, S., Lenz, O., Schlodder, E., Zebger, I., Andersen, L. K., et al. (2005b). Reduction of unusual iron-sulfur clusters in the H_2-sensing regulatory NiFe hydrogenase from *Ralstonia eutropha* H16. *J. Biol. Chem.* 280, 19488–19495. doi: 10.1074/jbc.M500601200

Bürstel, I., Hummel, P., Siebert, E., Wisitruangsakul, N., Zebger, I., Friedrich, B., et al. (2011). Probing the origin of the metabolic precursor of the CO ligand in the catalytic center of [NiFe] hydrogenase. *J. Biol. Chem.* 286, 44937–44944. doi: 10.1074/jbc.M111.309351

Bürstel, I., Siebert, E., Frielingsdorf, S., Zebger, I., Friedrich, B., and Lenz, O. (2016). CO synthesized from the central one-carbon pool as source for the iron carbonyl in O_2-tolerant [NiFe]-hydrogenase. *Proc. Natl. Acad. Sci. U.S.A.* 113, 14722–14726. doi: 10.1073/pnas.1614656113

Bürstel, I., Siebert, E., Winter, G., Hummel, P., Zebger, I., Friedrich, B., et al. (2012). A universal scaffold for synthesis of the $Fe(CN)_2(CO)$ moiety of [NiFe] hydrogenase. *J. Biol. Chem.* 287, 38845–38853. doi: 10.1074/jbc.M112.376947

Casadaban, M. J., and Cohen, S. N. (1979). Lactose genes fused to exogenous promoters in one step using a Mu-lac bacteriophage: *in vivo* probe for transcriptional control sequences. *Proc. Natl. Acad. Sci. U.S.A.* 76, 4530–4533. doi: 10.1073/pnas.76.9.4530

Casalot, L., and Rousset, M. (2001). Maturation of the [NiFe] hydrogenases. *Trends Microbiol.* 9, 228–237. doi: 10.1016/S0966-842X(01)02009-1

Caserta, G., Lorent, C., Pelmenschikov, V., Schoknecht, J., Yoda, Y., Hildebrandt, P., et al. (2020). *In vitro* assembly as a tool to investigate catalytic intermediates of [NiFe]-hydrogenase. *ACS Catal.* 10, 13890–13894. doi: 10.1021/acscatal.0c04079

De Lacey, A. L., Fernández, V. M., Rousset, M., and Cammack, R. (2007). Activation and inactivation of hydrogenase function and the catalytic cycle: spectroelectrochemical Studies. *Chem. Rev.* 107, 4304–4330. doi: 10.1021/CR0501947

Eberz, G., Eitinger, T., and Friedrich, B. (1989). Genetic determinants of a nickel-specific transport system are part of the plasmid-encoded hydrogenase gene cluster in *Alcaligenes eutrophus*. *J. Bacteriol.* 171, 1340–1345. doi: 10.1128/jb.171.3.1340-1345.1989

Eitinger, T., and Friedrich, B. (1991). Cloning, nucleotide sequence, and heterologous expression of a high-affinity nickel transport gene from *Alcaligenes eutrophus*. *J. Biol. Chem.* 266, 3222–3227. doi: 10.1016/S0021-9258(18)49977-2

Eitinger, T., and Mandrand-Berthelot, M. A. (2000). Nickel transport systems in microorganisms. *Arch. Microbiol.* 173, 1–9. doi: 10.1007/s002030050001

Fan, Q., Caserta, G., Lorent, C., Lenz, O., Neubauer, P., and Gimpel, M. (2021a). Optimization of culture conditions for oxygen-tolerant regulatory [NiFe]-hydrogenase production from *Ralstonia eutropha* H16 in *Escherichia coli*. *Microorganisms* 9:1195. doi: 10.3390/microorganisms9061195

Fan, Q., Neubauer, P., and Gimpel, M. (2021b). Production of soluble regulatory hydrogenase from *Ralstonia eutropha* in *Escherichia coli* using a fed-batch-based autoinduction system. *Microb. Cell Fact.* 20:201. doi: 10.1186/s12934-021-01690-4

Fan, Q., Neubauer, P., Lenz, O., and Gimpel, M. (2020). Heterologous hydrogenase overproduction systems for biotechnology—An overview. *Int. J. Mol. Sci.* 21:5890. doi: 10.3390/ijms21165890

Fontecilla-Camps, J. C., Volbeda, A., Cavazza, C., and Nicolet, Y. (2007). Structure/function relationships of [NiFe]- and [FeFe]-hydrogenases. *Chem. Rev.* 107, 4273–4303. doi: 10.1021/cr050195z

Forzi, L., and Sawers, R. G. (2007). Maturation of [NiFe]-hydrogenases in *Escherichia coli*. *Biometals* 20, 565–578. doi: 10.1007/s10534-006-9048-5

Fritsch, J., Lenz, O., and Friedrich, B. (2013). Structure, function and biosynthesis of O_2-tolerant hydrogenases. *Nat. Rev. Microbiol.* 11, 106–114. doi: 10.1038/nrmicro2940

Hartmann, S., Frielingsdorf, S., Caserta, G., and Lenz, O. (2020). A membrane-bound [NiFe]-hydrogenase large subunit precursor whose C-terminal extension is not essential for cofactor incorporation but guarantees optimal maturation. *Microbiologyopen* 9, 1197–1206. doi: 10.1002/mbo3.1029

Kaluarachchi, H., Altenstein, M., Sugumar, S. R., Balbach, J., Zamble, D. B., and Haupt, C. (2012). Nickel binding and [NiFe]-hydrogenase maturation by the metallochaperone SlyD with a single metal-binding site in *Escherichia coli*. *J. Mol. Biol.* 417, 28–35. doi: 10.1016/j.jmb.2012.01.037

Kim, H. J., Jeong, H., Hwang, S., Lee, M.-S., Lee, Y.-J., Lee, D.-W., et al. (2014). Short-term differential adaptation to anaerobic stress via genomic mutations by *Escherichia coli* strains K-12 and B lacking alcohol dehydrogenase. *Front. Microbiol.* 5:476. doi: 10.3389/fmicb.2014.00476

Kim, J. Y., Jo, B., and Cha, H. (2010). Production of biohydrogen by recombinant expression of [NiFe]-hydrogenase 1 in *Escherichia coli*. *Microb. Cell Fact.* 9:54. doi: 10.1186/1475-2859-9-54

Kim, J. Y. H., Jo, B. H., and Cha, H. J. (2011). Production of biohydrogen by heterologous expression of oxygen-tolerant *Hydrogenovibrio marinus* [NiFe]-hydrogenase in *Escherichia coli*. *J. Biotechnol.* 155, 312–319. doi: 10.1016/j.jbiotec.2011.07.007

Kleihues, L., Lenz, O., Bernhard, M., Buhrke, T., and Friedrich, B. (2000). The H_2 sensor of *Ralstonia eutropha* is a member of the subclass of regulatory [NiFe] hydrogenases. *J. Bacteriol.* 182, 2716–2724. doi: 10.1128/JB.182.10.2716-2724.2000

Kosman, D. J. (2013). Iron metabolism in aerobes: managing ferric iron hydrolysis and ferrous iron autoxidation. *Coord. Chem. Rev.* 257, 210–217. doi: 10.1016/j.ccr.2012.06.030

Lacasse, M. J., and Zamble, D. B. (2016). [NiFe]-hydrogenase maturation. *Biochemistry* 55, 1689–1701. doi: 10.1021/acs.biochem.5b01328

Lau, C. K. Y., Krewulak, K. D., and Vogel, H. J. (2016). Bacterial ferrous iron transport: the Feo system. *FEMS Microbiol. Rev.* 40, 273–298. doi: 10.1093/femsre/fuv049

Lauterbach, L., and Lenz, O. (2013). Catalytic production of hydrogen peroxide and water by oxygen-tolerant [NiFe]-hydrogenase during H_2 cycling in the presence of O_2. *J. Am. Chem. Soc.* 135, 17897–17905. doi: 10.1021/ja408420d

Leach, M. R., Zhang, J. W., and Zamble, D. B. (2007). The role of complex formation between the *Escherichia coli* hydrogenase accessory factors HypB and SlyD. *J. Biol. Chem.* 282, 16177–16186. doi: 10.1074/jbc.M610834200

Lenz, O., Lauterbach, L., and Frielingsdorf, S. (2018). O_2-tolerant [NiFe]-hydrogenases of *Ralstonia eutropha* H16: Physiology, molecular biology, purification, and biochemical analysis. *Methods Enzymol.* 613, 117–151. doi: 10.1016/bs.mie.2018.10.008

Lenz, O., Lauterbach, L., Frielingsdorf, S., and Friedrich, B. (2015). "Oxygen-tolerant hydrogenases and their biotechnological potential," in *Biohydrogen*, ed. M. Rögner (Berlin: De Gruyter), 61–96. doi: 10.1515/9783110336733.61

Lenz, O., Ludwig, M., Schubert, T., Bürstel, I., Ganskow, S., Goris, T., et al. (2010). H_2 conversion in the presence of O_2 as performed by the membrane-bound [NiFe]-hydrogenase of *Ralstonia eutropha*. *ChemPhysChem* 11, 1107–1119. doi: 10.1002/cphc.200901002

Lenz, O., Strack, A., Tran-Betcke, A., and Friedrich, B. (1997). A hydrogen-sensing system in transcriptional regulation of hydrogenase gene expression in Alcaligenes species. *J. Bacteriol.* 179, 1655–1663. doi: 10.1128/JB.179.5.1655-1663.1997

Lenz, O., Zebger, I., Hamann, J., Hildebrandt, P., and Friedrich, B. (2007). Carbamoylphosphate serves as the source of CN^-, but not of the intrinsic CO

in the active site of the regulatory [NiFe]-hydrogenase from *Ralstonia eutropha*. *FEBS Lett.* 581, 3322–3326. doi: 10.1016/j.febslet.2007.06.027

Lubitz, W., Ogata, H., Ru, O., and Reijerse, E. (2014). Hydrogenases. *Chem. Rev.* 114, 4081–4148. doi: 10.1021/cr4005814

Lutz, S., Jacobi, A., Schlensog, V., Böhm, R., Sawers, G., and Böck, A. (1991). Molecular characterization of an operon (*hyp*) necessary for the activity of the three hydrogenase isoenzymes in *Escherichia coli*. *Mol. Microbiol.* 5, 123–135. doi: 10.1111/j.1365-2958.1991.tb01833.x

Messenger, S. L., and Green, J. (2003). FNR-mediated regulation of *hyp* expression in *Escherichia coli*. *FEMS Microbiol. Lett.* 228, 81–86. doi: 10.1016/S0378-1097(03)00726-2

Ogata, H., Lubitz, W., and Higuchi, Y. (2016). Structure and function of [NiFe] hydrogenases. *J. Biochem.* 160, 251–258. doi: 10.1093/jb/mvw048

Paschos, A., Bauer, A., Zimmermann, A., Zehelein, E., and Böck, A. (2002). HypF, a carbamoyl phosphate-converting enzyme involved in [NiFe] hydrogenase maturation. *J. Biol. Chem.* 277, 49945–49951. doi: 10.1074/jbc.M204601200

Peters, J. W., Schut, G. J., Boyd, E. S., Mulder, D. W., Shepard, E. M., Broderick, J. B., et al. (2015). [FeFe]- and [NiFe]-hydrogenase diversity, mechanism, and maturation. *Biochim. Biophys. Acta Mol. Cell Res.* 1853, 1350–1369. doi: 10.1016/j.bbamcr.2014.11.021

Pierik, A. J., Schmelz, M., Lenz, O., Friedrich, B., and Albracht, S. P. J. (1998). Characterization of the active site of a hydrogen sensor from *Alcaligenes eutrophus*. *FEBS Lett.* 438, 231–235. doi: 10.1016/S0014-5793(98)01306-4

Pinske, C., Bönn, M., Krüger, S., Lindenstrauß, U., and Sawers, R. G. (2011). Metabolic deficiences revealed in the biotechnologically important model bacterium *Escherichia coli* BL21(DE3). *PLoS One* 6:e22830. doi: 10.1371/journal.pone.0022830

Pinske, C., Sargent, F., and Sawers, R. G. (2015). SlyD-dependent nickel delivery limits maturation of [NiFe]-hydrogenases in late-stationary phase *Escherichia coli* cells. *Metallomics* 7, 683–690. doi: 10.1039/c5mt00019j

Pinske, C., Thomas, C., Nutschan, K., and Sawers, R. G. (2019). Delimiting the function of the C-terminal extension of the *Escherichia coli* [NiFe]-hydrogenase 2 large subunit precursor. *Front. Microbiol.* 10:2223. doi: 10.3389/fmicb.2019.02223

Rangarajan, E. S., Asinas, A., Proteau, A., Munger, C., Baardsnes, J., Iannuzzi, P., et al. (2008). Structure of [NiFe] hydrogenase maturation protein HypE from *Escherichia coli* and its interaction with HypF. *J. Bacteriol.* 190, 1447–1458. doi: 10.1128/JB.01610-07

Rathnayake, I., Megharaj, M., Krishnamurti, G., Bolan, N., and Naidu, R. (2013). Heavy metal toxicity to bacteria–Are the existing growth media accurate enough to determine heavy metal toxicity? *Chemosphere* 90, 1195–1200. doi: 10.1016/j.chemosphere.2012.09.036

Reissmann, S., Hochleitner, E., Wang, H., Paschos, A., Lottspeich, F., Glass, R. S., et al. (2003). Taming of a poison: biosynthesis of the NiFe-hydrogenase cyanide ligands. *Science* 299, 1067–1070. doi: 10.1126/science.1080972

Roncaroli, F., Bill, E., Friedrich, B., Lenz, O., Lubitz, W., and Pandelia, M.-E. (2015). Cofactor composition and function of a H_2-sensing regulatory hydrogenase as revealed by Mössbauer and EPR spectroscopy. *Chem. Sci.* 6, 4495–4507. doi: 10.1039/c5sc01560j

Roseboom, W., Blokesch, M., Böck, A., and Albracht, S. P. J. (2005). The biosynthetic routes for carbon monoxide and cyanide in the Ni-Fe active site of hydrogenases are different. *FEBS Lett.* 579, 469–472. doi: 10.1016/j.febslet.2004.12.013

Schollmeyer, J. (2020). *Bioprocess Development for the Production of a S-methyl-5′-thio-Adenosine Phosphorylase in Escherichia coli*. Master thesis. Berlin: TU Berlin.

Schulz, A. C., Frielingsdorf, S., Pommerening, P., Lauterbach, L., Bistoni, G., Neese, F., et al. (2020). Formyltetrahydrofolate decarbonylase synthesizes the active site CO ligand of O_2-tolerant [NiFe] hydrogenase. *J. Am. Chem. Soc.* 142, 1457–1464. doi: 10.1021/jacs.9b11506

Schwartz, E., Fritsch, J., and Friedrich, B. (2013). "H_2-metabolizing prokaryotes," in *The Prokaryotes: Prokaryotic Physiology and Biochemistry*, eds E. Rosenberg, E. F. DeLong, S. Lory, E. Stackebrandt, F. Thomson (Heidelberg, Berlin: Springer), 119–199. doi: 10.1007/978-3-642-30141-4_65

Senger, M., Stripp, S. T., and Soboh, B. (2017). Proteolytic cleavage orchestrates cofactor insertion and protein assembly in [NiFe]-hydrogenase biosynthesis. *J. Biol. Chem.* 292, 11670–11681. doi: 10.1074/jbc.M117.788125

Soboh, B., Stripp, S. T., Bielak, C., Lindenstrauß, U., Braussemann, M., Javaid, M., et al. (2013). The [NiFe]-hydrogenase accessory chaperones HypC and HybG of *Escherichia coli* are iron- and carbon dioxide-binding proteins. *FEBS Lett.* 587, 2512–2516. doi: 10.1016/j.febslet.2013.06.055

Soini, J., Ukkonen, K., and Neubauer, P. (2008). "High cell density media for *Escherichia coli* are generally designed for aerobic cultivations - consequences for large-scale bioprocesses and shake flask cultures. *Microb. Cell Fact.* 7:26. doi: 10.1186/1475-2859-7-26

Vignais, P. M., and Billoud, B. (2007). Occurrence, classification, and biological function of hydrogenases: an overview. *Chem. Rev.* 107, 4206–4272. doi: 10.1021/cr050196r

Watanabe, S., Matsumi, R., Atomi, H., Imanaka, T., and Miki, K. (2012). Crystal structures of the HypCD complex and the HypCDE ternary complex: transient intermediate complexes during [NiFe] hydrogenase maturation. *Structure* 20, 2124–2137. doi: 10.1016/j.str.2012.09.018

Waugh, R., and Boxer, D. H. (1986). Pleiotropic hydrogenase mutants of *Escherichia coli* K12: growth in the presence of nickel can restore hydrogenase activity. *Biochimie* 68, 157–166. doi: 10.1016/S0300-9084(86)81080-X

Wolf, I., Buhrke, T., Dernedde, J., Pohlmann, A., and Friedrich, B. (1998). Duplication of *hyp* genes involved in maturation of [NiFe] hydrogenases in *Alcaligenes eutrophus* H16. *Arch. Microbiol.* 170, 451–459. doi: 10.1007/s002030050666

Wolfram, L., Friedrich, B., and Eitinger, T. (1995). The *Alcaligenes eutrophus* protein HoxN mediates nickel transport in *Escherichia coli*. *J. Bacteriol.* 177, 1840–1843. doi: 10.1128/JB.177.7.1840-1843.1995

Wu, L. -F., Mandrand-Berthelot, M. -A., Waugh, R., Edmonds, C. J., Holt, S. E., and Boxer, D. H. (1989). Nickel deficiency gives rise to the defective hydrogenase phenotype of *hydC* and *fnr* mutants in *Escherichia coli*. *Mol. Microbiol.* 3, 1709–1718. doi: 10.1111/j.1365-2958.1989.tb00156.x

Conflict of Interest: PN is a shareholder of EnPresso GmbH.

The remaining authors declare that the research was conducted in the absence of any commercial or financial relationships that could be construed as a potential conflict of interest.

Publisher's Note: All claims expressed in this article are solely those of the authors and do not necessarily represent those of their affiliated organizations, or those of the publisher, the editors and the reviewers. Any product that may be evaluated in this article, or claim that may be made by its manufacturer, is not guaranteed or endorsed by the publisher.

Paper IV

Implementation of a high cell density fed-batch for heterologous production of active [NiFe]-hydrogenase in *Escherichia coli*

Qin Fan, Saskia Waldburger, Peter Neubauer, Sebastian L. Riedel and Matthias Gimpel

Microb. Cell Fact. **21, 193**

Fan *et al. Microbial Cell Factories* (2022) 21:193
https://doi.org/10.1186/s12934-022-01919-w

Microbial Cell Factories

RESEARCH Open Access

Implementation of a high cell density fed-batch for heterologous production of active [NiFe]-hydrogenase in *Escherichia coli* bioreactor cultivations

Qin Fan, Saskia Waldburger, Peter Neubauer, Sebastian L. Riedel and Matthias Gimpel*

Abstract

Background: O_2-tolerant [NiFe]-hydrogenases offer tremendous potential for applications in H_2-based technology. As these metalloenzymes undergo a complicated maturation process that requires a dedicated set of multiple accessory proteins, their heterologous production is challenging, thus hindering their fundamental understanding and the development of related applications. Taking these challenges into account, we selected the comparably simple regulatory [NiFe]-hydrogenase (RH) from *Cupriavidus necator* as a model for the development of bioprocesses for heterologous [NiFe]-hydrogenase production. We already reported recently on the high-yield production of catalytically active RH in *Escherichia coli* by optimizing the culture conditions in shake flasks.

Results: In this study, we further increase the RH yield and ensure consistent product quality by a rationally designed high cell density fed-batch cultivation process. Overall, the bioreactor cultivations resulted in $^{>}130$ mg L^{-1} of catalytically active RH which is a more than 100-fold increase compared to other RH laboratory bioreactor scale processes with *C. necator*. Furthermore, the process shows high reproducibility of the previously selected optimized conditions and high productivity.

Conclusions: This work provides a good opportunity to readily supply such difficult-to-express complex metalloproteins economically and at high concentrations to meet the demand in basic and applied studies.

Keywords: Metalloprotein, Regulatory hydrogenase, High cell density fed-batch, *Escherichia coli*, [NiFe]-hydrogenase

Introduction

In view of global warming and depletion of natural resources, scientists are struggling to look for renewable and environmentally friendly alternative energy systems. Hydrogenases, which are complex metalloenzymes capable of reversibly catalyzing the conversion of H_2 into protons and electrons, can serve a valuable model for these tasks [1, 2]. Although most hydrogenases are typically inhibited or irreversibly inactivated even by trace amounts of O_2 or CO, certain O_2-tolerant [NiFe]-hydrogenases capable of sustaining the catalytic activity in the presence of O_2, are widely distributed in nature [3, 4]. To date, the most well-characterized O_2-tolerant [NiFe]-hydrogenases come from *Cupriavidus necator* (formerly *Ralstonia eutropha*) H16, which houses four different types of these hydrogenases (membrane-bound hydrogenase (MBH), soluble NAD^+-reducing hydrogenase (SH), actinobacterial-like hydrogenase (AH), regulatory hydrogenase (RH) [5, 6]. Over several decades, technical systems that use O_2-tolerant [NiFe]-hydrogenases have been developed. These systems offer

*Correspondence: matthias.gimpel@tu-berlin.de

Chair of Bioprocess Engineering, Technische Universität Berlin, Ackerstr. 76, ACK24, D-13355 Berlin, Germany

tremendous potential applications in e.g. light-driven H_2 production [7–9], H_2-driven biofuel cells [10–12] or H_2-mediated cofactor regeneration [13–15]. However, at present, their biotechnological applications is still hardly feasible due to the low product yields and long process times by cultivation of the native producers [16–19]. Similarly, the heterologous production of these hydrogenases is challenging due to the complicated maturation process and the high specificity of the required maturation proteins [20]. To improve accessibility of hydrogenases, we recently developed a heterologous production system for [NiFe]-hydrogenases in the robust and genetically tractable production host *Escherichia coli* by the example of the O_2-tolerant regulatory [NiFe]-hydrogenase from *C. necator* [21].

The RH functions as H_2 sensor regulating the expression of energy-converting hydrogenases (MBH, SH operons) in the presence of H_2 [22, 23]. It consists of two heterodimers, each formed by the large HoxC subunit (52 kDa) harboring the H_2-activating [$NiFe(CN)_2CO$]-cofactor and the small HoxB subunit (36 kDa) with three [4Fe4S]-clusters [5, 24]. A truncated version, called RH_{stop} protein, that consists of the single HoxBC heterodimer capable of H_2-oxidation in vitro, has been widely used for spectroscopic studies [25–29]. Previously, this truncated protein as well as wildtype RH were obtained from batch cultivations of *C. necator* at very low yields of 0.1–1 mg L^{-1} ($<$ 0.1 mg g^{-1}) [30–32]. Recently, we achieved by heterologous production in *E. coli* BL21 Gold approx. 300 mg L^{-1} RH in shake flasks by the use of the fed-batch-like EnPresso® growth system [33, 34]. However, despite the high yield the product was inactive due to the absence of the [NiFe] cofactor [33]. The biosynthesis and incorporation of the [NiFe] cofactor into the apo-hydrogenase requires nickel and iron as well as six accessory proteins encoded by the *hyp1* operon [35–37]. Furthermore, we achieved the production of catalytically active RH in aerobically grown *E. coli* BL21 derivatives by co-expressing the *C. necator hyp1* operon as well as the HoxN high-affinity nickel permease and the dedicated HypX maturase and addition of $NiCl_2$ [21].

The enzyme-based glucose-releasing EnPresso® medium is based on a typical *E. coli* mineral salt medium supplemented with a non-metabolizable polymer as carbon source. The glucose release from the polymer can be controlled by the amount of enzyme added to the culture, resulting in a quasi-linear increase in cell densities despite permanent glucose limitation [38]. In such growth system proteins are produced under optimal metabolic conditions, thus reducing the risk of incorrectly folding and increasing the portion of soluble proteins, as has been confirmed by the production of different recombinant proteins [38–41]. Small-scale cultivations in the EnPresso growth system e.g. in microwell-plates or shake-flasks are suitable for estimation and optimization of transferable process parameters, however, the yields stay lower compared to benchtop bioreactors due to lower oxygen transfer rates, restricted glucose availability and the impossibility to provide an exponential feed rate [39, 42]. Hence, the next rational step was the development of a high cell density fed-batch process. Generally, *E. coli* can be successfully cultivated in bioreactors up to high cell densities by applying a glucose limited fed-batch mode. In this mode, a highly concentrated glucose solution is continuously fed to the reactor as the growth limiting component, and thus the growth rate can be adapted to the oxygen transfer rate, so that aerobic cultivation conditions can be ensured even at high cell densities [43, 44]. In this study, a rationally designed parallelized fed-batch bioreactor process was developed to produce RH at high cell densities. We believe that the data reported herein provide a reasonable bioprocess development approach for realizing difficult-to-express metalloprotein production to meet the demand for active enzyme in basic and applied studies.

Materials and methods

Bacterial strains

E. coli strain BQF8RH8 (BL21-Gold [F^-*ompT hsdS*(r_B–m_B–) *dcm*$^+$ *Tet*^{R} *gal endA Hte*] carrying plasmids pQF8 and pQF18) [21] was used as the production host. The plasmid pQF8 contains the genes encoding the RH structural subunits under control of a $P_{lac\text{-}CTU}$ promoter, while the plasmid pQF18 harbors the native maturation genes encoding the auxiliary proteins HypA1B1F1CDEX and the nickel permease HoxN under the control of a P_{tac} promoter [21].

Growth media

All main cultures were performed using a defined mineral salt medium (MSM), as described recently [41]. Additionally, a macro element solution was prepared as a 10 × stock containing 146 g L^{-1} K_2HPO_4, 40 g L^{-1} $NaH_2PO_4 \times H_2O$, 20 g L^{-1} Na_2SO_4, 25 g L^{-1} $(NH_4)_2SO_4$, 5 g L^{-1} NH_4Cl, 10 g L^{-1} $(NH_4)_2$-H-citrate and separately autoclaved for further use in the feeding solution.

For preparation of precultures LB medium (5 g L^{-1} yeast extract, 10 g L^{-1} tryptone, 5 g L^{-1} NaCl for preculture 1) and EnPresso® B medium (EnPresso GmbH, Germany, for preculture 2) were used. For selection, 25 µg mL^{-1} chloramphenicol and 25 µg mL^{-1} kanamycin were added to all cultures.

Pre-experiments in 24 deepwell plates

To test cell growth and RH expression in MSM under different nickel or iron concentrations, a 24 deepwell

flat-bottom OxoDish® (OD24) plate (PreSens Precision Sensing GmbH, Germany), was used for the pre-experiments. The plate is equipped with oxygen sensors at the bottom of each well, which allows *on-line* measurement of dissolved oxygen concentration (DO). *E. coli* BQF8RH8 was first grown in 50 mL of MSM medium containing 9 g L^{-1} glucose in a 250-mL Ultra-Yield™ flask (UYF; Thomson Instrument Company, USA) sealed with a sterile AirOtop membrane (Thomson Instrument Company, USA) at 37 ℃, 250 rpm for 2 h until an optical density at 600 nm (OD_{600}) of approx. 0.6 was attained, and then 3 mL of culture were distributed into each well of the 24 OxoDish plate. Subsequently, 50 µM IPTG for induction of protein expression and different concentrations of $NiSO_4$ (0, 30, 50, 100, 500, 1000 µM) together with 0.1 mM $FeCl_3$ or different $FeCl_3$ concentrations (0, 30, 50, 100, 500, 1000 µM) together with 0.1 mM $NiSO_4$ were added to the wells. The cultivations were performed at 30 ℃, 250 rpm (Infors HT, 25 mm amplitude, Switzerland) for 21 h of induction. At the end of the cultivation, 3 mL culture broth from each well were collected in two 1.5-mL tubes followed by centrifugation at 4 ℃ with at 16 000 × *g* for 10 min. The cell pellets were stored at -80 ℃ for further analysis.

Preculture and inoculation conditions for the fed-batch bioreactor cultivations

To ensure a sufficient cell density for inoculation of the bioreactor, a two-step preculture was used. For the 1st pre-culture, 25 mL LB medium in a 125-mL UYF (Thomson Instrument Company, USA) sealed with a sterile AirOtop membrane (Thomson Instrument Company, USA) were inoculated with scratch of colonies from a fresh LB agar plate and incubated for 6 – 8 h at 30 ℃ and 200 rpm (Infors HT, 50 mm amplitude, Switzerland). Next, 1 mL of the pre-seed LB culture was used to inoculate 150 mL EnPresso B medium supplemented with 3 U L^{-1} reagent A according to the manufacturer's instructions (EnPresso GmbH, Germany). The fed-batch like preculture was performed in a 1000-mL single-use polycarbonate sensor flask (SFS-HP5-PSt3, PreSens Precision Sensing GmbH, Germany), which allows *on-line* monitoring of pH, DO and biomass. The culture was shaken at 30 ℃ and 200 rpm for 20 h reaching an OD_{600} of about 7 (Additional file 1: Fig. S1). Afterwards, the bioreactor was inoculated with the fed-batch like preculture to an initial OD_{600} of approx. 0.2. To prevent foam formation, 0.01% (v v^{-1}) sterile antifoam 204 (Sigma-Aldrich, Germany) was added to all precultures.

Bioreactor fed-batch culture conditions

The high cell density fed-batch fermentation for heterologous RH production was performed in a 3.7-L bench-top bioreactor with 2 L working volume (KLF2000, Bioengineering AG, Switzerland) with following parameters: the temperature was set to 30 ℃ and 18 ℃ before and after induction, respectively, pH was kept at 7.0 ± 0.2 by controlled feeding of 25% (v v^{-1}) ammonia solution. The bioreactors were equipped with two six-blade Rushton impellers mounted with a distance of 1.5 times the stirrer diameter. The initial stirring speed and air flow were set to 400 rpm and 0.05 vvm, respectively. In order to maintain the DO value above 20% during the fed-batch cultivation, both parameters were stepwise increased manually until their maximum (1,200 rpm, 2 vvm). Foaming was controlled by manual pulse additions with 0.1 mL antifoam when foam appeared.

The fed-batch cultivations started with an initial batch phase in 2 L MSM medium. After glucose depletion (as indicated by zero residual glucose and a sharp increase in DO), the external glucose feeding was initiated exponentially at a specific growth rate (μ_{set}) set to approx. 70% of μ_{max} in the batch phase according to Eq. 1.

$$F(t) = F_0 * e^{\mu_{set} * t} \quad (1)$$

The initial feed rate F_0 (L h^{-1}) was calculated according to Eq. 2. The biomass concentration (X) was estimated from a previous correlation of OD_{600} with cell dry weight (CDW) values. One unit of OD_{600} corresponds to a cell dry weight of 0.3 g L^{-1} [45]. The specific growth rate (μ) was calculated for the period between two consecutive OD_{600} measurements and fitted with the best spline. The biomass/substrate yield $Y_{x/s}$ was calculated from the batch phase with the initial glucose concentration (S). S_i represents the glucose concentration of the feed solution, and X_0 and V_0 are the biomass concentration and culture volume at the start of the fed-batch phase, respectively.

$$F_0 = \frac{\mu_{set}}{Y_{x/s} * S_i}(X_0 V_0) \quad (2)$$

The feeding solution consisted of 650 g L^{-1} glucose supplemented with 10% (v v^{-1}) macro element solution and 0.2% (v v^{-1}) trace element solution, as well as 1 g L^{-1} thiamine. When a stirring speed of 1,200 rpm and aeration rate of 2 vvm were reached (corresponding to an OD_{600} of about 75), RH production was induced by addition of 150 µM IPTG per OD_{600} of 75. In parallel 0.3 mM $NiSO_4$ and 1.5 mM $FeCl_3$ were added per OD_{600} of 75. After induction, the feeding rate was kept constant and eventually decreased to avoid anaerobic growth or overflow metabolism. At the beginning of induction, the inducer was also added to the feeding solution at a concentration of 150 µM and constantly fed to the bioreactor with a total additional IPTG of approx. 90 µmol per 2 L bioreactor culture. The production phase was carried out

for 132 h at 18 ℃ under glucose-limited conditions. During the whole fed-batch cultivation, 4 mL of 1 M $MgSO_4$ was added aseptically to the bioreactor with each OD_{600} increase of ~ 20.

Sampling and analytical methods of the bioreactor fermentation

Before induction, sampling was performed every 2 h, whereas sampling was carried out in larger time intervals after induction. At every sampling point, the OD_{600} was measured manually in duplicates with a spectrophotometer (Ultraspec 3300, GE Healthcare, USA) at a dilution (in 0.9% $NaCl_{aq}$) in a measurement range of 0.2–0.8.

For CDW determination, duplicates of 2 mL aliquots of the culture were harvested in pre-weighted 2-mL tubes by centrifugation (21,500 × *g*, 4 ℃, 10 min). The pellets were washed under the same conditions with 0.9% $NaCl_{aq}$ to remove residual culture medium. After centrifugation, the washed pellets were dried at 80 ℃ for 24 h and the CDW was determined by weighing the dried cell-containing tubes. The supernatants were analyzed with a Cedex Bio HT Analyzer (Roche Diagnostics International AG, Switzerland) using test kits for glucose, Mg^{2+}, ammonia, acetate and iron (Glucose Bio HT, Magnesium Bio HT, NH3 Bio HT, Acetate V2 Bio HT, Iron Bio HT).

Additionally, 1 mL broth samples were collected at the selected sampling times for total protein analysis. The samples were centrifuged (21,500×*g*, 4 ℃, 10 min), the supernatant discarded and the pellet stored at − 80 ℃ until further analysis. For soluble RH purification, cells were harvested from 20 mL culture samples followed by centrifugation at 8,000×*g*, 4 ℃ for 10 min (Eppendorf, Germany) at different times after induction and pellets were stored at − 80 ℃.

Off-gas data performed with a $BlueInOne_{FERM}$-sensor gas analyzer for parallel measurement of O_2 and CO_2 concentrations (BlueSens gas sensor GmbH, Germany) was recorded for both bioreactors during the fed-batch cultivations, and served for the determination of the oxygen uptake rate (Q_{O2}), carbon dioxide production rate (Q_{CO2}), respiration coefficient (RQ) and the volumetric oxygen transfer coefficient (k_La) based on the gas mass balance.

RH purification

For total protein analysis, the pellets were resuspended in 2 × SDS sample buffer normalized to an OD_{600} of 25 and heated at 95 ℃ for 20 min. After cooling and centrifugation 12 µL of the SDS-denatured samples were separated in 12% PAA gels. Subsequently, proteins were transferred onto a PVDF membrane (0.45 µm pore size, Carl Roth, Germany) by semi-dry blotting in a Transblot Turbo Transfer system (Bio-Rad, Germany) at 1.3 A/25 V for 30 min. Detection of Strep-tagged HoxB was carried out as described previously [33, 34].

For soluble protein purification cell pellets were resuspended in 4 mL buffer A (100 mM Tris–HCl, pH 8.0, 150 mM NaCl) per g wet cells supplemented with 1 g L^{-1} lysozyme and 1 mM PMSF. The cells were disrupted by sonicating using the UP200S sonicator (Hielscher Ultrasonics GmbH, Germany, 30 s on/off, 7 mm sonotrode diameter, 60% amplitude) for 2.5 min per 2 g of wet cell weight. The cell-free extracts were centrifuged at 8,000×*g*, 4 ℃ for 1.5 h (Eppendorf, Germany) and the supernatant was collected (SE) and immediately applied to Strep-Tactin Superflow columns (IBA, Göttingen, Germany) for soluble RH purification. RH purification and quantification were carried out as previously described [21, 33, 34].

Western blotting

Western blotting was performed as described recently [33]. For soluble and insoluble protein analysis, 100 µL aliquots lysate suspension after sonication were centrifuged at 16,000×*g*, 4 ℃ for 45 min. The supernatant was transferred into a fresh 1.5-mL tube (soluble fraction) and mixed with 100 µL 2 × SDS sample buffer, whilst the pellet containing insoluble proteins and cell debris was resuspended in 200 µL 2 × SDS sample buffer. Afterwards, the samples were incubated at 95 ℃ for 10 min or 20 min for soluble and insoluble fractions, respectively. 15 µL of each sample were applied for SDS-PAA gel and subsequent Western blot analysis.

Results and discussion

Metal effect on cell growth and active RH production in glucose MSM

Previously we used the fed-batch like EnPresso system to screen essential process parameters, e.g. production strain, inducer concentration, production temperature or metal ion supplementation, required for active RH production in deepwell plates or shake flasks [21, 33]. This guarantees that the same cultivation mode (fed-batch mode) is used for small-scale optimization and for large-scale bioreactor cultivation. However, numerous studies have shown that high nickel supplementation has a significantly more negative effect on cell viability in MSM compared to complex media [46–48]. So before proceeding with bioreactor cultures, we analyzed the effects of nickel and/or iron additions on cell growth and active RH production in glucose MSM cultures.

Thus, we performed deepwell plate cultivations of *E. coli* strain BQF8RH8 in 3 mL MSM with 9 g L^{-1} glucose supplemented with different concentrations of $NiSO_4$ or $FeCl_3$ as described in Materials and methods. The dissolved oxygen concentration (Fig. 1A and

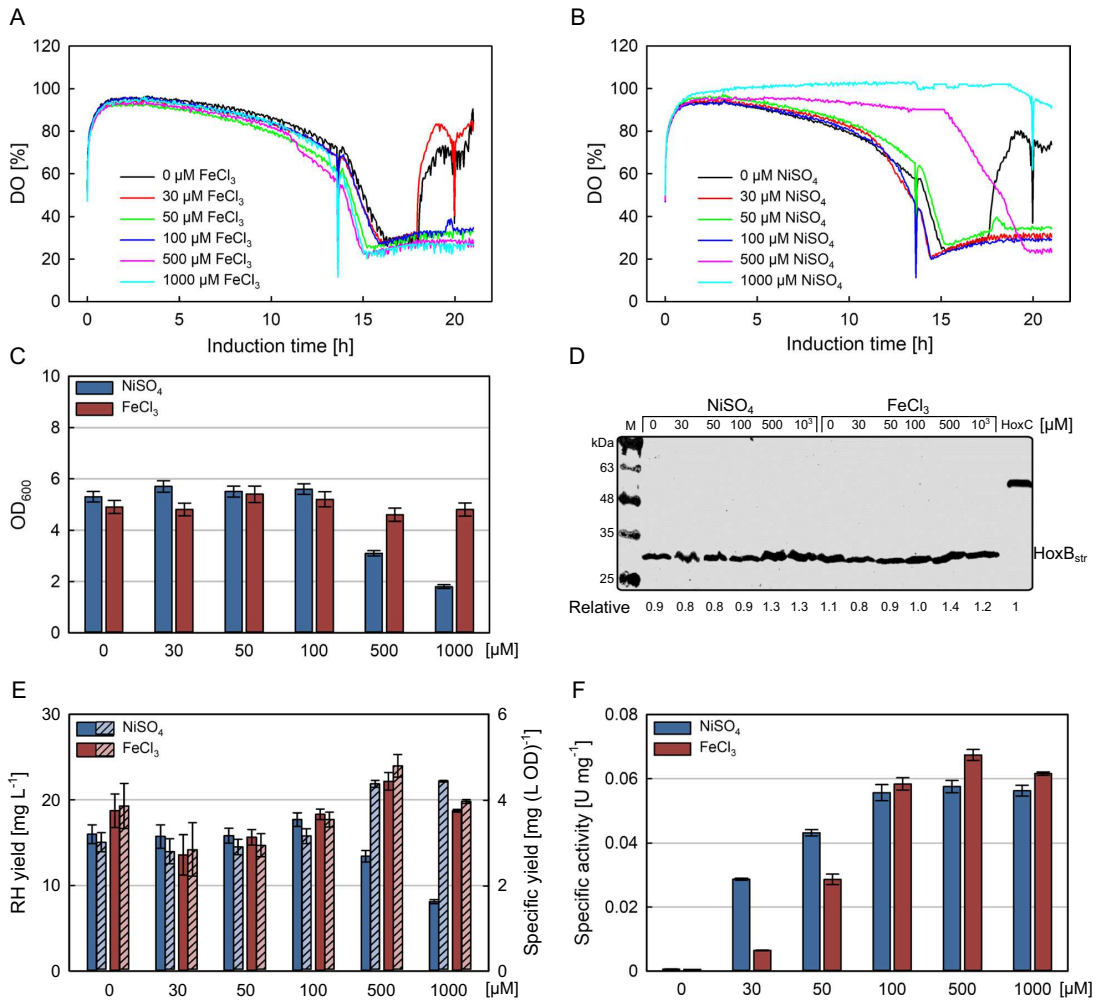

Fig. 1 Screening of nickel and iron concentrations in mineral salt medium. Cells were grown in mineral salt medium with 9 g L^{-1} glucose. After induction with 50 µM IPTG, 3 mL culture were distributed in 24-deepwell plates at 30 ℃, 250 rpm and supplemented with different nickel or iron concentrations. 0.1 mM $FeCl_3$ was added for nickel screenings while 0.1 mM $NiSO_4$ was added for iron screenings. For RH detection 3 mL cells were normalized to an OD_{600} of 30 with 50 mM KH_2PO_4/K_2HPO_4 buffer pH 7.0 and sonicated followed by centrifugation. 12 µL soluble protein sample was separated on 12% polyacrylamide gels followed by Western blotting where HoxB from RH was detected using anti-Strep tag antibody. 1 µg $HoxC_{str}$ was used as control. **A**, **B** profiles of online dissolved oxygen concentration (DO) of the cultures after induction. **C** Final OD_{600} of cultures, **D** Western Blot (WB) analysis of soluble crude extracts. Bands were quantified relative to the control $HoxC_{str}$ using ImageJ as shown below the blots. **E** soluble RH yields (without slash) and specific yields (with slash) as quantified from WB analysis, **F** specific activities measured from soluble crude extracts. All measured ODs and yields are the mean of two independent technical replicates

B) was measured *on-line* over the entire induction time as an indicator for cell growth. In addition, the final OD (Fig. 1C), total RH (Fig. 1D and E) and its activity in the soluble protein extract (Fig. 1F) were determined at the end of cultivation. With increasing cell growth, more oxygen is required, which leads to a decrease in the DO level. In case of iron addition, no differences in oxygen consumption irrespective of the iron concentration were observed (Fig. 1A), suggesting no negative impact on cell growth. On the contrary, the increase of the DO level after about 17 h at 0 and 30 mM $FeCl_3$ (Fig. 1A) indicates a drop in the metabolic activity of the cells that might

be the consequence of an iron deficiency caused by an increased iron demand due to RH production. While the addition of up to 100 µM $NiCl_2$ lead to a similar decrease of the DO level as in the case of $FeCl_3$, addition of 0.5 or 1 mM $NiCl_2$ resulted in a significantly reduced DO consumption, which indicates a significant reduction of cell growth or prolonged cellular adaptation of the strain in mineral salt medium (Fig. 1B). Interestingly, without additional nickel, a rise in the DO level is also observed after about 16 h of induction (Fig. 1B), indicating a limitation of nickel analogous to the iron limitation. In both cases, the results of the DO curves are confirmed by the final ODs (Fig. 1C). Similarly, none of the tested iron or nickel additions affected the specific RH production (Fig. 1D, E), thus higher nickel concentrations resulted in a significant decrease in total RH yield due to the reduced growth (Fig. 1E). However, increasing metal concentrations of up to 0.1 mM nickel or 0.5 mM iron had a positive effect on the specific RH activity, which ceased to increase at higher metal ion concentrations (Fig. 1F). This is in line with previous studies on recombinant [NiFe]-hydrogenase production in *E. coli* showing the highest in vitro activity at 25–30 µM $NiCl_2$ in modified mineral salt medium cultures [49–52]. Hence, nickel and iron concentrations of 0.1 mM and 0.5 mM, respectively, were selected for the following bioreactor cultivations.

High cell density fed-batch cultivation

As cultivations in shake flasks with EnPresso B medium cannot meet the possible hydrogenase demand for an industrial application, production in a larger scale and higher cell density is necessary. Thus, we aimed to develop a glucose-limited high cell density fed-batch in a benchtop bioreactor. The cultivations were performed in a 3.7-L lab-scale bioreactor filled with 2 L of MSM minimal medium containing an initial glucose concentration of 8.5 g L^{-1} as sole carbon source. The process was divided into three phases (Fig. 2A): (i) an initial batch phase, followed (ii) by an exponential feeding phase after which the RH production was induced by the addition of IPTG, and (iii) finally the production phase with constant feeding until the end of cultivation. During the 18 h batch phase, the initial glucose was completely consumed, as indicated by offline glucose measurements (Fig. 2B). Whenever the DO dropped below 30% either the stirrer speed or the aeration rate were increased manually to avoid oxygen limitation (Additional file 1: Fig. S2A). At the end of the batch phase the culture reached an OD_{600} of 11 (CDW of 4.2 g L^{-1}) and a maximal specific growth rate (μ_{max}) of 0.25 h^{-1} (Fig. 2A). In the batch phase, a biomass yield of 0.5 g biomass g^{-1} glucose was determined, which is slightly higher than the range of the most *E. coli* strains (0.35–0.48 g g^{-1}), indicating stress-free growth and effective incorporation of the supplied carbon into biomass [53]. After glucose depletion, an exponential feed with concentrated (650 g L^{-1}) glucose solution was started. The feed rate was calculated to ensure a targeted specific growth rate of 0.18 h^{-1} (Fig. 2A). During the whole process, the DO was maintained above 20% by gradually increasing air flow rate or stirring speed to prevent oxygen limitation or anaerobic conditions, as this would lead to the accumulation of acetate or other mixed acid fermentation products that are detrimental to cell growth and recombinant protein production [44, 54, 55]. The exponential feed was stopped after 29 h, when an OD_{600} of approx. 75 was reached (corresponding to a CDW of 28.5 g L^{-1}, Fig. 2A). After the exponential feeding phase, the temperature was reduced to 18 °C and RH production induced by IPTG addition. Simultaneously, $NiCl_2$ and $FeCl_3$ were added to provide sufficient metal ions for RH maturation. A constant feed rate was applied during the production phase, which was gradually decreased due to the lower glucose consumption at 18 °C to avoid acetate accumulation [56–58]. Nevertheless, the cells continued to grow with a specific growth rate below 0.01 h^{-1} until the end of the cultivation, reaching a final OD_{600} and CDW of 150 and 66 g L^{-1}, respectively (Fig. 2A). However, neither glucose nor acetate accumulated during the production phase (Fig. 2B). Since addition of IPTG led to a decrease of respiration, the DO level rose and was maintained at 75% during the production phase (Additional file 1: Fig. S2A).

During the cultivation, a final biomass concentration (66.3 g L^{-1} CDW) was reached by consumption of a total of 438.2 g glucose, corresponding to an average yield of biomass per substrate $Y_{X/S}$ of 0.3 g g^{-1} (Additional file 1: Fig. S2B). The obtained OD_{600} of 150 is fivefold higher compared to fed-batch-like EnPresso shake flask cultivations (OD_{600} of 30–40) [21, 33, 34] and even 32-times higher than in batch MSM cultivations performed in deepwell plates (Fig. 1C). It is estimated that the volumetric oxygen transfer coefficient (k_La) value in the stirred-tank bioreactor is about threefold higher compared to the 250-mL UYF at 200 rpm (~ 422 h^{-1}) [59], thus, enabling aerobic cultivation to high cell densities. As the biomass increased, the gas flow rate was increased up to 2 vvm at a stirring speed of 1,200 rpm (Additional file 1: Fig. S2A). By this way, based on the sensor for exhaust gas analysis, a maximal k_La value of approx.1,200 h^{-1} was determined during the growth phase, which is comparable to other *E. coli* cultivations with the same bioreactor system [41]. The respiration quotient (RQ) as a ratio of carbon dioxide produced per oxygen consumed increased after the feed start, and immediately decreased slightly after the induction followed by maintaining at a relatively constant value of about 1 until the end of the cultivation (Additional

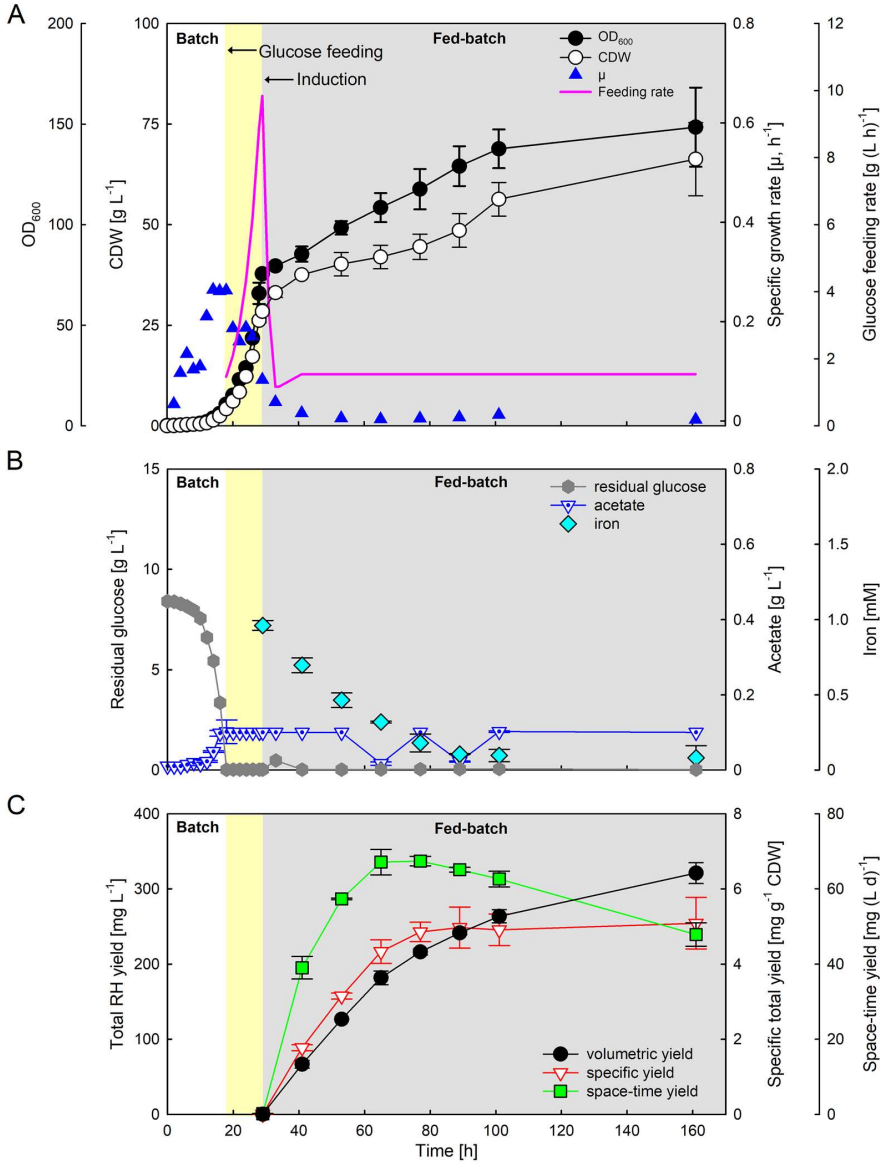

Fig. 2 High cell density fed-batch bioreactor cultivation for RH production with *E. coli* BL21-Gold pQF8 and pQF18. **A** Cell growth curve, biomass, specific growth rate and glucose feeding rate. **B** Residual glucose concentration, acetate and iron concentrations measured from culture supernatant. **C** The yields for total volumetric, specific, and space–time RH production were determined from Western blotting analysis after induction. The three phases of the process are shown by different color backgrounds: white batch phase, yellow exponential feeding phase, and gray production phase. All values are the mean of two independent technical replicates from two independent biological replicates

file 1: Fig S2C). The RQ close to 1 indicates an equilibrium between respiration, cell growth and carbon dioxide production without accumulation of byproducts, e.g. acetate or lactose, which is in line with the acetate measurements (Fig. 2B).

In parallel to induction with IPTG, 1.5 mM $FeCl_3$ and 0.3 mM $NiCl_2$ were added to provide sufficient metal ions for RH maturation. The iron concentration in the medium decreases steadily as iron is required for the hydrogenase production, and finally levels off at a value of approx. 80 µM, suggesting that sufficient iron is available in the medium (Fig. 2B). To follow the RH production during the production process, samples were collected at different time points after induction and used for the determination of the total RH concentration. The Western blotting analyses indicate that the RH is stably produced and gradually accumulated approx. 320 mg L^{-1} (Additional file 1: Figs. S3 and 2C). Similarly, the specific yield increased to about 5 mg RH g^{-1} CDW in the first 48 h after induction and remained at this level thereafter (Fig. 2C), thereby further demonstrating the stability of the RH production over the entire duration of the process.

Evaluation of RH yield and activity

The soluble RH yield and the enzymatic activity are decisive criteria for assessing the success of a cultivation. To follow the RH production, 20 mL samples were collected at different time points after induction and used for purification of the soluble RH and subsequent measurement of its enzymatic activity. As expected, both volumetric and specific RH yield increased over time (Fig. 3A). While the volumetric yield increased steadily due to the increasing biomass in the reactor and reached a final level of 133 mg L^{-1}, the specific yield reaches a maximum of about 2 mg g^{-1} CDW already at 48 h after induction and does not increase significantly further until the end of the cultivation after 132 h of induction (Fig. 3A). Unfortunately, the amount of purified soluble RH corresponds to only about 40% of the total RH yield (Figs. 2C and 3A). When analyzing the protein content of sonication-lysed cells, half of the total RH amount was still found in the insoluble cell fraction (Additional file 1: Fig S4), which has not been observed in shake flask cultivations [21, 33, 34]. The difference may be related to the much higher cell densities and time of cultivation which affect the adaptation of the cellular system in connection to the protein synthesis system and the stress responses. It may be hypothesized that the extracellular cAMP level could be one of the key factors which would affect the expression strength and thus the balance between correctly folding and aggregation of target protein [60]. Besides product formation at high cell densities, expression at low growth rates may provide a positive effect by an increased stress resistance, which could be important in response to environmental changes caused by high cell density cultivations [61]. Nevertheless, previous studies in the measurement of the stringent response ppGpp level during the very slow growth for both recombinant and non-recombinant *E. coli* fed-batch processes, indicate the segregation of a part of the cell population into viable but nonculturable cells at very slow growth rates ($\leq$0.02 h^{-1}) [62, 63]. Thus, those may serve as analytical focus points for further improvements in terms of RH activity and solubility in larger scale high cell density bioreactor cultivations.

The space–time yield increases with the volumetric yield, at least at the beginning of the production phase. However, it reaches a maximum of approx. 24 mg (L d)$^{-1}$ after 48 h of induction and then starts to decrease steadily (Fig. 3A). Nevertheless, the soluble protein yield is still more than 130-fold higher than the RH yield obtained from bioreactor cultivations of the native producer *C. necator* [30] and even several thousand-times higher than that of the *Pyrococcus furiosus* [NiFe]-hydrogenase heterologously produced in *E. coli* [49], further demonstrating the value of our cultivation strategy.

Similar to the increase in protein yield, the specific and absolute RH activity increase and reach final values of 1.23 U mg^{-1} and 160 U L^{-1}, respectively (Fig. 3B). The activities and yields achieved were 1.3 and 160 times higher than those obtained from *C. necator* H16, respectively. [30]. However, compared to our recently reported data from shake flask cultivations the specific RH activity is about 2.5-fold lower [21]. The specific activity is proportional to the amount of cofactor formed and incorporated into the apo-enzyme, thus it is possible that the RH apoprotein cannot receive cofactors as efficiently as the enzyme produced in shake flasks, presumably due to different medium used. In deepwell plate experiments with MSM medium (Fig. 1) or EnPresso shake flask cultivations [21], the highest RH activity was achieved by addition of 0.1 mM $NiSO_4$ at an OD_{600} of 5 or 8, while in the bioreactor cultivation 0.3 mM $NiSO_4$ was added only once at an OD_{600} of 75 (Fig. 2). Thus, the lower specific RH activity obtained in the bioreactor cultivations might be attributed to the lower concentration of added nickel relative to the higher cell densities, resulting in insufficient nickel being delivered to the cells. Nevertheless, the production of soluble RH is significantly higher in the bioreactor, thus compensating for the lower specific activity compared to the shake flasks.

Conclusion

In this study, the scalability and robustness of the heterologous RH production process from small-scale cultivation to laboratory-scale bioreactors was successfully

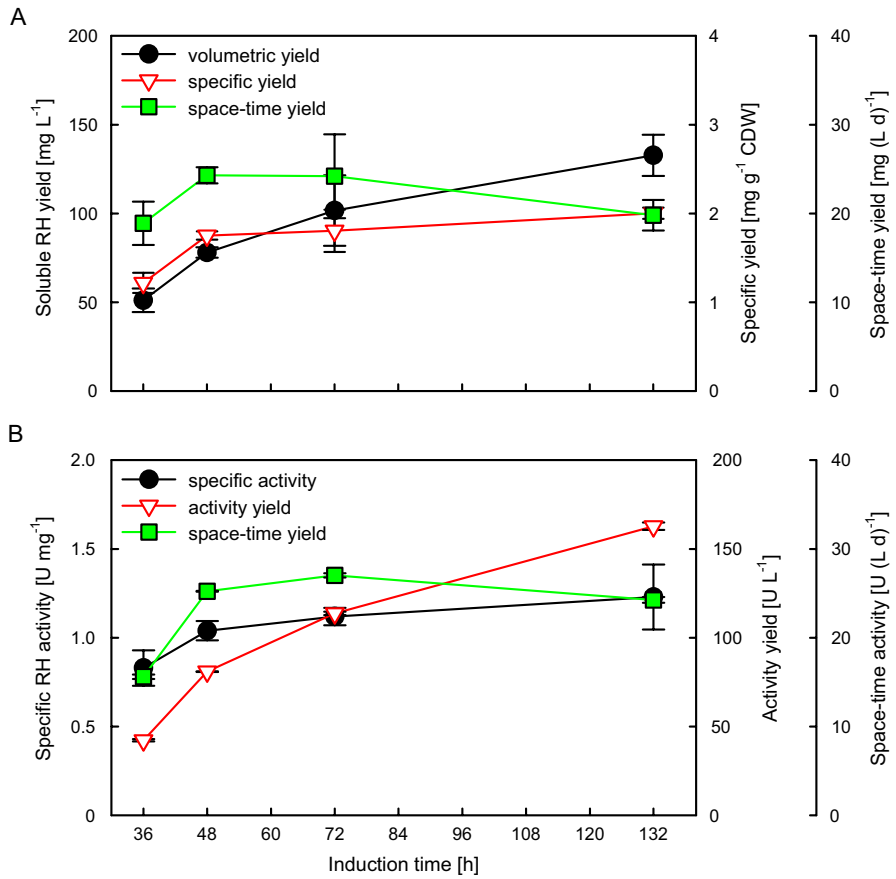

Fig. 3 Soluble RH production and activity yield obtained from the fed-batch bioreactor fermentation. 20 mL cells were collected at different induction times from two parallelized bioreactor under the same conditions. Cells were disrupted with sonication on ice (60% amptitude, 7 mm sonotrode, 30 s on/off, 10 min) followed by centrifugation (8000×*g*, 4 ℃, 90 min). The clarified lysates were purified using Strep-Tactin columns (CV of 500 µL). **A** The eluted RH amounts were quantified with SDS-PAGE analysis and **B** the activities of the purified RH samples were measured in vitro. All values are the mean of two independent technical replicates from two independent biological replicates

demonstrated. The high cell density fed-batch cultivation resulted in a soluble active RH yield of more than 130 mg L^{-1} and as high as 320 mg L^{-1} for total RH titers, based on a pure glucose limiting feeding strategy. Our results are promising as they show that active RH production is not disturbed by scaling effects, demonstrating the robustness of the hydrogenase production process when providing reproducible growth conditions at different scales. However, a limitation of the current scale-up study is that the highest specific RH activity achieved in previous shake flask scales [21] could not yet be maintained in the bioreactor scale, suggesting potential for further optimization, e.g. in media requirements. In addition, further research will be necessary to elucidate whether the inducer IPTG concentration enables to satisfy the induction behavior of individual cells at high cell density cultures at both macroscopic and microscopic levels, as it can trigger stress responses in *E. coli* leading to pre-induced cells remaining induced and non-induced cells. Nevertheless, we strongly believe that the data reported herein qualitatively and quantitatively provides a reasonable approach for the development of bioprocesses for the production of difficult-to-express metalloproteins to meet the needs in basic and applied studies. The developed bioreactor cultivation system for the production of active [NiFe]-hydrogenases, provides a good opportunity for an economical supply of such metalloenzymes in high concentrations, facilitating basic and applied research on these proteins as well as their

potential industrial application. Furthermore, there are also broader implications for the future development of biotechnological production systems for heterologous functional complex heteromeric metalloproteins.

Supplementary Information

The online version contains supplementary material available at https://doi.org/10.1186/s12934-022-01919-w.

Additional file 1: Figure S1. Profiles of dissolved oxygen concentration, pH and biomass of the 2nd preculture in EnPresso B medium. **Figure S2**. Supplementary information of the fed-batch bioreactor cultivations, **Figure S3.** Western Blot analysis of total RH production during the fed-batch bioreactor fermentation, **Figure S4**. Soluble and insoluble fractions of RH with Western blotting analysis.

Acknowledgements
We wish to thank Dr. Oliver Lenz and Janna Schoknecht for the opportunity to use the spectroscopic facility for in vitro activity measurements. We thank Roche CustomBiotech (Mannheim, Germany) for the supply of the Cedex Bio HT Analyzer. We acknowledge support by the German Research Foundation and the Open Access Publication Fund of TU Berlin.

Author contributions
MG, QF, SW, SR, PN participated in experimental design and interpretation of the results. QF carried out all molecular biological and biochemical experiments. QF and SW performed the bioreactor cultivation experiments. SR supervised the bioreactor cultivations. QF performed the activity measurements. All authors analyzed the data with major contributions from QF and MG. QF drafted the original manuscript. MG, SW, PN and SR revised the manuscript. All authors read and approved the final manuscript.

Funding
Open Access funding enabled and organized by Projekt DEAL. This work was supported by the Cluster of Excellence "Unifying Systems in Catalysis" (UniSysCat) coordinated by the Technische Universität Berlin and its graduate school, Berlin International Graduate School of Natural Sciences and Engineering (BIGNSE), funded by the German Research Foundation (DFG) under Germany's Excellence Strategy (EXC 2008/1–390540038). QF obtained a grant from the German Academic Exchange Service (DAAD).

Availability of data and materials
All data generated or analyzed during this study are included in this published article [and its supplementary information files].

Declarations

Ethics approval and consent to participate
Not applicable.

Consent for publication
Not applicable.

Competing interests
The authors declare no competing interests.

Received: 27 July 2022 Accepted: 7 September 2022
Published online: 19 September 2022

References

1. Fontecilla-Camps JC, Amara P, Cavazza C, Nicolet Y, Volbeda A. Structure-function relationships of anaerobic gas-processing metalloenzymes. Nature. 2009;460:814–22.
2. Greening C, Biswas A, Carere CR, Jackson CJ, Taylor MC, Stott MB, et al. Genomic and metagenomic surveys of hydrogenase distribution indicate H_2 is a widely utilised energy source for microbial growth and survival. ISME J. 2016;10:761–77.
3. Greening C, Constant P, Hards K, Morales SE, Oakeshott JG, Russell RJ, et al. Atmospheric hydrogen scavenging: from enzymes to ecosystems. Appl Environ Microbiol. 2015;81:1190–9.
4. Lubitz W, Ogata H, Ru O, Reijerse E. Hydrogenases. Chem Rev. 2014;114:4081–148.
5. Pierik AJ, Schmelz M, Lenz O, Friedrich B, Albracht SPJ. Characterization of the active site of a hydrogen sensor from *Alcaligenes eutrophus*. FEBS Lett. 1998;438:231–5.
6. Lenz O, Lauterbach L, Frielingsdorf S, Friedrich B. Oxygen-tolerant hydrogenases and their biotechnological potential. In: Rögner M, editor. Biohydrogen. Berlin: DE GRUYTER; 2015. p. 61–96.
7. Krassen H, Schwarze A, Friedrich B, Ataka K, Lenz O, Heberle J. Photosynthetic hydrogen production by a hybrid complex of photosystem I and [NiFe]-hydrogenase. ACS Nano. 2009;3:4055–61.
8. Schwarze A, Kopczak MJ, Rogner M, Lenz O. Requirements for construction of a functional hybrid complex of photosystem I and [NiFe]-hydrogenase. Appl Environ Microbiol. 2010;76:2641–51.
9. Zhang L, Morello G, Carr SB, Armstrong FA. Aerobic photocatalytic H_2 production by a [NiFe] hydrogenase engineered to place a silver nanocluster in the electron relay. J Am Chem Soc. 2020;142:12699–707.
10. Cracknell JA, Vincent KA, Armstrong FA. Enzymes as working or inspirational electrocatalysts for fuel cells and electrolysis. Chem Rev. 2008;108:2439–61.
11. De Poulpiquet A, Marques-Knopf H, Wernert V, Giudici-Orticoni MT, Gadiou R, Lojou E. Carbon nanofiber mesoporous films: efficient platforms for bio-hydrogen oxidation in biofuel cells. Phys Chem Chem Phys. 2014;16:1366–78.
12. Xu L, Armstrong FA. Optimizing the power of enzyme-based membraneless hydrogen fuel cells for hydrogen-rich H_2–air mixtures. Energy Environ Sci. 2013;6:2166–71.
13. Reeve HA, Lauterbach L, Ash PA, Lenz O, Vincent KA. A modular system for regeneration of NAD cofactors using graphite particles modified with hydrogenase and diaphorase moieties. Chem Commun. 2012;48:1589–91.
14. Lauterbach L, Lenz O, Vincent KA. H_2-driven cofactor regeneration with $NAD(P)^+$-reducing hydrogenases. FEBS J. 2013;280:3058–68.
15. Preissler J, Reeve HA, Zhu T, Nicholson J, Urata K, Lauterbach L, et al. Dihydrogen-driven NADPH recycling in imine reduction and P450-catalyzed oxidations mediated by an engineered O2-tolerant hydrogenase. ChemCatChem. 2020;12:4853–61.
16. Mertens R, Liese A. Biotechnological applications of hydrogenases. Curr Opin Biotechnol. 2004;15:343–8.
17. Atomi H, Sato T, Kanai T. Application of hyperthermophiles and their enzymes. Curr Opin Biotechnol. 2011;22:618–26.
18. Friedrich B, Fritsch J, Lenz O. Oxygen-tolerant hydrogenases in hydrogen-based technologies. Curr Opin Biotechnol. 2011;22:358–64.
19. Kim JYH, Cha HJ. Recent progress in hydrogenase and its biotechnological application for viable hydrogen technology. Korean J Chem Eng. 2013;30:1–10.
20. Fan Q, Neubauer P, Lenz O, Gimpel M. Heterologous hydrogenase overproduction systems for biotechnology—An overview. Int J Mol Sci. 2020;21:5890.
21. Fan Q, Caserta G, Lorent C, Zebger I, Neubauer P, Lenz O, et al. High-yield production of catalytically active regulatory [NiFe]-hydrogenase from *Cupriavidus necator* in *Escherichia coli*. Front Microbiol. 2022;13: 894375.
22. Lenz O, Strack A, Tran-Betcke A, Friedrich B. A hydrogen-sensing system in transcriptional regulation of hydrogenase gene expression in *Alcaligenes* species. J Bacteriol. 1997;179:1655–63.
23. Lenz O, Friedrich B. A novel multicomponent regulatory system mediates H_2 sensing in *Alcaligenes eutrophus*. Proc Natl Acad Sci. 1998;95:12474–9.
24. Kleihues L, Lenz O, Bernhard M, Buhrke T, Friedrich B. The H_2 sensor of *Ralstonia eutropha* is a member of the subclass of regulatory [NiFe] hydrogenases. J Bacteriol. 2000;182:2716–24.
25. Brecht M, van Gastel M, Buhrke T, Friedrich B, Lubitz W. Direct detection of a hydrogen ligand in the [NiFe] center of the regulatory H_2-Sensing Hydrogenase from *Ralstonia eutropha* in its reduced state by HYSCORE and ENDOR Spectroscopy. J Am Chem Soc. 2003;125:13075–83.

26. Ash PA, Liu J, Coutard N, Heidary N, Horch M, Gudim I, et al. Electrochemical and infrared spectroscopic studies provide insight into reactions of the NiFe regulatory hydrogenase from *Ralstonia eutropha* with O_2 and CO. J Phys Chem B. 2015;119:13807–15.
27. Roncaroli F, Bill E, Friedrich B, Lenz O, Lubitz W, Pandelia ME. Cofactor composition and function of a H_2-sensing regulatory hydrogenase as revealed by Mössbauer and EPR spectroscopy. Chem Sci. 2015;6:4495–507.
28. Horch M, Schoknecht J, Mroginski MA, Lenz O, Hildebrandt P, Zebger I. Resonance raman spectroscopy on [NiFe] hydrogenase provides structural insights into catalytic intermediates and reactions. J Am Chem Soc. 2014;136:9870–3.
29. Caserta G, Pelmenschikov V, Lorent C, Tadjoung Waffo AF, Katz S, Lauterbach L, et al. Hydroxy-bridged resting states of a [NiFe]-hydrogenase unraveled by cryogenic vibrational spectroscopy and DFT computations. Chem Sci. 2021;12:2189–97.
30. Bernhard M, Buhrke T, Bleijlevens B, De Lacey AL, Fernandez VM, Albracht SPJ, et al. The H_2 sensor of *Ralstonia eutropha*. J Biol Chem. 2001;276:15592–7.
31. Buhrke T, Brecht M, Lubitz W, Friedrich B. The H_2 sensor of *Ralstonia eutropha*: Biochemical and spectroscopic analysis of mutant proteins modified at a conserved glutamine residue close to the [NiFe] active site. JBIC J Biol Inorg Chem. 2002;7:897–908.
32. Buhrke T, Löscher S, Lenz O, Schlodder E, Zebger I, Andersen LK, et al. Reduction of unusual iron-sulfur clusters in the H_2-sensing regulatory NiFe hydrogenase from *Ralstonia eutropha* H16. J Biol Chem. 2005;280:19488–95.
33. Fan Q, Caserta G, Lorent C, Lenz O, Neubauer P, Gimpel M. Optimization of culture conditions for oxygen-tolerant regulatory [NiFe]-hydrogenase production from *Ralstonia eutropha* H16 in *Escherichia coli*. Microorganisms. 2021;9:1195.
34. Fan Q, Neubauer P, Gimpel M. Production of soluble regulatory hydrogenase from *Ralstonia eutropha* in *Escherichia coli* using a fed-batch-based autoinduction system. Microb Cell Fact. 2021;20:1–22.
35. Buhrke T, Bleijlevens B, Albracht SPJ, Friedrich B. Involvement of *hyp* gene products in maturation of the H_2-sensing [NiFe] hydrogenase of *Ralstonia eutropha*. J Bacteriol. 2001;183:7087–93.
36. Lacasse MJ, Zamble DB. [NiFe]-hydrogenase maturation. Biochemistry. 2016;55:1689–701.
37. Fritsch J, Lenz O, Friedrich B. Structure, function and biosynthesis of O_2-tolerant hydrogenases. Nat Rev Microbiol. 2013;11:106–14.
38. Krause M, Ukkonen K, Haataja T, Ruottinen M, Glumoff T, Neubauer A, et al. A novel fed-batch based cultivation method provides high cell-density and improves yield of soluble recombinant proteins in shaken cultures. Microb Cell Fact. 2010;9:11.
39. Šiurkus J, Panula-Perälä J, Horn U, Kraft M, Rimšeliene R, Neubauer P. Novel approach of high cell density recombinant bioprocess development: optimisation and scale-up from microlitre to pilot scales while maintaining the fed-batch cultivation mode of *E. coli* cultures. Microb Cell Fact. 2010;9:35.
40. Li J, Jaitzig J, Lu P, Süssmuth RD, Neubauer P. Scale-up bioprocess development for production of the antibiotic valinomycin in *Escherichia coli* based on consistent fed-batch cultivations. Microb Cell Fact. 2015;14:83.
41. Ongey EL, Santolin L, Waldburger S, Adrian L, Riedel SL, Neubauer P. Bioprocess development for lantibiotic ruminococcin-A production in *Escherichia coli* and kinetic insights into LanM enzymes catalysis. Front Microbiol. 2019;10:2133.
42. Krause M, Neubauer A, Neubauer P. The fed-batch principle for the molecular biology lab: controlled nutrient diets in ready-made media improve production of recombinant proteins in *Escherichia coli*. Microb Cell Fact. 2016;15:1–14.
43. Jung G, Denefle P, Becquart J, Mayaux JF. High-cell density fermentation studies of recombinant *Escherichia coli* strains expressing human interleukin-1β. Ann l'Institut Pasteur/Microbiologie. 1988;139:129–46.
44. Shiloach J, Fass R. Growing *E. coli* to high cell density—A historical perspective on method development. Biotechnol Adv. 2005;23:345–57.
45. Soini J, Ukkonen K, Neubauer P. High cell density media for *Escherichia coli* are generally designed for aerobic cultivations – consequences for large-scale bioprocesses and shake flask cultures. Microb Cell Fact. 2008;7:26.
46. Rowe JL, Starnes GL, Chivers PT. Complex transcriptional control links NikABCDE-dependent nickel transport with hydrogenase expression in *Escherichia coli*. J Bacteriol. 2005;187:6317–23.
47. Macomber L, Hausinger RP. Mechanisms of nickel toxicity in microorganisms. Metallomics. 2011;3:1153–62.
48. Schiffels J, Pinkenburg O, Schelden M, Aboulnaga EHAA, Baumann MEM, Selmer T. An innovative cloning platform enables large-scale production and maturation of an oxygen-tolerant [NiFe]-hydrogenase from *Cupriavidus necator* in *Escherichia coli*. PLoS ONE. 2013;8: e68812.
49. Sun J, Hopkins RC, Jenney FE, McTernan PM, Adams MWW. Heterologous expression and maturation of an NADP-dependent [NiFe]-Hydrogenase: a key enzyme in biofuel production. PLoS ONE. 2010;5: e10526.
50. Kim JY, Jo B, Cha H. Production of biohydrogen by recombinant expression of [NiFe]-hydrogenase 1 in *Escherichia coli*. Microb Cell Fact. 2010;9:54.
51. Kim JYH, Jo BH, Cha HJ. Production of biohydrogen by heterologous expression of oxygen-tolerant *Hydrogenovibrio marinus* [NiFe]-hydrogenase in *Escherichia coli*. J Biotechnol. 2011;155:312–9.
52. Ghosh D, Bisaillon A, Hallenbeck PC. Increasing the metabolic capacity of *Escherichia coli* for hydrogen production through heterologous expression of the *Ralstonia eutropha* SH operon. Biotechnol Biofuels. 2013;6:122.
53. Fahnert B, Lilie H, Neubauer P. Inclusion bodies: Formation and utilisation. Adv Biochem Eng Biotechnol. 2004;89:93–142.
54. Xu B, Jahic M, Blomsten G, Enfors SO. Glucose overflow metabolism and mixed-acid fermentation in aerobic large-scale fed-batch processes with *Escherichia coli*. Appl Microbiol Biotechnol. 1999;51:564–71.
55. Lin HY, Mathiszik B, Xu B, Enfors SO, Neubauer P. Determination of the maximum specific uptake capacities for glucose and oxygen in glucose-limited fed-batch cultivations of *Escherichia coli*. Biotechnol Bioeng. 2001;73:347–57.
56. Sandén AM, Prytz I, Tubulekas I, Förberg C, Le H, Hektor A, et al. Limiting factors in *Escherichia coli* fed-batch production of recombinant proteins. Biotechnol Bioeng. 2003;81:158–66.
57. Neubauer P, Lin HY, Mathiszik B. Metabolic load of recombinant protein production: inhibition of cellular capacities for glucose uptake and respiration after induction of a heterologous gene in *Escherichia coli*. Biotechnol Bioeng. 2003;83:53–64.
58. Hoffmann F, Rinas U. Stress induced by recombinant protein production in *Escherichia coli*. Adv Biochem Eng Biotechnol. 2004;89:73–92.
59. Glazyrina J, Materne E, Hillig F, Neubauer P, Junne S. Two-compartment method for determination of the oxygen transfer rate with electrochemical sensors based on sulfite oxidation. Biotechnol J. 2011;6:1003–8.
60. Lin H, Hoffmann F, Rozkov A, Enfors SO, Rinas U, Neubauer P. Change of extracellular cAMP concentration is a sensitive reporter for bacterial fitness in high-cell-density cultures of *Escherichia coli*. Biotechnol Bioeng. 2004;87:602–13.
61. Neubauer P, Winter J. Expression and fermentation strategies for recombinant protein production in *Escherichia coli*. Recombinant protein production with prokaryotic and eukaryotic cells. A comparative view on host physiology. Dordrecht: Springer; 2001. p. 195–258.
62. Neubauer P, Hunan M, Tiirnkvist M, Larsson G, Enfors SO. Response of guanosine tetraphosphate to glucose fluctuations in fed-batch cultivations of *Escherichia coli*. J Biotechnol. 1995;43:195–204.
63. Teich A, Meyer S, Lin HY, Andersson L, Enfors SO, Neubauer P. Growth rate related concentration changes of the starvation response regulators σS and ppGpp in glucose-limited fed-batch and continuous cultures of *Escherichia coli*. Biotechnol Prog. 1999;15:123–9.

Publisher's Note

8. Appendix

8.1. Construction of expression vectors and oligonucleotides

All destination plasmids were constructed via a conventional restriction enzyme-digestion technology. The destination vector pCTUT7, which harbored a pBR322 origin of replication (*ori*) and a CTU promoter, a derivative of lac promoter (Kraft et al. 2007), was used for *hoxBC* expression, whereas the vector pGK16 containing a pWV01 *ori* was used for construction of *hyp* maturase expression plasmid. Expression from both plasmids is Isopropyl β-D-1-thiogalactopyranoside (IPTG) inducible; pCTUT7 possesses a high copy number, whereas pGK16 has a moderate copy number. The plasmids are stabilized by chloramphenicol and kanamycin resistance genes. In addition, all plasmids contained the heterologous *Bacillus subtilis* BsrF transcription terminator (Preis et al. 2009) placed at the 3' end of the plasmid vector. An overview of description of the plasmids is shown in Table 2.1 and plasmid maps are found in Figure 4.1. All expression constructs were confirmed to be accurate by DNA sequencing (LGC Genomics, Berlin, Germany) and transformed into appropriate *E. coli* strains based on different production purposes, respectively.

Oligonucleotide primers for PCR amplification or plasmid DNA sequencing were designed with the help of the Clone Manager (Sci-Ed software) or SnapGene 5.2 software. All the primers were chemically synthesized and obtained from Sigma-Aldrich (Taufkirchen, Germany) and listed in Table 2.2 in details.

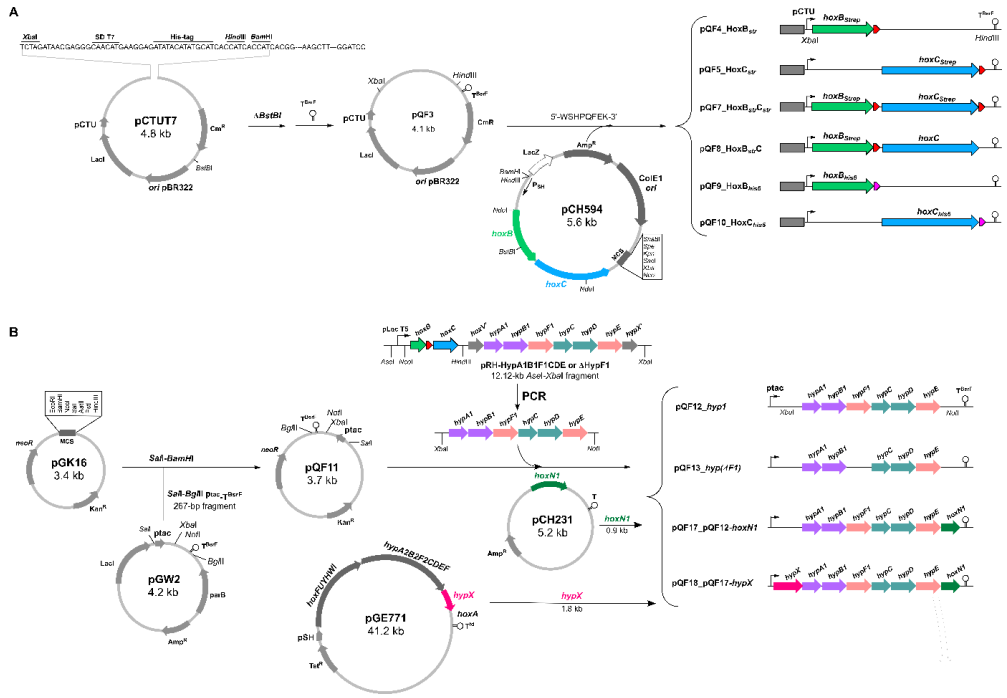

Figure 4.1 Description of expression vector maps with all necessary features.
(A) Overview of the construction pathway for expression plasmids encoding RH structural subunit HoxBC; (B) Overview of the construction pathway for expression plasmids encoding maturation proteins required.

Table 2.1 Overview of description of the destination vectors constructed in this work

Plasmid	Description	Ref.
pUC19	*E. coli* cloning vector, Amp^R, P_{lac}, MCS	(Yanisch-Perron et al. 1985)
pCH594	*E. coli* cloning vector, Amp^R, P_{SH}, *hoxBCJ*	(Kleihues et al. 2000)
pRHB1	pUC19 with insertion of *hoxB* from pCH594, Amp^R	This work
pRHB2	pRHB1 with insertion of $hoxB_{strep}$ from pRHB1, Amp^R	This work
pCTUT7	*E. coli* cloning vector, Cm^R, P_{lac}, MCS	(Kraft et al. 2007)
pQF1	pCTUT7 with deletion of unique BstBI site, CmR	This work
pQF2	pQF1 with integration of $hoxB_{strep}$ from pRHB2, Cm^R	This work
pQF3	pQF1 with integration of *bsrF* 3' mRNA transcription terminator, Cm^R	This work
pQF4	pQF3 with insertion of $hoxB_{strep}$ from pRHB2, Cm^R	This work
pQF5	pQF3 with insertion of $hoxC_{strep}$ from pCH594, Cm^R	This work
pQF6	pRHB2 with integration of *hoxC* from pCH594, Amp^R	This work
pQF7	pQF2 with insertion of $hoxC_{strep}$ from pQF5, Cm^R	This work
pQF8	pQF3 with integration of $hoxB_{strep}hoxC$ from pQF6, Cm^R	This work
pQF9	pQF3 with insertion of $hoxB_{his}$ from pQF4, Cm^R	This work
pQF10	pQF3 with insertion of $hoxC_{his}$ from pQF5, Cm^R	This work
pGK14	*E. coli*, *S. thermophilus* shuttle vector Ery^R	(Brantl 1994)
pGK16	pGK14 derivative, exchange of Ery^R with Km^R, MCS	Gimpel, unpublished
pGW2	*E. coli* expression vector, P_{tac}, Amp^R, MCS, T_{BsrF}	(Schollmeyer 2020)

pRH-Hyp	pCM62 with *hoxBC* and *hyp1* operon (*hypA1B1F1CDE*), Tet^R	(Lenz et al. 2007)
pRH-Hyp(ΔF1)	pCM62 with *hoxBC* and *hyp1(ΔF1)* operon (*hypA1B1CDE*), Tet^R	(Lenz et al. 2007)
pCH231	pBluescript KS^+ with *hoxN1*, Amp^R	(Eitinger and Friedrich 1991)
pGE771	pEDY309 with *hoxFUYHWI-hypA2B2F2CDEX-hoxA*, P_{SH}, Tet^R	(Lauterbach and Lenz 2013)
pQF11	pGK16 with P_{tac}, MCS, T_{BsrF} from pGW2, Km^R	This work
pQF12	pQF11 with insertion of *hyp1* operon from pRH-Hyp, Km^R	This work
pQF13	pQF11 with insertion of *hyp1(ΔF1)* operon from pRH-Hyp(ΔF1), Km_R	This work
pQF14	pUC19 with insertion of *hyp1* operon from pRH-Hyp, Amp^R	This work
pQF15	pUC19 with insertion of *hyp1(ΔF1)* operon from pRH-Hyp(ΔF1), Amp^R	This work
pQF16	pGK16 with integration of *bsrF* transcription terminator, Km^R	This work
pQF17	pQF12 with integation of *hoxN1* from pCH231, Km^R	This work
pQF18	pQF17 with integration of *hypX* from pGE771, Km^R	This work

Table 2.2 Oligonucleotides used in this work

Name	Oligonucleotide sequence	Restriction enzyme
Deletion of *BstB1*-site on the vector pCTUT7		
MG0034_f	CGTCGACTCGAGCTCGCTGCAGA	*PstI, XhoI, SalI, SacI*
MG0035_r	CGTCTGCAGCGAGCTCGAGTCGA	
Insertion of *B. subtilis bsrF* transcription terminator		
MG0051_f	GATCCAAGCTTAAAAAGGCGTTTGCCTTAGCCAAACGCCTTTTTAGATCT ACTAGT	
MG0052_r	GATCCAAGCTTAAAAAGGCGTTTGCCTTAGCCAAACGCCTTTTTAGATCT ACTAGT	
Cloning of *hoxB* with a C-terminal Strep-tag II instead of 55 amino acids		
MG0038_f	AGT**TCTAGA**TGGCTTGGAGGAGAAATGAACGCGCCTGTATGT	*XbaI*
MG0039_r	GTTTGGTGGAAGGGGTGGCCGGGCTCCTCAAAGCCGGGTTCAGTGCAA	
MG0040_r2	ATC**AAGCTT**A**TTTTTCGAACTGCGGGTGGCTCCA**AGCAGAGGGTGTTT GGTGGAAGGGGTGG	*HindIII*
Cloning of *hoxC* with a C-terminal Strep-tag II		
MG0043_f	ATG**TCTAGA**AATAGGAGGCGAGCATGGAAC	*XbaI*
MG0044_r	ACT**AAGCTT**A**TTTCTCAAACTGCGGGTGGCTCCA**AGCAGAATGCACG GTGCACACCATGCAG	*HindIII*
Cloning *hoxC* and *hoxB*$_{Strep}$ on the same vector (*RH*$_{stop}$)		
MG0041_f	CAG**TTCGAA**AAATAGGAGGCGAGCATGGAACGTTTG	*BstBI*
MG0042_r	ATC**AAGCTT**TCAATGCACGGTGCACACCATG	*HindIII*
Cloning of *hoxB* with a C-terminal His_6-tag instead of 55 amino acids		

MG0129_r	ATC**AAGCTT**A**GTGATGGTGATGGTGATG**GGATCCTGTTTGGTGGAAGG GGTGGC	*HindIII*
Cloning of *hoxC* with a C-terminal His_6-tag		
MG0130_r	ACT**AAGCTT**A**GTGATGGTGATGGTGATG**GGATCCAGCAGAATGCACG GTGCACACCATGC	*HindIII*
Cloning of *hyp1* operon (*hypA1B1F1CDE*) or *hyp1(DF1)* operon (*hypA1B1CDE*)		
MG0162_f	ATC**AAGCTT**CATGCATGAGCTCAGCCTGG	*HindIII*
MG0163_r	ATC**GACGTC**AACAAATGCGCGGAAGCTG	*AatII*
MG0164_f	TCA**TCTAGA**CGGAGTCTTTGGGAGATACTG	*XbaI*
MG0168_r	ACT**GCGGCCGC**TTAACAAATGCGCGGAAGCTG	*NotI*
Cloning of *hoxN1*		
MG0226_f	ATC**GCGGCCGC**ACAGGAGACTTCCAGCATGTTCCA	*NotI*
MG0227_r	ACT**GCGGCCGC**TTAACATGAACTTGTCGGCCAGGA	*NotI*
Cloning of *hypX*		
MG0243_f	AGT**TCTAGA**GCGAGTCGGCTATGCGCATATTGC	*XbaI*
MG0244_r	ATG**TCTAGA**TCAAGATCGTTTCCCCGCAAGTGC	*XbaI*
Primers used for sequencing		
M13-24R	CGGATAACAATTTCACACAGG	
MG0046	CGAACGTGGCGAGAAAGGA	
MG0047	TTGCGGCAATCGCCAGCCTGT	
MG0090	GCTTGCTGCAACTCTCTCAG	
RTG0049	ATGAAAGGGGATTTTATGCGT	
MG0160	TAC CTC CAC GCC ACA CAA CTT G	
MG0161	TAC GTG GCG AAC GAA GGT AAA TTG	
MG0170	ATCATCGCATCTGTTATACGACG	
MG0174	AGCATCCAGTCTAGCCACTC	
MG0175	CACATCTGCGCTTCGATGTAGC	
MG0176	CGGAATACGATCTGAGAGAACCC	
MG0177	ATGGCAAGGAACACCACCTC	
MG0178	AGACGGTAGCGAACAGCTTG	
MG0179	GTCGATTAGAATGCCCGCTG	
MG0228	ATCGCGGCCGCACAGGAGACTTCCAGCATGTTCCA	
MG0245	GCGCATATTGACAACAAGCGG	

f: forward primer; r: reverse primer; bold: restriction sites; bold red- or green-colored: insertion of C-terminal Strep-tag II or His_6-tag.

8.2. Purification and storage of RH samples

The purified hydrogenase preparation can be stored at -80 ℃ for activity measurements or spectroscopic analysis. However, the enzyme activity tends to be partially inactivated by freeze-thaw cycles. Rapid freezing of the enzyme solution in liquid nitrogen could reduce the loss of activity. Thus, purified Hox proteins were quickly flash-frozen in liquid nitrogen and stored at -80 ℃ for several years without any loss of activity.

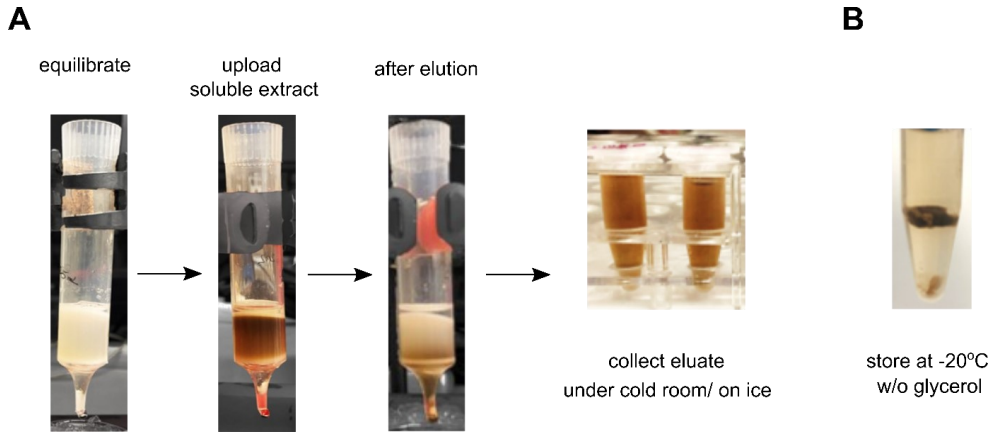

Figure 4.2 Purification process of recombinant RH protein produced from *E. coli* using Strep-tag affinity chromatography (A) and precipitation of concentrated purified RH stored at -20 °C without glycerol (B).

8.3. The concept of spectroscopic techniques

8.3.1. *In vitro* H_2-oxidation activity measurement of RH

An uptake hydrogenase activity assay allows for assessment of the in *vitro* H_2-oxidation activity of enzyme via coupling to the reduction of an artificial electron acceptor, which in this work was the redox dye methylene blue. While the oxidized form of this dye is blue, the reduced form is colorless, and so this color change can be quantified by measuring the absorbance at a specific wavelength in a spectrophotometer. Here, H_2-mediated reduction of methylene blue is measured spectrophotometrically as described previously (Podzuweit et al. 1987; Lenz et al. 2018) using a Cary50 UV-vis spectrophotometer (Varian, Agilent) with temperature controller (Varian, Agilent). The reaction is performed in a 3 ml specific optical glass cuvette (1 cm path length) sealed with a rubber septum. The methylene blue is added to the cuvette filled by 1.9 mL reaction buffer containing 50 mM K_2HPO_4/KH_2PO_4, pH 7.0 to a final concentration of 200 µM, respectively. After saturating the mixture solution by bubbling with H_2 gas for 2 min, the protein samples are injected. The absorbance change at 570 nm is carried out at 30 °C using the data obtained from the slope of a linear absorbance versus time plot. The enzyme activity can be quantified by relating the calculated slope of the activity curve to the cuvette/sample dimensions, the extinction coefficient and the protein concentration as Eq. 1:

$$\text{Specific activity } [\frac{U}{mg}] = \frac{\text{Slope} * v_{assay}}{\varepsilon * v_{enzyme} * c_{enzyme} * l} \qquad \text{Eq. 1}$$

ε = molar extinction coefficient of 13.1 mM^{-1} cm^{-1} at 570 nm

v_{assay} = total volume (in mL) of assay

v_{enzyme} = volume (in mL) of enzyme used

c_{enzyme} = concentration (in mg/mL) of enzyme used

l = length (in cm) of cuvette.

One unit (U) of specific enzyme activity corresponds to 1 µmol H_2 oxidized (corresponding to 1 µmol methylene blue reduced) per min per 1 mg of protein.

8.3.2. Infrared spectroscopy

Infrared (IR) spectroscopy probes molecular vibrations of atoms based on the resonant absorption of photons in the IR region. In comparison of that UV and visible light (0.2-0.78 μm) absorption due to electronic transitions in molecules, infrared light (2.5-25 μm) is absorbed due to vibration and rotation of molecules and the energy involved is smaller. To absorb light a molecule must have a bond within its structure that can exhibit what is referred to "dipole moment" which means electrons within a bond are not shared equally. In a molecule, interatomic chemical bonds can stretch as if they are springs. If the energy associated with such stretching vibrations is closed to that of IR light, molecules absorb IR light and vibrate. The vibration induced by IR light are restricted to those involving a change in dipole moment. Generally, stronger bonds and light atoms will vibrate at a high stretching frequency (wavenumber) (Larkin 2017).

In large biomolecular systems there is a huge number of normal modes that are IR-active and this situation calls for experimental principles that allow selective probing of molecular vibrations e.g., those can be associated with certain functional sites in metalloproteins. Local stretching vibrational information of the diatomic CN^- (2100-2040 cm^{-1}) and CO (1970-1900 cm^{-1}) ligands of the iron in the active center of [NiFe]-hydrogenases can be accessible via normal modes containing only few dominating internal coordinates or exhibiting natural frequencies in a range of the IR spectrum that is free of other absorptions (Happe et al. 1997; Pierik et al. 1999; De Lacey et al. 2007). Figure 4.3 shows an example of visualization of CO and CN stretching modes detected in the IR spectra of as-isolated oxidized form of regulatory hydrogenase from *R. eutropha* (Horch et al. 2019). Vibrational frequencies of these modes are sensitive to details of the active site, so that each redox-structural [NiFe] state exhibits a distinct signature of three absorption signals (at 1943, 2071 and 2080 cm^{-1} for RH in active as-isolated oxidized form). The frequencies of susceptibility to changes of the electron density distribution of the bimetallic center may be attributed to their conspicuous σ-donor and π-acceptor capabilities (Bagley et al. 1995, Darensbourg et al. 2000). IR senses variations of the electron density distribution in the bimetallic complex, in spite of without immediate insight into the structure of the [NiFe]-center. Therefore, the vibrational information detected by IR spectroscopy has

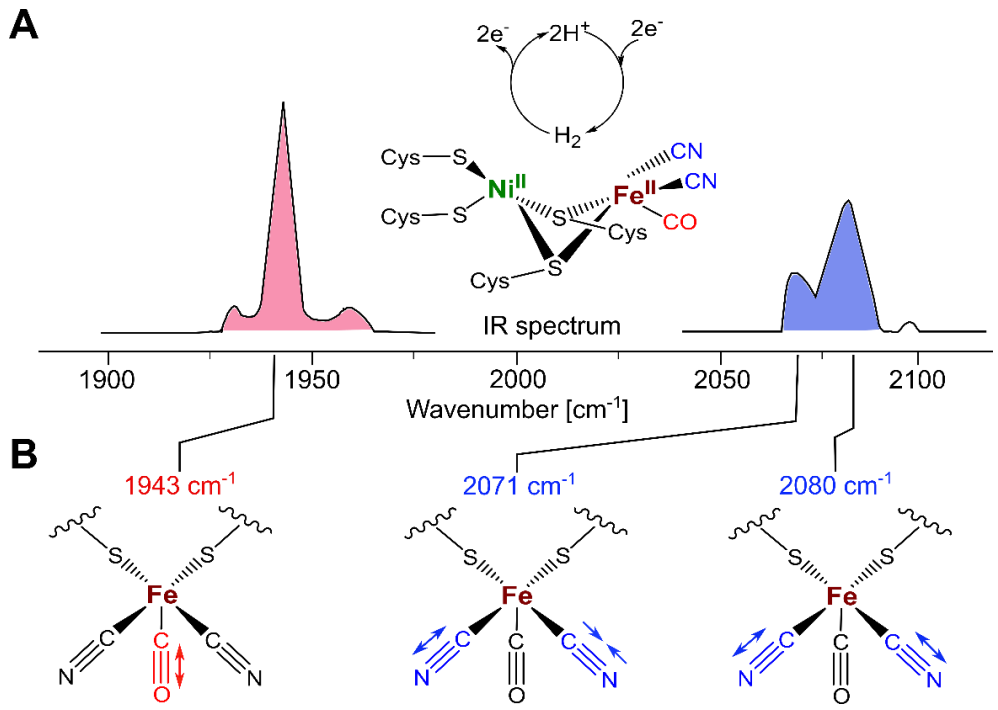

Figure 4.3 IR absorption spectrum and stretching modes of regulatory [NiFe]-hydrogenase *Re*RH from *R. eutropha*.
(A) IR absorption spectrum and active site structure of as-isolated oxidized *Re*RH in the Ni_a-S state, the H_2-accepting intermediate of [NiFe]-hydrogenases. (B) Visualization of CO (red) and CN (blue) stretching modes detected in the IR spectra of [NiFe]-hydrogenases. The *Re*RH active site produces an IR absorption spectrum containing three peaks at 1943, 2071 and 2080 cm-1 that have been assigned to the fundamental transitions (ground to first excited state, $\nu = 0 - 1$) of one CO and two CN stretching vibrations (Horch et al. 2019).

been widely used as structural probes of all states of the active site towards characterization of the diatomic CN^- and CO ligands of the Fe (De Lacey et al. 2007; Lubitz et al. 2014).

8.3.3. Electron paramagnetic resonance spectroscopy

Electron paramagnetic resonance (EPR) spectroscopy is a selective technique that uses microwaves to detect and characterize the structure and dynamics of paramagnetic centers, e.g., radicals and transition-metal ions. The interactions of radicals and transition metals with an external magnetic field and the local environment are investigated by absorbing irradiated microwaves to different extents. Since metalloproteins e.g., [NiFe]-hydrogenases mostly contain transition metals

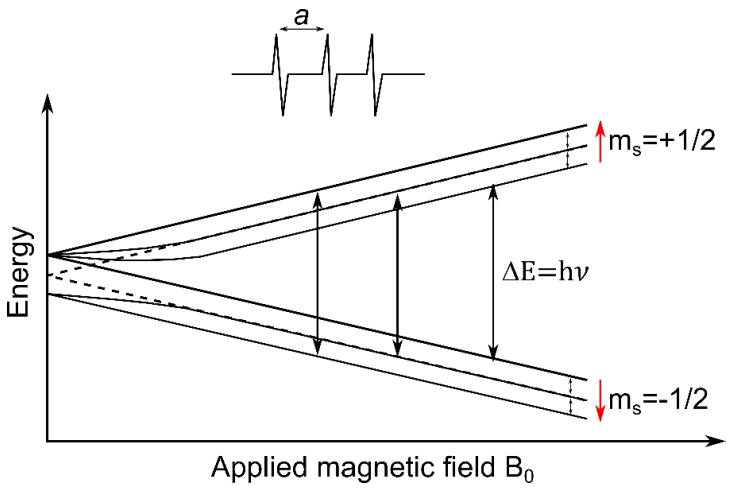

Figure 4.4 General principle of EPR spectroscopy on the external magnetic field. At low fields, where the hyperfine and Zeeman interactions are of comparable magnitude, there is a noticeable deviation from liner behavior. The magnitude of the splitting is given by sympol *a*, expressed in magnetic field units (mT).

responsible for function, probes for EPR are naturally present in these enzymes thereby providing detailed information about isolated proteins that are inaccessible to crystallography. Insight into the electronic structure can be gained through EPR spectroscopy: information about binding, structural changes and functional mechanisms can be obtained via magnetic parameters e.g., g-values, hyperfine or quadrupole values (García-Rubio 2013). In [NiFe]-hydrogenases, several spin-bearing clusters are present which are paramagnetic depending on the redox state, on the one hand the active [NiFe]-center itself, on the other hand one or more [FeS]-clusters. However, EPR spectroscopy is restricted to paramagnetic Ni states, whereas information about the active site Fe (Fe^{II}, S=0) is largely inaccessible.

The electron has a quantum mechanical intrinsic angular momentum, the spin S, which is linked to a magnetic moment via the Bohr magneton μ_B and the g-factor (as a characteristic parameter of the spin system) of the free electrons g_e. The magnetic moment has the energy in the magnetic field. Without an external magnetic field, the two possible spin orientations with the values for the magnetic spin quantum number $m_s = \pm 1/2$ are energetically degenerate. By applying a magnetic field, the degeneracy in the z-direction is typically removed. As depicted in Figure 4.4 of Zeeman splitting, $m_s = +1/2$ corresponds to the setting of the spin parallel to the

external magnetic field, $m_s = -1/2$ on the other hand antiparallel. The energy difference scales linearly with the strength of the magnetic field:

$$\Delta E = g_e \mu_B B_0 \quad \text{Eq. 2}$$

When the resonance condition Eq. 3 is fulfilled, an electromagnetic alternating field of suitable frequency (ν) and polarization can induce a transition between the energy levels exactly:

$$h\nu = g_e \mu_B B_0 \quad \text{Eq. 3}$$

Continuous-wave EPR detects changes in the energy state of a species upon the absorption of incident electromagnetic radiation, where the excitable species is an unpaired electron. The EPR spectrum of a paramagnetic center is sensitive to spin-spin interactions between unpaired electrons and nuclear spins (hyperfine interaction) and between unpaired electrons and other paramagnetic centers. Furthermore, different interactions between considered spin and its environment given by a spin Hamiltonian operator which describes the energy of the quantum mechanical system are typically considered for EPR spectroscopy, including hyperfine interaction, nuclear quadrupole interaction, zero field interaction, exchange interaction, nuclear Zeeman and electron Zeeman interaction. The basic theoretical background of various EPR methods and practical applications can be found in numerous reports (Weil and Bolton 2007, Hagen 2009, Hoff 2012).

8.3.4. UV-visible absorption spectroscopy

UV-visible absorption spectroscopy is a widely used analytical technique that measures the amounts of discrete wavelengths of UV or visible light that are absorbed by or transmitted through a sample in comparison to a reference. Light has a certain amount of energy which is inversely proportional to its wavelength. Electrons in different bonding surrounding in a substance require a different specific amount of energy to promote the electrons to a higher energy state which can be detected as absorption, thus resulting in that the absorption of light occurs for different wavelengths in different substances. To identify or analyze different substances, Therefore, UV-visible spectroscopy can locate the specific wavelengths corresponding to the maximum absorbance to identify or analyze different substances and give information presented as a graph (typically referred to as an absorption

spectrum) of absorbance, optical density or transmittance as a function of wavelength (Bosch Ojeda and Sanchez Rojas 2013; Picollo et al. 2019).

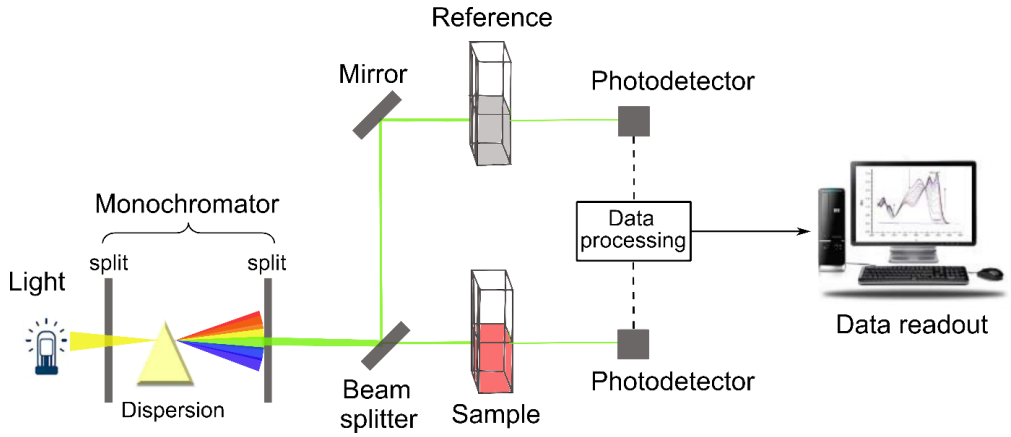

Figure 4.5 Schematic diagram of a UV-visible spectrophotometer.

A UV-visible spectrophotometer usually contains the main components such as light source, wavelength selector, sample, detector and output device, as depicted in Figure 4.5. In this work, the UV-visible spectra are recorded in a Cary300 UV-vis spectrophotometer (Varian™, Agilent, Santa Clara, USA). The measurement was performed in 100 µL quartz cuvettes (Varian, optical path length 1 cm) at RT and a scanning speed of 600 nm per min in the wavelength range of 250-800 nm. The respective storage buffer served as a reference for the baseline. For measurements of the spectrum of an oxidized sample, 100 µL of the sample is used directly after purification (as-isolated). For reduction, the same sample is sealed airtight with a rubber septum and gassed with N_2 followed by gassing H_2.

9. References

Ã, S. C. A., Robinson, A. K., and Rodriguez-Quinones, F. (2003). Bacterial iron homeostasis. FEMS Microbiol. Lett. 27, 215–237.

Abou-Hamdan, A., Ceccaldi, P., Lebrette, H., Gutiérrez-Sanz, O., Richaud, P., Cournac, L., et al. (2015). A threonine stabilizes the NiC and NiR catalytic intermediates of [NiFe]-hydrogenase. J. Biol. Chem. 290, 8550–8558.

Adams, M. W. W. (1990). The structure and mechanism of iron-hydrogenases. Biochim. Biophys. Acta - Bioenerg. 1020, 115–145.

Ahmed, M. E., Adam, S., Saha, D., Fize, J., Artero, V., Dey, A., et al. (2020). Repurposing a bio-inspired NiFe hydrogenase model for CO_2 reduction with selective production of methane as the unique C-based product. ACS Energy Lett. 5, 3837–3842.

Albareda, M., Pacios, L. F., and Palacios, J. M. (2019). Computational analyses, molecular dynamics, and mutagenesis studies of unprocessed form of [NiFe] hydrogenase reveal the role of disorder for efficient enzyme maturation. Biochim. Biophys. Acta - Bioenerg. 1860, 325–340.

Allakhverdiev, S. I., Thavasi, V., Kreslavski, V. D., Zharmukhamedov, S. K., Klimov, V. V., Ramakrishna, S., et al. (2010). Photosynthetic hydrogen production. J. Photochem. Photobiol. C Photochem. Rev. 11, 101–113.

Anane, E., García, Á. C., Haby, B., Hans, S., Krausch, N., Krewinkel, M., et al. (2019). A model-based framework for parallel scale-down fed-batch cultivations in mini-bioreactors for accelerated phenotyping. Biotechnol. Bioeng. 116, 2906–2918.

Andrews, S. C., Berks, B. C., McClay, J., Ambler, A., Quail, M. A., Golby, P., et al. (1997). A 12-cistron *Escherichia coli* operon (*hyf*) encoding a putative proton-translocating formate hydrogenlyase system. Microbiology 143, 3633–3647.

Andrews, S., Norton, I., Salunkhe, A. S., Goodluck, H., Aly, W. S. M., Mourad-agha, H., et al. (2013). Control of iron metabolism in bacteria. Metallomics and the Cell (Springer Dordrecht), 203-239.

Appel, J., Hueren, V., Boehm, M., and Gutekunst, K. (2020). Cyanobacterial in vivo solar hydrogen production using a photosystem I–hydrogenase (PsaD-HoxYH) fusion complex. Nat. Energy 5, 458–467.

Arlt, C., Nutschan, K., Haase, A., Ihling, C., Tänzler, D., Sinz, A., et al. (2021). Native mass spectrometry identifies the HybG chaperone as carrier of the $Fe(CN)_2CO$ group during maturation of *E. coli* [NiFe]-hydrogenase 2. Sci. Rep. 11, 1–12.

Armstrong, F. A., Belsey, N. A., Cracknell, J. A., Goldet, G., Parkin, A., Reisner, E., et al. (2009). Dynamic electrochemical investigations of hydrogen oxidation and production by enzymes and implications for future technology. Chem. Soc. Rev. 38, 36–51.

Armstrong, F. A., and Hirst, J. (2011). Reversibility and efficiency in electrocatalytic energy conversion and lessons from enzymes. Proc. Natl. Acad. Sci. 108, 14049–14054.

Ash, P. A., Liu, J., Coutard, N., Heidary, N., Horch, M., Gudim, I., et al. (2015). Electrochemical and infrared spectroscopic studies provide insight into reactions of the NiFe regulatory hydrogenase from *Ralstonia eutropha* with O_2 and CO. J. Phys. Chem. B 119, 13807–13815.

Atomi, H., Sato, T., and Kanai, T. (2011). Application of hyperthermophiles and their enzymes. Curr. Opin. Biotechnol. 22, 618–626.

Bagley, K. A., Duin, E. C., Roseboom, W., Albracht, S. P. J., and Woodruff, W. H. (1995). Infrared-detectable group senses changes in charge density on the nickel center in hydrogenase from *Chromatium vinosum*. Biochemistry 34, 5527–5535.

Ballantine, S. P., and Boxer, D. H. (1985). Nickel-containing hydrogenase isoenzymes from anaerobically grown *Escherichia coli* K-12. J. Bacteriol. 163, 454–459.

Banci, L., and Bertini, I. (2013). Metallomics and the cell: Some definitions and general comments.

in Metal Ions in Life Sciences (Springer London), 1–13.

Bareither, R., and Pollard, D. (2011). A review of advanced small-scale parallel bioreactor technology for accelerated process development: Current state and future need. Biotechnol. Prog. 27, 2–14.

Beauchene, N. A., Mettert, E. L., Moore, L. J., Keleş, S., Willey, E. R., and Kiley, P. J. (2017). O_2 availability impacts iron homeostasis in *Escherichia coli*. Proc. Natl. Acad. Sci. 114, 12261–12266.

Beauchene, N. A., Myers, K. S., Chung, D., Park, D. M., Weisnicht, A. M., Keleş, S., et al. (2015). Impact of anaerobiosis on expression of the iron-responsive Fur and RyhB regulons. MBio 6, 1947–1962.

Benemann, J. (1996). Hydrogen Production: Progress and prospects. Nat. Biotechnol. 14, 1101–1103.

Bernhard, M., Benelli, B., Hochkoeppler, A., Zannoni, D., and Friedrich, B. (1997). Functional and structural role of the cytochrome b subunit of the membrane-bound hydrogenase complex of *Alcaligenes eutrophus* H16. Eur. J. Biochem. 248, 179–186.

Bernhard, M., Buhrke, T., Bleijlevens, B., De Lacey, A. L., Fernandez, V. M., Albracht, S. P. J., et al. (2001). The H_2 sensor of *Ralstonia eutropha*. J. Biol. Chem. 276, 15592–15597.

Birrell, J. A., Laurich, C., Reijerse, E. J., Ogata, H., and Lubitz, W. (2016). Importance of hydrogen bonding in fine tuning the [2Fe-2S] cluster redox potential of HydC from *Thermotoga maritima*. Biochemistry 55, 4344–4355.

Bleijlevens, B., Buhrke, T., Van Der Linden, E., Friedrich, B., and Albracht, S. P. J. (2004). The auxiliary protein HypX provides oxygen tolerance to the soluble [NiFe]-hydrogenase of *Ralstonia eutropha* H16 by way of a cyanide ligand to nickel. J. Biol. Chem. 279, 46686–46691.

Blériot, C., Effantin, G., Lagarde, F., Mandrand-Berthelot, M.-A., and Rodrigue, A. (2011). RcnB is a periplasmic protein essential for maintaining intracellular Ni and Co concentrations in *Escherichia coli*. J. Bacteriol. 193, 3785–3793.

Blesken, C., Olfers, T., Grimm, A., and Frische, N. (2016). The microfluidic bioreactor for a new era of bioprocess development. Eng. Life Sci. 16, 190–193.

Blokesch, M., Albracht, S. P. J., Matzanke, B. F., Drapal, N. M., Jacobi, A., and Böck, A. (2004a). The complex between hydrogenase-maturation proteins HypC and HypD is an intermediate in the supply of cyanide to the active site iron of [NiFe]-hydrogenases. J. Mol. Biol. 344, 155–167.

Blokesch, M., Magalon, A., and Böck, A. (2001). Interplay between the specific chaperone-like proteins HybG and HypC in maturation of hydrogenases 1, 2, and 3 from *Escherichia coli*. J. Bacteriol. 183, 2817–2822.

Blokesch, M., Paschos, A., Bauer, A., Reissmann, S., Drapal, N., and Böck, A. (2004b). Analysis of the transcarbamoylation-dehydration reaction catalyzed by the hydrogenase maturation proteins HypF and HypE. Eur. J. Biochem. 271, 3428–3436.

Blokesch, M., Paschos, A., Theodoratou, E., Bauer, A., Hube, M., Huth, S., et al. (2002). Metal insertion into NiFe-hydrogenases. Biochem. Soc. Trans. 30, 674–680.

Blommel, P. G., Becker, K. J., Duvnjak, P., and Fox, B. G. (2007). Enhanced bacterial protein expression during auto-induction obtained by alteration of Lac repressor dosage and medium composition. Biotechnol. Prog. 23, 585–598.

Böck, A., King, P. W., Blokesch, M., and Posewitz, M. C. (2006). Maturation of hydrogenases. Adv. Microb. Physiol. 51, 1–225.

Bonocora, R. P., Smith, C., Lapierre, P., and Wade, J. T. (2015). Genome-scale mapping of *Escherichia coli* σ54 reveals widespread, conserved intragenic binding. PLoS Genet. 11, 1–30.

Bortolus, M., Costantini, P., Doni, D., and Carbonera, D. (2018). Overview of the maturation

machinery of the H-Cluster of [FeFe]-Hydrogenases with a focus on HydF. Int. J. Mol. Sci. 19, 3118.

Bosch Ojeda, C., and Sanchez Rojas, F. (2013). Recent applications in derivative ultraviolet/visible absorption spectrophotometry: 2009–2011: A review. Microchem. J. 106, 1–16.

Boyd, E. S., Thomas, K. M., Dai, Y., Boyd, J. M., and Outten, F. W. (2014). Interplay between oxygen and Fe-S cluster biogenesis: Insights from the Suf pathway. Biochemistry 53, 5834–5847.

Brantl, S. (1994). The *copR* gene product of plasmid p1P501 acts as a transcriptional repressor at the essential *repR* promoter. Mol. Microbiol. 14, 473–483.

Braun, V. (2003). Iron uptake by *Escherichia coli*.

Braun, V., and Hantke, K. (2011). Recent insights into iron import by bacteria. Curr. Opin. Chem. Biol. 15, 328–334.

Brecht, M., van Gastel, M., Buhrke, T., Friedrich, B., and Lubitz, W. (2003). Direct detection of a hydrogen ligand in the [NiFe] center of the regulatory H_2-Sensing Hydrogenase from *Ralstonia eutropha* in its reduced state by HYSCORE and ENDOR Spectroscopy. J. Am. Chem. Soc. 125, 13075–13083.

Buhrke, T., Bleijlevens, B., Albracht, S. P. J., and Friedrich, B. (2001). Involvement of *hyp* gene products in maturation of the H_2-sensing [NiFe] hydrogenase of *Ralstonia eutropha*. J. Bacteriol. 183, 7087–7093.

Buhrke, T., and Friedrich, B. (1998). *hoxX* (*hypX*) is a functional member of the *Alcaligenes eutrophus hyp* gene cluster. Arch. Microbiol. 170, 460–463.

Buhrke, T., Lenz, O., Krauss, N., and Friedrich, B. (2005a). Oxygen tolerance of the H_2-sensing [NiFe] hydrogenase from *Ralstonia eutropha* H16 is based on limited access of oxygen to the active site. J. Biol. Chem. 280, 23791–23796.

Buhrke, T., Lenz, O., Porthun, A., and Friedrich, B. (2004). The H_2-sensing complex of *Ralstonia eutropha*: Interaction between a regulatory [NiFe] hydrogenase and a histidine protein kinase. Mol. Microbiol. 51, 1677–1689.

Buhrke, T., Löscher, S., Lenz, O., Schlodder, E., Zebger, I., Andersen, L. K., et al. (2005b). Reduction of unusual iron-sulfur clusters in the H_2-sensing regulatory NiFe hydrogenase from *Ralstonia eutropha* H16. J. Biol. Chem. 280, 19488–19495.

Burgdorf, T., Lenz, O., Buhrke, T., Van Der Linden, E., Jones, A. K., Albracht, S. P. J., et al. (2005). [NiFe]-hydrogenases of *Ralstonia eutropha* H16: Modular enzymes for oxygen-tolerant biological hydrogen oxidation. J. Mol. Microbiol. Biotechnol. 10, 181–196.

Bürstel, I., Hummel, P., Siebert, E., Wisitruangsakul, N., Zebger, I., Friedrich, B., et al. (2011). Probing the origin of the metabolic precursor of the CO ligand in the catalytic center of [NiFe] hydrogenase. J. Biol. Chem. 286, 44937–44944.

Bürstel, I., Siebert, E., Frielingsdorf, S., Zebger, I., Friedrich, B., and Lenz, O. (2016). CO synthesized from the central one-carbon pool as source for the iron carbonyl in O_2-tolerant [NiFe]-hydrogenase. Proc. Natl. Acad. Sci. U. S. A. 113, 14722–14726.

Bürstel, I., Siebert, E., Winter, G., Hummel, P., Zebger, I., Friedrich, B., et al. (2012). A universal scaffold for synthesis of the $Fe(CN)_2(CO)$ moiety of [NiFe] hydrogenase. J. Biol. Chem. 287, 38845–53.

Buurman, G., Shima, S., and Thauer, R. K. (2000). The metal-free hydrogenase from methanogenic archaea: Evidence for a bound cofactor. FEBS Lett. 485, 200–204.

Cammack, R., Bagyinka, C., and Kovacs, K. L. (1989). Spectroscopic characterization of the nickel and iron-sulphur clusters of hydrogenase from the purple photosynthetic bacterium *Thiocapasa roseopersicina*. 2. Electron spin-echo spectroscopy. Eur. J. Biochem. 182, 363–366.

Cartron, M. L., Maddocks, S., Gillingham, P., Craven, C. J., and Andrews, S. C. (2006). Feo-Transport of ferrous iron into bacteria. in BioMetals (Springer), 143–157.

Casalot, L., and Rousset, M. (2001). Maturation of the [NiFe] hydrogenases. Trends Microbiol. 9,

228–237.

Caserta, G., Lorent, C., Ciaccafava, A., Keck, M., Breglia, R., Greco, C., et al. (2020a). The large subunit of the regulatory [NiFe]-hydrogenase from *Ralstonia eutropha* - a minimal hydrogenase? Chem. Sci. 11, 5453–5465.

Caserta, G., Lorent, C., Pelmenschikov, V., Schoknecht, J., Yoda, Y., Hildebrandt, P., et al. (2020b). In vitro assembly as a tool to investigate catalytic intermediates of [NiFe]-hydrogenase. ACS Catal. 10, 13890–13894.

Caserta, G., Pelmenschikov, V., Lorent, C., Tadjoung Waffo, A. F., Katz, S., Lauterbach, L., et al. (2021). Hydroxy-bridged resting states of a [NiFe]-hydrogenase unraveled by cryogenic vibrational spectroscopy and DFT computations. Chem. Sci. 12, 2189–2197.

Ceccaldi, P., Schuchmann, K., Müller, V., and Elliott, S. J. (2017). The hydrogen dependent CO_2 reductase: The first completely CO tolerant FeFe-hydrogenase. Energy Environ. Sci. 10, 503–508.

Cohen, J., Kim, K., Posewitz, M., Ghirardi, M. L., Schulten, K., Seibert, M., et al. (2005). Molecular dynamics and experimental investigation of H_2 and O_2 diffusion in [Fe]-hydrogenase. in Biochemical Society Transactions (Portland Press Limited), 80–82.

Constant, P., Chowdhury, S. P., Hesse, L., Pratscher, J., and Conrad, R. (2011). Genome data mining and soil survey for the novel group 5 [NiFe]-hydrogenase to explore the diversity and ecological importance of presumptive high-affinity H_2-oxidizing bacteria. Appl. Environ. Microbiol. 77, 6027–6035.

Constant, P., Chowdhury, S. P., Pratscher, J., and Conrad, R. (2010). Streptomycetes contributing to atmospheric molecular hydrogen soil uptake are widespread and encode a putative high-affinity [NiFe]-hydrogenase. Environ. Microbiol. 12, 821–829.

Corless, E. I., Mettert, E. L., Kiley, P. J., and Antony, E. (2020). Elevated expression of a functional Suf pathway in *Escherichia* sulfur cluster-containing protein. J. Bacteriol. 202, 1–11.

Cowart, R. E. (2002). Reduction of iron by extracellular iron reductases: Implications for microbial iron acquisition. Arch. Biochem. Biophys. 400, 273–281.

Crabtree, G. W., and Dresselhaus, M. S. (2008). The hydrogen fuel alternative. MRS Bull. 33, 421–428.

Cracknell, J. A., Vincent, K. A., and Armstrong, F. A. (2008a). Enzymes as working or inspirational electrocatalysts for fuel cells and electrolysis. Chem. Rev. 108, 2439–2461.

Cracknell, J. A., Vincent, K. A., Ludwig, M., Lenz, O., rbel Friedrich, B., and Armstrong, F. A. (2008b). Enzymatic oxidation of H_2 in atmospheric O_2 : The electrochemistry of energy generation from trace H_2 by aerobic microorganisms. J. AM. CHEM. SOC 130, 424–425.

Cracknell, J. A., Wait, A. F., Lenz, O., Friedrich, B., and Armstrong, F. A. (2009). A kinetic and thermodynamic understanding of O_2 tolerance in [NiFe]-hydrogenases. Proc. Natl. Acad. Sci. U. S. A. 106, 20681–6.

Daegelen, P., Studier, F. W., Lenski, R. E., Cure, S., and Kim, J. F. (2009). Tracing ancestors and relatives of *Escherichia coli* B, and the derivation of B strains REL606 and BL21(DE3). J. Mol. Biol. 394, 634–643.

Darensbourg, M. Y., Lyon, E. J., and Smee, J. J. (2000). The bio-organometallic chemistry of active site iron in hydrogenases. Coord. Chem. Rev. 206–207, 533–561.

de Graef, M. R., Alexeeva, S., Snoep, J. L., and Teixeira de Mattos, M. J. (1999). The steady-state internal redox state (NADH/NAD) reflects the external redox state and is correlated with catabolic adaptation in *Escherichia coli*. J. Bacteriol. 181, 2351–7.

de la Garza, L., Jeong, G., Liddell, P. A., Sotomura, T., Moore, T. A., Moore, A. L., et al. (2003). Enzyme-based photoelectrochemical biofuel cell. J. Phys. Chem. B 107, 10252–10260.

De Lacey, A. L., Fernández, V. M., Rousset, M., and Cammack, R. (2007). Activation and inactivation of hydrogenase function and the catalytic cycle: Spectroelectrochemical studies. Chem. Rev. 107, 4304–4330.

De Pina, K., Desjardin, V., Mandrand-Berthelot, M.-A., Giordano, G., and Wu, L.-F. (1999). Isolation and characterization of the *nikR* gene encoding a nickel-responsive regulator in *Escherichia coli*. J. Bacteriol. 181, 670–674.

de Reuse, H., Vinella, D., and Cavazza, C. (2013). Common themes and unique proteins for the uptake and trafficking of nickel, a metal essential for the virulence of *Helicobacter pylori*. Front. Cell. Infect. Microbiol. 3, 94.

Demuez, M., Cournac, L., Guerrini, O., Soucaille, P., and Girbal, L. (2007). Complete activity profile of *Clostridium acetobutylicum* [FeFe]-hydrogenase and kinetic parameters for endogenous redox partners. FEMS Microbiol. Lett. 275, 113–121.

Dernedde, J., Eitinger, T., Patenge, N., and Friedrich, B. (1996). Are part of a hydrogenase-maturation system. Proteins 358, 351–358.

Dole, F., Fournel, A., Magro, V., Hatchikian, E. C., Bertrand, P., and Guigliarelli, B. (1997). Nature and electronic structure of the Ni-X dinuclear center of *Desulfovibrio gigas* hydrogenase. Implications for the enzymatic mechanism. Biochemistry 36, 7847–7854.

Dörr, M., Fibinger, M. P. C., Last, D., Schmidt, S., Santos-Aberturas, J., Böttcher, D., et al. (2016). Fully automatized high-throughput enzyme library screening using a robotic platform. Biotechnol. Bioeng. 113, 1421–1432.

Duché, O., Elsen, S., Cournac, L., and Colbeau, A. (2005). Enlarging the gas access channel to the active site renders the regulatory hydrogenase HupUV of *Rhodobacter capsulatus* O_2 sensitive without affecting its transductory activity. FEBS J. 272, 3899–3908.

Durmowicz, M. C., and Maier, R. J. (1997). Roles of HoxX and HoxA in biosynthesis of hydrogenase in *Bradyrhizobium japonicum*. J. Bacteriol. 179, 3676–3682.

Eitinger, T., and Friedrich, B. (1991). Cloning , nucleotide sequence , and heterologous expression of a high-affinity nickel transport gene from *Alcaligenes eutrophus*. J. Biol. Chem. 266, 3222–3227.

Eitinger, T., and Mandrand-Berthelot, M. A. (2000). Nickel transport systems in microorganisms. Arch. Microbiol. 173, 1–9.

Evans, C. R., Fan, Y., and Ling, J. (2019). Increased mistranslation protects *E. coli* from protein misfolding stress due to activation of a RpoS-dependent heat shock response. FEBS Lett. 593, 3220–3227.

Evans, D. J., and Pickett, C. J. (2003). Chemistry and the hydrogenases. Chem. Soc. Rev. 32, 268–275.

Evans, R. M., Brooke, E. J., Wehlin, S. A. M., Nomerotskaia, E., Sargent, F., Carr, S. B., et al. (2016). Mechanism of hydrogen activation by [NiFe] hydrogenases. Nat. Chem. Biol. 12, 46–50.

Ezraty, B., Vergnes, A., Banzhaf, M., Duverger, Y., Huguenot, A., Brochado, A. R., et al. (2013). Fe-S cluster biosynthesis controls uptake of aminoglycosides in a ROS-less death pathway. Science 340, 1583–1587.

Fahnert, B., Lilie, H., and Neubauer, P. (2004). "Inclusion bodies: Formation and utilisation," in Advances in Biochemical Engineering/Biotechnology, 93–142.

Fan, Q. (2017). Impact of oscillating nutrient starvation simulated in a two-compartment scale-down system on metabolic responses of recombinant Escherichia coli and production of non-canonical amino acids. Master thesis (unpublished), Techenische Universität Berlin.

Fan, Q., Neubauer, P., Lenz, O., and Gimpel, M. (2020). Heterologous hydrogenase overproduction systems for biotechnology—An overview. Int. J. Mol. Sci. 21, 5890.

Fauque, G., Peck Jr, H. D., Moura, J. J. G., Huynh, B. H., Berlier, Y., DerVartanian, D. V, et al. (1988). The three classes of hydrogenases from sulfate-reducing bacteria of the genus *Desulfovibrio*. FEMS Microbiol. Lett. 54, 299–344.

Faust, G., Stand, A., and Weuster-Botz, D. (2015). IPTG can replace lactose in auto-induction media to enhance protein expression in batch-cultured *Escherichia coli*. Eng. Life Sci. 15, 824–829.

Fernández-Castané, A., Caminal, G., and López-Santín, J. (2012a). Direct measurements of IPTG enable analysis of the induction behavior of *Escherichia coli* in high cell density cultures. Microb. Cell Fact. 11, 1–9.

Fernández-Castané, A., Vine, C. E., Caminal, G., and López-Santín, J. (2012b). Evidencing the role of lactose permease in IPTG uptake by *Escherichia coli* in fed-batch high cell density cultures. J. Biotechnol. 157, 391–398.

Flanagan, L. A., and Parkin, A. (2016). Electrochemical insights into the mechanism of NiFe membrane-bound hydrogenases. Biochem. Soc. Trans. 44, 315–328.

Foerster, S., Gastel, M. van, Brecht, M., and Lubitz, W. (2005). An orientation-selected ENDOR and HYSCORE study of the Ni-C active state of *Desulfovibrio vulgaris* Miyazaki F hydrogenase. JBIC J. Biol. Inorg. Chem. 10, 51–62.

Fontecilla-Camps, J. C., Amara, P., Cavazza, C., Nicolet, Y., and Volbeda, A. (2009). Structure-function relationships of anaerobic gas-processing metalloenzymes. Nature 460, 814–822.

Fontecilla-Camps, J. C., Volbeda, A., Cavazza, C., and Nicolet, Y. (2007). Structure/function relationships of [NiFe]- and [FeFe]-hydrogenases. Chem. Rev. 107, 4273–4303.

Förster, A. H., and Gescher, J. (2014). Metabolic engineering of *Escherichia coli* for production of mixed-acid fermentation end products. Front. Bioeng. Biotechnol. 2, 16.

Forzi, L., Hellwig, P., Thauer, R. K., and Sawers, R. G. (2007). The CO and CN^- ligands to the active site Fe in [NiFe]-hydrogenase of *Escherichia coli* have different metabolic origins. FEBS Lett. 581, 3317–3321.

Forzi, L., and Sawers, R. G. (2007). Maturation of [NiFe]-hydrogenases in *Escherichia coli*. in BioMetals (Springer US), 565–578.

Frey, M. (2002). Hydrogenases: Hydrogen-activating enzymes. ChemBioChem 3, 153–160.

Friedrich, B., Buhrke, T., Burgdorf, T., and Lenz, O. (2005). A hydrogen-sensing multiprotein complex controls aerobic hydrogen metabolism in *Ralstonia eutropha*. Biochem. Soc. Trans. 33, 97–101.

Friedrich, B., Fritsch, J., and Lenz, O. (2011). Oxygen-tolerant hydrogenases in hydrogen-based technologies. Curr. Opin. Biotechnol. 22, 358–364.

Friedrich, B., Heine, E., Finck, A., and Friedrich, C. G. (1981). Nickel requirement for active hydrogenase formation in *Alcaligenes eutrophus*. J. Bacteriol. 145, 1144–1149.

Friedrich, C. G. (1982). Depression of hydrogenase during limitation of electron donors and derepression of ribulosebisphosphate carboxylase during carbon limitation of *Alcaligenes eutrophus*. J. Bacteriol. 149, 203–210.

Fritsch, J., Lenz, O., and Friedrich, B. (2011). The maturation factors HoxR and HoxT contribute to oxygen tolerance of membrane-bound [NiFe] hydrogenase in *Ralstonia eutropha* H16. J. Bacteriol. 193, 2487–2497.

Fritsch, J., Lenz, O., and Friedrich, B. (2013). Structure, function and biosynthesis of O_2-tolerant hydrogenases. Nat. Rev. Microbiol. 11, 106–114.

García-Rubio, I. (2013). Pulsed EPR: Principles and examples of applications to hemeproteins. in Encyclopedia of Biophysics (Springer, Berlin, Heidelberg), 2115–2124.

Garcin, E., Vernede, X., Hatchikian, E. C., Volbeda, A., Frey, M., and Fontecilla-Camps, J. C. (1999). The crystal structure of a reduced [NiFeSe] hydrogenase provides an image of the activated catalytic center. Structure 7, 557–566.

Gasper, R., Scrima, A., and Wittinghofer, A. (2006). Structural insights into HypB, a GTP-binding protein that regulates metal binding. J. Biol. Chem. 281, 27492–27502.

Gerken, H., Vuong, P., Soparkar, K., and Misra, R. (2020). Roles of the ENVZ/OMPR two-component system and porins in iron acquisition in *Escherichia coli*. MBio 11, 1–18.

Ghirardi, M. L., Posewitz, M. C., Maness, P.-C., Dubini, A., Yu, J., and Seibert, M. (2007). Hydrogenases and hydrogen photoproduction in oxygenic photosynthetic organisms. Annu. Rev. Plant Biol. 58, 71–91.

Giel, J. L., Nesbit, A. D., Mettert, E. L., Fleischhacker, A. S., Wanta, B. T., and Kiley, P. J. (2013). Regulation of iron-sulphur cluster homeostasis through transcriptional control of the Isc pathway by [2Fe-2S]-IscR in *Escherichia coli*. Mol. Microbiol. 87, 478–492.

Giel, J. L., Rodionov, D., Liu, M., Blattner, F. R., and Kiley, P. J. (2006). IscR-dependent gene expression links iron-sulphur cluster assembly to the control of O_2-regulated genes in *Escherichia coli*. Mol. Microbiol. 60, 1058–1075.

Girbal, L., Von Abendroth, G., Winkler, M., Benton, P. M. C., Meynial-Salles, I., Croux, C., et al. (2005). Homologous and heterologous overexpression in *Clostridium acetobutylicum* and characterization of purified clostridial and algal Fe-only hydrogenases with high specific activities. Appl. Environ. Microbiol. 71, 2777–2781.

Goff, A. Le, Artero, V., Jousselme, B., Tran, P. D., Guillet, N., Métayé, R., et al. (2009). From hydrogenases to noble metal-free catalytic nanomaterials for H_2 production and uptake. Science 326, 1384–1387.

Gombert, A. K., and Kilikian, B. V. (1998). Recombinant gene expression in *Escherichia coli* cultivation using lactose as inducer. J. Biotechnol. 60, 47–54.

Goris, T., Wait, A. F., Saggu, M., Fritsch, J., Heidary, N., Stein, M., et al. (2011). A unique iron-sulfur cluster is crucial for oxygen tolerance of a [NiFe]-hydrogenase. Nat. Chem. Biol. 7, 310–318.

Görke, B., and Stülke, J. (2008). Carbon catabolite repression in bacteria: many ways to make the most out of nutrients. Nat. Rev. Microbiol. 6, 613–624.

Gottesman, S. (1996). Proteases and Their targents in *Escherichia coli*. Annu. Rev. Genet. 30, 465–506.

Goulhen, F., Gloter, A., Guyot, F., and Bruschi, M. (2006). Cr(VI) detoxification by *Desulfovibrio vulgaris* strain Hildenborough: Microbe–metal interactions studies. Appl. Microbiol. Biotechnol. 71, 892–897.

Goyal, A., Marcandalli, G., … V. M.-J. of the A., and 2020, U. (2020). Competition between CO_2 reduction and hydrogen evolution on a gold electrode under well-defined mass transport conditions. ACS Publ. 142, 4161.

Grabski, A., Mehler, M., and Drott, D. (2005). The overnight express autoinduction system: High-density cell growth and protein expression while you sleep. Nat. Methods 2, 233–235.

Grass, G. (2006). Iron transport in *Escherichia coli*: All has not been said and done. BioMetals 19, 159–172.

Greening, C., Biswas, A., Carere, C. R., Jackson, C. J., Taylor, M. C., Stott, M. B., et al. (2016). Genomic and metagenomic surveys of hydrogenase distribution indicate H_2 is a widely utilised energy source for microbial growth and survival. ISME J. 10, 761–777.

Greening, C., Constant, P., Hards, K., Morales, S. E., Oakeshott, J. G., Russell, R. J., et al. (2015). Atmospheric hydrogen scavenging: From enzymes to ecosystems. Appl. Environ. Microbiol. 81, 1190–1199.

Grodberg, J., and Dunn, J. J. (1989). Comparison of *Escherichia coli* K-12 outer membrane protease OmpT and *Salmonella typhimurium* E protein. J. Bacteriol. 171, 2903–2905.

Gross, R., Simon, J., and Kröger, A. (1999). The role of the twin-arginine motif in the signal peptide encoded by the *hydA* gene of the hydrogenase from *Wolinella succinogenes*. Arch. Microbiol. 1999 1724 172, 227–232.

Gyaneshwar, P., Paliy, O., McAuliffe, J., Jones, A., Jordan, M. I., and Kustu, S. (2005). Lessons from *Escherichia coli* genes similarly regulated in response to nitrogen and sulfur limitation. Proc. Natl. Acad. Sci. U. S. A. 102, 3453–3458.

Haby, B., Hans, S., Anane, E., Sawatzki, A., Krausch, N., Neubauer, P., et al. (2019). Integrated robotic mini bioreactor platform for automated, parallel microbial cultivation with online data handling and process control. SLAS Technol. 24, 569–582.

Hans, S., Haby, B., Krausch, N., Barz, T., Neubauer, P., and Cruz-Bournazou, M. N. (2020). Automated conditional screening of multiple *Escherichia coli* strains in parallel adaptive fed-

batch cultivations. Bioengineering 7, 145.

Happe, R. P., Roseboom, W., Plerlk, A. J., Albracht, S. P. J., and Bagley, K. A. (1997). Biological activition of hydrogen. Nature 385, 126.

Happe, T., and Kaminski, A. (2002). Differential regulation of the Fe-hydrogenase during anaerobic adaptation in the green alga *Chlamydomonas reinhardtii*. Eur. J. Biochem. 269, 1022–1032.

Happe, T., Schütz, K., and Böhme, H. (2000). Transcriptional and mutational analysis of the uptake hydrogenase of the filamentous cyanobacterium *Anabaena variabilis* ATCC 29413. J. Bacteriol. 182, 1624–1631.

Hausinger, R. P. (1987). Nickel utilization by microorganisms. Microbiol. Rev. 51, 22–42.

Hemmerich, J., Noack, S., Wiechert, W., and Oldiges, M. (2018). Microbioreactor systems for accelerated bioprocess development. Biotechnol. J. 13, 1700141.

Higgins, K. A., Carr, C. E., and Maroney, M. J. (2012). Specific metal recognition in nickel trafficking. Biochemistry 51, 7816–7832.

Hiromoto, T., Ataka, K., Pilak, O., Vogt, S., Stagni, M. S., Meyer-Klaucke, W., et al. (2009). The crystal structure of C176A mutated [Fe]-hydrogenase suggests an acyl-iron ligation in the active site iron complex. FEBS Lett. 583, 585–590.

Hoffman, B. J., Broadwater, J. A., Johnson, P., Harper, J., Fox, B. G., and Kenealy, W. R. (1995). Lactose fed-batch overexpression of recombinant metalloproteins in *Escherichia coli* BL21(DE3): Process control yielding high levels of metal-incorporated, soluble protein. Protein Expr. Purif. 6, 646–654.

Horch, M., Lauterbach, L., Mroginski, M. A., Hildebrandt, P., Lenz, O., and Zebger, I. (2015). Reversible active site sulfoxygenation can explain the oxygen tolerance of a NAD^+-reducing [NiFe] hydrogenase and its unusual infrared spectroscopic properties. J. Am. Chem. Soc. 137, 2555–2564.

Horch, M., Lauterbach, L., Saggu, M., Hildebrandt, P., Lendzian, F., Bittl, R., et al. (2010). Probing the active site of an O_2-tolerant NAD^+-reducing [NiFe]-hydrogenase from *Ralstonia eutropha* H16 by in situ EPR and FTIR spectroscopy. Angew. Chemie - Int. Ed. 49, 8026–8029.

Horch, M., Schoknecht, J., Wrathall, S. L. D., Greetham, G. M., Lenz, O., and Hunt, N. T. (2019). Understanding the structure and dynamics of hydrogenases by ultrafast and two-dimensional infrared spectroscopy. Chem. Sci. 10, 8981–8989.

Horinouchi, T., Minamoto, T., Suzuki, S., Shimizu, H., and Furusawa, C. (2014). Development of an automated culture system for laboratory evolution. SLAS Technol. 19, 478–482.

Horner, D. S., Heil, B., Happe, T., and Embley, T. M. (2002). Iron hydrogenases – ancient enzymes in modern eukaryotes. Trends Biochem. Sci. 27, 148–153.

Huang, G., Wagner, T., Ermler, U., and Shima, S. (2020). Methanogenesis involves direct hydride transfer from H_2 to an organic substrate. Nat. Rev. Chem. 4, 213–221.

Hube, M., Blokesch, M., and Böck, A. (2002). Network of hydrogenase maturation in *Escherichia coli*: Role of accessory proteins HypA and HybF. J. Bacteriol. 184, 3879–3885.

Igor Stojiljkovic, Miloje Cobeljic, K. H. (1993). *Escherichia coli* K-12 ferrous iron uptake mutants are impaired in their ability to colonize the mouse intestine. FEMS Microbiol. Lett. 108, 111–115.

Ihara, M., Nishihara, H., Yoon, K.-S., Lenz, O., Friedrich, B., Nakamoto, H., et al. (2006). Light-driven hydrogen production by a hybrid complex of a [NiFe]-hydrogenase and the cyanobacterial photosystem I. Photochem. Photobiol. 82, 676.

Ikeda, T., and Kano, K. (2001). An electrochemical approach to the studies of biological redox reactions and their applications to biosensors, bioreactors, and biofuel cells. J. Biosci. Bioeng. 92, 9–18.

Ilina, Y., Lorent, C., Katz, S., Jeoung, J., Shima, S., Horch, M., et al. (2019). X-ray crystallography

and vibrational spectroscopy reveal the key determinants of biocatalytic dihydrogen cycling by [NiFe] Hydrogenases. Angew. Chemie Int. Ed. 58, 18710–18714.

Iwig, J. S., and Chivers, P. T. (2010). Coordinating intracellular nickel–metal-site structure-function relationships and the NikR and RcnR repressors. Nat. Prod. Rep. 27, 658.

Iwig, J. S., Rowe, J. L., and Chivers, P. T. (2006). Nickel homeostasis in *Escherichia coli*? the *rcnR-rcnA* efflux pathway and its linkage to NikR function. Mol. Microbiol. 62, 252–262.

Jacobi, A., Rossmann, R., and Böck, A. (1992). The *hyp* operon gene products are required for the maturation of catalytically active hydrogenase isoenzymes in *Escherichia coli*. Arch. Microbiol. 158, 444–451.

Jaganaman, S., Pinto, A., Tarasev, M., and Ballou, D. P. (2007). High levels of expression of the iron-sulfur proteins phthalate dioxygenase and phthalate dioxygenase reductase in *Escherichia coli*. Protein Expr. Purif. 52, 273–279.

Jagilinki, B. P., Ilic, S., Trncik, C., Tyryshkin, A. M., Pike, D. H., Lubitz, W., et al. (2020). In vivo biogenesis of a de novo designed iron-sulfur protein. ACS Synth. Biol. 9, 3400–3407.

Jensen, E. B., and Carlsen, S. (1990). Production of recombinant human growth hormone in *Escherichia coli*: expression of different precursors and physiological effects of glucose, acetate, and salts. Biotechnol. Bioeng. 36, 1–11.

Jeong, H., Barbe, V., Lee, C. H., Vallenet, D., Yu, D. S., Choi, S. H., et al. (2009). Genome sequences of *Escherichia coli* B strains REL606 and BL21(DE3). J. Mol. Biol. 394, 644–652.

Jervis, A. J., Crack, J. C., White, G., Artymiuk, P. J., Cheesman, M. R., Thomson, A. J., et al. (2009). The O_2 sensitivity of the transcription factor FNR is controlled by Ser24 modulating the kinetics of [4Fe-4S] to [2Fe-2S] conversion. Proc. Natl. Acad. Sci. 106, 4659–4664.

Jing, D., Guo, L., Zhao, L., Zhang, X., Liu, H., Li, M., et al. (2010). Efficient solar hydrogen production by photocatalytic water splitting: From fundamental study to pilot demonstration. International Journal of Hydrogen Energy, 7087–7097.

Jones, A. K., Lamle, S. E., Pershad, H. R., Vincent, K. A., Albracht, S. P. J., and Armstrong, F. A. (2003). Enzyme electrokinetics: Electrochemical studies of the anaerobic interconversions between active and inactive states of *Allochromatium vinosum* [NiFe]-hydrogenase. J. Am. Chem. Soc. 125, 8505–8514.

Jones, A. K., Lenz, O., Strack, A., Buhrke, T., and Friedrich, B. (2004). NiFe Hydrogenase Active Site Biosynthesis: Identification of Hyp Protein Complexes in *Ralstonia eutropha*. Biochemistry 43, 13467–13477.

Jugder, B.-E., Welch, J., Aguey-Zinsou, K.-F., and Marquis, C. P. (2013). Fundamentals and electrochemical applications of [Ni–Fe]-uptake hydrogenases. RSC Adv. 3, 8142.

Jung, G., Denefle, P., Becquart, J., and Mayaux, J. F. (1988). High-cell density fermentation studies of recombinant *Escherichia coli* strains expressing human interleukin-1β. Ann. l'Institut Pasteur/Microbiologie 139, 129–146.

Junker, B. H., and Wang, H. Y. (2006). Bioprocess monitoring and computer control: Key roots of the current PAT initiative. Biotechnol. Bioeng. 95, 226–261.

Kalia, V. C., Lal, S., Ghai, R., Mandal, M., and Chauhan, A. (2003). Mining genomic databases to identify novel hydrogen producers. Trends Biotechnol. 21, 152–156.

Kalms, J., Schmidt, A., Frielingsdorf, S., Utesch, T., Gotthard, G., von Stetten, D., et al. (2018). Tracking the route of molecular oxygen in O_2-tolerant membrane-bound [NiFe] hydrogenase. Proc. Natl. Acad. Sci. U. S. A., 201712267.

Kammler, M., Schon, C., and Hantke, K. (1993). Characterization of the ferrous iron uptake system of *Escherichia coli*. J. Bacteriol. 175, 6212–6219.

Kanygin, A., Milrad, Y., Thummala, C., Reifschneider, K., Baker, P., Marco, P., et al. (2020). Rewiring photosynthesis: A photosystem I-hydrogenase chimera that makes H_2: In vivo. Energy Environ. Sci. 13, 2903–2914.

Karyakin, A. A., Morozov, S. V., Karyakina, E. E., Zorin, N. A., Perelygin, V. V., and Cosnier, S.

(2005). Hydrogenase electrodes for fuel cells. Biochem. Soc. Trans. 33, 73–75.

Kehres, D. G., Lawyer, C. H., and Maguire, M. E. (1998). The CorA magnesium transporter gene family. Microb. Comp. Genomics 3, 151–169.

Khoroshilova, N., Popescu, C., Munck, E., Beinert, H., and Kiley, P. J. (1997). Iron-sulfur cluster disassembly in the FNR protein of *Escherichia coli* by O_2: [4Fe-4S] to [2Fe-2S] conversion with loss of biological activity. Proc. Natl. Acad. Sci. 94, 6087–6092.

Kiley, P. J., and Beinert, H. (1998). Oxygen sensing by the global regulator, FNR: the role of the iron-sulfur cluster. FEMS Microbiol. Rev. 22, 341–352.

Kim, J. Y. H., Jo, B. H., and Cha, H. J. (2011). Production of biohydrogen by heterologous expression of oxygen-tolerant Hydrogenovibrio marinus [NiFe]-hydrogenase in *Escherichia coli*. J. Biotechnol. 155, 312–319.

Kim, J. Y., Jo, B., and Cha, H. (2010). Production of biohydrogen by recombinant expression of [NiFe]-hydrogenase 1 in *Escherichia coli*. Microb. Cell Fact. 9, 54.

Kleihues, L., Lenz, O., Bernhard, M., Buhrke, T., and Friedrich, B. (2000). The H_2 sensor of *Ralstonia eutropha* is a member of the subclass of regulatory [NiFe] hydrogenases. J. Bacteriol. 182, 2716–2724.

Kopito, R. (2000). Aggresomes, inclusion bodies and protein aggregation. Trends Cell Biol. 10, 524-530.

Korbas, M., Vogt, S., Meyer-Klaucke, W., Bill, E., Lyon, E. J., Thauer, R. K., et al. (2006). The iron-sulfurcluster-free hydrogenase (Hmd) is a metalloenzyme with a novel iron binding motif. J. Biol. Chem. 281, 30804–30813.

Kortluke, C., Horstmann, K., Schwartz, E., Rohde, M., Binsack, R., and Friedrich, B. (1992). A gene complex coding for the membrane-bound hydrogenase of *Alcaligenes eutrophus* H16. J. Bacteriol. 174, 6277–6289.

Kosman, D. J. (2013). Iron metabolism in aerobes: Managing ferric iron hydrolysis and ferrous iron autoxidation. Coord. Chem. Rev. 257, 210–217.

Kotik, M., Kočanová, M., Marešová, H., and Kyslík, P. (2004). High-level expression of a fungal pyranose oxidase in high cell-density fed-batch cultivations of *Escherichia coli* using lactose as inducer. Protein Expr. Purif. 36, 61–69.

Kraft, M., Knüpfer, U., Wenderoth, R., Kacholdt, A., Pietschmann, P., Hock, B., et al. (2007). A dual expression platform to optimize the soluble production of heterologous proteins in the periplasm of *Escherichia coli*. Appl. Microbiol. Biotechnol. 76, 1413–1422.

Krassen, H., Schwarze, A., Friedrich, B., Ataka, K., Lenz, O., and Heberle, J. (2009). Photosynthetic hydrogen production by a hybrid complex of photosystem I and [NiFe]-hydrogenase. ACS Nano 3, 4055–4061.

Krause, M., Ukkonen, K., Haataja, T., Ruottinen, M., Glumoff, T., Neubauer, A., et al. (2010). A novel fed-batch based cultivation method provides high cell-density and improves yield of soluble recombinant proteins in shaken cultures. Microb. Cell Fact. 9, 11.

Krishnan, A., Qian, X., Ananyev, G., Lun, D. S., and Dismukes, G. C. (2018). "Rewiring of cyanobacterial metabolism for hydrogen production: Synthetic biology approaches and challenges," in Advances in Experimental Medicine and Biology, 171–213.

Kubas, G. J. (2007). Fundamentals of H_2 binding and reactivity on transition metals underlying hydrogenase function and H_2 production and storage. Chem. Rev. 107, 4152–4205.

Kwon, S., Watanabe, S., Nishitani, Y., Kawashima, T., Kanai, T., Atomi, H., et al. (2018). Crystal structures of a [NiFe] hydrogenase large subunit HyhL in an immature state in complex with a Ni chaperone HypA. Proc. Natl. Acad. Sci. 115, 7045–7050.

Lamle, S. E., Albracht, S. P. J., and Armstrong, F. A. (2004). Electrochemical potential-step investigations of the aerobic interconversions of [NiFe]-hydrogenase from *allochromatium vinosum*: Insights into the puzzling difference between unready and ready oxidized inactive states. J. Am. Chem. Soc. 126, 14899–14909.

Larkin, P. (2017). Infrared and raman spectroscopy: Principles and spectral interpretation. Elsevier.

Lau, C. K. Y., Krewulak, K. D., and Vogel, H. J. (2016). Bacterial ferrous iron transport: The Feo system. FEMS Microbiol. Rev. 40, 273–298.

Lauermann, G., Häussinger, P., Lohmüller, R., and Watson, A. (2000). Hydrogen, 1. Properties and occurrence. Wiley-VCH, Weinheim.

Lauterbach, L., Idris, Z., Vincent, K. A., and Lenz, O. (2011a). Catalytic properties of the isolated diaphorase fragment of the NAD^+-reducing [NiFe]-hydrogenase from *Ralstonia eutropha*. PLoS One 6, e25939-25951.

Lauterbach, L., and Lenz, O. (2013). Catalytic production of hydrogen peroxide and water by oxygen-tolerant [NiFe]-hydrogenase during H_2 cycling in the presence of O_2. J. Am. Chem. Soc. 135, 17897–17905.

Lauterbach, L., Lenz, O., and Vincent, K. A. (2013). H_2-driven cofactor regeneration with $NAD(P)^+$-reducing hydrogenases. FEBS J. 280, 3058–3068.

Lauterbach, L., Liu, J., Horch, M., Hummel, P., Schwarze, A., Haumann, M., et al. (2011b). The hydrogenase subcomplex of the NAD^+-reducing [NiFe] hydrogenase from *Ralstonia eutropha* - Insights into catalysis and redox interconversions. Eur. J. Inorg. Chem. 2011, 1067–1079.

Lazazzera, B. A., Beinert, H., Khoroshilova, N., Kennedy, M. C., and Kiley, P. J. (1996). DNA binding and dimerization of the Fe−S-containing FNR protein from *Escherichia coli* are regulated by oxygen. J. Biol. Chem. 271, 2762–2768.

Leach, M. R., Zhang, J. W., and Zamble, D. B. (2007). The role of complex formation between the *Escherichia coli* hydrogenase accessory factors HypB and SlyD. J. Biol. Chem. 282, 16177–16186.

Lee, K.-C., Yeo, W.-S., and Roe, J.-H. (2008). Oxidant-responsive induction of the *suf* Operon, encoding a Fe-S assembly system, through Fur and IscR in *Escherichia coli*. J. Bacteriol. 190, 8244–8247.

Lenz, O. (2020). Hydrogen comes alive. Nat. Energy 5, 426–427.

Lenz, O., Bernhard, M., Buhrke, T., Schwartz, E., and Friedrich, B. (2002). The hydrogen-sensing apparatus in *Ralstonia eutropha*. J. Mol. Microbiol. Biotechnol. 4, 255–262.

Lenz, O., and Friedrich, B. (1998). A novel multicomponent regulatory system mediates H_2 sensing in *Alcaligenes eutrophus*. Proc. Natl. Acad. Sci. 95, 12474–12479.

Lenz, O., Lauterbach, L., and Frielingsdorf, S. (2018). "O_2-tolerant [NiFe]-hydrogenases of *Ralstonia eutropha* H16: Physiology, molecular biology, purification, and biochemical analysis," in Methods in Enzymology (Elsevier Inc.), 117–151.

Lenz, O., Ludwig, M., Schubert, T., Bürstel, I., Ganskow, S., Goris, T., et al. (2010). H_2 conversion in the presence of O_2 as performed by the membrane-bound [NiFe]-hydrogenase of *Ralstonia eutropha*. ChemPhysChem 11, 1107–1119.

Lenz, O., Strack, A., Tran-Betcke, A., and Friedrich, B. (1997). A hydrogen-sensing system in transcriptional regulation of hydrogenase gene expression in *Alcaligenes* species. J. Bacteriol. 179, 1655–1663.

Lenz, O., Zebger, I., Hamann, J., Hildebrandt, P., and Friedrich, B. (2007). Carbamoylphosphate serves as the source of CN^-, but not of the intrinsic CO in the active site of the regulatory [NiFe]-hydrogenase from *Ralstonia eutropha*. FEBS Lett. 581, 3322–3326.

Li, J., Jaitzig, J., Lu, P., Süssmuth, R. D., and Neubauer, P. (2015). Scale-up bioprocess development for production of the antibiotic valinomycin in *Escherichia coli* based on consistent fed-batch cultivations. Microb. Cell Fact. 14, 83.

Li, Z., Kessler, W., van den Heuvel, J., and Rinas, U. (2011). Simple defined autoinduction medium for high-level recombinant protein production using T7-based *Escherichia coli* expression systems. Appl. Microbiol. Biotechnol. 91, 1203–1213.

Liao, C.-H., Huang, C.-W., and Wu, J. C. S. (2012). Hydrogen production from semiconductor-based photocatalysis via water splitting. Catalysts 2, 490–516.

Liebgott, P. P., De Lacey, A. L., Burlat, B., Cournac, L., Richaud, P., Brugna, M., et al. (2011). Original design of an oxygen-tolerant [NiFe] hydrogenase: Major effect of a valine-to-cysteine mutation near the active site. J. Am. Chem. Soc. 133, 986–997.

Lill, S. O. N., and Siegbahn, P. E. M. (2009). An autocatalytic mechanism for NiFe-hydrogenase: Reduction to Ni(I) followed by oxidative addition. Biochemistry 48, 1056–1066.

Lin, H., Hoffmann, F., Rozkov, A., Enfors, SO., Rinas, U., Neubauer, P. (2004). Change of extracellular cAMP concentration is a sensitive reporter for bacterial fitness in high-cell-density cultures of *Escherichia coli*. Biotechnol. Bioeng. 87, 602–13.

Loiseau, L., Gerez, C., Bekker, M., Ollagnier-de Choudens, S., Py, B., Sanakis, Y., et al. (2007). ErpA, an iron sulfur (FeS) protein of the A-type essential for respiratory metabolism in *Escherichia coli*. Proc. Natl. Acad. Sci. 104, 13626–13631.

Lubitz, W., Ogata, H., Ru, O., and Reijerse, E. (2014). Hydrogenases. Chem. Rev. 114, 4081–4148.

Lubner, C. E., Grimme, R., Bryant, D. A., and Golbeck, J. H. (2010a). Wiring photosystem I for direct solar hydrogen production. Biochemistry 49, 404–414.

Lubner, C. E., Knörzer, P., Silva, P. J. N., Vincent, K. A., Happe, T., Bryant, D. A., et al. (2010b). Wiring an [FeFe]-hydrogenase with Photosystem I for light-induced hydrogen production. Biochemistry 49, 10264–10266.

Ludwig, M., Cracknell, J. A., Vincent, K. A., Armstrong, F. A., and Lenz, O. (2009a). Oxygen-tolerant H_2 oxidation by membrane-bound [NiFe] hydrogenases of *Ralstonia* species. J. Biol. Chem. 284, 465–477.

Ludwig, M., Schubert, T., Zebger, I., Wisitruangsakul, N., Saggu, M., Strack, A., et al. (2009b). Concerted action of two novel auxiliary proteins in assembly of the active site in a membrane-bound [NiFe] hydrogenase. J. Biol. Chem. 284, 2159–2168.

Lukey, M. J., Parkin, A., Roessler, M. M., Murphy, B. J., Harmer, J., Palmer, T., et al. (2010). How *Escherichia coli* is equipped to oxidize hydrogen under different redox conditions. J. Biol. Chem. 285, 3928–3938.

Lukey, M. J., Roessler, M. M., Parkin, A., Evans, R. M., Davies, R. A., Lenz, O., et al. (2011). Oxygen-tolerant [NiFe]-hydrogenases: The individual and collective importance of supernumerary cysteines at the proximal Fe-S cluster. J. Am. Chem. Soc. 133, 16881–16892.

Luli, G. W., and Strohl, W. R. (1990). Comparison of growth, acetate production, and acetate inhibition of *Escherichia coli* strains in batch and fed-batch fermentations. Appl. Environ. Microbiol. 56, 1004–1011.

Lupacchini, S., Appel, J., Stauder, R., Bolay, P., Klähn, S., Lettau, E., et al. (2021). Rewiring cyanobacterial photosynthesis by the implementation of an oxygen-tolerant hydrogenase. Metab. Eng. 68, 199–209.

Lutz, B. J., Fan, Z. H., Burgdorf, T., and Friedrich, B. (2005). Hydrogen sensing by enzyme-catalyzed electrochemical detection. Anal. Chem. 77, 4969–4975.

Lutz, S., Jacobi, A., Schlensog, V., Böhm, R., Sawers, G., and Böck, A. (1991). Molecular characterization of an operon (*hyp*) necessary for the activity of the three hydrogenase isoenzymes in *Escherichia coli*. Mol. Microbiol. 5, 123–135.

Lyon, E. J., Shima, S., Boecher, R., Thauer, R. K., Grevels, F.-W., Bill, E., et al. (2004a). Carbon monoxide as an intrinsic ligand to iron in the active site of the iron−sulfur-cluster-free hydrogenase H_2-forming methylenetetrahydromethanopterin dehydrogenase asrevealed by infrared spectroscopy. J. Am. Chem. Soc. 126, 14239–14248.

Lyon, E. J., Shima, S., Buurman, G., Chowdhuri, S., Batschauer, A., Steinbach, K., et al. (2004b). UV-A/blue-light inactivation of the 'metal-free' hydrogenase (Hmd) from methanogenic archaea. Eur. J. Biochem. 271, 195–204.

Macomber, L., and Hausinger, R. P. (2011). Mechanisms of nickel toxicity in microorganisms. Metallomics 3, 1153–1162.

Makui, H., Roig, E., Cole, S. T., Helmann, J. D., Gros, P., and Cellier, M. F. M. (2000). Identification of the *Escherichia coli* K-12 Nramp orthologue (MntH) as a selective divalent metal ion transporter. Mol. Microbiol. 35, 1065–1078.

Marbach, A., and Bettenbrock, K. (2012). *lac* operon induction in *Escherichia coli*: Systematic comparison of IPTG and TMG induction and influence of the transacetylase LacA. J. Biotechnol. 157, 82–88.

Massanz, C., Fernandezz, V. M., and Friedrich, B. (1997). C-terminal extension of the H_2-activating subunit, HoxH, directs maturation of the NAD-reducing hydrogenase in *Alcaligenes eutrophus*. Eur. J. Biochem. 245, 441–448.

Massanz, C., and Friedrich, B. (1999). Amino acid replacements at the H_2-activating site of the NAD-reducing hydrogenase from *Alcaligenes eutrophus*. Biochemistry 38, 14330–14337.

Massé, E., and Gottesman, S. (2002). A small RNA regulates the expression of genes involved in iron metabolism in *Escherichia coli*. Proc. Natl. Acad. Sci. U. S. A. 99, 4620–4625.

Massé, E., Vanderpool, C. K., and Gottesman, S. (2005). Effect of RyhB small RNA on global iron use in *Escherichia coli*. J. Bacteriol. 187, 6962–6971.

Masse, E., and Arguin, M. (2005). Ironing out the problem: New mechanisms of iron homeostasis. Trends Biochem. Sci. 30, 462–468.

Mayer, S., Junne, S., Ukkonen, K., Glazyrina, J., Glauche, F., Neubauer, P., et al. (2014). Lactose autoinduction with enzymatic glucose release: Characterization of the cultivation system in bioreactor. Protein Expr. Purif. 94, 67–72.

Mazoch, J., and Kučera, I. (2002). Control of gene expression by FNR-like proteins in facultatively anaerobic bacteria. Folia Microbiol. (Praha). 47, 95–103.

McDowall, J. S., Hjersing, M. C., Palmer, T., and Sargent, F. (2015). Dissection and engineering of the *Escherichia coli* formate hydrogenlyase complex. FEBS Lett. 589, 3141–3147.

McDowall, J. S., Murphy, B. J., Haumann, M., Palmer, T., Armstrong, F. A., and Sargent, F. (2014). Bacterial formate hydrogenlyase complex. Proc. Natl. Acad. Sci. U. S. A. 111, E3948–E3956.

Melis, A., Seibert, M., and Happe, T. (2004). Genomics of green algal hydrogen research. Photosynth. Res. 82, 277–288.

Menon, N. K., Chatelus, C. Y., Dervartanian, M., Wendt, J. C., Shanmugam, K. T., Peck, H. D., et al. (1994). Cloning, sequencing, and mutational analysis of the *hyb* operon encoding *Escherichia coli* hydrogenase 2. J. Bacteriol. 176, 4416–4423.

Menon, N. K., Robbins, J., Peck, H. D., Chatelus, C. Y., Choi, E. S., and Przybyla, A. E. (1990). Cloning and sequencing of a putative *Escherichia coli* [NiFe] hydrogenase-1 operon containing six open reading frames. J. Bacteriol. 172, 1969–1977.

Menon, N. K., Robbins, J., Wendt, J. C., Shanmugam, K. T., and Przybyla, A. E. (1991). Mutational analysis and characterization of the *Escherichia coli hya* operon, which encodes [NiFe] hydrogenase 1. J. Bacteriol. 173, 4851–4861.

Mersch, D., Lee, C. Y., Zhang, J. Z., Brinkert, K., Fontecilla-Camps, J. C., Rutherford, A. W., et al. (2015). Wiring of photosystem II to hydrogenase for photoelectrochemical water splitting. J. Am. Chem. Soc. 137, 8541–8549.

Mertens, R., and Liese, A. (2004). Biotechnological applications of hydrogenases. Curr. Opin. Biotechnol. 15, 343–348.

Messenger, S. L., and Green, J. (2003). FNR-mediated regulation of *hyp* expression in *Escherichia coli*. FEMS Microbiol. Lett. 228, 81–86.

Mettert, E. L., and Kiley, P. J. (2015). How is Fe-S cluster formation regulated? Annu. Rev. Microbiol. 69, 505–526.

Mettert, E. L., Outten, F. W., Wanta, B., and Kiley, P. J. (2008). The impact of O_2 on the Fe–S cluster biogenesis requirements of *Escherichia coli* FNR. J. Mol. Biol. 384, 798–811.

Meyer, J. (2007). [FeFe] hydrogenases and their evolution: A genomic perspective. Cell. Mol. Life

Sci. 64, 1063–1084.

Mogk, A., Kummer, E., and Bukau, B. (2015). Cooperation of Hsp70 and Hsp100 chaperone machines in protein disaggregation. Front. Mol. Biosci. 2, 22.

Montet, Y., Amara, P., Volbeda, A., Vernede, X., Hatchikian, E. C., Field, M. J., et al. (1997). Gas access to the active site of Ni-Fe hydrogenases probed by X-ray crystallography and molecular dynamics. Nat. Struct. Biol. 4, 523–6.

Morozov, S. V., Karyakina, E. E., Zadvornyi, O. A., Zorin, N. A., Varfolomeev, S. D., and Karyakin, A. A. (2002). Bioelectrocatalysis by hydrogenase *Th. Roseopersicina* immobilized on carbon materials. Russ. J. Electrochem. 2002 381 38, 97–102.

Mouesca, J., Fontecilla-Camps, J. C., and Amara, P. (2013). The structural plasticity of the proximal [4Fe3S] cluster is responsible for the O_2 tolerance of membrane-bound [NiFe] Hydrogenases. Angew. Chemie 125, 2056–2060.

Mulder, D. W., Shepard, E. M., Meuser, J. E., Joshi, N., King, P. W., Posewitz, M. C., et al. (2011). Insights into [FeFe]-Hydrogenase Structure, Mechanism, and Maturation. Structure 19, 1038–1052.

Nakamura, M., Saeki, K., and Takahashi, Y. (1999). Hyperproduction of recombinant ferredoxins in *Escherichia coli* by coexpression of the ORF1-ORF2-iscS-iscU-iscA-hscB-hscA-fdx-ORF3 gene cluster. J. Biochem. 126, 10–18.

Navarro, C., Wu, L., and France, C. (1993). The *nik* operon of *Escherichia coli* encodes a periplasmic binding-protein-dependent transport system for nickel. Mol. Microbiol. 9, 1181–1191.

Nesbit, A. D., Giel, J. L., Rose, J. C., and Kiley, P. J. (2009). Sequence-specific binding to a subset of IscR-regulated promoters does not require IscR Fe–S cluster ligation. J. Mol. Biol. 387, 28–41.

Neubauer, P., Anane, E., Junne, S., and Cruz Bournazou, M. N. (2020). "Potential of integrating model-based design of experiments approaches and process analytical technologies for bioprocess scale-down," in Digital Twins, eds. C. Herwig, Ralf Pörtner, and Johannes Möller (Springer, Berlin), 1–28.

Neubauer, P., and Cruz-Bournazou, M. (2017). Continuous bioprocess development: methods for control and characterization of the biological system. Contin. Biomanufacturing Innov. Technol. Methods, John Wiley & Sons: Hoboken, NJ, USA.

Neubauer, P., Cruz, N., Glauche, F., Junne, S., Knepper, A., and Raven, M. (2013). Consistent development of bioprocesses from microliter cultures to the industrial scale. Eng. Life Sci. 13, 224–238.

Neubauer, P., Fahnert, B., Lilie, H., and Villaverde, A. (2006). "Protein inclusion bodies in recombinant Bacteria," in inclusions in prokaryotes (Berlin/Heidelberg: Springer-Verlag), 237–292.

Neubauer, P., Hunan, M., Tiirnkvist, M., Larsson, G., Enfors, SO. (1995). Response of guanosine tetraphosphate to glucose fluctuations in fed-batch cultivations of *Escherichia coli*. J. Biotechnol. 43, 195–204.

Neubauer, P., and Winter, J. (2001). "Expression and fermentation strategies for recombinant protein production in *Escherichia Coli*," in Recombinant Protein Production with Prokaryotic and Eukaryotic Cells. A Comparative View on Host Physiology (Springer, Dordrecht), 195–258.

Nicolet, Y., Cavazza, C., and Fontecilla-Camps, J. C. (2002). Fe-only hydrogenases: Structure, function and evolution. in Journal of Inorganic Biochemistry (Elsevier), 1–8.

Nicolet, Y., Piras, C., Legrand, P., Hatchikian, C. E., and Fontecilla-Camps, J. C. (1999). *Desulfovibrio desulfuricans* iron hydrogenase: The structure shows unusual coordination to an active site Fe binuclear center. Structure 7, 13–23.

Niu, S., Thomson, L. M., and Hall, M. B. (1999). Theoretical characterization of the reaction

intermediates in a model of the nickel-iron hydrogenase of *Desulfovibrio gigas*. J. Am. Chem. Soc. 121, 4000–4007.

Ogata, H., Hirota, S., Nakahara, A., Komori, H., Shibata, N., Kato, T., et al. (2005). Activation process of [NiFe] hydrogenase elucidated by high-resolution X-ray analyses: Conversion of the ready to the unready state. Structure 13, 1635–1642.

Ogata, H., Kellers, P., and Lubitz, W. (2010). The crystal structure of the [NiFe] hydrogenase from the photosynthetic bacterium *Allochromatium vinosum*: Characterization of the oxidized enzyme (Ni-A state). J. Mol. Biol. 402, 428–444.

Ogata, H., Lubitz, W., and Higuchi, Y. (2009). [NiFe] hydrogenases: structural and spectroscopic studies of the reaction mechanism. Dalt. Trans. 0, 7577.

Ogata, H., Lubitz, W., and Higuchi, Y. (2016). Structure and function of [NiFe] hydrogenases. J. Biochem. 160, 251–258.

Ohki, Y., Yasumura, K., Kuge, K., Tanino, S., Ando, M., Li, Z., et al. (2008). Thiolate-bridged dinuclear iron(tris-carbonyl)–nickel complexes relevant to the active site of [NiFe] hydrogenase. Proc. Natl. Acad. Sci. 105, 7652–7657.

Olson, J. W., Mehta, N. S., and Maier, R. J. (2001). Requirement of nickel metabolism proteins HypA and HypB for full activity of both hydrogenase and urease in *Helicobacter pylori*. Mol. Microbiol. 39, 176–182.

Ongey, E. L., Santolin, L., Waldburger, S., Adrian, L., Riedel, S. L., and Neubauer, P. (2019). Bioprocess development for lantibiotic ruminococcin-A production in *Escherichia coli* and kinetic insights into LanM enzymes catalysis. Front. Microbiol. 10, 2133.

Outten, F. W., Djaman, O., and Storz, G. (2004). A suf operon requirement for Fe-S cluster assembly during iron starvation in *Escherichia coli*. Mol. Microbiol. 52, 861–872.

Pandelia, M. E., Ogata, H., and Lubitz, W. (2010). Intermediates in the catalytic cycle of [NiFe] hydrogenase: Functional spectroscopy of the active site. ChemPhysChem 11, 1127–1140.

Paschos, A., Bauer, A., Zimmermann, A., Zehelein, E., and Böck, A. (2002). HypF, a carbamoyl phosphate-converting enzyme involved in [NiFe] hydrogenase maturation. J. Biol. Chem. 277, 49945–49951.

Paschos, A., Glass, R. S., and Böck, A. (2001). Carbamoylphosphate requirement for synthesis of the active center of [NiFe]-hydrogenases. FEBS Lett. 488, 9–12.

Patzer, S. I., and Hantke, K. (1999). SufS is a NifS-like protein, and SufD is necessary for stability of the [2Fe-2S] FhuF protein in *Escherichia coli*. J. Bacteriol. 181, 3307–3309.

Pei, X. L., Wang, Q. Y., Li, C. L., Qiu, X. F., Xie, K. L., Huang, L. F., et al. (2011). Efficient production of a thermophilic 2-deoxyribose-5-phosphate aldolase in glucose-limited fed-batch cultivations of *Escherichia coli* by continuous lactose induction strategy. Appl. Biochem. Biotechnol. 165, 416–425.

Peters, J. M., Vangeloff, A. D., and Landick, R. (2011). Bacterial transcription terminators: The RNA 3′-end chronicles. J. Mol. Biol. 412, 793–813.

Peters, J. W. (1999). Structure and mechanism of iron-only hydrogenases. Curr. Opin. Struct. Biol. 9, 670–676.

Peters, J. W., Lanzilotta, W. N., Lemon, B. J., and Seefeldt, L. C. (1998). X-ray crystal structure of the Fe-only hydrogenase (CpI) from *Clostridium pasteurianum* to 1.8 angstrom resolution. Science 282, 1853–8.

Peters, J. W., Schut, G. J., Boyd, E. S., Mulder, D. W., Shepard, E. M., Broderick, J. B., et al. (2015). [FeFe]- and [NiFe]-hydrogenase diversity, mechanism, and maturation. Biochim. Biophys. Acta - Mol. Cell Res. 1853, 1350–1369.

Petkun, S., Shi, R., Li, Y., Asinas, A., Munger, C., Zhang, L., et al. (2011). Structure of hydrogenase maturation protein HypF with reaction intermediates shows two active sites. Structure 19, 1773–1783.

Picollo, M., Aceto, M., and Vitorino, T. (2019). UV-Vis spectroscopy. Phys. Sci. Rev. 4.

Pierik, A. J., Roseboom, W., Happe, R. P., Bagley, K. A., and Albracht, S. P. J. (1999). Carbon monoxide and cyanide as intrinsic ligands to iron in the active site of [NiFe]-hydrogenases. $NiFe(CN)_2CO$, biology's way to activate H_2. J. Biol. Chem. 274, 3331–3337.

Pierik, A. J., Schmelz, M., Lenz, O., Friedrich, B., and Albracht, S. P. J. (1998). Characterization of the active site of a hydrogen sensor from *Alcaligenes eutrophus*. FEBS Lett. 438, 231–235.

Pinske, C., Bönn, M., Krüger, S., Lindenstrauß, U., and Sawers, R. G. (2011). Metabolic deficiences revealed in the biotechnologically important model bacterium *Escherichia coli* BL21(DE3). PLoS One 6, e22830.

Pinske, C., Jaroschinsky, M., Linek, S., Kelly, C. L., Sargent, F., and Sawers, R. G. (2015a). Physiology and bioenergetics of [NiFe]-hydrogenase 2-catalyzed H_2-consuming and H_2 -producing reactions in *Escherichia coli*. J. Bacteriol. 197, 296–306.

Pinske, C., Jaroschinsky, M., and Sawers, R. G. (2013). Levels of control exerted by the Isc iron–sulfur cluster system on biosynthesis of the formate hydrogenlyase complex. Microbiology 159, 1179–1189.

Pinske, C., Sargent, F., and Sawers, R. G. (2015b). SlyD-dependent nickel delivery limits maturation of [NiFe]-hydrogenases in late-stationary phase *Escherichia coli* cells. Metallomics 7, 683–690.

Pinske, C., and Sawers, R. G. (2012). Delivery of iron-sulfur clusters to the hydrogen-oxidizing [NiFe]-hydrogenases in *Escherichia coli* requires the A-Type carrier proteins ErpA and IscA. PLoS One 7, e31755.

Pinske, C., and Sawers, R. G. (2016). Anaerobic formate and hydrogen metabolism. EcoSal Plus 7.

Podzuweit, H. G., Schneider, K., and Knüttel, H. (1987). Comparison of the membrane-bound hdyrogenases from *Alcaligenes eutrophus* H16 and *Alcaligenes eutrophus* type strain. Biochim. Biophys. Acta-Biomembr. 905, 435–446.

Popescu, C. V., Bates, D. M., Beinert, H., Munck, E., and Kiley, P. J. (1998). Mossbauer spectroscopy as a tool for the study of activation/inactivation of the transcription regulator FNR in whole cells of *Escherichia coli*. Proc. Natl. Acad. Sci. 95, 13431–13435.

Preis, H., Eckart, R. A., Gudipati, R. K., Heidrich, N., and Brantl, S. (2009). CodY activates transcription of a small RNA in *Bacillus subtilis*. J. Bacteriol. 191, 5446–57.

Preissler, J., Reeve, H. A., Zhu, T., Nicholson, J., Urata, K., Lauterbach, L., et al. (2020). Dihydrogen-driven NADPH recycling in imine reduction and P_{450}-catalyzed oxidations mediated by an engineered O_2-tolerant hydrogenase. ChemCatChem 12, 4853–4861.

Py, B., and Barras, F. (2010). Building Fe-S proteins: Bacterial strategies. Nat. Rev. Microbiol. 8, 436–446.

Py, B., Moreau, P. L., and Barras, F. (2011). Fe–S clusters, fragile sentinels of the cell. Curr. Opin. Microbiol. 14, 218–223.

Quail, M. A., Haydon, D. J., and Guest, J. R. (1994). The *pdhR-aceEF-lpd* operon of *Escherichia coli* expresses the pyruvate dehydrogenase complex. Mol. Microbiol. 12, 95–104.

Rajagopalan, S., Teter, S. J., Zwart, P. H., Brennan, R. G., Phillips, K. J., and Kiley, P. J. (2013). Studies of IscR reveal a unique mechanism for metal-dependent regulation of DNA binding specificity. Nat. Struct. Mol. Biol. 2013 206 20, 740–747.

Ratzka, J., Lauterbach, L., Lenz, O., and Ansorge-Schumacher, M. B. (2012). Stabilisation of the NAD^+-reducing soluble [NiFe]-hydrogenase from *Ralstonia eutropha* H16 through modification with methoxy-poly(ethylene) glycol. J. Mol. Catal. B Enzym. 74, 219–223.

Reeve, H. A., Ash, P. A., Park, H., Huang, A., Posidias, M., Tomlinson, C., et al. (2017). Enzymes as modular catalysts for redox half-reactions in H_2-powered chemical synthesis: From biology to technology. Biochem. J. 474, 215–230.

Reeve, H. A., Lauterbach, L., Lenz, O., and Vincent, K. A. (2015). Enzyme-modified particles for

selective biocatalytic hydrogenation by hydrogen-driven NADH recycling. ChemCatChem 7, 3480–3487.

Reissmann, S., Hochleitner, E., Wang, H., Paschos, A., Lottspeich, F., Glass, R. S., et al. (2003). Taming of a poison: Biosynthesis of the NiFe-hydrogenase cyanide ligands. Science (80-.). 299, 1067–1070.

Rey, L., Fernández, D., Brito, B., Hernando, Y., Palacios, J. M., Imperial, J., et al. (1996). The hydrogenase gene cluster of *Rhizobium leguminosarum* bv. *viciae* contains an additional gene (*hypX*), which encodes a protein with sequence similarity to the N^{10}-formyltetrahydrofolate-dependent enzyme family and is required for nickel-dependent hydrogen. Mol. Gen. Genet. 252, 237–248.

Richard, D. J., Sawers, G., Sargent, F., McWalter, L., and Boxer, D. H. (1999). Transcriptional regulation in response to oxygen and nitrate of the operons encoding the [NiFe] hydrogenases 1 and 2 of *Escherichia coli*. Microbiology 145, 2903–2912.

Riesenberg, D., and Guthke, R. (1999). High-cell-density cultivation of microorganisms. Appl. Microbiol. Biotechnol. 51, 422–430.

Roche, B., Aussel, L., Ezraty, B., Mandin, P., Py, B., and Barras, F. (2013). Reprint of: Iron/sulfur proteins biogenesis in prokaryotes: Formation, regulation and diversity. Biochim. Biophys. Acta-Bioenerg. 1827, 923–937.

Rodrigue, A., Effantin, G., and Mandrand-Berthelot, M. A. (2005). Identification of *rcnA* (*yohM*), a nickel and cobalt resistance gene in *Escherichia coli*. J. Bacteriol. 187, 2912–2916.

Roessler, M. M., Evans, R. M., Davies, R. A., Harmer, J., and Armstrong, F. A. (2012). EPR spectroscopic studies of the Fe-S clusters in the O_2-tolerant [NiFe]-hydrogenase Hyd-1 from *Escherichia coli* and characterization of the unique [4Fe-3S] cluster by HYSCORE. J. Am. Chem. Soc. 134, 15581–15594.

Roncaroli, F., Bill, E., Friedrich, B., Lenz, O., Lubitz, W., and Pandelia, M.-E. (2015). Cofactor composition and function of a H_2-sensing regulatory hydrogenase as revealed by Mössbauer and EPR spectroscopy. Chem. Sci. 6, 4495–4507.

Roseboom, W., Blokesch, M., Böck, A., and Albracht, S. P. J. (2005). The biosynthetic routes for carbon monoxide and cyanide in the Ni-Fe active site of hydrogenases are different. FEBS Lett. 579, 469–472.

Rossmann, R., Maier, T., Lottspeich, F., and Böck, A. (1995). Characterisation of a protease from *Escherichia coli* involved in hydrogenase maturation. Eur. J. Biochem. 227, 545–550.

Rowe, J. L., Starnes, G. L., and Chivers, P. T. (2005). Complex transcriptional control links NikABCDE-dependent nickel transport with hydrogenase expression in *Escherichia coli*. J. Bacteriol. 187, 6317–6323.

Ruff, A., Szczesny, J., Marković, N., Conzuelo, F., Zacarias, S., Pereira, I. A. C., et al. (2018). A fully protected hydrogenase/polymer-based bioanode for high-performance hydrogen/glucose biofuel cells. Nat. Commun. 9, 1–10.

Saggu, M., Teutloff, C., Ludwig, M., Brecht, M., Pandelia, M.-E., Lenz, O., et al. (2010). Comparison of the membrane-bound [NiFe] hydrogenases from *R. eutropha* H16 and *D. vulgaris* Miyazaki F in the oxidized ready state by pulsed EPR. Phys. Chem. Chem. Phys. 12, 2139.

Saggu, M., Zebger, I., Ludwig, M., Lenz, O., Friedrich, B., Hildebrandt, P., et al. (2009). Spectroscopic insights into the oxygen-tolerant membrane-associated [NiFe] hydrogenase of *Ralstonia eutropha* H16. J. Biol. Chem. 284, 16264–16276.

Saini, A., Mapolelo, D. T., Chahal, H. K., Johnson, M. K., and Outten, F. W. (2010). SufD and SufC ATPase activity are required for iron acquisition during in vivo Fe-S cluster formation on SufB. Biochemistry 49, 9402–9412.

Sargent, F. (2016). "The model [NiFe]-hydrogenases of *Escherichia coli*," in Advances in microbial physiology (Academic Press), 433–507.

Sawers, G., and Suppmann, B. (1992). Anaerobic induction of pyruvate formate-lyase gene

expression is mediated by the ArcA and FNR proteins. J. Bacteriol. 174, 3474–3478.

Sawers, R. G. (2005). Formate and its role in hydrogen production in *Escherichia coli*. Biochem Soc Trans 33, 42–46.

Sawers, R. G., Ballantine, S. P., and Boxer, D. H. (1985). Differential expression of hydrogenase isoenzymes in *Escherichia coli* K-12: Evidence for a third isoenzyme. J. Bacteriol. 164, 1324–1331.

Schäfer, C., Bommer, M., Hennig, S. E., Jeoung, J. H., Dobbek, H., and Lenz, O. (2016). Structure of an actinobacterial-type [NiFe]-hydrogenase reveals insight into O_2-tolerant H_2 Oxidation. Structure 24, 285–292.

Schäfer, C., Friedrich, B., and Lenza, O. (2013). Novel, oxygen-insensitive group 5 [NiFe]-hydrogenase in *Ralstonia eutropha*. Appl. Environ. Microbiol. 79, 5137–5145.

Schick, M., Xie, X., Ataka, K., Kahnt, J., Linne, U., and Shima, S. (2012). Biosynthesis of the iron-guanylylpyridinol cofactor of [Fe]-hydrogenase in methanogenic archaea as elucidated by stable-isotope labeling. J. Am. Chem. Soc. 134, 3271–3280.

Schiffels, J., Pinkenburg, O., Schelden, M., Aboulnaga, E. H. A. A., Baumann, M. E. M., and Selmer, T. (2013). An innovative cloning platform enables large-scale production and maturation of an oxygen-tolerant [NiFe]-hydrogenase from *Cupriavidus necator* in *Escherichia coli*. PLoS One 8, e68812.

Schink, B., and Schlegel, H. G. (1979). The membrane-bound hydrogenase of *Alcaligenes eutrophus*. I. Solubilization, purification, and biochemical properties. BBA - Enzymol. 567, 315–324.

Schmid, I., and Aschoff, J. (2017). A scalable software framework for data integration in bioprocess development. Eng. Life Sci. 17, 1159–1165.

Schneider, K., and Schlegel, H. G. (1976). Purification and properties of soluble hydrogenase from *Alcaligenes eutropha* H16. FEMS Microbiol. Lett. 452, 66–80.

Schollmeyer, J. (2020). Bioprocess devopment for the production of a S-methyl-5'-thio-adenosine phosphorylase in *Escherichia coli*. Master thesis (unpublished), Technische Universität Berlin.

Schwartz, C. J., Djaman, O., Imlay, J. A., and Kiley, P. J. (2000). The cysteine desulfurase, IscS, has a major role in in vivo Fe-S cluster formation in *Escherichia coli*. Proc. Natl. Acad. Sci. 97, 9009–9014.

Schwartz, E., Henne, A., Cramm, R., Eitinger, T., Friedrich, B., and Gottschalk, G. (2003). Complete nucleotide sequence of pHG1: A *Ralstonia eutropha* H16 megaplasmid encoding key enzymes of H_2-based lithoautotrophy and anaerobiosis. J. Mol. Biol. 332, 369–383.

Schwartz, E., Fritsch, J., and Friedrich, B. (2013). "H_2-metabolizing prokaryotes," in The Prokaryotes, ed. F. T. E. Rosenberg, E. F. DeLong, S. Lory, E. Stackebrandt (Heidelberg, Berlin: Springer), 119–199.

Schwarze, A., Kopczak, M. J., Rogner, M., and Lenz, O. (2010). Requirements for construction of a functional hybrid complex of photosystem I and [NiFe]-hydrogenase. Appl. Environ. Microbiol. 76, 2641–2651.

Shiloach, J., and Fass, R. (2005). Growing *E. coli* to high cell density—A historical perspective on method development. Biotechnol. Adv. 23, 345–357.

Shima, S., Lyon, E. J., Sordel-Klippert, M., Kauß, M., Kahnt, J., Thauer, R. K., et al. (2004). The cofactor of the iron–sulfur cluster free hydrogenase Hmd: structure of the light-inactivation product. Angew. Chemie Int. Ed. 43, 2547–2551.

Shima, S., Pilak, O., Vogt, S., Schick, M., Stagni, M. S., Meyer-Klaucke, W., et al. (2008). The crystal structure of [Fe]-hydrogenase reveals the geometry of the active site. Science 321, 572–575.

Shima, S., and Thauer, R. K. (2007). A third type of hydrogenase catalyzing H_2 activation. Chem. Rec. 7, 37–46.

Shimizu, N., Fukuzono, S., Fujimori, K., Nishimura, N., and Odawara, Y. (1988). Fed-batch cultures of recombinant *Escherichia coli* with inhibitory substance concentration monitoring. J. Ferment. Technol. 66, 187–191.

Shomura, Y., Yoon, K. S., Nishihara, H., and Higuchi, Y. (2011). Structural basis for a [4Fe-3S] cluster in the oxygen-tolerant membrane-bound [NiFe]-hydrogenase. Nature 479, 253–256.

Shomura, Y. (2019). "Structural insights into the protective mechanisms against O_2 in the [NiFe]-hydrogenases," in Advances in Bioorganometallic Chemistry (Elsevier), 365–377.

Siegbahn, P. E. M., Tye, J. W., and Hall, M. B. (2007). Computational studies of [NiFe] and [FeFe] hydrogenases. Chem. Rev. 107, 4414–4435.

Silakov, A., Wenk, B., Reijerse, E., and Lubitz, W. (2009). ^{14}N HYSCORE investigation of the H-cluster of [FeFe] hydrogenase: Evidence for a nitrogen in the dithiol bridge. Phys. Chem. Chem. Phys. 11, 6592–6599.

Smith, R. L., and Maguire, M. E. (1998). Microbial magnesium transport: Unusual transporters searching for identity. Mol. Microbiol. 28, 217–226.

Soboh, B., Adrian, L., and Stripp, S. T. (2022). An in vitro reconstitution system to monitor iron transfer to the active site during the maturation of [NiFe]-hydrogenase. J. Biol. Chem. 298, 102291.

Soboh, B., Stripp, S. T., Bielak, C., Lindenstrauß, U., Braussemann, M., Javaid, M., et al. (2013). The [NiFe]-hydrogenase accessory chaperones HypC and HybG of *Escherichia coli* are iron- and carbon dioxide-binding proteins. FEBS Lett. 587, 2512–2516.

Soboh, B., Stripp, S. T., Muhr, E., Granich, C., Braussemann, M., Herzberg, M., et al. (2012). [NiFe]-hydrogenase maturation: Isolation of a HypC-HypD complex carrying diatomic CO and CN^- ligands. FEBS Lett. 586, 3882–3887.

Sommer, C., Volk, N., and Pietzsch, M. (2011). Model based optimization of the fed-batch production of a highly active transglutaminase variant in *Escherichia coli*. Protein Expr. Purif. 77, 9–19.

Spiro, S., and Guest, J. R. (1990). FNR and its role in oxygen-regulated gene expression in *Escherichia coli*. FEMS Microbiol. Lett. 75, 399–428.

Stephenson, M., and Stickland, L. H. (1931). Hydrogenase: A bacterial enzyme activating molecular hydrogen: The properties of the enzyme. Biochem. J. 25, 205–214.

Stripp, S. T., Oltmanns, J., Müller, C. S., Ehrenberg, D., Schlesinger, R., Heberle, J., et al. (2021). Electron inventory of the iron-sulfur scaffold complex HypCD essential in [NiFe]-hydrogenase cofactor assembly. Biochem. J. 478, 3281–3295.

Stripp, S. T., Soboh, B., Lindenstrauss, U., Braussemann, M., Herzberg, M., Nies, D. H., et al. (2013). HypD is the scaffold protein for Fe-$(CN)_2$CO cofactor assembly in [NiFe]-hydrogenase maturation. Biochemistry 52, 3289–3296.

Studier, F. W., Daegelen, P., Lenski, R. E., Maslov, S., and Kim, J. F. (2009). Understanding the differences between genome sequences of *Escherichia coli* B strains REL606 and BL21(DE3) and comparison of the *E. coli* B and K-12 genomes. J. Mol. Biol. 394, 653–680.

Sumner, I., and Voth, G. A. (2012). Proton transport pathways in [NiFe]-hydrogenase. J. Phys. Chem. B 116, 2917–2926.

Sun, J., Hopkins, R. C., Jenney, F. E., McTernan, P. M., and Adams, M. W. W. (2010). Heterologous expression and maturation of an NADP-dependent [NiFe]-hydrogenase: A key enzyme in biofuel production. PLoS One 5, e10526.

Sutton, V. R., Stubna, A., Patschkowski, T., Münck, E., Beinert, H., and Kiley, P. J. (2004). Superoxide destroys the $[2Fe\text{-}2S]^{2+}$ cluster of FNR from *Escherichia coli*. Biochemistry 43, 791–798.

Szczesny, J., Birrell, J. A., Conzuelo, F., Lubitz, W., Ruff, A., and Schuhmann, W. (2020). Redox-polymer-based high-current-density gas-diffusion H_2-oxidation bioanode using [FeFe] hydrogenase from *Desulfovibrio desulfuricans* in a membrane-free biofuel cell. Angew. Chemie 59, 16506–16510.

Tai, H., Nishikawa, K., Higuchi, Y., Mao, Z., and Hirota, S. (2019). Cysteine SH and glutamate COOH contributions to [NiFe] hydrogenase proton transfer revealed by highly sensitive FTIR spectroscopy. Angew. Chemie 131, 13419–13424.

Takács, M., Tóth, A., Bogos, B., Varga, A., Rákhely, G., and Kovács, K. L. (2008). Formate hydrogenlyase in the hyperthermophilic archaeon, *Thermococcus litoralis*. BMC Microbiol. 8, 1–12.

Teich, A., Meyer, S., Lin, HY., Andersson, L., Enfors, SO., Neubauer, P (1999). Growth rate related concentration changes of the starvation response regulators σS and ppGpp in glucose-limited fed-batch and continuous cultures of *Escherichia coli*. Biotechnol. Prog. 15, 123–9.

Teodor, A. H., Sherman, B. D., Ison, Z. Y., Ooi, E. J., Bergkamp, J. J., and Bruce, B. D. (2020). Green catalysts: Applied and synthetic photosynthesis. Catalysts 10, 1016.

Thauer, R. K., Kaster, A.-K., Goenrich, M., Schick, M., Hiromoto, T., and Shima, S. (2010). Hydrogenases from methanogenic archaea, nickel, a novel cofactor, and H_2 storage. Annu. Rev. Biochem. 79, 507–536.

Theodoratou, E., Huber, R., and Böck, A. (2005). [NiFe]-Hydrogenase maturation endopeptidase: structure and function. Biochem. Soc. Trans. 33, 108–111.

Thiemermann, S., Dernedde, J., Bernhard, M., Schroeder, W., Massanz, C., and Friedrich, B. (1996). Carboxyl-terminal processing of the cytoplasmic NAD-reducing hydrogenase of *Alcaligenes eutrophus* requires the *hoxW* gene product. J. Bacteriol. 178, 2368–2374.

Tishkov, V. I., and Popov, V. O. (2006). Protein engineering of formate dehydrogenase. Biomol. Eng. 23, 89–110.

Tolla, D. A., and Savageau, M. A. (2010). Regulation of aerobic-to-anaerobic transitions by the FNR cycle in *Escherichia coli*. J. Mol. Biol. 397, 893–905.

Tran-Betcke, A., Warnecke, U., Bocker, C., Zaborosch, C., and Friedrich, B. (1990). Cloning and nucleotide sequences of the genes for the subunits of NAD-reducing hydrogenase of *Alcaligenes eutrophus* H16. J. Bacteriol. 172, 2920–2929.

Tran, Q. H., Arras, T., Becker, S., Holighaus, G., Ohlberger, G., and Unden, G. (2000). Role of glutathione in the formation of the active form of the oxygen sensor FNR ([4Fe-4S]·FNR) and in the control of FNR function. Eur. J. Biochem. 267, 4817–4824.

Ukkonen, K., Mayer, S., Vasala, A., and Neubauer, P. (2013). Use of slow glucose feeding as supporting carbon source in lactose autoinduction medium improves the robustness of protein expression at different aeration conditions. Protein Expr. Purif. 91, 147–154.

Unden, G., Achebach, S., Holighaus, G., Tran, H. Q., Wackwitz, B., and Zeuner, Y. (2002). Control of FNR function of Escherichia coli by O2 and reducing conditions. in Journal of Molecular Microbiology and Biotechnology, 263–268.

Unden, G., and Schirawski, J. (1997). The oxygen-responsive transcriptional regulator FNR of *Escherichia coli*: The search for signals and reactions. Mol. Microbiol. 25, 205–210.

Uppada, V., Bhaduri, S., and Noronha, S. B. (2014). Cofactor regeneration - an important aspect of biocatalysis. Curr. Sci. 106, 946–957.

Utschig, L. M., Soltau, S. R., and Tiede, D. M. (2015). Light-driven hydrogen production from photosystem I-catalyst hybrids. Curr. Opin. Chem. Biol. 25, 1–8.

van der Giezen, M., Tovar, J., and Clark, C. G. (2005). "Mitochondrion-derived organelles in protists and fungi," in International Review of Cytology, 175–225.

Van Der Linden, E., Faber, B. W., Bleijlevens, B., Burgdorf, T., Bernhard, M., Friedrich, B., et al. (2004). Selective release and function of one of the two FMN groups in the cytoplasmic NAD^+-reducing [NiFe]-hydrogenase from *Ralstonia eutropha*. Eur. J. Biochem. 271, 801–808.

Van Gastel, M., Stein, M., Brecht, M., Schröder, O., Lendzian, F., Bittl, R., et al. (2006). A single-crystal ENDOR and density functional theory study of the oxidized states of the [NiFe] hydrogenase from *Desulfovibrio vulgaris* Miyazaki F. J. Biol. Inorg. Chem. 11, 41–51.

Velayudhan, J., Hughes, N. J., Mccolm, A. A., Bagshaw, J., Clayton, C. L., Andrews, S. C., et al. (2000). Iron acquisition and virulence in *Helicobacter pylori* : A major role for FeoB , a high-affinity ferrous iron transporter. Mol. Microbiol. 37, 274–286.

Velez-Suberbie, M. L., Betts, J. P. J., Walker, K. L., Robinson, C., Zoro, B., and Keshavarz-Moore, E. (2018). High throughput automated microbial bioreactor system used for clone selection and rapid scale-down process optimization. Biotechnol. Prog. 34, 58–68.

Vignais, P. (2001). Classification and phylogeny of hydrogenases. FEMS Microbiol. Rev. 25, 455–501.

Vignais, P. M., and Billoud, B. (2007). Occurrence, Classification, and biological function of hydrogenases: An overview. Chem. Rev. 107, 4206–4272.

Vignais, P. M., and Colbeau, A. (2004). Molecular biology of microbial hydrogenases. Curr. Issues Mol. Biol. 6, 159–188.

Vijayaraghavan, K., and Mohd Soom, M. A. (2006). Trends in bio-hydrogen generation – A review. Environ. Sci. 3, 255–271.

Vincent, K. A., Cracknell, J. A., Clark, J. R., Ludwig, M., Lenz, O., Friedrich, B., et al. (2006). Electricity from low-level H_2 in still air–an ultimate test for an oxygen tolerant hydrogenase. Chem. Commun. 187, 5033–5035.

Vincent, K. A., Cracknell, J. A., Lenz, O., Zebger, I., Friedrich, B., and Armstrong, F. A. (2005). Electrocatalytic hydrogen oxidation by an enzyme at high carbon monoxide or oxygen levels. Proc. Natl. Acad. Sci. U. S. A. 102, 16951–16954.

Vincent, K. A., Parkin, A., and Armstrong, F. A. (2007). Investigating and exploiting the electrocatalytic properties of hydrogenases. Chem. Rev. 107, 4366–4413.

Vinella, D., Brochier-Armanet, C., Loiseau, L., Talla, E., and Barras, F. (2009). Iron-sulfur (Fe/S) protein biogenesis: Phylogenomic and genetic studies of A-type carriers. PLoS Genet. 5, e1000497.

Vinella, D., Loiseau, L., de Choudens, S. O., Fontecave, M., and Barras, F. (2013). In vivo [Fe-S] cluster acquisition by IscR and NsrR, two stress regulators in *Escherichia coli*. Mol. Microbiol. 87, 493–508.

Volbeda, A., Amara, P., Darnault, C., Mouesca, J.-M., Parkin, A., Roessler, M. M., et al. (2012). X-ray crystallographic and computational studies of the O_2-tolerant [NiFe]-hydrogenase 1 from *Escherichia coli*. Proc. Natl. Acad. Sci. 109, 5305–5310.

Volbeda, A., Charon, M.-H., Piras, C., Hatchikian, E. C., Frey, M., and Fontecilla-Camps, J. C. (1995). Crystal structure of the nickel–iron hydrogenase from *Desulfovibrio gigas*. Nature 373, 580–587.

Volbeda, A., Darnault, C., Parkin, A., Sargent, F., Armstrong, F. A., and Fontecilla-Camps, J. C. (2013). Crystal structure of the O_2-Tolerant membrane-bound hydrogenase 1 from *Escherichia coli* in complex with its cognate cytochrome b. Structure 21, 184–190.

Volbeda, A., Garcin, E., Piras, C., De Lacey, A. L., Fernandez, V. M., Hatchikian, E. C., et al. (1996). Structure of the [NiFe] hydrogenase active site: Evidence for biologically uncommon Fe ligands. J. Am. Chem. Soc. 118, 12989–12996.

Volbeda, A., Martin, L., Barbier, E., Gutiérrez-Sanz, O., De Lacey, A. L., Liebgott, P. P., et al. (2015). Crystallographic studies of [NiFe]-hydrogenase mutants: Towards consensus structures for the elusive unready oxidized states. J. Biol. Inorg. Chem. 20, 11–22.

Volbeda, A., Martin, L., Cavazza, C., Matho, M., Faber, B. W., Roseboom, W., et al. (2005). Structural differences between the ready and unready oxidized states of [NiFe] hydrogenases. J. Biol. Inorg. Chem. 10, 239–249.

Volbeda, A., Mouesca, J. M., Darnault, C., Roessler, M. M., Parkin, A., Armstrong, F. A., et al. (2018). X-ray structural, functional and computational studies of the O_2 -sensitive *E. coli* hydrogenase-1 C19G variant reveal an unusual [4Fe–4S] cluster. Chem. Commun. 54, 7175–7178.

Wait, A. F., Parkin, A., Morley, G. M., Dos Santos, L., and Armstrong, F. A. (2010).

Characteristics of enzyme-based hydrogen fuel cells using an oxygen-tolerant hydrogenase as the anodic catalyst. J. Phys. Chem. C 114, 12003–12009.

Wang, P. H., Best, R. B., and Blumberger, J. (2011). Multiscale simulation reveals multiple pathways for H_2 and O_2 transport in a [NiFe]-hydrogenase. J. Am. Chem. Soc. 133, 3548–3556.

Wang, S., Huang, H., Kahnt, J., and Thauer, R. K. (2013). A reversible electron-bifurcating ferredoxin- and NAD-Dependent [FeFe]-Hydrogenase (HydABC) in *Moorella thermoacetica*. J. Bacteriol. 195, 1267–1275.

Watanabe, K., and Oikawa, H. (2007). Robust platform for de novo production of heterologous polyketides and nonribosomal peptides in *Escherichia coli*. Org. Biomol. Chem. 5, 593–602.

Waugh, R., and Boxer, D. H. (1986). Pleiotropic hydrogenase mutants of *Escherichia coli* K12: growth in the presence of nickel can restore hydrogenase activity. Biochimie 68, 157–166.

Wayne Outten, F. (2015). Recent advances in the Suf Fe-S cluster biogenesis pathway: Beyond the Proteobacteria. Biochim. Biophys. Acta - Mol. Cell Res. 1853, 1464–1469.

Weckbecker, A., Gröger, H., and Hummel, W. (2010). Regeneration of nicotinamide coenzymes: principles and applications for the synthesis of chiral compounds. Adv. Biochem. Eng. Biotechnol. 120, 195–242.

Winter, G., Dökel, S., Jones, A. K., Scheerer, P., Krauss, N., Höhne, W., et al. (2010). Crystallization and preliminary X-ray crystallographic analysis of the [NiFe]-hydrogenase maturation factor HypF1 from *Ralstonia eutropha* crystallization communications. Acta Crystallographica Section F: Structural Biology and Crystallization Communications 66, 452–455.

Wolf, I., Buhrke, T., Dernedde, J., Pohlmann, A., and Friedrich, B. (1998). Duplication of *hyp* genes involved in maturation of [NiFe] hydrogenases in *Alcaligenes eutrophus* H16. Arch. Microbiol. 170, 451–459.

Wolfram, L., Friedrich, B., and Eitinger, T. (1995). The *Alcaligenes eutrophus* protein HoxN mediates nickel transport in *Escherichia coli*. J. Bacteriol. 177, 1840–1843.

Wollers, S., Layer, G., Garcia-Serres, R., Signor, L., Clemancey, M., Latour, J.-M., et al. (2010). Iron-Sulfur (Fe-S) Cluster Assembly. J. Biol. Chem. 285, 23331–23341.

Wombwell, C., Caputo, C. A., and Reisner, E. (2015). [NiFeSe]-hydrogenase chemistry. Acc. Chem. Res. 48.

Worst, D. J., M. Gerrits, M., Vandenbroucke-Grauls, C. M. J. E., and Kusters, J. G. (1998). *Helicobacter pylori ribBA*-mediated riboflavin production is involved in iron acquisition. J. Bacteriol. 180, 1473–1479.

Wu, L. -F, Mandrand-Berthelot, M. -A, Waugh, R., Edmonds, C. J., Holt, S. E., and Boxer, D. H. (1989). Nickel deficiency gives rise to the defective hydrogenase phenotype of *hydc* and *fnr* mutants in *Escherichia coli*. Mol. Microbiol. 3, 1709–1718.

Wulff, P., Thomas, C., Sargent, F., and Armstrong, F. A. (2016). How the oxygen tolerance of a [NiFe]-hydrogenase depends on quaternary structure. J. Biol. Inorg. Chem. 21, 121–134.

Wurm, D. J., Hausjell, J., Ulonska, S., Herwig, C., and Spadiut, O. (2017a). Mechanistic platform knowledge of concomitant sugar uptake in *Escherichia coli* BL21(DE3) strains. Sci. Rep. 7, 45072.

Wurm, D. J., Herwig, C., and Spadiut, O. (2017b). "How to determine interdependencies of glucose and lactose uptake rates for heterologous protein production with *Escherichia coli*," in Methods in Molecular Biology (Humana Press Inc.), 397–408.

Yanisch-Perron, C., Vieira, J., and Messing, J. (1985). Improved M13 phage cloning vectors and host strains: Nucleotide sequences of the M13mpl8 and pUC19 vectors. Gene 33, 103–119.

Zhang, B., Crack, J. C., Subramanian, S., Green, J., Thomson, A. J., Le Brun, N. E., et al. (2012). Reversible cycling between cysteine persulfide-ligated [2Fe-2S] and cysteine-ligated [4Fe-4S] clusters in the FNR regulatory protein. Proc. Natl. Acad. Sci. U. S. A. 109, 15734–15739.

Recent doctoral theses at Bioprocess Engineering, TU Berlin

1. Felix Kaspar (2021) Analytical methods and thermodynamic frameworks for efficient biocatalytic nucleoside synthesis via nucleoside phosphorylases
2. Sebastian Hans (2021) Accelerating biological screenings through the combination of high-throughput and modeling
3. Robert Giessmann (2020) Prediction of kinetics and yields of nucleoside phosphorylase reactions and derived enzymatic reaction cascades
4. Klaus Pellicer Alborch (2020) Cocci chain length distribution as control parameter in scaling lactic acid fermentations
5. Ángel Córcoles García (2019) Molecular genetic approaches to decrease mis- incorporation of non-canonical branched chain amino acids into a recombinant protein in *Escherichia coli*
6. Moonsung Cho (2019) Suspension of a point-mass-loaded filament in non-uniform flows: the ballooning flight of spiders
7. Sarah Kamel (2019) Enzymatic synthesis of α-D-pentosefuranose-1-phosphate
8. Heba Yehia Mohamed (2019) Chemoenzymatic synthesis of nucleoside analogs as potential medicinal agents
9. Funda C. Ertem (2019) Life cycle assessment and modeling approaches as a combined evaluation tool for sustainable control strategies at biogas plants
10. Emmanuel Anane (2019) Model based strategies for scale-down studies in fed- batch cultivation of *Escherichia coli* expressing protein
11. Ekaterina Osmekhina (2018) Quantitative approach for detection of RNA and proteins by sandwich hybridization technology
12. Elvis Legala Ongey (2018) Reconstruction of the lanthipeptide ruminococcin-A biosynthesis machinery in *Escherichia coli* and structural characterization
13. Anika Bockisch (2018) Mobile multi-parameter measurements for the dynamic analysis of gradients in brewing vessels
14. Juan Antonio Arzate (2018) Modeling and simulation of biogas production based on anaerobic digestion of energy crops and manure
15. Anna Maria Marbá (2018) Monitoring of the single-cell morphology for the evaluation of microbial eukaryotic bioprocesses

Full copies of the theses are available at https://depositonce.tu-berlin.de/.